# Unearthing the background of Naturalis *Tyrannosaurus rex*: taphonomy, stratigraphy and paleoenvironment

**Master Thesis Report**
MSc Earth Sciences
Vrije Universiteit Amsterdam

**Pim Kaskes**
Student nr: 1891790

**Supervisors:**
Dr. Klaudia F. Kuiper
Prof. Dr. Jan Smit
Dr. Anne S. Schulp

**Final version**
14 July 2016

VU UNIVERSITY AMSTERDAM

Naturalis Biodiversity Center

**Cover photo:** a large skull of a new, relatively complete and exceptionally well-preserved individual of *Tyrannosaurus rex* is unearthed by scientists of Naturalis Biodiversity Center (Leiden, the Netherlands) and Black Hills Institute (Hill City, South Dakota, USA). The specimen of this famous carnivorous dinosaur was excavated in August and September 2013 from a fluvial sandstone deposit of the Upper Cretaceous Hell Creek Formation in eastern Montana, USA. The geological context of this specimen, nicknamed Trix, forms the subject of this Master Thesis Project (photo by Servaas Neijens, National Geographic Nederland).

# Table of Contents

# Abstract

In August 2013, Naturalis Biodiversity Center in Leiden and the Black Hills Institute (Hill City, USA) excavated a new specimen of *Tyrannosaurus rex* on the Murray Ranch, south of Jordan, eastern Montana, USA. The partial skeleton of this famous carnivorous dinosaur was found in a fluvial sandstone deposit of the Upper Maastrichtian Hell Creek Formation on the western margin of the Williston Basin. The specimen, currently registered in Leiden as RGM 792.000, is a relatively complete and exceptionally well-preserved adult containing an articulated skull, left shoulder girdle, furcula, much of the vertebral column and rib cage, pelvis, right leg and a large part of the tail. In September 2014, a geological field campaign was conducted on the Murray Ranch to study three aspects of this fossil locality: the taphonomy and sedimentary context (1), the paleoenvironmental conditions (2) and the age of the paleontological site (3).

The specimen was partly disarticulated with the right leg and pelvis separated c. 10 m from the skull block. Rip-up clasts and climbing ripples observed at the excavation site pointed towards high paleocurrent strengths. Additional grain-size and thermogravimetric analysis showed that the unique 3D preservation of this *Tyrannosaurus rex* is linked to a rapid burial under a 3.20 m thick blanket of poorly consolidated, well sorted, fine sand with a high carbonate content. It is hypothesized that a single, massive flood event buried this dinosaur shortly after its death within days to weeks. Furthermore, the sandstone was not compacted and therefore prevented bone deformation. Lastly, the high carbonate content, represented by angular, detrital dolomite grains, protected the skeleton against subsequent leaching. These characteristics of the sand body entombing the *Tyrannosaurus rex* provided the perfect recipe for its excellent preservation.

A paleoenvironmental reconstruction, based on field evidence and pollen analysis, showed that the ecosystem of this *Tyrannosaurus rex* was characterized by meandering rivers surrounded by densely vegetated floodplains and shallow lakes. The various palynomorph taxa indicated the presence of a high biodiversity, subtropical forest dominated by angiosperms. The regional climate was subtropical with probably a clear dry and wet season, explaining the seasonal flood events of which one buried this specimen.

The age of the fossil locality was determined using an integrated stratigraphic approach combining litho-, magneto-, bio- and cyclostratigraphy. Paleomagnetic measurements of the different sections all showed a normal polarity that coincided with chron C30N and thereby excluded a stratigraphic position in the upper part of the Hell Creek Formation. Combined with the presence of the biostratigraphic marker species *Aquilapollenites collaris*, an age range between c. 66.8 and 67.2 Ma was established. Milankovitch cyclicity within the fluvial sediments, related to enhanced monsoonal activity, was suggested, but was not possible to test without a solid first order age model. Therefore, to further refine the age of the fossil site, a more detailed magneto- and biostratigraphic study is necessary.

Based on the results of this study, it is recommended to incorporate similar contextual, high-resolution geological research to other future dinosaur discoveries. Using this multidisciplinary approach, it is possible to better understand and reconstruct the mode of life of the associated animal, its habitat, the cause of death, its fossilization process and the conditions under which the specimen became preserved over millions of years.

**Keywords:** *Tyrannosaurus rex*, Theropoda, Hell Creek Formation, Maastrichtian, taphonomy, paleoenvironment and integrated stratigraphy

# Preface

This report documents the results of my Master Thesis Project in partial fulfillment of the Master Earth Sciences - program at the Vrije Universiteit (VU), Amsterdam, the Netherlands. This Master Thesis Project + extension (in total 39 ECTS) comprises two tracks within the Earth Sciences program, namely the 'Solid Earth' and 'Paleoclimatology and Geo-ecosystems' track and therefore has two course codes (AM_450199 and AM_450201). This research project was carried out at the VU and was supervised by Dr. Klaudia F. Kuiper (VU), Prof. Dr. Jan Smit (VU) and Dr. Anne S. Schulp (Naturalis Biodiversity Center and VU). One aspect of the lab-activities involved the magnetostratigraphic measurements at Paleomagnetic Laboratory Fort Hoofddijk of Utrecht University (UU) and this forms the extension of my project.

My Master Thesis Project focuses on the geological context of the recent discovery of a unique specimen of the famous carnivorous dinosaur *Tyrannosaurus rex* by Naturalis Biodiversity Center (national natural history museum in Leiden, the Netherlands). This beautiful fossil was discovered by Michele and Blaine Lunstad in May 2013 during a stroll over the ranch of Lige and Mary-Ann Murray south of the town of Jordan, Garfield County, eastern Montana, USA. Blaine Lunstad phoned local fossil-hunter Clayton Phipps who confirmed the exposed skull was part of a *T. rex* (Fig 0.1). Phipps contacted Peter Larson, director of the Black Hills Institute in South Dakota, who informed Naturalis about this discovery. In August 2013, a collaborative excavation started between Naturalis and the Black Hills Institute and within two weeks a relatively complete and remarkably well-preserved *Tyrannosaurus rex* was unearthed. This specimen, currently registered as RGM 792.000, will become the centerpiece in the new dinosaur gallery of the renovated natural history museum in Leiden. In September and October 2014, I went back to the dig site in Montana to perform additional fieldwork to place this *T. rex* in a detailed geological framework. The field- and lab results of this study are presented in this report.

**Fig. 0.1.** From left to right: Land owners Lige and Mary Ann Murray, discoverers Michele and Blaine Lunstad and local paleontologist Clayton Phipps posing with the skull of the *Tyrannosaurus rex* of Naturalis Biodiversity Center (photo: Servaas Neijens, National Geographic Nederland).

The objectives of my Master Thesis are three-fold: first of all, I would like to know why this specific *Tyrannosaurus rex* specimen is so exceptionally well-preserved within a sandstone deposit of the Cretaceous Hell Creek Formation. Therefore, a detailed sedimentological (including grain-size analysis and thin section petrography), geochemical (e.g. thermogravimetric analysis) and taphonomic (e.g. examination of the bone articulation) study was carried out at the excavation site to establish possible post-mortem scenarios. My second main research question is: what was the paleoenvironment of this *T. rex*? A landscape and vegetational reconstruction was interpreted on basis of pollen-analysis combined with field evidence and comparisons with literature about the Hell Creek Formation. At last, I am eager to provide an answer to the question when this particular *T. rex* lived. Using an integrated stratigraphic approach by combining litho-, magneto-, bio- and cyclostratigraphy on various sections within the study area, I hope to establish an as accurately as possible age model for this fossil site within the Late Cretaceous.

This report is subdivided into five major chapters. In **Chapter 1,** an extensive literature study is performed to provide the reader with background information concerning the species *Tyrannosaurus rex* in general, the geological setting of the Williston Basin in North America, the characteristics of the regional Hell Creek Formation, the specimen itself, the local study area, the research aims and the multidisciplinary approach. **Chapter 2** deals with the methodology and materials used during the field campaign in eastern Montana in 2014 and the subsequent lab-activities at the VU and UU. The results of this study, subdivided over the three main questions regarding taphonomy, paleoenvironment, and age-determination, are presented in **Chapter 3**. The data is interpreted in **Chapter 4** per three research questions separately, as well as in a combined manner in order to provide possible burial and paleoenvironmental reconstructions of the *T. rex* locality through time. **Chapter 5** summarizes the major findings of this study and in the following **Outlook** chapter**,** recommendations, other ideas and remaining questions are provided for future research. Lastly, various detailed maps of the study area, photo-overviews and sedimentological graphs of specific sections, the raw grain-size, thermogravimetry, pollen and paleomagnetism dataset and an overview of the *Tyrannosaurus rex* discoveries over the last century are listed in the **Appendices**. All photographs in this report are made by the author or his supervisors, unless stated otherwise.

By means of this Master Thesis Project, I have been able to answer a large part of the research questions regarding the geological context of the Naturalis *Tyrannosaurus rex*. However, during the academic process, some new, interesting research questions arose which are certainly worthwhile to study in the near future. This report may serve as a solid basis for future research plans or educational and expositional activities concerning the Naturalis *T. rex* specimen, which recently received the 'royal' nickname 'Trix'. From September 2016 onwards, the skeleton of this dinosaur will arrive in the museum in Leiden and will be part of a new *T. rex* exhibition open for public.

For me, it was an honor to work on this fascinating, extinct creature and it was an exciting experience to be able to reconstruct glimpses of the ancient world of Trix!

Pim Kaskes

14 July 2016

Master student Geology
Vrije Universiteit Amsterdam
pim.kaskes@gmail.com

# 1. Introduction

In this chapter, a literature review is provided with state-of-the-art background information about the species *Tyrannosaurus rex* in general and the sedimentary basin (Williston Basin) and rock formation (Hell Creek Formation) where the Naturalis-specimen has been found. Finally, the specimen itself, the local study area and the research aims and approach of this Master Thesis project are described in detail.

## 1.1. *Tyrannosaurus rex*

In this paragraph, the discovery, phylogeny and evolution of the species *Tyrannosaurus rex* is described, followed by a section summarizing the most important anatomical features and growth characteristics. Subsequently, the most recent and controversial ideas about its paleobiology are reviewed and finally the paleobiogeographic aspects of *T. rex* in western North-America are reported.

### 1.1.1. The 'Tyrant Lizard King' and its family

*Tyrannosaurus rex* was one of the largest carnivorous dinosaurs of all time and was the apex predator of the latest Cretaceous continental ecosystems of western North America (e.g. Brusatte et al., 2010; Larson, 2008). *Tyrannosaurus rex*, commonly abbreviated to *T. rex*, received its iconic name (meaning 'Tyrant Lizard King', in reference to its size) after its first description in 1905 by Henry Fairfield Osborn, a professor and founder of the department of vertebrate paleontology at the American Museum of Natural History (AMNH) in New York. The initial paper (Osborn, 1905, Fig. 1.1A) was based on a partial skeleton (specimen name: CM 9380, originally AMNH 973) discovered in 1902 during a field expedition under the supervision of the museum's chief fossil collector Barnum Brown. This holotype specimen was found in a sandstone deposit from the Upper Cretaceous (Maastrichtian) Hell Creek Formation (then called Laramie Formation) near Jordan, Garfield County, eastern Montana, USA. This holotype locality is situated relatively close to the excavation site of the Naturalis specimen, namely c. 70 km to the north.

To be precise, in his first paper Osborn mentioned another large tyrannosaurid, *Dynamosaurus imperiosus,* based on a partial skeleton and skull found by Barnum Brown in 1900 in Wyoming. *Dynamosaurus* was thought to have osteoderms (bony plates), a characteristic that distinguished it from *Tyrannosaurus*. Doubts about association of the reported osteoderms with the type of *Dynamosaurus* (AMNH 5866) were expressed (Osborn, 1905), and Osborn later regarded *Dynamosaurus imperiosus* and *Tyrannosaurus rex* as the same species (Osborn, 1906). The name *Tyrannosaurus* has priority in taxonomy, as it preceded *Dynamosaurus* in the description (Breithaupt et al., 2008; Brochu, 2003). In his 1906 paper, Osborn published more detailed descriptions and illustrations of the collected material of the holotype *T. rex* specimen. It was one of these figures (Fig. 1.1B) that formed the basis for the first life restoration of a *Tyrannosaurus rex* in (an incorrect) upright position that would gradually become the accepted image of this fearsome, carnivorous dinosaur in the public eye. This way, *T. rex* became the archetypal dinosaur from the early 1900's and appeared in virtually every popular venue, ranging from comic books, toys, games, park exhibits and movies such as The Lost World in 1925 (based on artwork of Charles Richard Knight) and the famous Jurassic Park series from 1993 onwards (Glut, 2008).

Besides being such a pop culture icon, the species *T. rex* is also a valuable research subject and has currently become an ancient exemplar animal used to study many themes in vertebrate paleontology (Brusatte et al., 2010). *T. rex* is the largest known theropod in North America and also the largest member of the subfamily of so-called Tyrannosauroidea. This relatively derived group of theropod dinosaurs is more closely related to birds (Aves) than to other large theropods such as Allosauroids and Spinosaurids (Fig 1.2.). The Tyrannosauroidea are the most intensively studied extinct group of dinosaurs thanks to their large sample sizes and a revolution of new discoveries over the last decades in e.g. Alaska (Fiorillo and Tykoski, 2014), Mongolia (Brusatte et al., 2009), China (Li et al., 2010; Lü et al., 2014; Xu et al., 2012;) and Uzbekistan (Brusatte et al., 2016). Recent cladistic analysis (Brusatte & Carr, 2016; Brusatte et al., 2010) showed that the Tyrannosauroidea originated already in the Middle Jurassic, but remained relatively small and ecologically marginal until the latest Cretaceous (Fig. 1.3). The Northern Hemisphere continental ecosystems of the final 20 Myr of the Mesozoic were dominated by the family of Tyrannosauridae (indicated in red in Fig. 1.2 and 1.3) with *T. rex* as largest member and ultimate evolutionary form.

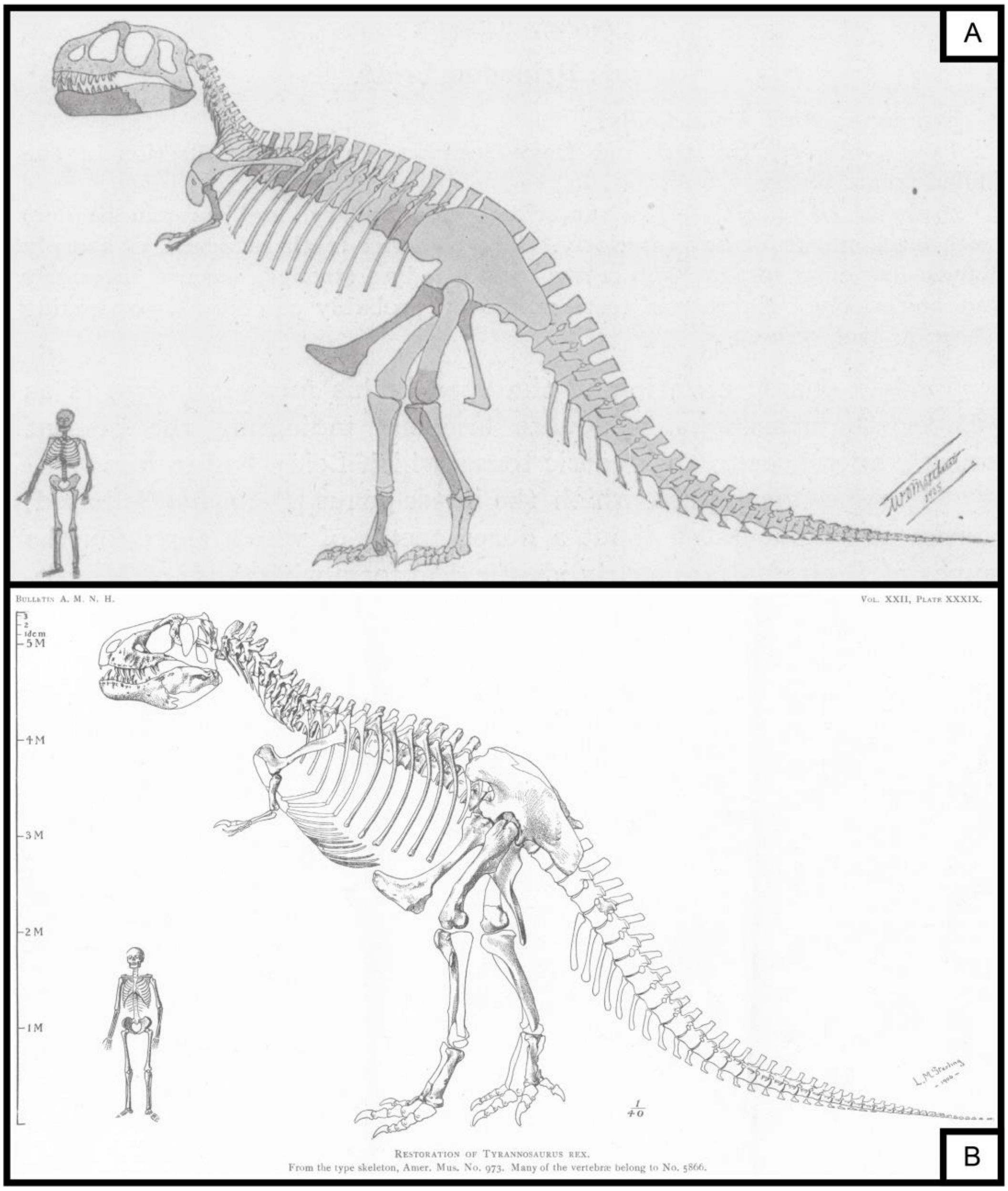


**Fig. 1.1.** Osborns first skeletal reconstruction of *Tyrannosaurus rex* **(A)**, drawn by W.D. Matthew, based on a skeleton that was not fully collected or prepared during publication (Osborn, 1905). His second, revised version, drawn by L. M. Sterling **(B)**, was based on specimen AMNH 973 and included parts of AMNH 5866 (the in first instance *Dynamosaurus* specimen) and parts of AMNH 5881 (a very partial skeleton found by Brown in 1905) (Osborn, 1906). It clearly shows the massive skull with huge teeth, robust pelvis, tiny forelimbs, elongated hindlimbs and long tail of this carnivorous dinosaur, although the upright, lizard-like posture has nowadays changed into a more agile, horizontal, bird-like stature.

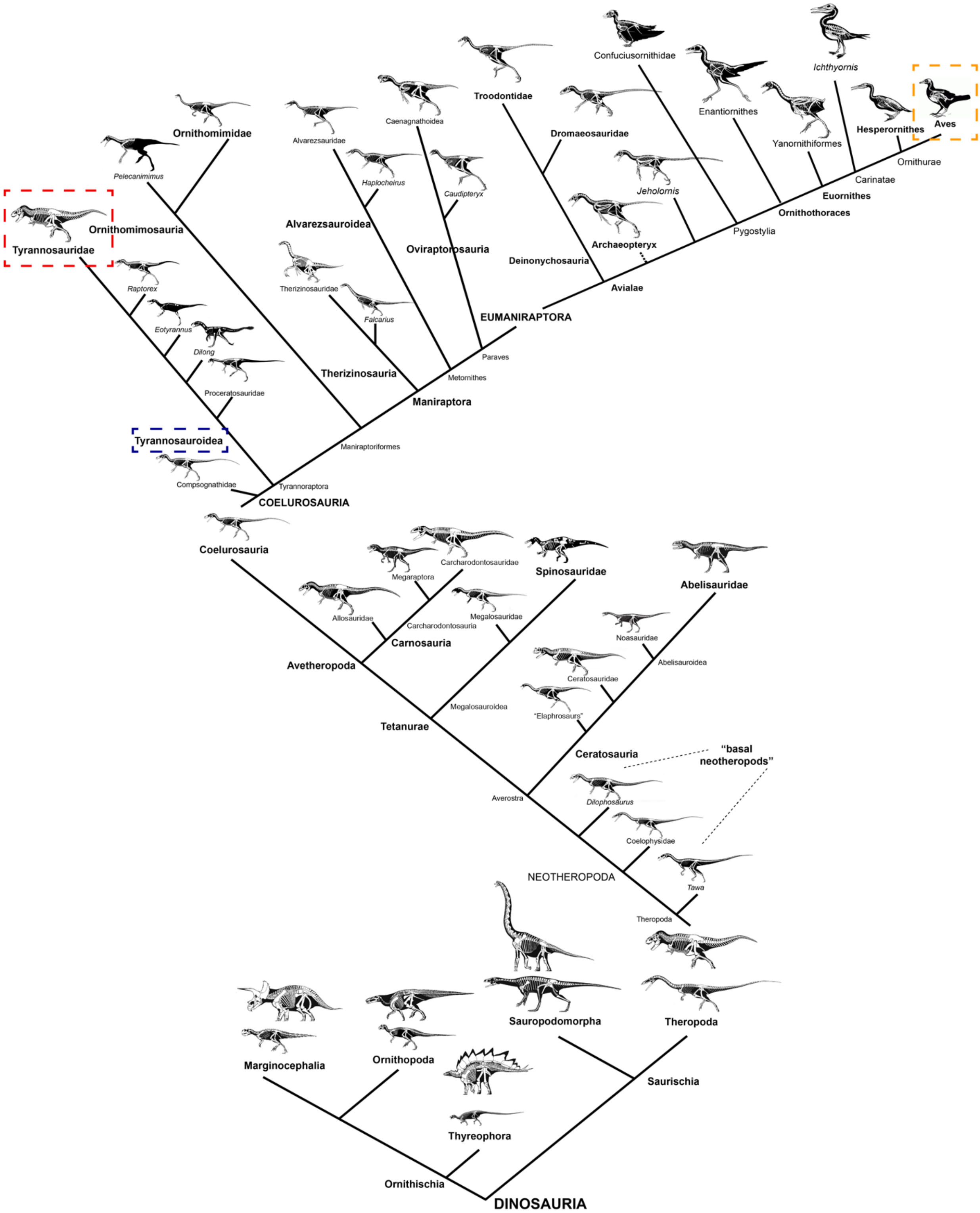


**Fig. 1.2.** Simplified cladogram of the clade of Dinosauria showing the evolutionary and phylogenetic relationships between the order of Saurischia, suborder of Theropoda, the Coelurosauria, Tyrannosauroidea (indicated with blue) and Tyrannosauridae (indicated with red). Furthermore, the relationship between theropod dinosaurs and modern day birds (Aves, indicated with orange) is provided (modified from Brusatte, 2008; Holtz, 2015).

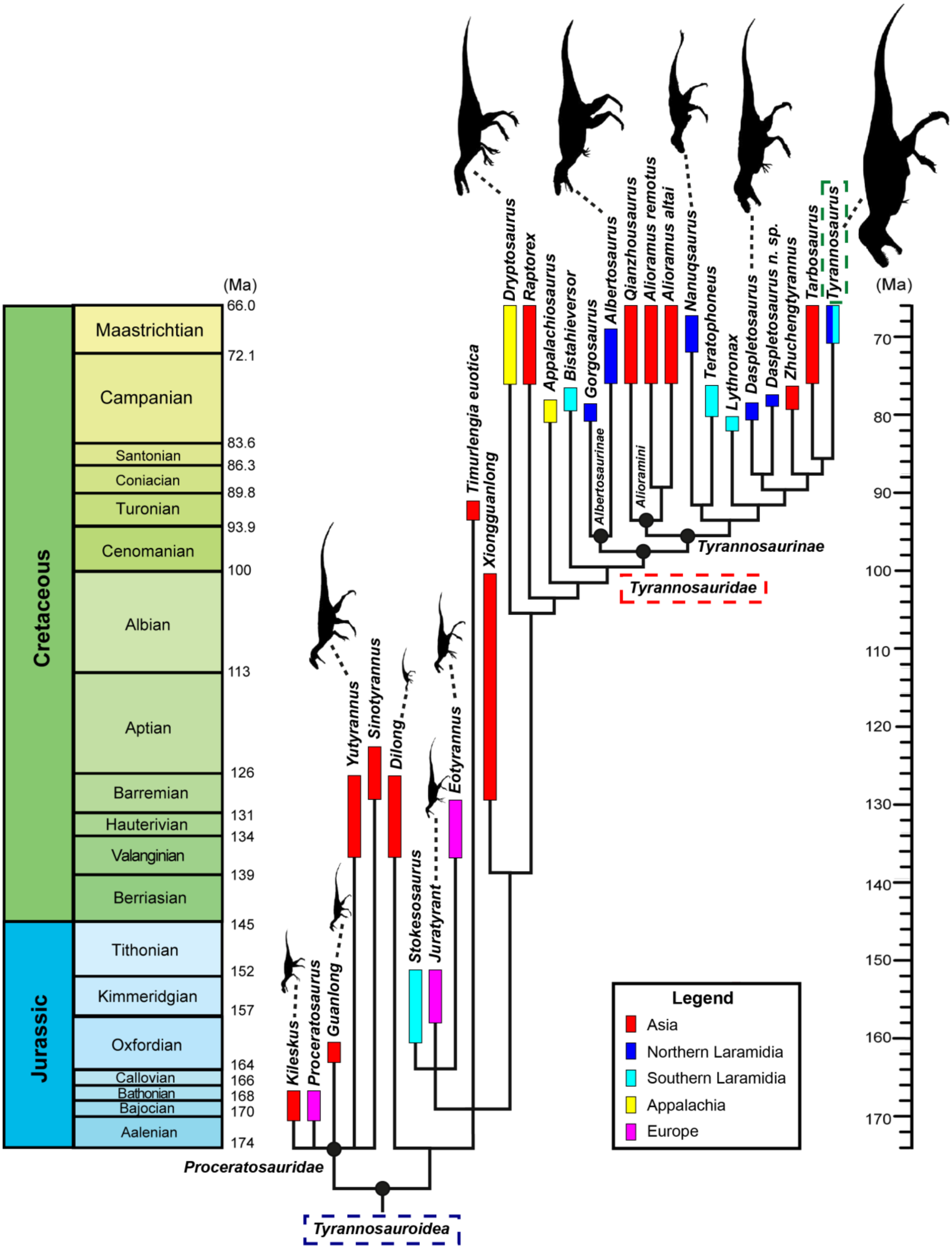


**Fig. 1.3.** Phylogenetic position of the genus *Tyrannosaurus* (indicated with green) among the subfamily of Tyrannosauroidea (indicated with blue) set to the most recent developed geologic timescale (Gradstein et al., 2012). Thick bars indicate uncertainty of geological range for a given taxon and the color of the bars marks the suggested Mesozoic landmass where the specific Tyrannosauroid taxon lived, indicating that *T. rex* was present on the entire Laramidia continent (after Loewen et al., 2013). Branches of the phylogeny are not scaled to time. Taxon silhouettes are in relative proportion and scaled to total body length *(T. rex* measures 13 meters). The

phylogenetic relationships of the Tyrannosauroidea are assessed by a cladistic analysis using the 'parsimony analysis' method of Brusatte et al. (2010), Brusatte & Benson (2013) and Brusatte and Carr (2016) with the most recent discovery of the Mid-Cretaceous aged *Timurlengia euotica* added (Brusatte et al., 2016).

### 1.1.2. Anatomy and ontogeny

New discoveries and more advanced technologies over the last decade have shed new light on the anatomy and appearance of Tyrannosauridae, including external, internal and soft-tissue morphology. *Tyrannosaurus rex* and its closest kin were all bipedal carnivores and their external body plan is in general characterized by a large and deep skull with powerful neck and jaw muscles, robust and serrated teeth to crush bone and cut meat, small arms with only two fingers, long, strong hindlimbs and a long tail to balance their massive head (Brochu, 2003; Sereno et al., 2009).

Morphometric analysis within different *Tyrannosaurs rex* specimens showed distinct gracile and robust morphotypes that are thought to represent sexual dimorphism within the same species (Larson, 2008). Direct gender-specific evidence came from the hindlimb of a *T. rex* specimen nicknamed 'B-rex' (MOR 1125), where medullary bone was identified. This calcium phosphate deposit is regulated by levels of estrogens, is used for shelling in eggs in living birds and is thus a reproductive tissue only found in pregnant animals (Schweitzer et al., 2005). Detailed laboratory tests showed that the unique chemical composition of medullary bone in extant birds is indeed retained in the femur of this *T. rex* and that the chemistry is not linked to bone diseases like osteopetrosis (Schweitzer et al., 2016). According to the nomenclature of Larson (2008), MOR 1125 is a robust morphotype, characterized by e.g. a thicker femur. Hence, it is assumed that the robust morphotype of *T. rex* represents the female.

Exceptionally well-preserved fossils of Tyrannosauroidea have shown to feature integumentary structures and other soft tissues, which rarely fossilize in dinosaurs. Recent discoveries of basal Tyrannosauroidea in China, such as *Dilong* (Xu et al., 2004) and *Yutyrannus* (Xu et al., 2010) (Fig. 1.3), have been reported to preserve branched, filamentous integumentary covering, interpreted as protofeathers likely used for display. Direct fossil evidence for feathers in the species *Tyrannosaurus rex* has not (yet) been reported, but this may be related to preservational issues of fossil skin. A well-preserved *T. rex* specimen known as Wyrex (BHI 6230) holds some small skin impressions that clearly show scales and no (proto)feathers (Larson, P., 2014, pers. comm.). Schweitzer et al. (2005) documented the recovery of soft tissue from the marrow cavity of a fossilized leg bone from *T. rex* specimen MOR 1125. Bifurcating blood vessels, fibrous bone matrix tissue, blood cells and even traces of possible protein sequences were recognized (Asara et al., 2008). However, there is heavy skepticism concerning the quality of preservation and thus the biomolecular and genetic use of these proteins to establish the evolutionary relationship between birds and dinosaurs (e.g. Pevzner et al., 2008).

For a long period of time, scientists were wondering how multi-ton dinosaurs such as *T. rex* reached such massive body sizes and how their skeletons developed from an embryo phase towards a full-grown adult stage. In 2004, Erickson et al. provided quantitative data on the life history of Tyrannosauridae such as growth rates, life span and adult size for the first time. Histological analysis (by counting growth lines within a bone thin section) was performed to determine the ages at death of dinosaurs. Combined with estimations of the body size (based on measured femur sizes) this made comparative growth-curve reconstructions for several dinosaur species possible. *Tyrannosaurus rex* differs from its closest relatives by an extraordinary accelerated growth with a maximum rate of 2.1 kg per day. *T. rex* clearly attained its enormous size thanks to this enhanced growth rate rather than extending its life span, because it reached skeletal maturity already at an age of c. 20 years, but most individuals rarely lived longer than 25 years. A full-grown *T. rex*, such as the world-famous and most complete specimen of *T. rex* nicknamed Sue (FMNH PR 2081), has a body length of 12.29 m, stands 4 m tall at the hips, was at least 28 years old and has an estimated body mass of more than 6000 kg (Erickson et al., 2004;

Hutchinson et al., 2011).

It is suggested that *T. rex* skeletons showed pronounced changes during ontogenetic stages. Carr (1999) and Currie (2003) showed that, as individuals matured, the skulls and jaws of Tyrannosauridae deepened, ornamented structures enlarged and coarsened, the torso became longer and heavier, the forearms shortened and the teeth became larger and thicker. The morphological differences between young and old individuals can be so large that several growth stages were identified as different species.

One good example is the long-running debate about the validity of the proposed Tyrannosauridae species *Nanotyrannus lancensis* by Bakker et al. (1988). Carr (1999) published a paper identifying a number of derived cranial features that suggested the famous 'Cleveland holotype specimen' (CMNH 7541) to be a young *T. rex*. A recent review by Hone et al. (2016) deals with the question 'what is an adult dinosaur?'. They concluded that, following new age-determination techniques developed over the past decades, numerous individual dinosaurs had not reached maturity when they died, whereas at first glance many researchers thought these dinosaurs died in their adult stage. For example, histological analysis by the Museum of the Rockies suggests distinct allometric growth stages within ornithischian dinosaurs, such as ceratopsians (*Torosaurus* is an adult *Triceratops* according to Scanella & Horner, 2011) and pachycephalosaurids (*Dracorex hogwartsia* and *Stygimoloch spinifer* are a juvenile and subadult stage of *Pachycephalosaurus wyomingensis* as interpreted by Horner & Goodwin, 2009). A proposed high juvenile survivorship of *T. rex*, derived from an age-standardized ecological life table for a North American carnivorous dinosaur population, may explain the rarity of young *T. rex* specimens in museum collections (Erickson et al., 2006).

However, computerized tomography (CT) scanning of the Cleveland skull by Witmer & Ridgeley (2010) revealed some distinct indentations within the braincase region that differs from *T. rex* skulls. Since the Cleveland skull, two other proposed *N. lancensis* specimens have taken center stage in the debate, namely Jane (BMR P2002.4.1) and the theropod described as one of the 'Dueling Dinosaurs' (BHI 6437), which was found – just like the Naturalis *T. rex* - on the Murray Ranch in eastern Montana. Larson (2008, 2013a,b) strongly believes *N. lancensis* is a separate taxon, because e.g. its teeth are too finely serrated and closely packed to be those of a juvenile *T. rex*. In addition, Schmerge & Rothschild (2016) addressed the importance of the presence of a lateral dentary groove in the lower jaw of *N. lancensis* in comparison with *T. rex* that lacks this feature. According to the authors, this characteristic makes *Nanotyrannus* a distinct genus and places it as a sister to the Albertosaurinae instead of the Tyrannosaurinae, as earlier proposed (Currie, 2003). Because of the ongoing controversy about the validity of *Nanotyrannus*, the taxon has not (yet) been added to Fig. 1.3 (Brusatte & Carr, 2016).

Nonetheless, the *Nanotyrannus* question remains unresolved and new discoveries of a clear adult *Nanotyrannus* skeleton that is different from *T. rex* or a young tyrannosaur more similar to an adult *T. rex* than any *Nanotyrannus* specimen are essential (Switek, 2013 Nature). The 'Dueling Dinosaurs' specimen might solve this mystery, but it is currently unavailable for scientific research (Pringle, 2014).

### 1.1.3. Paleobiology

The paleobiology of *Tyrannosaurus rex* is probably the best understood of all dinosaurs, thanks to its popular appeal and an avalanche of new body fossils and trace fossils over the last two decades. Skeletons of both juveniles and adults, fossilized footprints, pathologic specimens, bones of their prey with bite marks, stomach contents and even coprolites give indications for, amongst others, diet and feeding style, social behavior and locomotion of this ancient predator (Brusatte et al., 2010).

*T. rex* had all the tools of a ferocious carnivore at the top of the food chain. It was a warm-blooded animal (Bakker, 1972) with a very efficient respiratory system composed of air-sacs similar to modern-day birds. Furthermore, thanks to CT scanning, new internal anatomical features of *Tyrannosaurus rex* have indicated that this animal led a predatory mode of life. Relatively large brain sizes, large olfactory lobes and elongate cochlear have been found in *T. rex* skulls which support a strong sense of smell together with an enhanced sensitivity to low-frequency sound and highly coordinated eye and head movements (Witmer & Ridgeley, 2009). Stevens (2006) described several reconstructed theropod heads based on casts that showed that the cranial design of *T. rex* differed from its closest kin in terms of more broadly separated, larger eyes high up in the skull. This gave *T. rex* an excellent binocular vision with a c. 55° of binocular overlap, and would allow not only observation of distant prey, but also accurate perception of the three-dimensional arrangement of potential obstacles to avoid during pursuit predation (Farlow et al., 1995). *T. rex* most powerful weapons were its robust and serrated teeth (up to c. 30 cm long each, including the root) that could crush bone easily. Biomechanical models that replicated the depth and size of fossil bite marks and recent dynamic musculoskeletal 3D models resulted in an estimated bite force for *T. rex* of at least 13.400 N to a maximum of 57.000 N, by far the highest bite forces estimated for any terrestrial animal (Erickson et al., 1996; Bates & Falkingham 2012). Rayfield (2004) performed stress-vector analysis on the cranium and demonstrated that the facial bones of *T. rex* were able to resist such large biting and tearing loading.

One of the most controversial discussions over the past decades was on whether *Tyrannosaurus rex* was an active hunter or a scavenger that solely fed on carcasses. The discovery of a huge, bone-bearing theropod coprolite (Chin et al., 1998) and numerous bite marks on ornithischian dinosaur bones (e.g. Erickson & Olson, 1996) showed that these herbivorous dinosaurs were on the menu of *T. rex*. However, until recently no physical evidence was found for *T. rex* hunting these live prey. In 2013, DePalma and colleagues found 'a smoking gun', namely the discovery of an embedded tooth crown of a *T. rex* in the tail vertebra of an *Edmontosaurus annectens* specimen with bone tissue that clearly regrew around it. This means that the hadrosaur should have survived the attack of the *T. rex* (DePalma et al., 2013). Today, most scientists agree that *T. rex* was an opportunistic carnivore and an ecological generalist that sometimes hunted and sometimes scavenged, just like modern-day hyenas do.

Recent examination of a relatively limited sample of tooth-marked bones of *T. rex* specimens provided direct evidence of cannibalism and even suggested that this cannibalistic behavior must have been a surprisingly common behavior in *Tyrannosaurus* (Longrich et al., 2011). Other clear evidence for gregarious behavior within *T. rex* have not yet been found. However, a detailed analysis of a monodominant bonebed of *Albertosaurus sarcophagus* specimens in Canada may suggest that these close cousins of *T. rex* (Fig. 1.3) were hunting in packs on herds of herbivorous dinosaurs (Currie & Eberth, 2010). In addition, McCrea et al. (2014) documented the world's first trackway attributable to tyrannosaurids and interpreted these ichnofossils from the Wapiti Formation in British Columbia as a set of tracks left behind by three tyrannosaurs moving in the same direction at the same time. It is not known to which tyrannosaurid species the tracks belong, but the authors stated that the inference that these three animals were moving as a social group (possibly as a hunting pack) is the most parsimonious interpretation (McCrea et al., 2014).

The function of the unusually tiny arms of *T. rex* is still under debate. Did *T. rex* used its forelimbs for mating, clutching or getting up from a prone position? Lipkin & Carpenter (2008) showed that without exception, no theropod dinosaur could extend its forelimbs beyond the snout, thus limiting its usefulness as a prey-grasping organ before the mouth was reached. However, careful biomechanical and pathological analysis of new material, did show that the forearm of *T. rex* was capable of resisting large forces and moving at high accelerations and may have been used to cling to prey. On the other hand, Lockley et al. (2008) saw no functional role in predation for the forelimb whatsoever.

Despite all its powerful tools for predatory behavior, *T. rex* was probably not a swift hunter. Some evidence for this statement can be derived from the fossil footprint record of this large theropod dinosaur, which is surprisingly sparse compared to its well-documented skeletal record (McCrea et al., 2014; Manning et al., 2007). A very recent discovery of a rare tyrannosaur fossilized trackway, which belongs to either a juvenile *T. rex* or an adult *Nanotyrannus lancensis*, in the Lance Formation near the town of Glenrock in eastern Wyoming aided in estimating its walking speed. Based on the length of the footprint, an estimation of the hip height of the trackmaker (1.56 to 2.07 m above the ground) and the distance between the footprints, Smith et al., (2016) calculated that the dinosaur's speed should lie between 4.5 and 8 kilometers per hour (2.8 to 5 miles per hour). However, this trackway is not from a running full grown-tyrannosaur and thus the estimation is not an indication of the maximum speed of *T. rex*.

Biomechanical computer modeling studies, for example the muscle mass estimates performed by Hutchinson et al. (2011), also show that *T. rex* speed and turning capability was rather slow compared to large athletic animals that live today such as ostriches and horses. Although its long legs, large pelvic muscles and hollow bones reduced body weight, it apparently did not make *T. rex* extremely fast. Hutchinson & Garcia (2001) calculated a maximum speed of c. 17 km/h, still faster than its most likely prey, namely ceratopsians and hadrosaurs (Manning, 2008). *Tyrannosaurus rex* is the only large theropod known from the uppermost Maastrichtian beds of North America, excluding the presence of the controversial *Nanotyrannus lancensis*. This implies a lower biodiversity in large predators than is observed in most other well sampled dinosaur faunal assemblages (Persons & Currie, 2016). It has been hypothesized that the more elongate hindlimbs of *N. lancensis* reflect a form of predatory ecological niche partitioning between *T. rex* and *N. lancensis*. Bakker (1988) suggested that the two tyrannosaurids are comparable to modern-day African lions and cheetahs, with the smaller, more gracile, and longer legged *Nanotyrannus* being adapted for high-speed running.

### 1.1.4. Biogeography

Because of a renaissance of new discoveries made by amateur and professional paleontologists over the last two decades, *Tyrannosaurus rex* has now become one of the most visible large theropod dinosaur in many museum collections. However, well-preserved, articulated and more than 5% complete skeletons of *T. rex* are still rather rare. N. Larson (2008) summarized all collected skeletons of *T. rex* up to August 2006. Each listed specimen in his overview has a minimum of 10 associated skeletal bones from several parts of the body or a fairly complete skull. The list excluded isolated bones and teeth as well as specimens that consisted of only a braincase and/or few skull bones, foot bones or caudal bones (Larson, 2008).

Given these criteria, Larson identified 46 specimens of *Tyrannosaurus rex* containing more than 5% identifiable bones collected over the past century, which are displayed in a map overview in Fig. 1.4 and listed in Appendix 6 (Table A.6). The location of the Naturalis *T. rex* is also indicated in Fig. 1.4 and is situated just south of the Hell Creek type locality in Garfield County, Montana. I added manually a number of new *T. rex* specimens bringing the total number to 70 skeletons as of May 2016. However, a more detailed study is recommended in the future to fill in the gaps of missing information, since many new specimens (especially the ones in private collections) lack for instance reliable bone counts and lithology data.

When taking a closer look at the distribution of these skeletons (Fig. 1.4), it is apparent that *T. rex* skeletons have only been found in western North America in a N-S striking band of sedimentary basins all the way from Alberta in the north to New Mexico in the south. However, a recent find of isolated theropod teeth from the upper part of the Lomas Coloradas Formation in northeastern Sonora, Mexico, might broaden the geographic distribution of *T. rex* even more. Using morphological and statistical analyses these teeth were assigned to the Tyrannosauridae and these specimens may represent the most southern record of the genus *Tyrannosaurus* in North America (Serrano-Branas et al., 2014). An additional discovery of a maxilla and a very large anterior caudal vertebra, attributed to the genus *Tyrannosaurus*, from the Javelina Formation in Big Bend National Park in West-Texas supported the idea of southern habitats of *T. rex* (Wick, 2014).

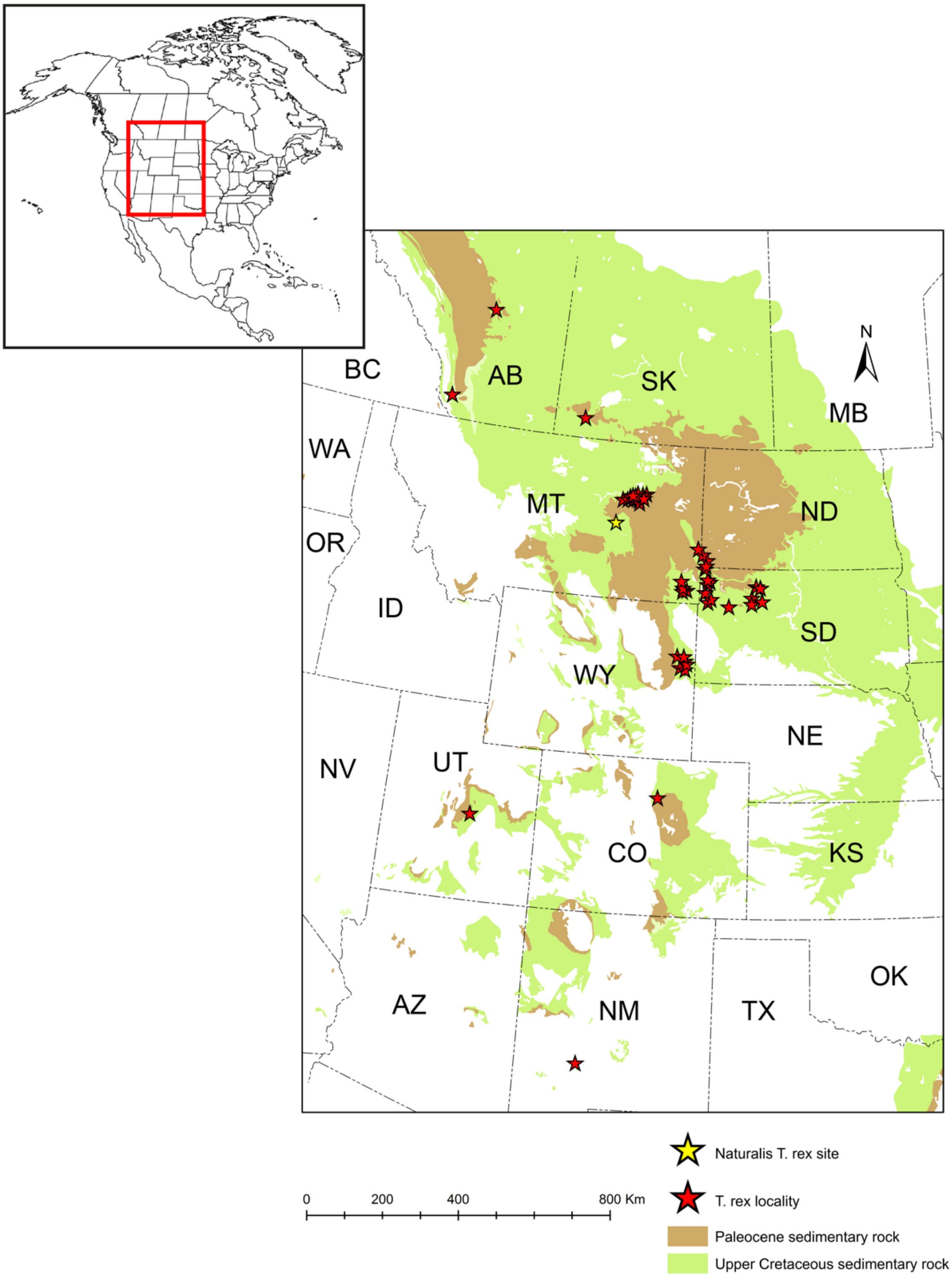


**Fig. 1.4.** Distribution of c. 50 excavated *Tyrannosaurus rex* skeletons (containing more than 5% identifiable bones) in western North America collected over the past century. These fossils have been found in the Upper Maastrichtian Hell Creek Formation and time-equivalent formations ranging from central Alberta in the north to southern New Mexico in the south and from central Utah in the west to north-central South Dakota in the east. The *T. rex* localities are adapted from N. Larson (2008) using the geological map of North America by Garrity & Soller (2009). At the moment c. 70 specimens of *T. rex* are known (see Appendix 6 for an extended overview), however, the most recent discoveries lack accurate geographic information and are hence not (yet) included in this map.

Horner et al. (1990) addressed the importance of the presence and extent of the Western Interior Seaway for the evolution and biogeographic zonation of North American dinosaur populations. The Western Interior Seaway (Fig. 1.5A) was a large epicontinental sea that formed in a foreland basin during the Mid-Cretaceous c. 110 Ma, lasted for almost 50 Myr, ran from present-day Alaska to the Gulf of Mexico and hence splitted North America in two continents: Laramidia in the east and Appalachia in the west (Kauffman, 1984). Little is known about the dinosaur fauna of Appalachia due to a lack of exposures, whereas the faunal assemblage of Laramidia is extremely well studied. Laramidia was a latitudinally elongate, but narrow landmass bounded by two biogeographic barriers: the mountains of the Upper Cretaceous Laramide Orogeny in the west and the Western Interior Seaway in the east (Loewen et al., 2013). During the Campanian, sea levels were relatively high and thus causing a restriction of the area of coastal plains. This 'habitat bottlenecking' triggered the subdivision of dinosaur communities into different provinces thereby stimulating evolutionary change in independent lineages and hence increasing the dinosaur biodiversity (Horner, 1992). On the contrary, the retreat of the Western Interior Seaway at the end of the Maastrichtian (Fig. 1.5B) re-linked the North American landmasses and reduced the provincialism and biodiversity in the dinosaurian fauna (Sampson et al., 2010).

Lehman (1987) identified three continental sedimentary provinces in Laramidia during the Maastrichtian stage: the alluvial plain, coastal lowland and intermontane basin sedimentary systems. He linked these so called 'lithosomes' to specific occurrences of the three herbivorous dinosaurs *Leptoceratops*, *Triceratops* and *Alamosaurus*, respectively (Fig. 1.6A) which represented three diverse dinosaur faunas that had little interchange during the Maastrichtian. The *Leptoceratops* fauna inhabited relatively cool, alluvial plain environments flanking the Rocky Mountains north of 35°N paleolatitude. This facies is represented by the Scollard and Willow Creek Formations in Canada (Sweet & Braman, 1992). The *Triceratops* fauna populated humid coastal floodplains and swamps bordering the retreating Western Interior Seaway, also north of 35°N latitude, exemplified by the Frenchman, Lance and Hell Creek Formations. The Naturalis *T. rex* locality represents this coastal lowland paleoenvironment. The *Alamosaurus* fauna inhabited intermontane basins south of 35°N latitude marked by seasonal, semi-arid conditions as seen in the North Horn, McRae and Javelina Formations. These three paleoenvironments were restricted habitats for endemic plant-eating dinosaurs (Fig. 1.6C), which can probably be explained by a combination of latitudinal climate variability, orogenic activity and variation in floral diversity (related to variations in rainfall and air temperature) between these distinct lithosomes (Lehman, 1987).

In contrast to coeval species of herbivorous dinosaurs, *Tyrannosaurus rex* was not dependent on variations in floral diversity and therefore able to adapt to different kind of paleoenvironments (Fig. 1.6B), ranging from humid coastal plains to upland arid basins, (Sampson and Loewen, 2007; Wick, 2014). Consequently, this carnivorous dinosaur exploited a wide range of prey species. *T. rex* lived as far north as Canada and possibly as far south as Mexico and thereby illustrating its widespread dominance as the apex predator of the Maastrichtian aged habitats on the continent of Laramidia. It has been hypothesized by Loewen et al. (2013) that the full isolation of Laramidia coincided with the origin of the Tyrannosauridae. Much of the initial diversification within this clade might be related to separation of sedimentary basins during transgressions of the Western Interior Seaway. Finally, phases of sea level lowering during the Campanian and Maastrichtian might have resulted in the dispersal of tyrannosaurids into eastern Asia using an ancient 'Bering land bridge', as represented by e.g. the species *Tarbosaurus bataar* (Fig. 1.3), and into vast areas of the Laramidia landmass by *Tyrannosaurus rex* (Loewen et al., 2013).

On the other hand, the phylogeny of Brusatte & Carr (2016) implies no clear division between northern and southern species in Laramidia and hence a frequent interchange that is not so clearly linked to sea level fluctuations. They suggested that *T. rex* may have been an invasive species derived from Asia that immigrated to North America. This may help explain the presence of only one large-bodied tyrannosaurid in the Maastrichtian of North American in contrast to the coeval multi-tyrannosaurid fauna in Asia and the Campanian aged dinosaur faunas of e.g. Alberta and Montana (Brusatte & Carr, 2016). Future tyrannosaurid discoveries may answer this question in more detail.

The largest concentration of *T. rex* skeletons is present in the Williston Basin of eastern Montana, the western parts of the Dakotas and the eastern portion of Wyoming. The associated non-marine rocks are from the Hell Creek Formation or the time-equivalent Lance Formation and were deposited on the margin of the Western Interior Seaway (Archibald et al., 1982). In the next paragraph, the tectono-sedimentary evolution of this specific sedimentary basin is described in detail to understand the underlying processes of the deposition of the dinosaur-bearing rock formations in Montana.

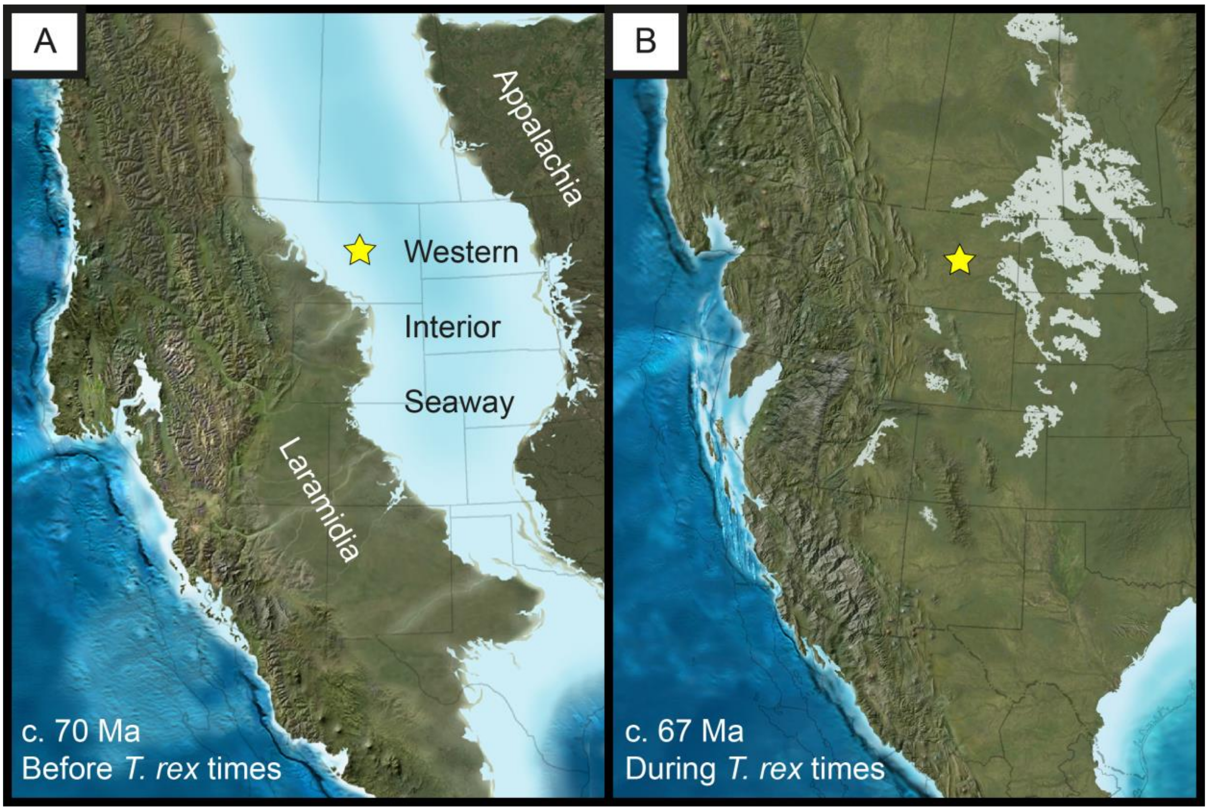


**Fig. 1.5.** Paleogeographical reconstructions of western North America during the Maastrichtian stage. Circa 70 Ma **(A)**, the Western Interior Seaway separated present-day North America in two continents, namely Laramidia in the west and Appalachia in the east. Due to ongoing uplift of the Rocky Mountains in the west and a global eustatic sea level fall, large parts of the Western Interior Seaway were vanished approximately 3 Myr later **(B)**. This regression allowed the growth and lateral migration of broad coastal plains populated by dinosaur species such as *Tyrannosaurus rex* and the deposition of fluvial sediments of the Hell Creek Formation. The yellow asterisk marks the Naturalis *T. rex* location in eastern Montana (from Blakey Paleogeographic maps: https://www2.nau.edu/rcb7/).

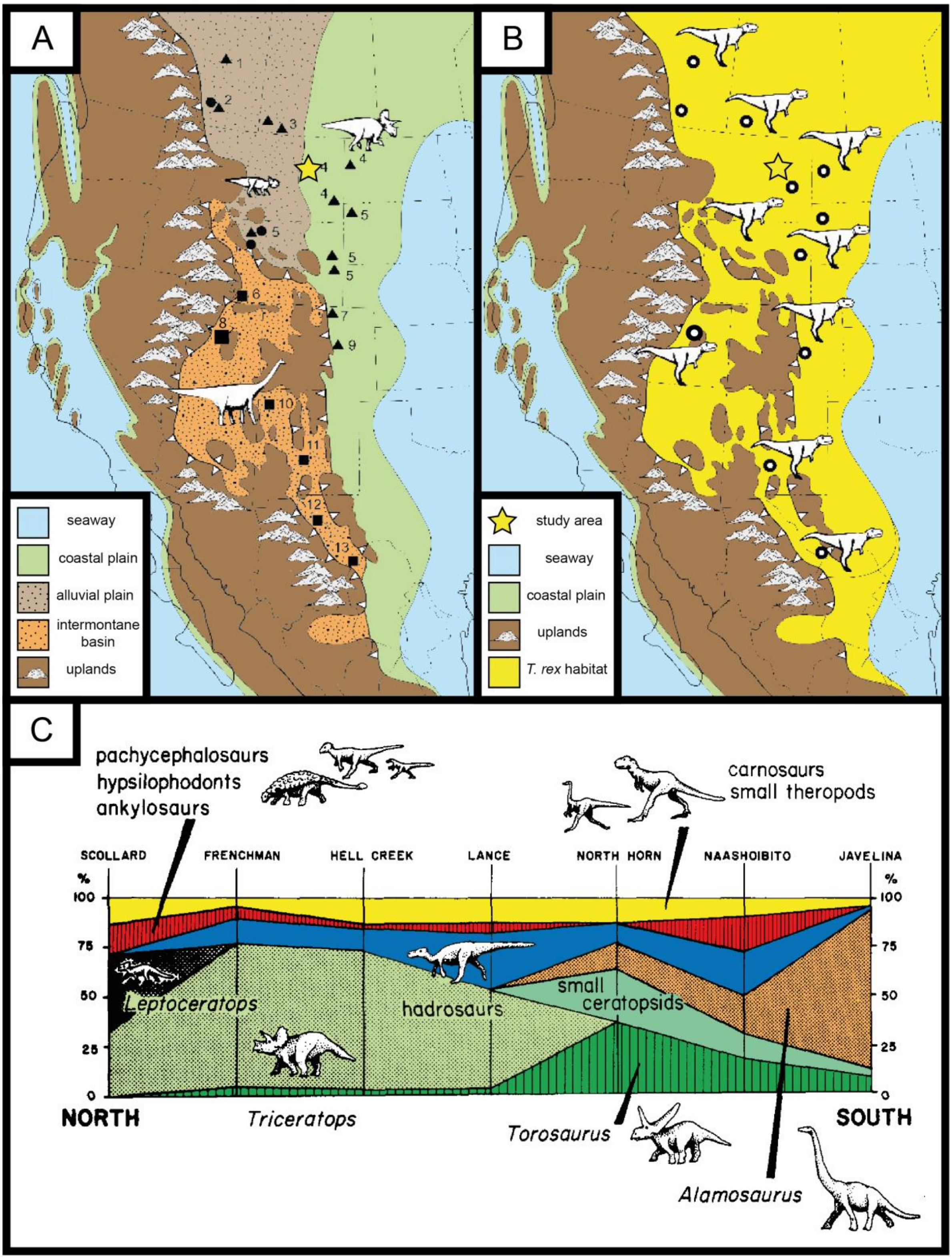
A
seaway
coastal plain
alluvial plain
intermontane basin
uplands
B
study area
seaway
coastal plain
uplands
T. rex habitat
C
pachycephalosaurs
hypsilophodonts
ankylosaurs
carnosaurs
small theropods
SCOLLARD
FRENCHMAN
HELL CREEK
LANCE
NORTH HORN
NAASHOIBITO
JAVELINA
%
100
75
50
25
0
Leptoceratops
hadrosaurs
small ceratopsids
NORTH
SOUTH
Triceratops
Torosaurus
Alamosaurus

**Fig. 1.6.** A reconstruction of Late Maastrichtian paleogeography, paleoenvironments and dinosaur biogeography for the Western Interior of North America (modified from Sampson & Loewen, 2007). Several paleoenvironments are mapped combined with known paleogeographic distribution of three herbivorous dinosaurs **(A).** *Alamosaurus sanjuanensis* occurrences are indicated with a square and this species is restricted to intermontane basins, whereas *Triceratops horridus* (triangles) solely lived on coastal plains and *Leptoceratops gracilis* (circles) on alluvial plains in the north. The numbers mark important fossil sites within specific geologic formations. These formations are indicated as follows: 1 = Scollard, 2 = Willow Creek, 3 = Frenchman, 4 = Hell Creek, 5 = Lance, 6 = Evanston, 7 = Laramie, 8 = North Horn, 9 = Denver, 10 = Kirtland Shale (Naashoibito Member), 11 = McRae, 12 = El Picacho, 13 = Javelina Formation. The known paleogeographic distribution of the theropod dinosaur *Tyrannosaurus rex* is displayed in **(B).** A schematic north-south profile **(C)** across western North America from Alberta towards Texas shows the latitudinal variation in the composition of Late Maastrichtian dinosaur megafaunas (modified from Lehman, 1987). Striking in these three figures is the large-scale distribution of *Tyrannosaurus rex* over the entire N-S extent of the Western Interior in contrast to the restricted habitats of the herbivorous dinosaurs *Leptoceratops*, *Triceratops* and *Alamosaurus*. The Naturalis *T. rex* locality is marked with a yellow asterisk.

## 1.2. Williston Basin

The Williston Basin (Fig 1.7) is a relatively large (c. 770.000 km$^2$), roughly circular, intracratonic, sedimentary basin situated in the Northern Great Plains of USA and Canada. It encompasses portions of the states of Montana, South Dakota, North Dakota and the adjacent Canadian Provinces of Manitoba and Saskatchewan. The basin is part of the North American craton and contains a relatively complete Late Cambrian through Tertiary sedimentary rock sequence that is characterized by six major stratigraphic sequences. The total thickness in the basin center is approximately 4900 m, but this thickness decreases to less than 3000 m in eastern Montana and to less than 1500 m along the basin margin (Pollastro et al. 2013; Peterson and MacCary, 1987). The stratigraphy and structure of the Williston basin is extensively studied due to its high petroleum potential. Since the first oil discoveries in the early 1950s, more than 20.000 exploratory boreholes have been drilled for oil and gas production (Kent & Christopher, 2008). The distribution and thickness of the Phanerozoic sediments in the Williston Basin is the result of a complex interplay between recurrent movement of Precambrian blocks as horsts, grabens or half-grabens, the influence of eustatic changes in sea level and the quantity and quality of available sediments (Anna et al., 2013). In this paragraph, a general description is given about the formation of the Williston Basin during the Paleozoic, its complex Mesozoic history of deposition and Sevier and Laramidian deformation and finally a brief discussion is provided concerning the Tertiary and Quaternary phase of widespread erosion in the area.

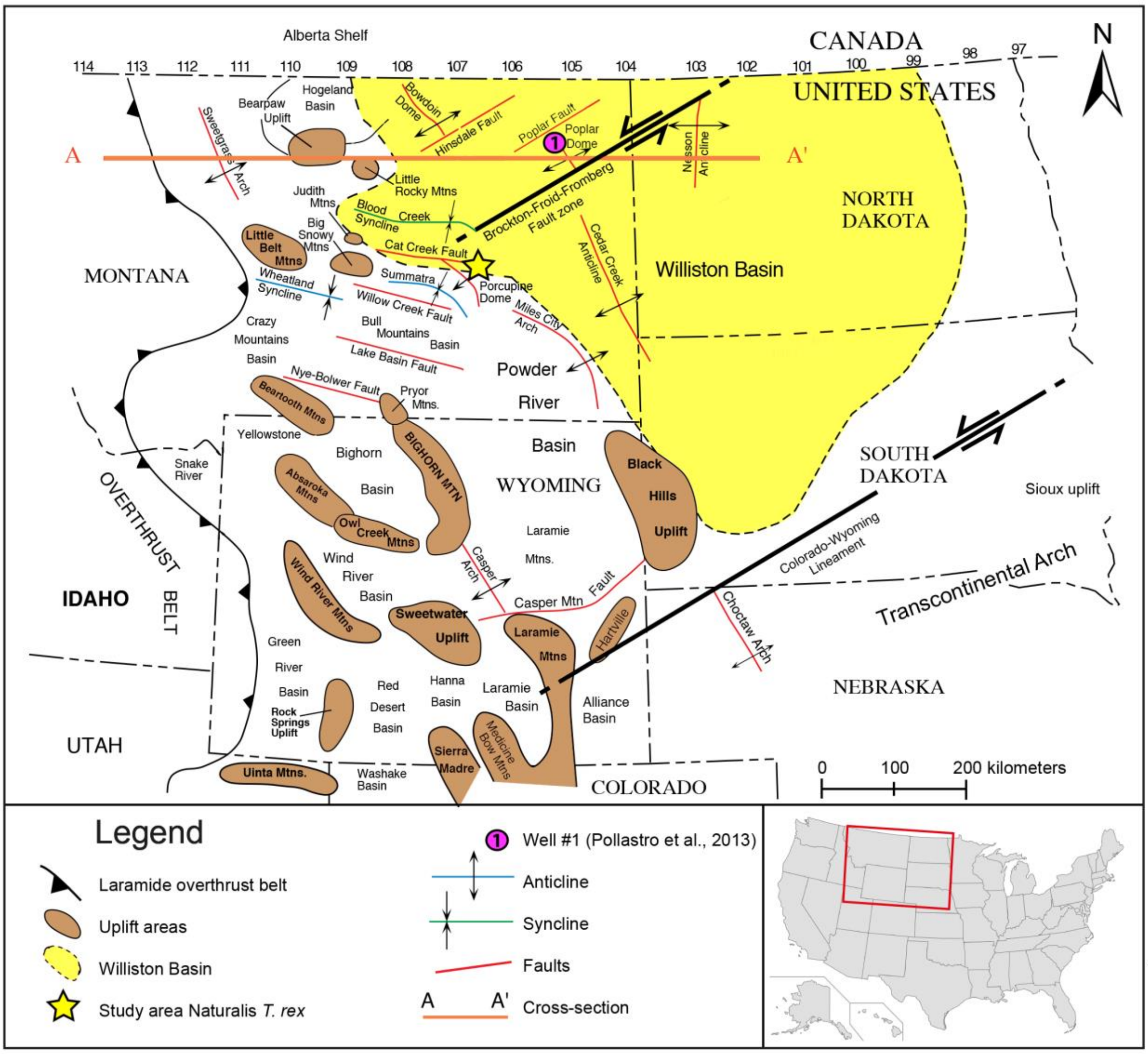

**Fig. 1.7.** Structural geological map of the US portion of the Williston Basin and surrounding areas showing present-day prominent structures in the subsurface. Inset shows the location on a map of the USA. The formation of the Williston Basin is thought to be linked to the Archean SW-NE striking, sinistral Brockton-Froid-Fromberg and Colorado-Wyoming Fault zone. The regional structural cross section A-A' is indicated on the structural map and represents Fig. 1.8. The purple well near the Poplar Dome corresponds to the location of the burial history curve of Pollastro et al. (2013), displayed in Fig. 1.9. The study area of the Naturalis *T. rex* is shown with the asterisk and is situated at the western boundary of the Williston Basin in the Central Montana Uplift region. The study area is dominated by the large-scale Blood Creek Syncline in the N, the Cat Creek Anticline in the W and the Porcupine Dome Uplift in the S. This structural geological map is modified from Peterson & MacCary (1987) and Pollastro et al. (2013).

### 1.2.1. Paleozoic history

The Williston Basin formed in the Late Ordovician (c. 495 Ma) with the creation of a large depressed tectonic block caused by strike-slip movement of two SW-NE oriented Archean sinistral shear systems, the Bronton-Froid-Fromberg fault zone and Colorado-Wyoming lineament (Gerhard et al., 1987). The Williston basin is known as a classic example of an intracratonic sag basin, because it was formed by strike slip movement, it did not show evidence of intense rifting, it has a rather circular shape and have shown multiple histories of subsidence (Coleman & Cahan, 2012).

A structural geological map of the US portion of the Williston Basin and surrounding areas reveals its extent and its deformational history (Fig. 1.7) The Williston basin is bordered to the west and south(west) by Laramide or rejuvenated Laramide structures including the Black Hills uplift, Miles City Arch, Porcupine Dome and Bowdoin Dome. To the north, the basin is bordered by the Bow Island Arch of the Alberta Shelf and the Canadian shield (not shown in Fig. 1.7), whereas the (south)eastern boundary is characterized by the Precambrian Transcontinental Arch and Sioux uplift (Anna et al., 2013). Other prominent structural features in the subsurface are the N-S-trending Nesson anticline and NW-trending Cedar Creek anticline, which have produced large volumes of oil and natural gas from several stratigraphic units.

Although the stratigraphic rock record in the Williston Basin is unusually complete in comparison with other basins (Fig. 1.8), episodic subsidence and erosional events have occurred throughout the history of the basin. This pattern is mainly steered by transgressive- and regressive cycles that caused episodes of basin filling and basin draining accompanied by repeated deposition of carbonates and clastics and subsequent erosion during sea level lowering. The Paleozoic strata of the Williston Basin consists mainly of marine carbonates, whereas the Mesozoic and Cenozoic sequence is dominated by marine and non-marine clastic rocks. Six complete transgressive-regressive cycles across a craton have been identified in the region from the Cambrian to the present (Fig. 1.9) and the associated sedimentary records, bounded by major unconformities, are in chronologic order known as the Sauk, Tippecanoe, Kaskaskia, Absaroka, Zuni and Tejas major sequences (Sloss, 1963).

During the Phanerozoic, water depths in the Williston basin were relatively shallow and hence a small change in paleowater depth caused substantial changes in sedimentation and depositional environment (Anna et al., 2013). Understanding these sedimentary dynamics is important, because, for example, during the Kaskaskia transgressive sequence the deposition of the oil-rich Bakken Formation took place (Anna et al., 2013). This succession represents the largest oil resource in the Williston basin and is a thin but widespread Upper Devonian to Lower Carboniferous sequence of highly organic-rich (and sealing) shales and sandstones that forms an ideal petroleum source, reservoir and seal rock (Pollastro et al., 2013).

In this thesis, the focus is on the Upper Cretaceous infill of the Williston Basin associated with the Zuni major sequence. Hence, a detailed sedimentary history of the Paleozoic, Triassic and Jurassic strata of the Williston Basin is not given here, but an overview can be found in Gerhard et al. (1990) and Peterson & MacCary (1987).

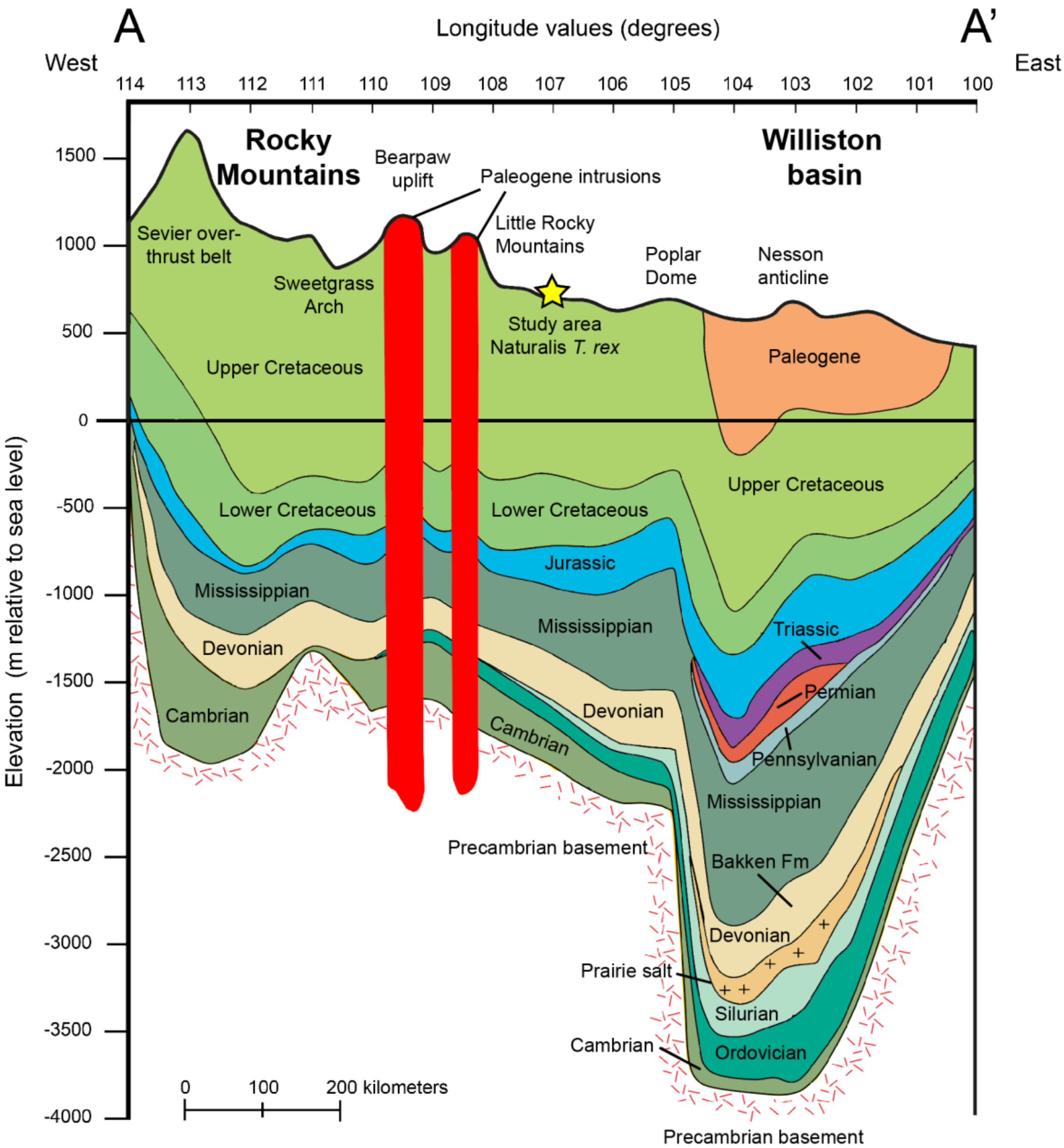


**Fig 1.8.** Generalized, large-scale W-E structural cross-section running from the Rocky Mountains in western Montana to the eastern edge of the Williston Basin in central North Dakota. It schematically shows the major structures, intrusions and stratigraphic units in the subsurface (modified from Shurr & Monson, 1995; Peterson & MacCary, 1987). The location of this regional cross-section A-A' is shown on the structural geological map of Fig 1.7. An approximately 4900 m thick Phanerozoic rock sequence was deposited in the Williston Basin with generally carbonate deposition in the Paleozoic and siliciclastic deposition in the Mesozoic and Cenozoic. The Naturalis *T. rex* site is located on the western margin of the Williston Basin.

### 1.2.2. Mesozoic history

The Mesozoic infill of the Williston Basin is dominated by the Zuni major sequence (Fig. 1.9). The Zuni comprises Jurassic and Cretaceous strata that is dominated by sandstone, siltstone and shale and minor carbonate and salt. There are three unconformities present in this interval; between the Upper Jurassic and Lower Cretaceous, between the Lower and Upper Cretaceous and in the Paleocene. Near the end of the Jurassic a transition from marine towards continental conditions occurred as represented by the dinosaur-bearing Morrison Formation, deposited between 155 and 148 Ma as a mosaic of riverine, lacustrine and floodplain environments developed on a vast alluvial plain nourished by debris from the ancestral Rocky Mountains (Dodson et al., 1980; Kowallis et al., 1998).

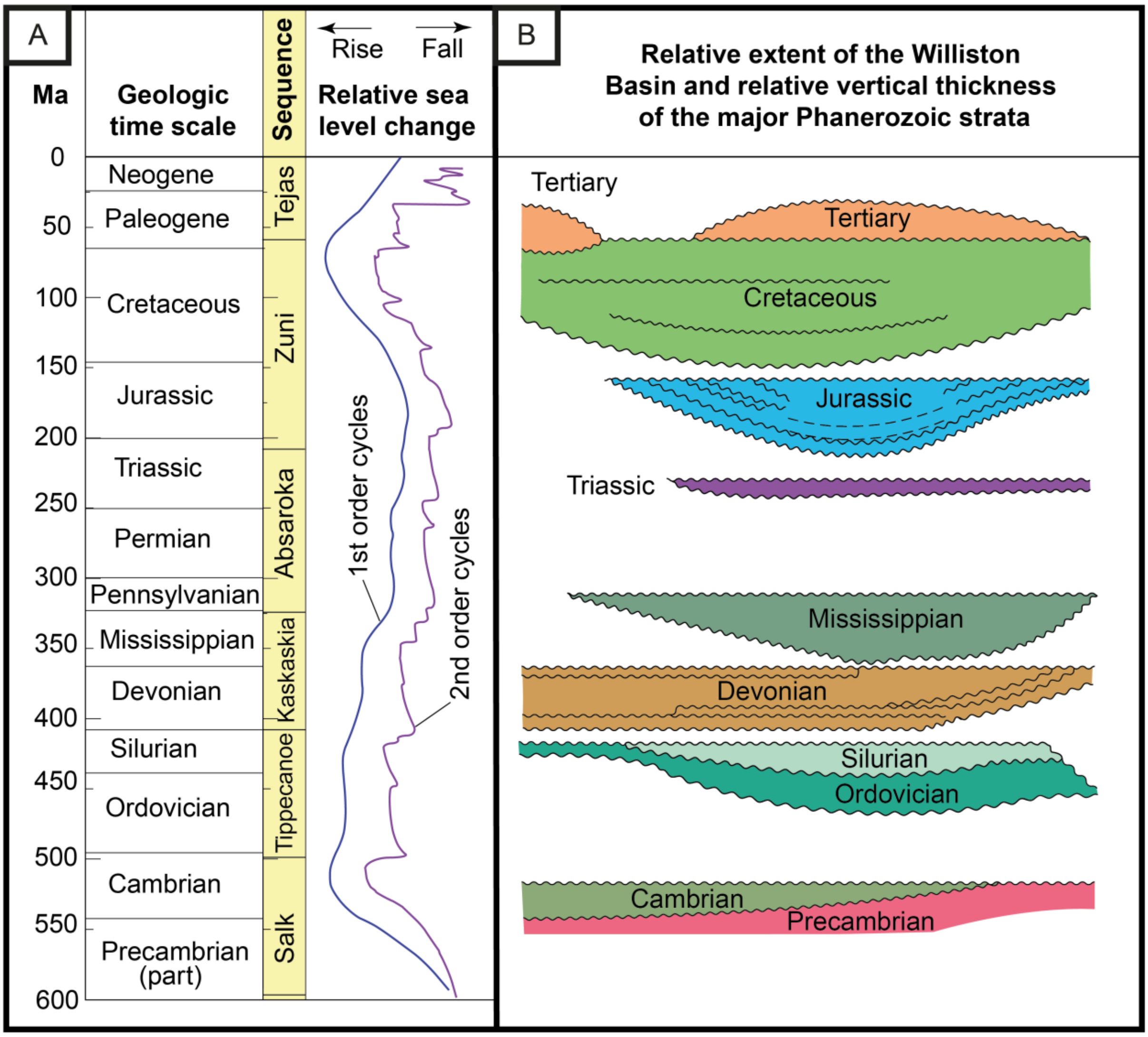


**Fig. 1.9.** Schematic diagram showing the six major stratigraphic sequences in the Williston Basin of Sloss (1963) and the first- and second order sea level curves from Vail et al. (1977) relative to the geologic time scale **(A)** (Gradstein et al., 2012). Schematic diagram showing the major slices of Phanerozoic strata in the Williston Basin which are bounded by unconformities **(B)**. The individual slices illustrate the relative horizontal extent and shape of the basin and shows also the effects of basin margin erosion. The approximate position of these slices relative to the six major sea level sequences of A is indicated, but this is not to scale, because the vertical axis shows relative thickness of the rocks that were deposited and does not resemble time (modified from Anna et al., 2013; Kent & Christopher, 2008).

The Cretaceous history in the Williston Basin is dominated by the presence of the epicontinental Western Interior Seaway (Fig 1.5) and tectonic activity caused by the Sevier and Laramide Orogeny. The rather complete Cretaceous beds in the Williston basin are c. 1400 m thick and are the result of a nearly continuous marine deposition for much of the Cretaceous Period. Berriasian to Barremian rocks are absent in the Williston Basin, due to a period of non-deposition and erosion which started in the Upper Jurassic (Condon, 2000). During the Aptian, the Williston Basin merged with a much larger, elongated basin known as the Western Interior Basin (Kauffmann, 1984). This classical example of a retro-arc foreland basin was formed due to the shallow subduction of the oceanic Farallon Plate beneath the continental North American Plate during the Sevier Orogeny (c. 140 Ma to 50 Ma). This convergent movement caused crustal thickening and created the Cordilleran fold- and thrust belt associated with numerous intrusive bodies and volcanic activity. The orogenic loading and subsequent lithospheric flexure resulted in the formation of a N-S elongated foreland basin between the fold-and thrust system in the west and a stable, broad cratonic platform in the east (DeCelles, 2004).

The Western Interior Basin was asymmetric with a steep sloping foredeep area in the west and a shallow, gentle sloping forebulge zone in the east. The ongoing tectonic loading and flexural response caused a variable void in accommodation space in the foreland basin. This acquired space was filled by transported erosional material from the topographic load, resulting in a continuous layered stratigraphy that wedged away from the mountain belt. The relatively continuous subsidence and filling of the thus created accommodation space combined with the longevity of the depositional basin allowed for the deposition of the thick and rather complete sequence of Cretaceous rocks (Fowler & Nisbet, 1985).

The interplay between worldwide fluctuations in sea-level (Haq et al., 1987) and tectonic activity (and associated regional sea level changes) mainly controlled the Cretaceous rock record in western North-America. From the Aptian onwards, the Western Interior foreland basin was able to accommodate a large inland sea known as the Western Interior Seaway. The first floodings occurred from the north, but a minor southern arm intruded slowly into the basin, meeting the northern tongue in Late Albian time in Colorado. At its peak sea level stand during the Turonian, the Western Interior Seaway was approximately 750 m deep, 4800 km long, 1600 km wide and extended from Arctic Canada and Alaska in the north to the Gulf of Mexico in the south and with probable intermittent connections to the Hudson's Bay region (Kauffman, 1984).

Condon (2000) identified five rock formations in the Early Cretaceous and thirteen in the Late Cretaceous of the Williston Basin in eastern Montana. Their sedimentary patterns were controlled by the numerous expansions and contractions of the Western Interior Seaway (Haq, 2014), as part of the Zuni major sequence. From the Santonian onwards, subsidence and sedimentation patterns changed in the Western Interior Basin in response to shallowing subduction angles and subduction of a thick oceanic slab as part of the Laramide Orogeny (c. 80 – 55 Ma). The subducted Farallon Plate eventually caused regional uplift, partitioning of the Western Interior Basin into Laramide uplifts and basins and withdrawal of the Western Interior Seaway (Blakey, 2004; DeCelles, 2004). Concerning the Williston Basin, the Laramide orogeny rejuvenated several pre-existing Precambrian basement faults to create regional basement-cored uplifts (e.g. the Black Hills, Miles City Arch, Porcupine Dome and Bowdoin Dome) and anticlines that serve as present-day oil traps (e.g. the Nesson and Cedar Creek Anticline) (Peterson & MacCary, 1987).

Marine sedimentation in the Williston Basin continued in the form of the Montana Group, overlying the Colorado Group, with the Late Santonian to Early Campanian Telegraph Creek and Eagle Sandstone Formations as basal units, comprising black shales, limestone concretions and calcareous, carbonaceous and silty sandstones. These two formations thin and pinch out eastward into the Gammon Shale, which contains noncalcareous shales, iron concretions and bentonite (weathered volcanic ash) beds (Condon, 2000). The overlying marine shales of the Claggett Shale of Middle Campanian age were the culmination of the first transgression within in the Montana Group. This sequence was followed by a regression and deposition of the non-marine, dinosaur-bearing Judith River and time-equivalent Late Campanian Two Medicine Formation.

A final large-scale transgression occurred at the end of the Campanian leading to the deposition of the fossiliferous, marine shales of the Bearpaw incursion. The Bearpaw Shale grades eastward into the Pierre Shale in areas where the underlying Judith River Formation is absent (Condon, 2000). The conformably overlying Early Maastrichtian Fox Hills Sandstone represents a thin, but widespread, regressive shoreface sandstone sequence and marks the top of the Montana Group. Finally, the Hell Creek Formation is the uppermost Cretaceous unit in the Williston Basin and is defined as a mostly non-marine succession of fluvial calcareous sandstones and floodplain/lacustrine silt- to mudstones. Like the Judith River Formation, the Hell Creek Formation is famous for its abundant fossil vertebrate fauna and it is interpreted as an eastern-prograding wedge composed of erosional materials shed from the Rocky Mountains in the west (Fastovsky & Bercovici, 2016). Eroded remnants along and near the Missouri River suggests the Hell Creek beds were once widespread over all of eastern Montana and large parts of North and South Dakota (McGookey et al., 1972).

### 1.2.3. Cenozoic history

The deposition of the Upper Maastrichtian Hell Creek Formation continued rather conformably into the Paleocene with the fluvial, swamp and lacustrine sediments of the Tullock Member of the Fort Union Formation (Fig. 1.12), which comprises extensive deposits of lignite and coal in the Williston Basin and marks also the end of the Zuni major sequence. In the lower Fort Union Formation, restricted to the east-central part of the basin, is a shallow marine rock unit present. This unit is known as the Cannonball Formation and represents the start of the Tejas major sequence and the final flooding of central North America at around 60 Ma, but this epeiric sea extent was less dramatic than during most of the Cretaceous Period. The rapid retreat of the Cannonball Sea during the Late Paleocene caused a regressive sequence including the Slope, Bullion Creek, Sentinel Butte and Golden Valley Formations in North Dakota and the Lebo Member of the upper Fort Union Formation in eastern Montana (Cherven & Jacob, 1985). Uplift from the Eocene onwards caused some alkalic, magmatic intrusions near the western edge of the Williston Basin and a long period of erosion and non-deposition (Wilson & Kyser, 1988).

The present-day landscape of the Northern Great Plains is primarily the work of two major forces that were operative during post-Cretaceous time. Firstly, a gentle but intermittent uplift was present that probably began in the late Eocene and may be still continuing into recent time (Jensen & Varnes, 1964). Secondly, successive invasions and retreats of Plio-Pleistocene ice sheets caused intense erosion in the area. The largely unconsolidated deposits that resulted from these events show a discontinuous distribution, uneven thickness and varied composition. The preglacial sediments in the western Williston Basin are part of a widespread group of Tertiary and Quaternary gravelly deposits laid down by rivers flowing east and northeast from the Rocky Mountains. Because of little lithological differences and scarcity of identifiable and dateable fossils, it is complicated to differentiate these gravel deposits. Two major preglacial units have been identified, namely the Late Miocene to Early Pliocene Flaxville Formation and the Early to Late Pleistocene Wiota gravels.

Climate models indicate that at least 25 major glacial episodes have occurred during the past 3.2 million years (e.g. Paillard, 1998). Continental icesheets probably advanced into the Williston Basin region during most, if not all, of those glacial periods. Moreover, the Rocky Mountains were probably covered with alpine icecaps during each of the glacial episodes. Meltwater from these alpine icecaps frequently crossed the Williston Basin only to be diverted along the margins of the continental ice sheets (Clausen, 1987). In Figure 1.11 the approximate maximum southern limit of the Laurentide ice sheet is indicated (Fulerton et al., 2004). A lack of continuous deposits in Montana and North Dakota hampers a clear distinction between e.g. the Illinoian (c. 191 – 130 ka) and Wisconsin (85 – 11 ka) glaciations (Soller, 2001). The study area of the Naturalis *T. rex* is located within close proximity of the margin of the (probably Illinoian) paleo-icesheet and must have been under repetitively periglacial influence during its Pleistocene history. The Pleistocene glacial deposits in the western Williston Basin consists of ground moraines dominated by glacial till and isolated erratics, fluviolacustrine sediments that were laid down on tongues of stagnant ice in the old Missouri River valley, glacial outwash (sandur) deposits of sandy gravel, and discontinuous terrace remnants (Jensen & Varnes, 1964). Finally, since the retreat of the last continental ice-sheet during the Holocene, rivers in the Williston Basin region have laid in their valleys extensive unconsolidated deposits of clay, silt, sand and fine gravel.

Besides deposition, intense erosion took place in the northern Great Plains during the Quaternary resulting in a progressive lowering of the landscape. Evidence for this deep erosion includes an erosional surface cutting across numerous stratigraphic units, a system of major escarpments, erosional remnants of previous topographic surfaces, and high-level drainage divides covered with alluvial sediments. Glacial erosion, aided by huge volumes of meltwater, probably scoured out systems of extremely wide and shallow glacial troughs in the Williston Basin region (Clausen, 1987). These valleys were cut in the easily-eroded claystone bedrock of for example the regional Bearpaw, Hell Creek and Fort Union Formations. The amount of erosion that have occurred in eastern Montana since the deposition of the Upper Cretaceous Hell Creek Formation is difficult to assess. However, with burial history diagrams it might be possible to estimate the Cenozoic erosion and hence quantify the total thickness of the sediments that should have lain above the Naturalis *T. rex* specimen. This is important to know in light of the taphonomic, sedimentologic and geochemical study to explain the unique preservation of this specimen, which will be discussed in more detail later on in this thesis.

The U.S. Geological Survey performed a recent geologic assessment in the US portion of the Williston Basin of technically recoverable shale oil in the Devonian and Lower Carboniferous Bakken Formation. A primary requirement for a continuous shale-oil accumulation is that the source rock and the associated reservoir rock was at sometime in its burial history within the thermal oil-generation window. Pollastro et al. (2013) measured the hydrogen index (amount of hydrocarbons generated relative to the total organic content in the rocks) and calculated the transformation index (the percentage of hydrocarbons expelled) for the Bakken Formation with respect to burial depth, time and temperature. They combined it with a one-dimensional modeling of burial history and thermal maturity using the methods of Roberts et al. (2008), which is shown in Fig. 1.10. They estimated a high heat flow of 95 mW/m$^2$ and found out that the oil generation of the Bakken Formation in the Poplar Dome area of the western part of the Williston Basin have reached peak generation. In addition, the amount of erosion at the well location was estimated at 2400 ft (c. 730 m).

Although the well of Fig. 1.10 is the closest known well location to the Naturalis *T. rex* site where burial history and erosion is modelled, a direct comparison between the two sites, that are c. 180 km apart, is difficult. Well #1 of Pollastro et al. (2013) is located in the Poplar Dome area which shows a complex anticlinal structure in the subsurface, is situated closer to the basin depocenter and was once covered by the Laurentide icesheet in contrast to the *T. rex* site that was located near the paleo-icesheet margin. In conclusion, the Naturalis *T. rex* locality most probably experienced less erosion than the Poplar Dome well, so a maximum of 730 m removed overburden can be established.

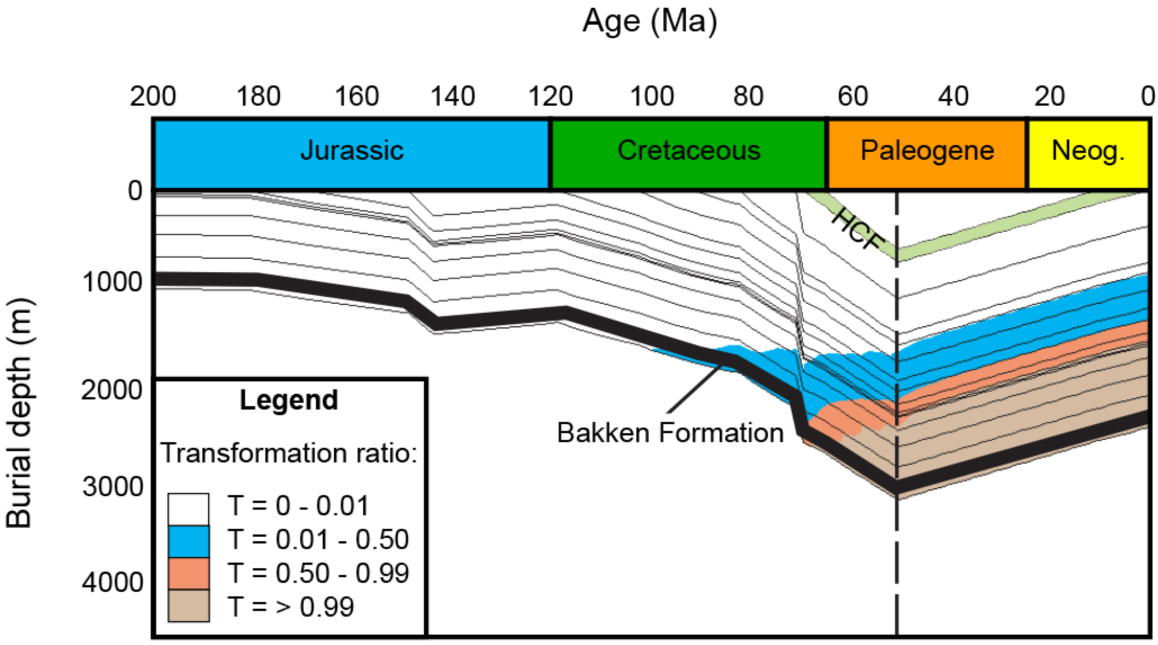


**Fig 1.10.** A generalized burial history curve at well location #1 in the high-maturity area of Poplar Dome in eastern Montana (modified from Pollastro et al., 2013), see the location of this well in Fig. 1.7. Colors represent calculated transformation ratios with respect to burial depth, time and temperature. The timing of the start, peak and end of oil generation (transformation ratios of 0.01, 0.50 and 0.99, respectively) shows that the oil generation of the Bakken Formation (thick bold line) at this particular location has gone to completion. Dashed line indicate maximum burial at about 50 Ma (Eocene) and the erosion was estimated at 2400 ft (c. 730 m). The burial and exposure history of the Hell Creek Formation (HCF) is indicated with a light-green band.

## 1.3. Hell Creek Formation

The Naturalis *Tyrannosaurus rex* specimen was discovered in rocks of the Upper Cretaceous Hell Creek Formation (HCF) in eastern Montana, USA. In this paragraph, a detailed description of the formation is given concerning geographic distribution, topographic expression, lithology, lower and upper stratigraphic boundary, age and duration, and its diverse flora and fauna.

### 1.3.1. Introduction

Barnum Brown was the first person to describe the Hell Creek beds and named the formation after the typical exposures in the valley of the Hell Creek and nearby tributaries of the Missouri River, north of Jordan, Garfield County, eastern Montana (Brown, 1907). He not only gave this uppermost Cretaceous dinosaur-bearing formation its classical name, but also collected many important fossil mollusks, plants and vertebrates (including *Tyrannosaurus. rex*) and set the foundation for understanding the transition between the end of the Mesozoic Era and the beginning of the mammal-dominated Cenozoic Era (Norell & Dingus, 2010).

During the rest of the 20th century, the interest in the Hell Creek area in eastern Montana was largely driven by the construction of the Fort Peck Dam and Reservoir and the search for oil, natural gas, coal and fossils (Clemens & Hartman, 2014). Since the 1980's the HCF became the focal point for many paleontologists and geologists to study the most complete terrestrially based fossil record of faunal and floral changes at the Cretaceous-Tertiary extinction event. Upon today, the interest in the HCF is still enormous given by the fact that recently two large special issues from the Geological Society of America (GSA) with state-of-the-art research were published (Hartman et al., 2002; Wilson et al., 2014).

The 2002 GSA Special Issue focused mainly on the previously rather unknown Hell Creek exposures in western North- and South Dakota, whereas the 2014 GSA Special Issue was dedicated to the results of the Hell Creek Project (1999-2010): a collaborative, multi-institutional field program initiated by Jack Horner of the Museum of the Rockies. The goal of this project was to amass a huge, new collection of fossil remains (plant, invertebrate, invertebrate, lower vertebrate, mammal and dinosaur specimens) from the HCF of eastern Montana, all of which would have precise geologic, stratigraphic and geographic data (Horner, 2014). The focus area was the type locality of the HCF, namely Hell Creek State Park on the southern shores of Fort Peck Reservoir in Garfield County (Fig. 1.11 and 1.15). The new achieved large collection of various Hell Creek fossils provided refined insights in changes of the relative abundance, diversity, ontogeny and biogeography in diverse biota (including dinosaurs) within the entire HCF and across the Cretaceous-Paleogene boundary.

### 1.3.2. Outcrop area and morphology

The geographic distribution of HCF exposures is concentrated around the Williston Basin in the states of Montana, North Dakota and South Dakota (Fig. 1.11). Time-equivalent (Upper Maastrichtian) dinosaur-bearing formations are known as the Scollard Formation in Alberta (Canada), the Frenchman Formation in Saskatchewan (Canada), the Lance Formation in Wyoming, the North Horn Formation in Utah, the McRae and Ojo Alamo Formation (with Naashoibito member) in New Mexico and the Javelina Formation in Texas (Fig 1.6C; Lehman, 1987).

Large-scale Quaternary erosion and the modern-day arid, continental climate in the Great Plains have created the typical rough Hell Creek 'badlands'-landscape of 'creeks' and 'buttes' (Fig. 1.12). The Hell Creek area is susceptible for intense natural erosion. Rainfall and freeze and thaw-cycles causes removal of the soft topsoil, exposing of fossils and washing of bone fragments down the steep slopes. The topographic expression of the HCF is hence directly linked to differential weathering of its lithology that consists mainly of interbedded soft mudstone and more solid sandstone beds. In general, the fine-grained intervals of the formation are poorly exposed and covered with modern prairie-vegetation such as sagebrush, grasses, cactuses and cottonwood. In outcrop, they form distinctive 'badlands' that typically exhibit the 'dirty popcorn' weathering texture characteristic of sediments rich in montmorillonite (Connor, 1992), a bentonitic clay that forms from weathering of volcanic ash. The organic rich layers of the HCF normally correspond with a slope break, because they weather out to gentle reentrants on steep hills. The badland surfaces are commonly protected by overlying resistant, compact, sheet-like sandstone units that form typical flat-topped mesas or buttes. Isolated dome-shaped hills and round-topped ridges stand as remnants of argillaceous sediments whose protective sandstone covers have been removed by recent erosion (Rigby and Rigby, 1990). Sandy intervals of the HCF that are less compacted and cemented show steep, fluted slopes where the sandstones 'simply melt away before a driving rain, like sugar' (Brown, 1907).

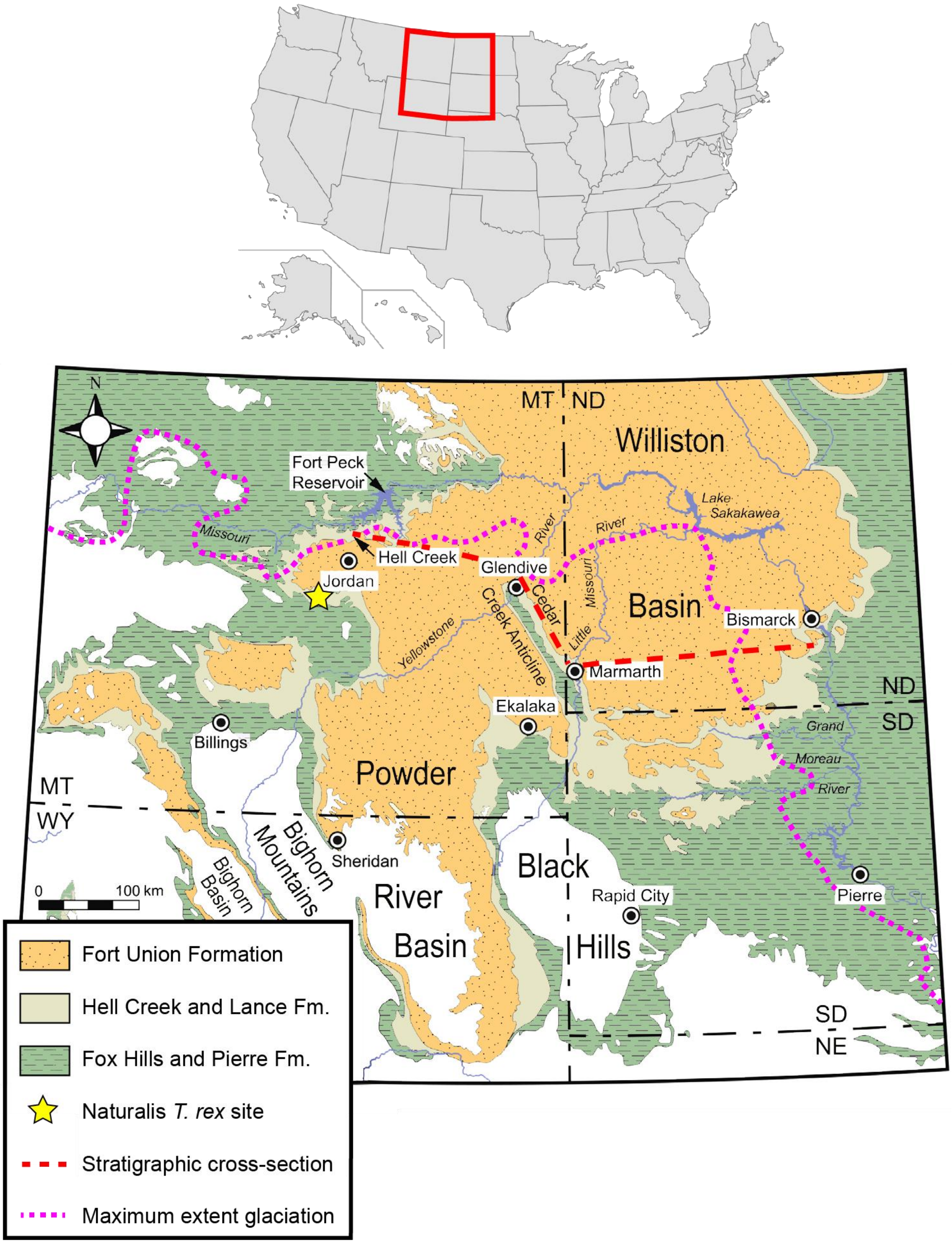

**Fig. 1.11.** Geological map of the Williston Basin and Powder River Basin in Montana (MT), Wyoming (WY), North Dakota (ND) and South Dakota (SD) indicating the exposures of Upper Cretaceous (in green) and Paleocene (in orange) rock formations. The approximate maximum extent of the Laurentide continental icesheet during the Pleistocene epoch is indicated with a magenta stippled line (derived from Fulerton et al., 2004; Soller, 2001). A stratigraphic W-E cross section (Fig. 1.13 and 1.16) is highlighted with a red dashed line and the excavation site of the Naturalis *T. rex* within the HCF is marked with a yellow asterisk (modified from Fastovsky & Bercovici, 2016; Johnson et al., 2002).

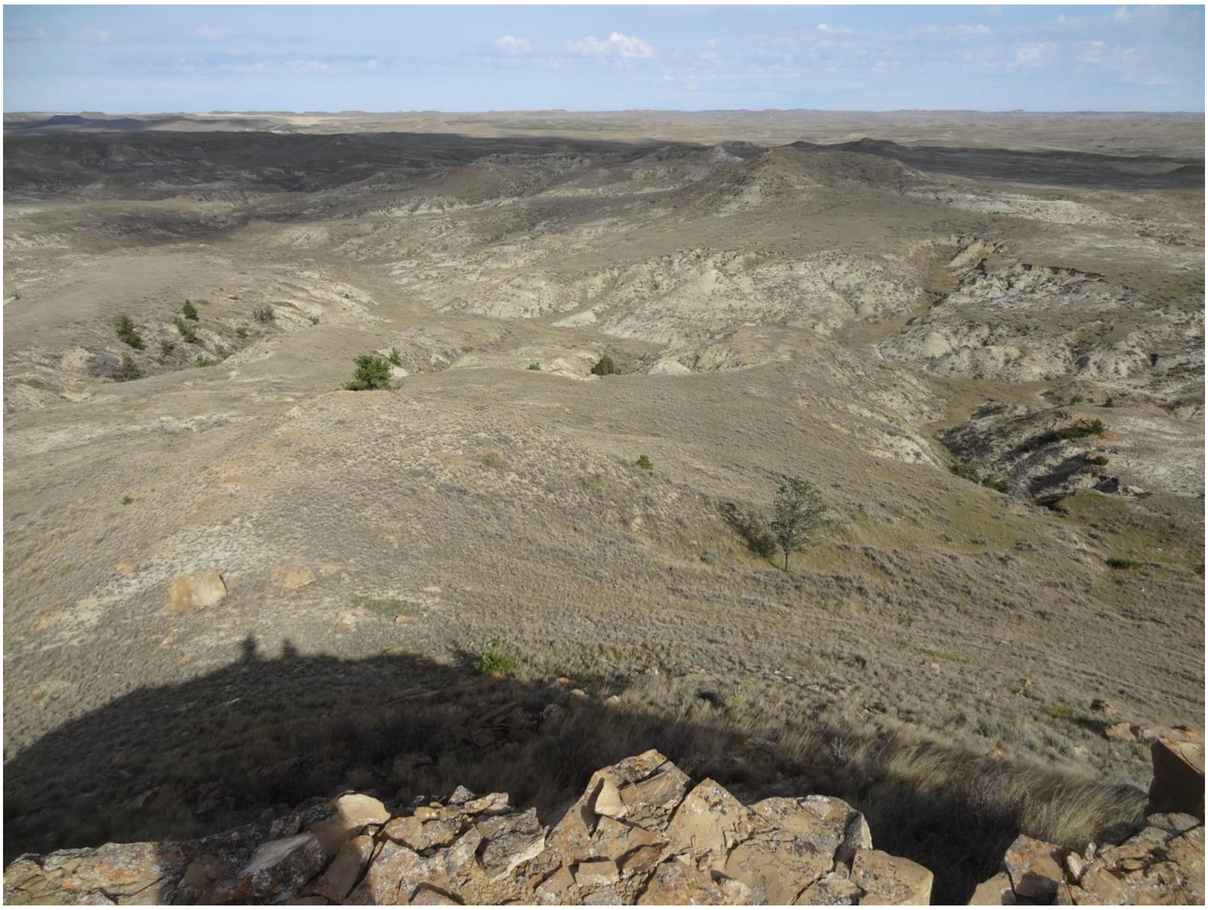

**Fig. 1.12.** Characteristic 'badlands' of the HCF in the study area of the Naturalis *T. rex* in eastern Montana showing 'creeks' incising in poorly exposed mudstone intervals and 'buttes' with flat-topped sandstones.

### 1.3.3. Lithology, thickness and lithostratigraphy

The HCF is a c. 100 m thick siliciclastic succession in the Williston Basin that consists predominantly of an alternation between soft claystone and shale (carbonaceous in part), siltstone and fine-to medium-grained sandstones. Often the more generalized term 'mudstone' is used to describe the fine-grained intervals of the HCF, which can essentially mean both claystone or siltstone depending on the grain-size range. Some of the carbonaceous shales in the upper part of the HCF can evolve into lignitic beds or lignites, although these coals are in general rare and discontinuous (Brown, 1907; Jensen & Varnes, 1964; Rigby & Rigby, 1990). In early literature the HCF was described as the 'somber beds' because of the contrast of the pale, olive gray and brown mudstone beds of the formation with the distinctly yellowish white, tan and buff colored underlying sandstones of the Fox Hills Formation (FHF) and the lighter, 'zebra-striped' yellowish gray strata of the overlying Tullock Member of the Fort Union Formation (FUF) (Brown, 1907).

The fluvially derived deposits of the HCF are by nature highly lenticular and cross cut each other in ways that inhibit high-precision lateral correlation and complicates accurate formational thickness determinations (Fastovsky & Dott, 1986). Furthermore, the HCF is little tectonically influenced, therefore mostly horizontal in the (sub)surface and usually thicker than the incision depth into the topographic relief (Johnson et al., 2002). For these reasons, the complete thickness of the HCF is mostly estimated and has only been measured at a few locations. Estimates in Montana have varied from c. 170 m in Garfield County (Brown, 1907) to 41 m (Collier and Knechtel, 1939) and 51-85 m in McCone County (Rigby and Rigby, 1990) whereas recent HCF measurements in North Dakota shows a thinning from c. 100 m in the SW to c. 70 m in the central part of the state (Murphy et al., 2002) (Fig. 1.13).

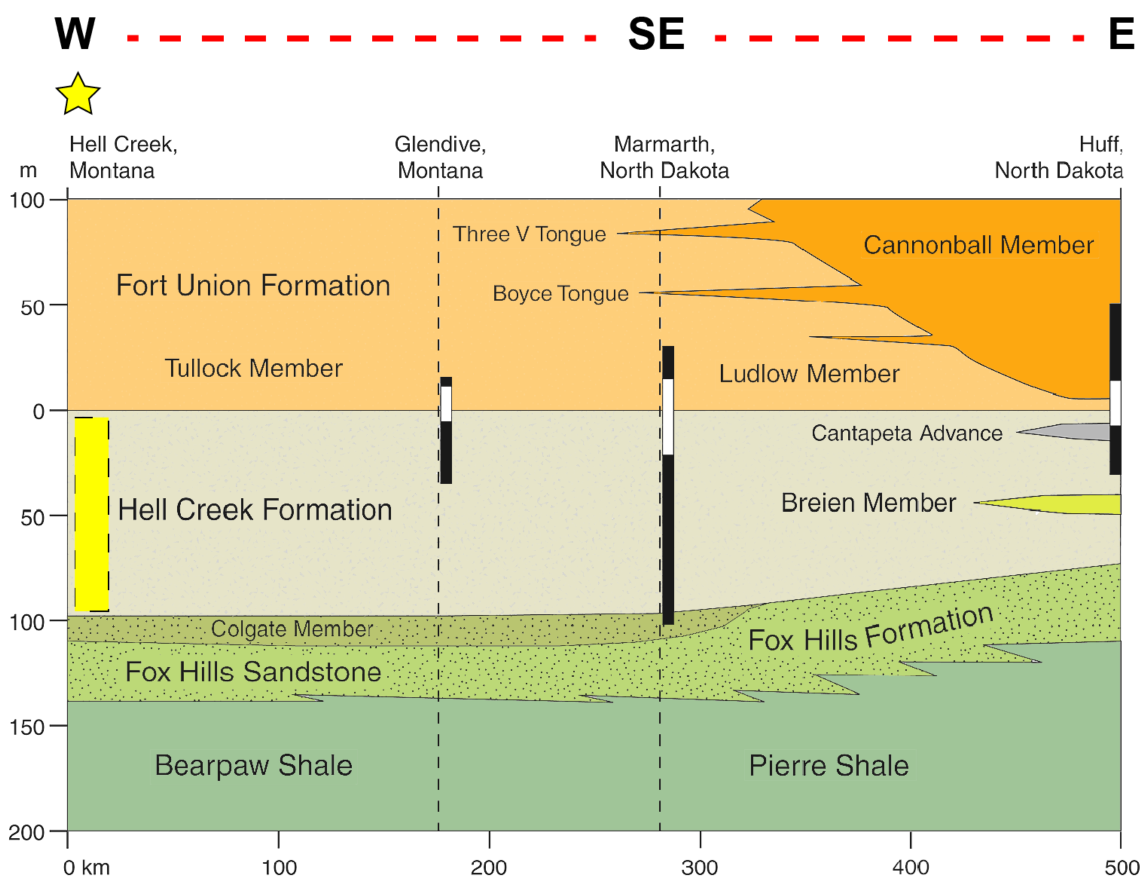


**Fig. 1.13.** Schematic stratigraphic cross-section running west to east from Hell Creek to Glendive in Montana towards Marmarth and Huff in North Dakota (see Fig. 1.11 for the map view of this cross section). The thickness of the HCF and adjacent strata is shown as well as paleomagnetic measurements at different sections (modified from Hicks et al., 2002; Johnson et al., 2002; Lund et al., 2002). The extent of the yellow rectangle is indicating one of the objectives of this study, namely the question at which lithostratigraphic and thus chronostratigraphic position within the HCF we can place the Naturalis *T. rex*.

Brown (1907) defined the HCF as fossiliferous continental freshwater deposits overlying the brackish to marine FHF and underlying the fluvial FUF. He subdivided the Hell Creek beds in an upper and lower member on basis of his fieldwork near the present-day south bank of Fort Peck Reservoir in Garfield County, Montana. The lower member consists of a massive sandstone and shows at the base an erosional unconformity with the FHF. The sandstones are fine-grained, massive, usually cross-bedded and composed of angular quartz grains loosely cemented with carbonate of lime (Brown, 1907). He also mentioned the clear presence of numerous concretions consisting of the same material as the surrounding sandstones, but harder, more compact, showing a concentric structure and often a loglike shape. Other concretions can be found as well, but these are irregular, purplish iron concretions. Brown (1907) describes his upper member of the HCF as an alternation between banded, bluish clays, lighter-colored, fossiliferous sandstones with less pronounced cross-bedding and thin layers of organic rich matter. Brown already noticed that the lignite beds above the HCF should belong to a different age and formation (namely FUF).

After the pioneering work of Barnum Brown, over the decades, many lithostratigraphic studies were performed under supervision of the state geological surveys to characterize the paleoenvironments and stratigraphic members of the HCF, for example by Frye (1969) and Moore (1976) in southwestern and south-central North Dakota and by Butler (1980) in the Glendive area in eastern Montana. These early studies established formal members of the HCF, but these members proved to be unrecognizable outside the limited area where they were described (Fastovsky & Bercovici, 2016). From the late 1980's onwards, modern sedimentological approaches (e.g. Fastovsky, 1987; Retallack, 1994) were carried out to understand the overall facies present in the HCF. However, most of these studies were focused only on the upper part of the HCF since the interest was on the biotic changes related to the K-Pg extinction event.

An exception was the work by Rigby & Rigby (1990), who created a composite lithostratigraphic column in the Bug Creek and Sand Arroyo quadrangles east of the Fort Peck Lake in McCone County, eastern Montana. They described a long section containing the FHF, HCF and Tullock and Lebo member of the FUF, as can be seen in the middle column in Fig. 1.14. Rigby & Rigby (1990) subdivided the HCF in an informal lower and upper member, separated by the Null coal. This 10 cm thick lignite interval contains abundant charcoal, characteristic amber fragments and a 1-2 cm thick bentonite (Smit et al., 1987). The Null coal crops out over most of the Bug Creek area and is the only known persistent coal from within the HCF since all other coal intervals are part of the overlying FUF. The Bug Creek composite log is incomplete though, because the famous Big Bugger, a large incised Paleocene channel, caused erosion in the Bug Creek area of more than 20 m (Smit et al., 1984).

Another important composite lithostratigraphic log of the HCF comes from Slope Counrty in North Dakota. Murphy et al. (2002) describes a composite section at Sunset Butte, located 18 km south of the town of Marmarth (Fig 1.11 and 1.13), which is based on five smaller sections that begin on the east bank of the Little Missouri River and extend to the top of the adjacent Sunset Butte. The complete section is 143 m thick, consisting of 8 m FHF, 100 m HCF and 35 m FUF, but in Fig. 1.14 only a small part of the FUF is shown. Although some individual groups of beds (e.g. channel sandstone bodies, popcorn weathered mudstones, carbonaceous shales or greenish-blue bentonites) can be traced across parts of the Sunset Butte transect, the HCF itself cannot be divided into member rank lithostratigraphic units in this area (Murphy et al., 2002). Several scientists used this Sunset Butte composite log to study the duration of the formation (Hicks et al., 2002) and the stratigraphic changes of palynoflora (Nichols, 2002), megaflora (Johnson, 2002) and vertebrate paleontology (e.g. Pearson et al., 2002).

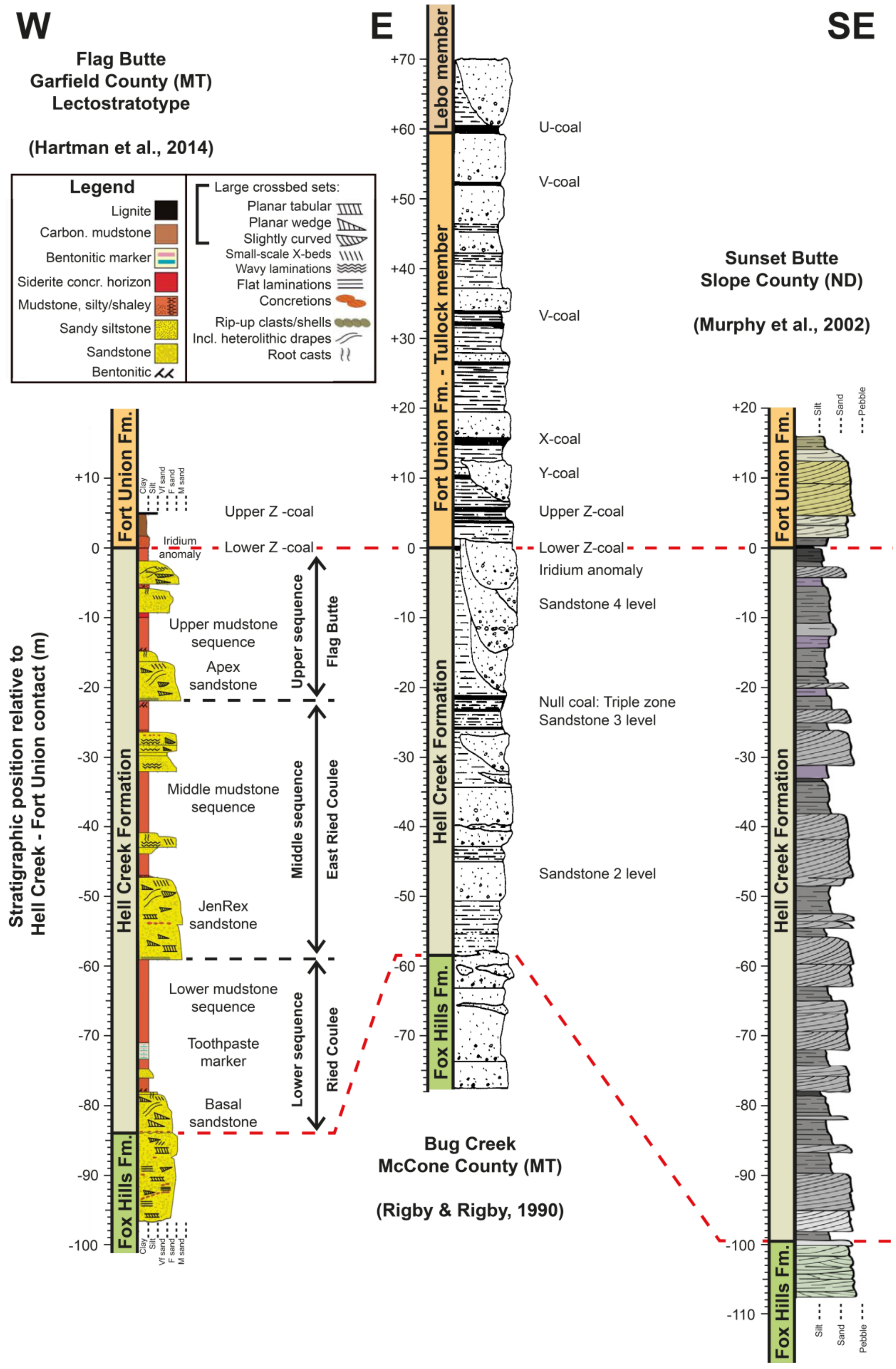
W
Flag Butte
Garfield County (MT)
Lectostratotype
(Hartman et al., 2014)
Legend
Lignite
Carbon. mudstone
Bentonitic marker
Siderite concr. horizon
Mudstone, silty/shaley
Sandy siltstone
Sandstone
Bentonitic
Large crossbed sets:
Planar tabular
Planar wedge
Slightly curved
Small-scale X-beds
Wavy laminations
Flat laminations
Concretions
Rip-up clasts/shells
Incl. heterolithic drapes
Root casts
Stratigraphic position relative to Hell Creek - Fort Union contact (m)
Fort Union Fm.
Hell Creek Formation
Fox Hills Fm.
Clay
Silt
Vf sand
F sand
M sand
Upper Z -coal
Iridium anomaly
Lower Z -coal
Upper mudstone sequence
Apex sandstone
Upper sequence
Flag Butte
Middle mudstone sequence
JenRex sandstone
Middle sequence
East Ried Coulee
Lower mudstone sequence
Toothpaste marker
Basal sandstone
Lower sequence
Ried Coulee
E
Lebo member
Fort Union Fm. - Tullock member
Hell Creek Formation
Fox Hills Fm.
U-coal
V-coal
V-coal
X-coal
Y-coal
Upper Z-coal
Lower Z-coal
Iridium anomaly
Sandstone 4 level
Null coal: Triple zone
Sandstone 3 level
Sandstone 2 level
Bug Creek
McCone County (MT)
(Rigby & Rigby, 1990)
SE
Sunset Butte
Slope County (ND)
(Murphy et al., 2002)
Silt
Sand
Pebble
+70
+60
+50
+40
+30
+20
+10
0
-10
-20
-30
-40
-50
-60
-70
-80
-90
-100
-110

**Fig 1.14** Three generalized, well-studied lithostratigraphic columns for the HCF to show the vertical variations within the formation throughout the Williston Basin. The formational contact between the HCF and FUF is chosen as a reference datum to compare the three columns. The first log is the Hell Creek lectostratotype from Flag Butte in Garfield County, Montana (see Fig 1.1.5. for the geographic location, 25 km north of Jordan), subdividing the formation in three distinct sequences bounded by large sandstone units (Hartman et al., 2014). The middle stratigraphic column derives from the Bug Creek and Sand Arroyo Quadrangles of McCone County, Montana (see Fig. 1.15. for the location) and shows a thin HCF related to intense erosion of Paleocene channels within the Cretaceous rocks (Rigby & Rigby, 1990). The column on the right is constructed from a composite section at Sunset Butte in the extensively studied Mud Buttes area in Bowman County, southwestern North Dakota (see Fig 1.11, Sunset Butte is located 18 km south of Marmarth). In Chapter 4, these lithostratigraphic columns of the HCF are used as reference to correlate with the Naturalis *T. rex* site.

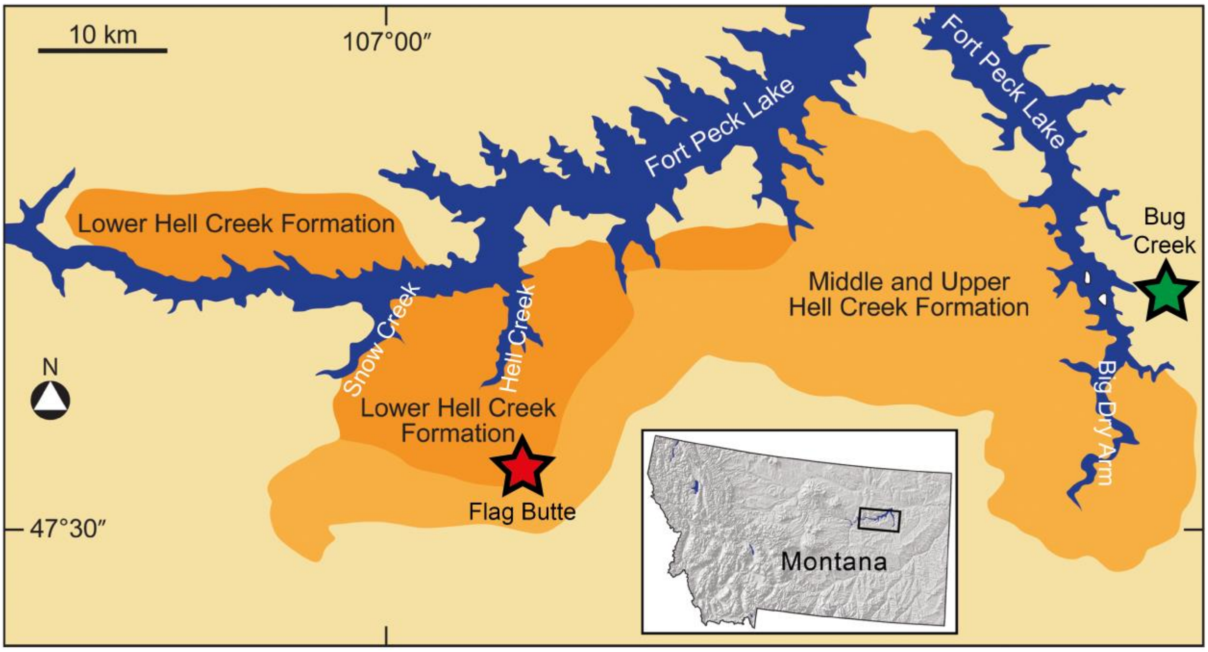


**Fig 1.15.** Schematic overview map of the Hell Creek type locality region in eastern Montana showing the general extent of the deposits of the Lower HCF (dark orange) and Middle and Upper HCF (light orange) along the shores of the Fort Peck Reservoir (modified from Horner et al., 2011)**.** In addition, the approximate positions of the Flag Butte lectostratotype (Hartman et al., 2014) and the Bug Creek stratotype (Rigby & Rigby, 1990) of Fig. 1.14 are indicated with stars.

In 1999, the Hell Creek Project started to establish a geologically well-constrained biotic overview of the entire HCF within its type locality on the southern shores of the Fort Peck Lake in Garfield County, eastern Montana (see the map view in Fig. 1.15). As part of this project, Jennifer Noël Flight, produced in her Master Thesis in 2004 for the first time a sophisticated sequence stratigraphic model of the Bearpaw formation, the FHF and the lower and upper member of the HCF. Unfortunately, most of Flights sections do not reach the contact with the FUF, so the regional thickness and lithofacies variations within the entire HCF are not well known. Following her pioneering work, Fowler (2009) published an abstract in which he subdivided the Hell Creek succession into three, possibly four sequences which are interpreted as 4$^{th}$ order base-level cycles. These so-called parasequences are superimposed on the 3$^{rd}$ order (0.5 – 3 Myr scale) base-level rise under which the HCF was deposited. This base-level rise is related to the retreat of the Western Interior Seaway and the filling of the created accommodation space within the Williston Basin in the Late Maastrichtian. Fowler (2009) stated that the sequence boundaries, each recognized by a laterally continuous disconformity followed by a large fluvial channel sandstone complex, defines the subdivision into the three members of the HCF in Garfield County.

This subdivision was refined by Hartman et al. (2014) who proposed a so-called 'lectostratotype' for the entire HCF, based on an 84.2 m thick succession at Flag Butte, Ried Coulee and East Ried Coulee, tributaries of the Hell Creek river in Garfield County. This composite section can serve as a framework of formational reference, because it is one of the few sections that has a base and top of the HCF visible in a single field of view and its division in three major units, each containing a major sandstone and a mudstone lithofacies, is interpreted as illustrative and representative for the formation (See the left column in Fig. 1.14; Hartman et al., 2014). The contact with the underlying FHF is characterized by the presence of the 'Basal Sandstone', followed by a c. 20 m thick sequence of variegated beds of mudstone and some siltstone. The 'JenRex Sandstone' is an informal name for the sandstone unit that indicates the base of the middle unit of the formation and is the most recognizable and traceable lithostratigraphic marker in the area (Fowler, 2009; Hartman et al., 2014). The overlying middle mudstone sequence is bounded by the third large sandstone body, namely the 'Apex Sandstone' that is typically located c. 26–30 m below the HCF – FUF formational contact. The 'Apex Sandstone' is followed by a mudstone interval which is separated by the so-called '10 Meter Sandstone', which is the informal name for a sandstone that typically occurs c. 10 m below the lower Z-coal of the FUF (Fowler, 2009).

Flight (2004) interpreted the fluvial sandstone bodies that bound the three informal Hell Creek members as the beginning of major 4th order lowstand sequences caused by sea level fall and renewed seaward progradation of the lower delta plain. This also resulted in the termination of the highstand system track that is represented by the overbank deposits of the different mudstone intervals. Scanella & Fowler (2010; 2014) used this sequence stratigraphic model to place a large number of specimens of Triceratops within a temporal framework and found anagenetic evolution in this genus of horned dinosaurs, for instance an increase in the length of the nasal horn over time. Horner et al. (2011) carried out an extensive dinosaur census study using the three informal members of the HCF and LeCain et al. (2014) performed magnetostratigraphy on the Flag Butte lectostratotype to constrain a temporal framework of the HCF.

Besides vertical variability within the HCF, the formation also shows distinct lateral lithologic variations. Fig. 1.16 displays schematically the changes from nonmarine facies in the west towards marine and brackish intercalations in the east. These marine tongues, known as the 'Breien Member' (Hoganson & Murphy, 2002) and 'Cantapeta Advance' (Murphy et al., 2002), are the precursors of the large transgressive phase of the Paleocene Cannonball Sea. These marine incursions indicate that the Western Interior Seaway, once thought to be absent in Hell Creek time, probably reached the recent eastern erosion-controlled outcrop margin of the HCF in the Dakotas. Hence, a large part of the HCF was likely deposited during an eustatic transgressive phase in contrast to many previous studies that favored a regressive sequential evolution of the HCF (Fastovsky & Bercovici, 2016).

Hoganson and Murphy (2002) described the Breien Member as a lithologically variable unit that consists of burrowed, greenish-gray, glauconitic sandstone and mudstone or burrowed, interbedded sandstone and mudstone with rare terrestrial and marine fossils. The Breien Member can be mapped over a large area of c. 6100 km$^2$ in south-central North Dakota (southwest of Bismarck, see the map in Fig. 1.11) and is therefore the only valid formal lithostratigraphic unit within the HCF, in contrast to the members described by Frye (1969) which are too localized and show only subtle lithofacies changes (Murphy et al., 2002). The Cantapeta Advance is located c. 10 m below the top of the HCF and is characterized by a yellowish, crossbedded sandstone bed that is burrowed by *Ophiomorpha*, which represents tidal conditions and thereby the very youngest Cretaceous marine influence in the Western Interior (Murphy et al., 2002).

### 1.3.4. Lower boundary

To calculate the thickness of the HCF and the duration of its deposition, it is crucial to study the characteristics of its contact with the underlying Fox Hills Sandstone. The FHF represents marine, marginal marine (tidal), brackish and less common non-marine deposits associated with a regressing sea during the Maastrichtian (Hartman & Kirkland, 2002). The Fox Hills lithology is dominated by yellow-white, crossbedded, very fine-grained, fossil-poor, calcareous sandstones with abundant loglike concretions. These sandstones can form steep, massive cliff faces, as exposed on the shores of the Fort Peck Lake (Rigby & Rigby, 1990). The top of the FHF is typically a 5 to 15 m thick, very fine to fine-grained sandstone commonly referred to as the Colgate Member (e.g. Belt et al., 1997). This member can be distinguished in the field from the overlying Hell Creek channel sandstone by its light gray to white weathered surfaces, grayish-green fresh surfaces (due to the presence of glauconite) and cleaner sandstone appearance.

The FHF is a good example of a diachronous sedimentary rock unit, meaning that the age of these deposits vary throughout the Williston Basin. As the shoreline of the Western Interior Seaway advanced or retreated throughout its Late Cretaceous history, a sequence of continuous sediments representing different environments (e.g. delta, beach, shallow water, open marine) was deposited. Although each facies may be continuous over a wide area, its age varies according to the position of the paleoshoreline. In the case of the FHF, due to Laramide uplift in the west, the paleoshoreline advanced to the east and thereby causing significant younger ages for the Fox Hills coastal sandstones in North Dakota compared to Montana. This diachronous pattern is clearly visible in the Wheeler diagram of Fig. 1.16 that shows the chronostratigraphic correlations known so far within the Williston Basin. In this figure it is visible that the HCF is also characterized by diachroneity throughout the Basin, although somewhat less pronounced than the FHF. The HCF is oldest in the eastern part, because some authors have interpreted that (especially in the west) a large temporal hiatus exists between the HCF and the FHF (Johnson et al., 2002).

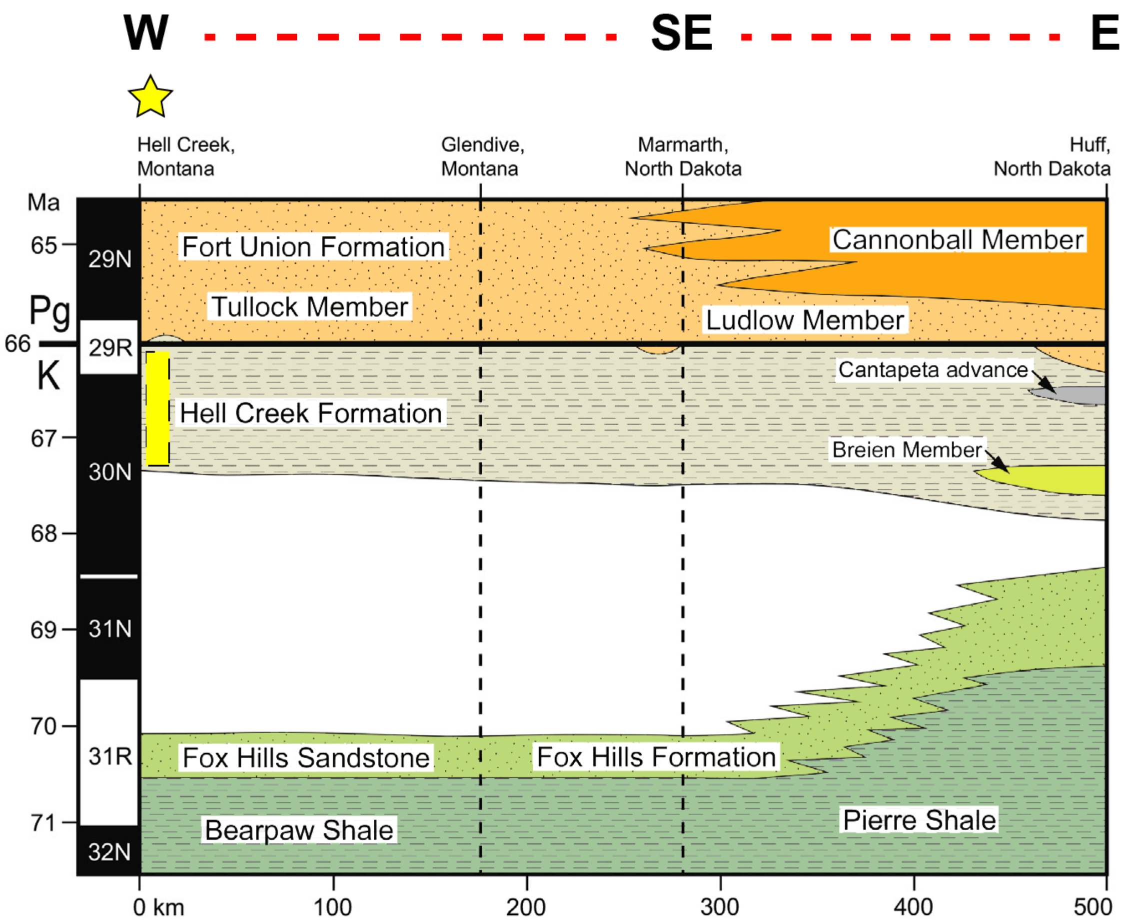

**Fig 1.16**. Schematic chronostratigraphic west-east cross-section of the Williston Basin showing a clear diachronous pattern of the regressive sequence of Bearpaw Shale, Fox Hills Sandstone and the HCF, resulting in a younger FHF and an older HCF in the eastern part compared to the western part in Montana (based on the interpretations of Fastovsky & Bercovici, 2016 and Johnson et al., 2002). The white space in the diagram marks a temporal hiatus of c. 2-3 Myr between the HCF and FHF. However, the presence and spatial and temporal extent of this unconformity at the base of the HCF is still debated (see section 1.3.4. and 1.3.6). See Fig. 1.11 for the map view of this cross section.

The lithological characteristics, the type of contact (conformable versus unconformable), and the age of the contact between the FHF and HCF is still under debate. The base of the HCF in North Dakota has been drawn by most authors at the base of a 0.3 to 1 m thick carbonaceous sandstone, siltstone, or mudstone directly above the white, clean sandstones of the Colgate member (Murphy et al., 2002). This thin carbonaceous bed is interpreted by Erickson (1992) as a paleosol, implying a period of quiescence and possible soil leaching into the underlying strata causing potentially the whitening of the Colgate sandstones (Fig 1.17). The basal contact in North Dakota is regionally conformable but locally, show relief of a few meters, due to scouring (Murphy et al., 2002).

In eastern Montana, the FHF-HCF contact can sometimes be more difficult to recognize when the Hell Creek Basal Sandstone is present (Fig. 1.15). The Basal Sandstone in Garfield County is slightly grayer in color and exhibit more fluted weathering than the upper FHF. The Hell Creek sandstones commonly exhibit lateral-accretion features and are encased within flood-basin deposits of a lower delta-plain origin in contrast to the tidally influenced, highly channelized sandstones of the Fox Hills (Hartman et al., 2014). Brown suggested in 1907 the existence of a possible timegap between the HCF and FHF, based on field observations of a disconformity that marked features of subaerial erosion. However, with additional fieldwork Brown came back to his original hypothesis and determined a conformable and thus gradational relationship between the brackish sediments of the FHF towards the fresh-water sediments of the Hell Creek (Brown, 1914). In the Bug Creek area in McCone county the HCF-FHF contact was assumed by Rigby & Rigby (1990) as conformable.

Johnson et al. (2002) claimed that there is a distinct possibility that the base of the HCF is significantly diachronous, since Hicks et al. (2002) and Lund et al. (2002) provided estimates of the age of the base of the HCF based on extrapolation of sedimentation rates: their estimates were 1.36 Ma and 2.5 Ma, respectively. In conclusion, more detailed sedimentary descriptions and better age estimates (i.e.: reliable radiometric dates) of the basal contact of the HCF are clearly needed to better understand the depositional mechanisms at the end of the Fox Hills period and the beginning of the Hell Creek strata. See paragraph 1.3.6 for a more detailed discussion about the complex nature of the FHF-HCF contact and its unresolved age.


**Fig. 1.17.** View on the Fox Hills-Hell Creek formational contact, as exposed near the boundary between Fergus and Petroleum County in Montana (Flight, 2004). A distinct color change is visible from the white sandstones of the Colgate member of the FHF towards the somber green-brown mudstones of the HCF. It is hypothesized that the white color of the Colgate sandstones is related to 'paleosol leaching' from the overlying Hell Creek carbonaceous strata and hence this soil formation may have caused a significant hiatus at the formational contact (Erickson, 1992; Lerbekmo, 2009).

### 1.3.5. Upper boundary

Already in early literature it was recognized that the upper boundary of the HCF, identified in first instance by the appearance of the first persistent lignitic coal interval, marked an important change in the fossil and geological record. Brown commented in his 1907-paper: "It is a most remarkable and significant fact that in no instance has a fragment of dinosaur bones been found in or above the lignite series by any of our party during five years' work in this region. On the contrary, crocodile and turtle remains were found all through the lignite horizon (which belongs now to the overlying Fort Union Formation). The sudden termination of the many highly specialized forms of dinosaurs indicates a considerable time hiatus or a sudden and marked change in geological conditions."

The top of the HCF is defined as a razor sharp boundary known as the Cretaceous-Paleogene (K-Pg) Boundary that marks the end of the Mesozoic era. This boundary is associated with the last of 'the big five' mass extinctions that life on Earth experienced in its long history (Benton, 1995). Not only non-avian dinosaurs went extinct during this devastating event, also pterosaurs, marine reptiles, ammonites, belemnites and marine micro-organisms such as coccolithophores and foraminifera were victims. Approximately 76% of all life on Earth disappeared including more than 30% of all marine genera (Barnosky et al., 2011).

After more than 35 years of intensive study, it is currently widely accepted that the K-Pg mass extinction is related to the impact of a single asteroid with a diameter of c. 10 km at present-day Chicxulub, on the Mexican peninsula of Yucatán (Alvarez et al., 1980; Smit & Hertogen, 1980). The geochemical and physical evidence for this extraterrestrial impact theory consists of a globally distributed ejecta blanket at the K-Pg boundary transition that is characterized by an anomalously high abundance of iridium and other platinum group elements, the presence of shocked quartz and the abundance of nickel-rich spinel bearing microkrystites (Bohor, 1990; Schulte et al., 2010; Smit, 1999). In 1991, the discovery of the c. 180 to 200 km diameter Chicxulub crater structure on the Yucatán peninsula in Mexico provided crucial additional information (Hildebrand et al, 1991).

Detailed modeling shows that a sequence of short-time events is associated with the bolide impact. The first hours after the impact were characterized by shock-wave induced earthquakes, slumping and tsunamis in the Gulf of Mexico that were affecting the Western Interior Seaway as far north as North Dakota (DePalma & Smit, 2015, pers. comm.). This early phase is also called the 'fireball-stage', because it generated a heat wave resulting in global wildfires (Robertson et al., 2004). Subsequently, the dust and sulfur aerosols, originating from anhydritic target rocks from the Yucatan surface, are predicted to have partially blocked incoming solar radiation (Pope et al., 1997). This 'impact winter' is proposed to have temporarily inhibited photosynthesis, resulting in a global collapse of marine and terrestrial food webs (Schulte et al., 2010; Kring, 2007). Vellekoop et al. (2014) quantified this impact winter using TEX86 paleothermometry of tsunamite sediments from the Brazos River section, Texas, USA. They measured a major decline in sea surface temperature during the first months to decades after the impact of at least 7 °C. On land, this post-impact cooling must have been even more severe.

Since the 1980's onwards, many geologists and paleontologists went to the Hell Creek area in Montana to study the extinction and survival patterns of terrestrial plants and animals associated with the K-Pg catastrophe. The well-exposed and continuous Upper Cretaceous and Paleogene deposits of the Hell Creek and Fort Union Formation in this region formed an ideal fossil record to investigate the rate and magnitude of disappearance of terrestrial biota and to compare these patterns with the marine realm. The terrestrial K-Pg boundary at the top of the HCF can be recognized in the field by the appearance of the first (lowest), laterally continuous (persistent) lignitic coal. This basal lignite is known as the 'lower Z-coal', based on the revised nomenclature of Collier & Knechtel (1939), that uses reversed-alphabetical labels for successively younger coals (Fig. 1.17). In addition, the formational contact can be identified as the top of the highest swelling 'popcorn weathered' claystone and the base of the first occurrence of variegated siltstone and claystone beds (Fastovsky, 1987). The contact is also often associated with a pronounced break in slope and a color change from somber, monotonous, gray-olive Hell Creek tones towards light brownish and yellowish 'zebra-striped' tones of the FUF (Fig. 1.17).

The study of fossil pollen and spores proved to be a powerful tool to recognize the sometimes bioturbated and discontinuous K-Pg boundary claystone, especially in situations where indicators of the Chicxulub impact (iridium anomaly, shocked quartz, Ni spinels) are absent. The Hell Creek palynoflora is relatively homogenous throughout the entire formation (Fastovsky & Bercovici, 2016), but at the K-Pg boundary it shows an abrupt c. 30% extinction combined with a distinctive fern spore spike. This spike indicates widespread deforestation due to a bolide-induced impact winter or massive wildfires that disrupted terrestrial ecosystems in such a catastrophic way that diverse plant communities are replaced by one dominated by a few species of fern (Tschudy et al., 1984, Vajda et al., 2001, Vajda & Bercovici, 2014).

Over the 500 km transect running from west to east in Fig. 1.13, the top of the HCF is always within a few meters, above or below, the defined K-Pg boundary (based on a coal interval associated with an iridium anomaly, fern spike and presence of shocked quartz). Therefore, the top of the HCF can be roughly seen as diachronous on a fine local scale, but essentially as isochronous on a regional scale (Nichols & Johnson, 2002; Sprain et al., 2015). This is the reason that in Fig. 1.13 the stratigraphic distance from the K-Pg boundary is used to calculate the formational thicknesses and why the Wheeler diagram in Fig. 1.16 uses the K-Pg boundary as a datum. The HCF-FUF contact is associated with a paleonvironmental transition from high-water table hydromorphic paleosols towards a Paleogene flooded landscape of the FUF which allowed large peat mires to grow (Fastovsky, 1987, Jerrett et al., 2015; Sprain et al., 2015).

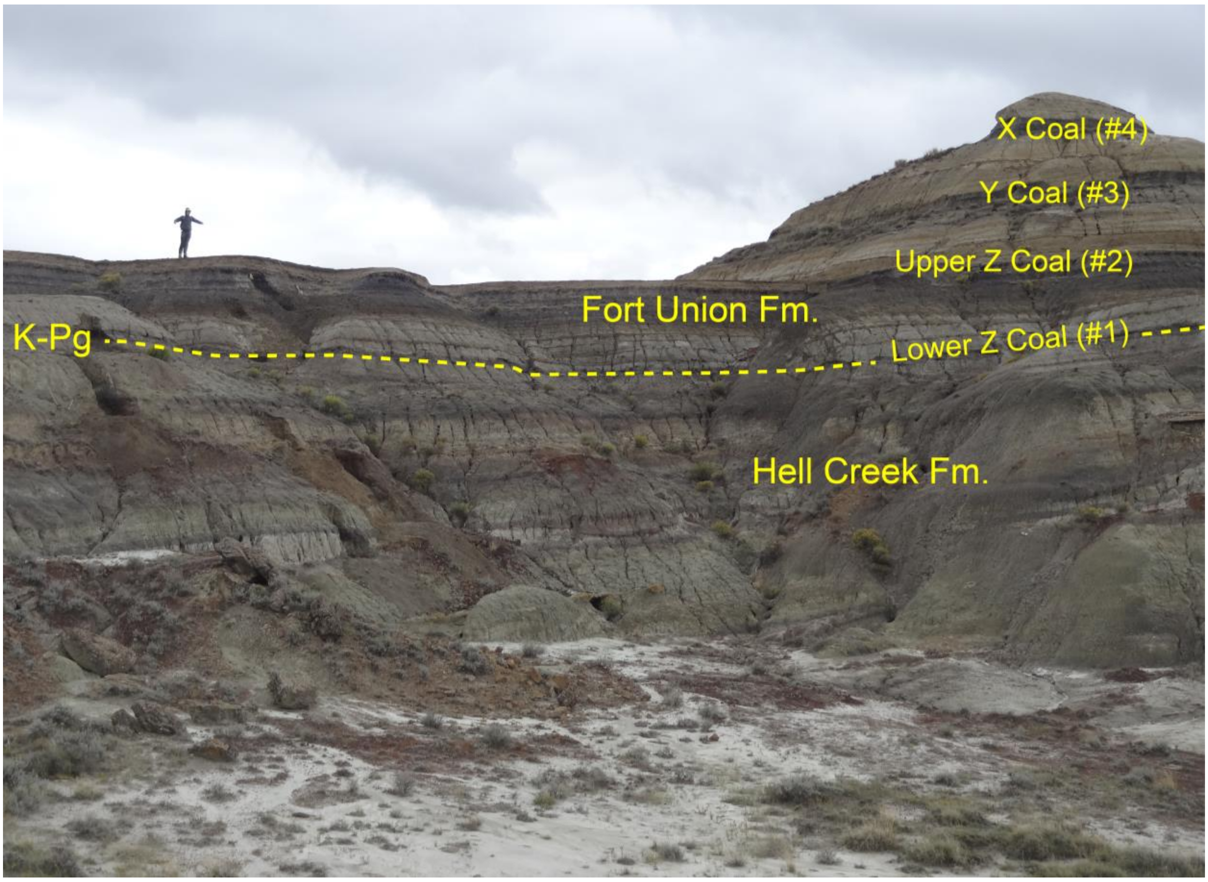


**Fig 1.18.** Hell Creek-Fort Union formational contact as exposed in the Flat Creek area north of Jordan, Garfield County, eastern Montana. The contact can be recognized based on a color and lithology change from relatively homogeneous somber olive, grey silty units of the HCF into the different coals of the FUF which are interbedded with golden-yellow striped sandy intervals. The approximate position of the K-Pg boundary at the base of the Lower Z Coal is indicated. Hemmo Abels (c. 2 m) for scale.

### 1.3.6. Age and duration

A range of different stratigraphic and geochronologic tools have been applied over the last decades to accurately define the age of the lower and upper boundary of HCF and thereby its duration, but this remains extremely challenging upon today. As mentioned before, due to the heterogeneity of the Hell Creek beds, lithostratigraphic correlation over large distances is nearly impossible. Moreover, approximately 60% of the HCF is composed of fine-grained (floodplain-related) sediments (Fastovsky, 1987) and hence the remaining 40% channel sandstone sequences, interpreted to be deposited geologically instantaneously, causes high variability in sedimentation rates throughout the formation.

Nevertheless, scientists tried to produce a stratigraphic framework of the HCF and to place fossil localities in a temporal context. The classical method to do this was to find a nearby exposure of either the top or the bottom of the formation and measuring the distance to that contact. However, this technique does not often allow for reliable placement of recovered specimens in areas in which neither the top nor the bottom contact of the HCF is exposed in relatively close proximity. In addition, this method would only work if all exposures of the HCF have a consistent thickness which is clearly not the case (see section 1.3.3.). Finally, as described in section 1.3.4., the FHF-HCF contact is interpreted by many authors to be unconformable and no clear absolute age has been established for this basal part of the formation. The most renowned lithostratigraphic marker bed of the HCF is the one just above it: the K-Pg boundary. The recognition of the boundary claystone can sometimes be difficult in the field and the associated iridium anomaly is at least as discontinuous as the coal deposits in which it can be found.

Due to the rarity of this iridium spike and the imprecision of other stratigraphic markers, other scientists tried to perform paleomagnetic studies. The first magnetostratigraphic analysis of the HCF was carried out by Archibald et al. (1982) and was based on four sections in Garfield and McCone Counties (Montana) that showed that the K-Pg boundary lies within magnetochron 29r of the geomagnetic polarity timescale (Gradstein et al., 2012) and the HCF comprises partly chron 29r and chron 30n. These sections were calibrated to the geochronologic time scale with a series of radiometric ages obtained from the Paleocene portion of the section by Swisher et al. (1993). The magnetostratigraphy was extended to central North Dakota and southwestern North Dakota with the work of Lund et al. (2002) and Hicks et al. (2002), respectively. However, these early studies lack time constraints stratigraphically below the K-Pg boundary and therefore hampers the determination of a precise age for the HCF and inhibits the correlation between fossil sites within the formation.

Therefore, Lerbekmo (2009) produced the first long terrestrial paleomagnetic record including the Bearpaw Formation, FHF and HCF, based on a road section near Hell Creek State Park north of Jordan, Garfield County. A geomagnetic reversal found in this section at the base of the Colgate member (uppermost FHF), was interpreted as the boundary between chron 30r and 30n. Lerbekmo calculated an average sedimentation rate for c29r (c. 83 m/Myr) and c30r (c. 100 m/Myr) and therefore assumed a normal accumulation rate for the 90 m thick c30n interval of c. 90 m/Myr. He used a duration of 1.9 Myr for c30n and thus the thickness of 30n should be c. 170 m. Consequently, a rock sequence of 80 m misses, representing a large hiatus with a magnitude of c. 0.9 Myr at the base of the HCF. It is hypothesized that this hiatus is attributed to subaerial exposure of the land that became subject of non-deposition or erosion. This is probably related to large eustatic sea level fall which equals a retreat of the Western Interior Seaway to central North Dakota of c. 500 km (Lerbekmo, 2009). Lerbekmo claimed that this sea level and water table drop caused a severe leaching of the sandstones of the Colgate member of the upper FHF, observable in the field as the white-weathering color related to the production of kaolinite (Fig. 1.17). He also stated that the regional disconformity at the top of the Colgate member is responsible for the high abundance of dinosaur skeletons (including *Tyrannosaurus rex)* within the Basal Sandstone (Fig 1.14), since bone material was eroded from older Hell Creek sediments and concentrated in this sandstone (Lerbekmo, 2009).

The most recent regional paleomagnetic study was published by LeCain et al. (2014) as part of the large-scale Hell Creek Project. They produced a high resolution magnetostratigraphic framework of the HCF lectostratotype section and a composite section in the Biscuit Butte area, together spanning the uppermost FHF, the entire HCF, and the Tullock Member of the Fort Union Formation. They also produced a 3D magnetostratigraphic plane using Differential GPS data tied to vertebrate fossil localities. LeCain et al. (2014) also found a reversal in the upper FHF, but they were not certain to link the reversed polarity zone to the short chron c30r without other age constraints than paleomagnetism. Johnson et al. (2002) interpreted that the FHF is deposited in chron c31r (Fig. 1.16), implying a much longer hiatus than suggested by Lerbekmo (2009). In conclusion, all of the paleomagnetic studies above are missing state-of-the-art geochronological tie-points, so determining sedimentation rates and the duration of the HCF remains complicated.

Absolute age control of the HCF comes predominantly from high-precision $^{40}Ar/^{39}Ar$ radioisotopic dating on the K-Pg boundary. This dating technique was carried out on well-preserved, sanidine crystals derived from volcanic ash fall-out deposits (for a summary of the $^{40}Ar/^{39}Ar$ dating method, see Kuiper, 2003). When volcanic ash is altered into clay in a terrestrial setting, the term tonstein is used. These tonsteins are only preserved in backswamp deposits. The dynamic Hell Creek rivers should have eroded away the soft unconsolidated volcanic ash very easily and therefore the dating was performed solely on coal-bearing K-Pg sections in the Hell Creek area. The most recent age for the K-Pg boundary is set on 66.043 ± 0.043 Ma (mean + analytical uncertainty, Renne et al., 2013). Renne et al. (2013) demonstrated that the lithostratigraphic contact between the HCF and Fort Union Formation coincides with the Chicxulub impact with a level of precision of 32.000 years, matching the Beloc droplets age. However, this is based on tephra geochronology in Garfield County (Montana), whereas dates to the east show that the K-Pg boundary in McCone County is located c. 2-3 below (Clemens, 2002) and in North Dakota 2-3 m above the formational contact (Johnson, 1992). In conclusion, the HCF-FUF contact is not completely synchronous with the K-Pg boundary throughout the entire Williston Basin, but the event-claystone itself (associated with the presence of an iridium anomaly, shocked quartz and fern spike) can certainly be used as an important regional correlative isochron (Moore et al., 2014).

Due to the scarcity of persistent lignite intervals within the HCF, the rest of the formation lacks absolute age control. The Null Coal in the Bug Creek area (Fig. 1.14) has recently been dated by Sprain et al. (2015), but this age (66.289 ± 0.051 Ma) is highly questionable. According to the magnetostratigraphic study of Swisher et al., (1993), the Null Coal in the Bug Creek area is positioned below the paleomagnetic reversal chron 30n-29r, but this is not in agreement with the determination of an older age for this reversal (66.398 Ma, after Ogg, 2012). Furthermore, Hicks et al (2002) made an attempt to date the Doaks Butte ash bed in Bowman County, southwesternmost North Dakota. However, this bentonitic ash layer, situated c. 75 m below the K-Pg boundary, only contained detrital K-feldspar. Single-crystal $^{40}Ar/^{39}Ar$ analyses provided a large range in ages that does not refine the age of the Hell Creek sequence and are thus unsuitable (Hicks et al., 2002).

A novel technique applied in recent years is known as chemostratigraphy based on carbon isotopes ($\delta^{13}C$). A -1‰ to –3‰ shift in carbon isotope composition have been well-documented in marine K-Pg boundary sections across the globe, related to a decreased flux of organic matter from the surface waters towards the deep ocean (D'Hondt, 2005). The presence of a robust marine K-Pg isotopic shift suggested to several authors that a terrestrial $\delta^{13}C$ excursion might also exist. This is linked to changes in the $\delta^{13}C$ of atmospheric $CO_2$ after the impact and this isotopic signature is preserved in the tissue of vascular land plants because they sample the $CO_2$ directly during photosynthesis (Arens et al., 2000). Indeed, modest negative $\delta^{13}C$ shifts ranging from 1‰ to –2.8‰ were obtained at or near K-Pg boundaries in Alberta (Therrien et al., 2007), Montana (Arens et al., 2014) and North Dakota (Arens & Jahren, 2002). Arens et al. (2014) produced a reference section throughout the entire HCF at Herman Ridge in westernmost Garfield County based on more than 300 $\delta^{13}C$ measurements on bulk C3 plant-derived sedimentary organic material. They also showed that the amount of organic content within the sediment samples - and thereby the associated depositional facies - does not bias the $\delta^{13}C$

signature. Nevertheless, a review by Grandpre et al. (2013), who measured the well-known Mud Buttes section in North Dakota, stated that the K-Pg isotopic shifts were statistically indistinguishable from any other $\delta^{13}C$ offsets recorded above and below the boundary and thus chemostratigraphy is of limited use. On the other hand, a recent study on Canadian coal seams by Jerrett et al. (2015) showed that reliable records of paleoatmospheric $\delta^{13}C$ can be extracted from terrestrial sediments that can be successfully correlated between sections more than 500 km apart. However, they only sampled lignites from the Paleocene, so more high resolution studies on specific lithologies throughout the HCF are needed to check whether this chemostratigraphic correlation can be applied on these Maastrichtian rocks.

Various forms of biostratigraphy have been applied in Upper Cretaceous and Paleocene rocks from the Williston Basin over the last decades. Early studies focused mainly on the diversity and evolution of mammals across the K-Pg boundary and extensive literature have been published about this faunal turnover (e.g. Van Valen & Sloan, 1977; Clemens, 2002). However, detailed biostratigraphy of the HCF based on North American Land Mammal Age (NALMA) zonations is not possible, since the entire unit is characterized by the Lancian mammal fauna and a relative scarcity of Mesozoic mammal fossils inhibits further subdivision. Similarly, subdivision of the HCF based on dinosaur fauna did not provide more detail since the entire formation is characterized by the *Triceratops* faunal assemblage that does not hold a large biodiversity (White et al., 1998).

A different approach that helps refining the temporal framework of the HCF is based on the study of fossil pollen and spores that belong to the Upper Maastrichtian *Wodehouseia spinata* Assemblage Zone. High resolution palynostratigraphy helps to identify the K-Pg boundary (linked to the presence of a fern spike), but also allow subdivision the HCF into biozones. Although at first glance the Hell Creek palynoflora is quite homogeneous, Nichols (2002) proposed five provisional subzones of the *Wodehouseia spinata* Assemblage Zone based on studies in the Mud Buttes area in southwestern North Dakota. These subzones, ranging from A to E (placed from the bottom of the HCF to the top), are defined by the stratigraphic range (first and last appearances) of ten distinct Maastrichtian angiosperm species which allow a clear separation between the lower 40 m and upper 60 m of the HCF.

The Western Interior is also famous for its well-constrained ammonite biostratigraphy. The marine facies underlying the HCF contains a high resolution ammonite zonation associated with numerous levels of datable marine, bentonitic levels (e.g. Cobban et al., 2006). The uppermost Bearpaw Formation comprises the youngest, reliable $^{40}Ar/^{39}Ar$ dated ammonite zones below the HCF, namely the middle of the *Baculites grandis* zone (70.66 ± 0.65 Ma) and the top of the *Baculites clinolobatus* zone (70.08 ± 0.37 Ma), both from Red Bird, Wyoming (Hicks et al., 1999, using the Taylor Creek Rhyolite standard at 28.23 Ma). These two zones are followed by the undated *Hoploscaphites birkelundi*, *Hoploscaphites nicolletti*, and *Jeletzkytes nebrascensis* zone, all found in the FHF. Interestingly, Hoganson & Murphy (2002) found an ammonite specimen identified as *Jeletzkytes cf. J. nebrascensis* in the marine Breien Member in south-central North Dakota. The occurrence of this specimen would imply that this part of the HCF was deposited at the time of the *Jeletzkytes nebrascensis* Zone (c. 68.0 – 68.7 Ma, following Gradstein et al., 2012), much older than previously thought. However, it only concerns a single, partial, poorly preserved ammonite specimen that could also be reworked from the underlying FHF.

Combining all known stratigraphic and geochronologic data, Hicks et al. (2002) made an attempt to establish the duration of the HCF based on five well-studied sections in Slope and Bowman County, southwestern North Dakota. By extrapolating the calculated sedimentation rate of the Cretaceous portion of chron 29r (333 kyr, based on an astronomically tuned South Atlantic deep-sea core by D'Hondt et al., 1996) through to the base of the HCF, the authors estimated the formation should be 1.36 Myr in duration. Hicks et al. (2002) acknowledges, however, that the time span of Hell Creek deposition can range between 1.9 and 1.05 Myr, all dependent on which precessional age estimate for chron 29r from the marine realm is used as input parameter. Using a Cretaceous chron 29r duration of 361 kyr and the Hell Creek thicknesses of Lerbekmo (2009) and LeCain et al. (2014), Wilson (2014) calculated two estimations for the timespan of deposition of the HCF, namely 1.80 Myr and 2.06 Myr. He eventually picked the mean value, 1.93 Myr, to use in his study about faunal dynamics within Maastrichtian and Danian mammals.

### 1.3.7. Flora and fauna

The HCF is famous for the preservation of an abundant and diverse flora and fauna in its latest Cretaceous fossil record. A warm, humid, subtropical climate reigned during Hell Creek time and this created a lush, fluvial ecosystem with wet soils and heavily forested, low-lying floodplains full of life (Fastovsky & Bercovici, 2016).

**Micro- and macroflora**

The rich and varied flora of the HCF is known from fossil leaves, seeds, cones, fossil wood, charcoal and as microscopic pollen and spores. The Hell Creek palynoflora is well-studied, but almost all publications contain solely sample intervals surrounding the K-Pg boundary. The only known palynological study comprising the entirety of the HCF is, to my knowledge, the paper by Nichols (2002) who reports a total of 115 pollen and spore taxa in southwestern North Dakota. On the other hand, Hotton (2002) identified over 281 HCF taxa in eastern Montana, not including fungal spores and algal cysts which are also present. This diverse pollen and spore assemblage resembles a lush, evergreen forest with an understory vegetation of mainly ferns and mosses, a canopy of gymnosperms (such as conifers) and an overall dominance in abundance and diversity of angiosperms (flowering plants) that occupied various habitats within the subtropical woodland.

This image is also confirmed by the rich macrofloral record of the HCF, extensively studied by paleobotanist Kirk Johnson and his colleagues in mostly North and South Dakota, that shows very diverse groups of rainforest type plants. Johnson (2002) reports a total of 328 plant morphotypes that can be subdivided into taxa of c. 90% angiosperm, 6% gymnosperms and 4% fern and fern allies. The angiosperms are mainly dicots (c. 97%), and can be subdivided into many palm species and trees similar to modern-day magnolia, laurel, platanus, sycamore and beech. The gymnosperms are represented by 18 species of conifer trees (including *Metasequoia* sp. and bald cypresses) and single species of *Gingko* and Cycads. Ferns and fern allies are subdivided in liverworts, horsetails, water mosses and club mosses. Johnson (2002) states that 'the Hell Creek forest is similar in general appearance to a living, mixed deciduous and evergreen broad-leafed forest, but differs from that general look by having palm trees, odd conifers and plants with an unusually high percentage of lobed leaves'. Considering the entire HCF, 78% of all terrestrial plant taxa went extinct at the K-Pg boundary (Nichols & Johnson, 2008) and as a consequence, the Paleocene flora of the FUF shows a much lower biodiversity and is dominated by taxa that were most common in Cretaceous mire environments (Johnson, 2002).

**Invertebrate fauna**

The invertebrate fauna preserved in the fossil record of the HCF is dominated by freshwater molluscs. Clemens & Hartman (2014) summarized the outcomes of the extensive collection of these molluscs. Most abundant are the unionid bivalves, the freshwater mussels from the family *Unionidae*, with *Pleurobema* and *Proparreysia* as important genera (Scholz & Hartman, 2007). Hartman (1998) listed 31 taxa of bivalves within the HCF, which all went extinct before or at the K-Pg boundary. In addition, exposures from the Breien Member of the HCF in south-central North Dakota provided a few finds of marine bivalves (e.g. oysters) and ammonites, similar to the FHF fossil record (Hartman & Kirkland, 2002). Freshwater clams are represented by the genus *Sphaerium* and the only known freshwater gastropod (snail) from the HCF is *Campeloma* sp. (Linkevich, 2013).

The presence of insects within the Hell Creek was for a long time only inferred from trace fossils in megaflora, in other words: insect-mediated damages on fossil leaves. This study can serve as a good proxy for insect diversity in past ecosystems, because many insect species today target specific plant species. Labandeira et al. (2002) discovered a total of 51 different plant-insect associations within the HCF, ranging from traces left by hole and margin feeders, mining and galling animals or piercing and sucking insects, pointing towards a very high insect biodiversity. DePalma et al. (2010) recorded the first clear body fossils of insects. These invertebrates were extraordinarily 3D preserved within large Cretaceous amber-deposits derived from Hell Creek siltstones from Harding County, South Dakota. Using micro-CT scans, the authors were able to visualize several high-quality Cretaceous insect species and identified them as part of the order of *Diptera* (containing flies and midges) and the suborder *Zygoptera* (including damselflies, similar to dragonflies, but smaller in size).

**Vertebrate fauna**

The HCF provides the finest record available of vertebrate fossils of all latest Cretaceous terrestrial paleoenvironments in the world (Fastovsky & Berocvici, 2016). The diversity of the most important vertebrate faunal groups will be briefly discussed below with a specific focus on the non-avian dinosaur (hereafter, dinosaur) assemblage.

Fish were core members of the shallow water communities of the HCF and can be subdivided in two large groups, namely the actinopterygians (ray-finned bony fish) and elasmobranchs (cartilaginous fish such as sharks and rays). Based on the investigation of isolated fish vertebrae and tooth-bearing elements from six vertebrate microfossil sites, three from the lower part and three from the upper part of the HCF in Montana, Brinkman et al. (2014) found 27 taxa of actinopterygians of which 17 are teleosts. Most abundant are the *Amiidae* (a family of basal ray-finned fishes of which the bowfin is the only extant species), *Lepisosteus* (a genus of gars or garpikes, the family *Lepisosteidae* still includes seven living species today) and *Coriops* (which shows similarities with the living freshwater bony fish *Arowana*, also known as bonytongue). Diversity within freshwater elasmobranchs from the HCF was examined by Cook et al. (2014) using teeth and dentary in microsites in Montana. The study revealed six taxa in the HCF, including species that are similar to modern-day guitarfishes (elongated rays) and nurse, and bamboo sharks, but these extinct species could tolerate freshwater conditions. The stingray *Dasyatis* sp. is only known from the FUF and the presence of the brackish water loving *Isnchyhiza* sp. in the Bug Creek section suggests that during upper Hell Creek time the Western Interior Seaway was not far away (Cook et al., 2014). The Breien member in southwestern North Dakota provided teeth and vertebrae from 13 species of marine sharks and rays and three species of actinopterygians (Hoganson & Murphy, 2002).

Amphibia in the HCF are known from findings of many salamander and some frog species. Wilson et al. (2014) revealed 11 species of salamander or salamander-like lissamphibians in the Hell Creek deposits and showed that, already during the final 400 kyr of the HCF, this diversity dropped in a step-wise pattern due to ecological instability possibly linked to the late Maastrichtian warming event (Wilf et al., 2003).

Following the pioneering work of Sloan & Van Valen (1965), many paleontologists went to the Hell Creek area to study Mesozoic mammals and their evolutionary pattern in association with the K-Pg extinction. A recent study by Wilson (2014) used a database of nearly 5000 specimens of fossil mammals from the HCF and lower FUF to quantify the temporal patterns in faunal dynamics across the K-Pg boundary. Mammals within the HCF are part of the Lancian NALMA zone and are represented by three large groups, namely the *Eutheria* (the group of the living placental mammals represented by 8 Hell Creek species and similar to modern-day rats), the *Metatheria* (similar to modern-day marsupial mammals, 11 species according to Wilson, 2014) and the *Multituberculata* (extinct taxon of rodent-like mammals that lived predominantly in trees, 13 species). Wilson (2014) found that the Hell Creek mammalian fauna remained relatively stable until 500 kyr before the KPg boundary when the relative abundance of the *Metatheria* declined. The Chicxulub impact caused c. 75% extinction of the Late Maastrichtian mammal species and the most important survivors were the *Multituberculatan* genera *Mesodma* and *Cimexomys,* the only survived marsupial genus *Peradectus* and the *Eutherian* order of *Cimolesta*. With the demise of the dinosaurs, the previously ecologically marginal mammals filled in the environmental niches of the FUF very quickly and the surviving genera radiated into diverse groups such as primitive ungulates and early primates (Wilson, 2014).

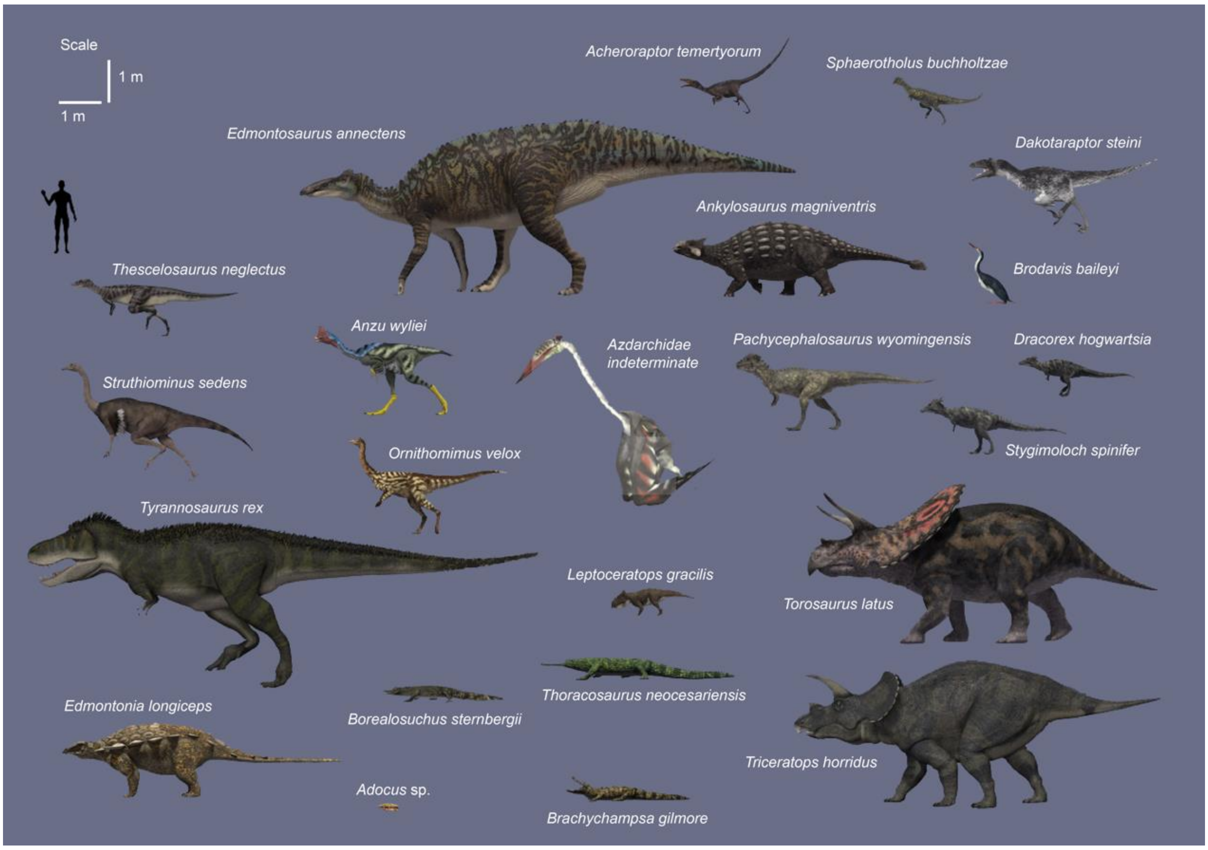


**Fig 1.18.** Reconstruction of the Hell Creek ‘reptilian’ vertebrate faunal assemblage (known as the *Triceratops* fauna) showing the most important vertebrates with estimated body sizes, excluding the controversial *Nanotyrannus* lancensis but including *Tyrannosaurus rex* and the recently discovered theropods *Anzu wyliei* and *Dakotaraptor steini*. Artist impression by James Kuether, updated on 2 November 2015.

Reptiles in the HCF include turtles, crocodiles, champsosaurs (similar to modern-day gavial crocodiles), snakes, lizards, pterosaurs (flying reptiles) and of course dinosaurs. Turtles are well-represented in the Hell Creek vertebrate fossil record and comprises 8 families of at least 19 genera (Holroyd et al., 2014), such as *Adocus* sp. (Fig 1.19). Three species of crocodile (*Brachychampsa montana*, *Borealosuchus sternbergii* and *Thoracosaurus neocesariensis*, see Fig. 1.19) and one species of champsosaur (*Champsosaurus* sp.) are known from the HCF (Pearson et al., 2012). These aquatic reptile groups suffered no significant extinction across the K-Pg boundary, probably attributed to their niche within the freshwater environment that could serve as a refugium for the post-impact perturbations. In contrast, land-dwelling organisms show a severe pattern of extinction, since they are strongly dependent upon the primary productivity of living plants on land (Sheehan & Fastovsky, 1992). Longrich et al. (2012) revised the diversity patterns of fossil squamates (lizards and snakes) across the K-Pg boundary and listed a species-total of 27 lizards and three snakes in the Late Maastrichtian of North America (of which the majority is present in the HCF, but not all species). The diverse Hell Creek land-dwelling lizard and snake fauna experienced a devastating extinction of c. 80% at the K-Pg boundary (Longrich et al., 2012). Pterosaurs are extremely rare in the HCF and the only known described remains comprise an isolated cervical vertebra of a large azhdarchid pterosaur, found in one of the field jackets of the *T. rex* specimen ‘Jane’ from Carter County, southeastern Montana. This single neck bone might belong to the genus *Quetzalcoatlus*, which had an estimated wingspan of 11-12 m, but precise determination is difficult (see Fig. 1.19; Henderson & Peterson, 2006).

The most famous inhabitants of the Hell Creek paleoenvironments are obviously the dinosaurs. In 1901, William T. Hornaday of the New York Zoological Society showed a nasal horn of *Triceratops* to Henry Fairfield Osborn of the AMNH and this culminated into the many field expeditions and discoveries by Barnum Brown in the Hell Creek area of Montana (Clemens & Hartman, 2014). More than a century of extensive, quantitative, field-based dinosaur research later, overwhelming evidence has been collected that show that dinosaur abundance and diversity did not decline throughout the HCF until the moment of their complete extinction at the K-Pg boundary, directly linked to the aftermath of the Chicxulub impact (e.g. Schulte et al., 2010; Brusatte et al., 2015). The dinosaur assemblage of the HCF is known as the *Triceratops* fauna (Fig. 1.19) following the nomenclature of Lehmann (1987), since this horned dinosaur is by far the most common dinosaur found within the formation and similar assemblages can be found in coeval formations that reflect coastal lowland environments. An overview of the 22 non-avian dinosaur species found so far in the Hell Creek deposits is given in Table 1.1, subdivided in Ornitischia (herbivores like ceratopsians, hadrosaurs, thescelosaurs, pachycephalosaurs and two families of ankylosaurs) and Saurichsia (carnivores/omnivores like *Tyrannosaurus rex*, ornithomimids, dromaeosaurs and the oviraptor-like caenagnathids). Important to note is that there is still some discussion present about the question whether some species are a valid taxon or should be an ontogenetic stage of an already existing species (see also paragraph 1.1.2). 'Avian dinosaurs', the antecedents of modern bird groups, also lived in the Hell Creek ecosystem. Longrich et al. (2013) identified 17 species of Maastrichtian birds of which seven 'archaic' species (e.g. *Brodavis* sp.) went extinct during the K-Pg boundary, alongside the non-avian dinosaurs.

**Table 1.1.** List of the 22 species within ten families of non-avian dinosaurs known from the Hell Creek Formation (as of April 2016), based on new discoveries over the last decade and the faunal studies from Russel & Manabe (2002), Pearson et al. (2002) and Weishampel et al. (2004).

| Ornitischia | Saurischia |
|---|---|
| **Ceratopsidae**<br>*Torosaurus latus*<br>*Triceratops horridus*<br>*Triceratops prorsus*<br>*Leptoceratops gracilis* | **Tyrannosauridae**<br>*Tyrannosaurus rex* (including *Nanotyrannus lancensis* in this overview) |
| **Hadrosauridae**<br>*Anatotitan copei*<br>*Edmontosaurus annectens* | **Ornithomimidae**<br>*Ornithomimus velox*<br>*Struthiomimus sedens* |
| **Thescelosauridae**<br>*Thescelosaurus neglectus*<br>*Thescelosaurus garbanii* | **Dromaeosauridae**<br>*Acheraptor temertyorum* (Evans et al., 2013)<br>*Dakotaraptor steini* (DePalma et al., 2015) |
| **Pachycephalosauridae**<br>*Pachycephalosaurus wyomingensis*<br>*Stygimoloch spinifer*<br>*Dracorex hogwartsia* (Bakker et al., 2006)<br>*Sphaerotholus buchholtzae* | **Caenagnathidae**<br>*Leptorhynchos elegans*<br>*Anzu wyliei* (Lamanna et al., 2014) |
| **Nodosauridae**<br>*Edmontonia longiceps*<br>*Denversaurus schlessmani* | |
| **Ankylosauridae**<br>*Ankylosaurus magniventris* | |

Sheehan et al (1990) and White et al. (1998) performed one of the first dinosaur population studies within the HCF, but they averaged their census count data over the entire formation and mainly looked at taphonomic patterns. More stratigraphic control was added by the extensive research of Pearson et al. (2002) which revealed a high-resolution vertebrate biostratigraphy of the entire HCF of southwestern North Dakota. However, in terms of dinosaur biodiversity, their database was also constrained by isolated finds of dinosaur bones and teeth within microsites. Horner et al. (2011) carried out the most recent dinosaur census count study of the HCF and they explicitly ignored microsites and focused on articulated/associated skeletons and specific lag deposits. In line of the large-scale Hell Creek Project, the authors added their dinosaur fossils (n = 181) from Garfield County (eastern Montana) in a comprehensive framework including information about geography, taphohistory (which they defined as the history of the specimen from death to final disposition within time and space), stratigraphy, phylogeny and (which was new) ontogeny. The stratigraphic control was based on the Flag Butte lectostratotype of Hartman et al. (2014) and their subdivision into three sequences.

The results of the census count by Horner et al. (2011) are shown in Fig. 1.20, with associated pie charts displaying dinosaur abundance. When averaged over the entire HCF, the seven major dinosaur genera are in decreasing relative abundance listed as follow: *Triceratops* (40%), *Tyrannosaurus* (24%), *Edmontosaurus* (20%), *Thescelosaurus* (8%), *Ornithomimus* (5%), *Pachycephalosaurus* (1%) and *Ankylosaurus* (1%) (Horner et al., 2011). This data clearly shows a high abundance of *Tyrannosaurus* rex fossils within the HCF and demonstrates its position as very successful, apex predator of its time. The presence of the small theropod *Troodon* sp. and other dromaeosaurs within the Hell Creek assemblage has been suggested in previous studies, but this record is scarce and only based on isolated tooth fragments. Therefore, Evans et al. (2013) stated that there is few evidence for more than a single dromaeosaur taxon, namely their new species *Acheroraptor temertyorum*. However, DePalma et al. (2015) proved their conclusion wrong with the discovery of the c. 6 m tall giant dromaeosaur species *Dakotaraptor steini*, which could live alongside *Tyrannosaurus rex* because it probably hunted on prey smaller than adult megaherbivores.

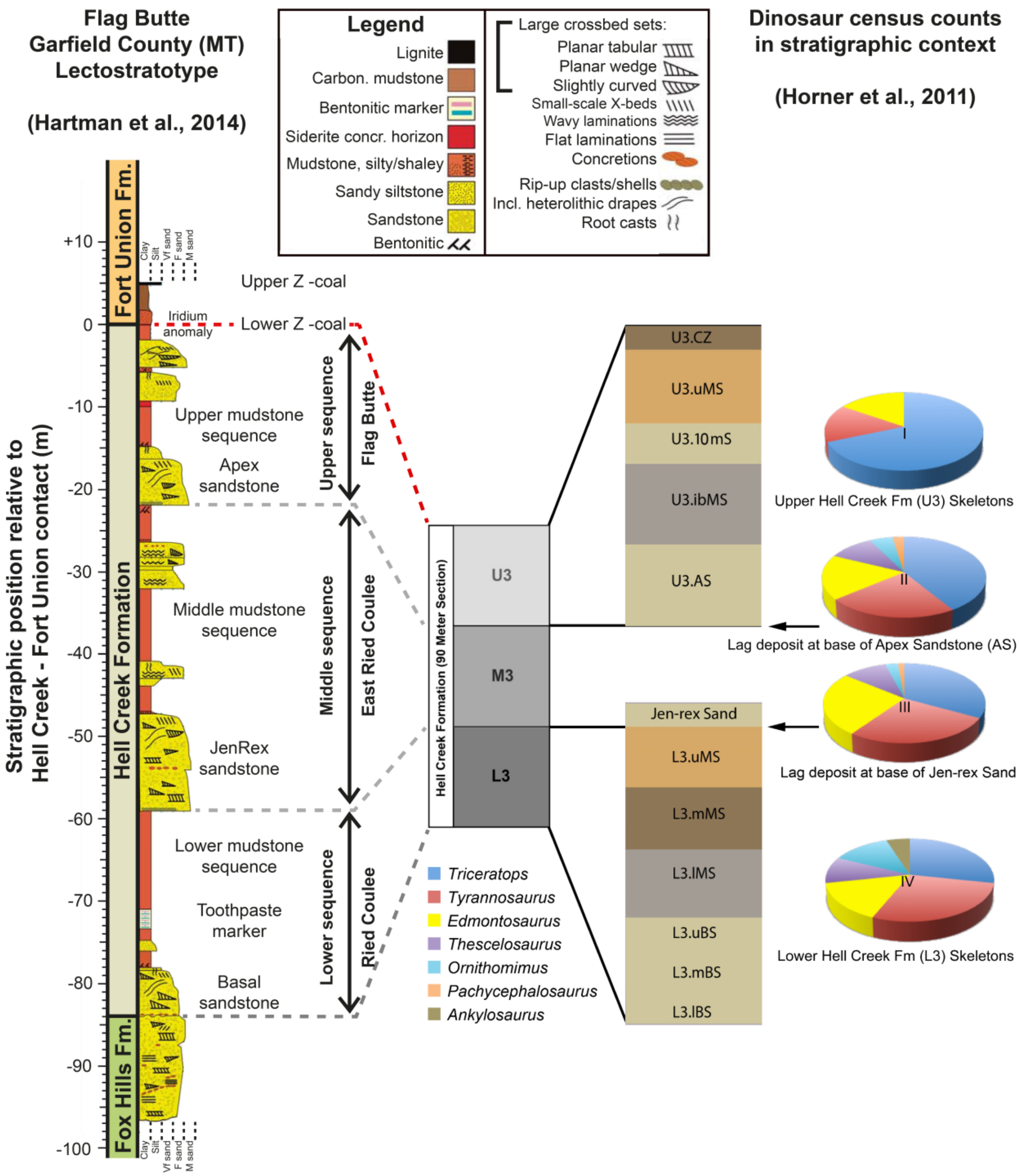


**Fig 1.20**. Overview of the Flag Butte lectostratotype (Hartman et al., 2014) and the associate dinosaur faunal distribution per stratigraphic sequence of the HCF (Horner et al., 2011). Note the relative high abundance of *Tyrannosaurus rex* fossils throughout the formation.

## 1.4. Specimen and study area

In May 2013, Blaine and Michele Lunstad discovered a new specimen of the carnivorous dinosaur *Tyrannosaurus rex* on the ranch of their neighbors Lige and Mary-Ann Murray. Together with local paleontologist Clayton Phipps they exposed a small part of the skull and pelvis and decided to cover it with a jacket to protect it against frost and other weather conditions. Subsequently, a joint excavation was carried out by Naturalis Biodiversity Center (Leiden, the Netherlands) and the Black Hills Institute (Hill City, South Dakota, USA) in August and September 2013 to unearth these dinosaur bones. The rock matrix encasing the fossil consists of a poorly consolidated sandstone and therefore the removal of the overburden using mechanical diggers and shovels occurred very quickly, as can be seen in Fig. 1.21A and 1.21B. Detailed sieving close to the temporary plaster jacketed skull was carried out to make sure no small bone and tooth fragments were lost (Fig. 1.21C). Screening around the pelvis revealed many pieces of rib, gastralia and presacral vertebrae. Approximately two meter above the pelvis-bearing layer a femur and a shoulder girdle were discovered. Soon it became apparent that the fossil locality consisted of bones belonging to only one individual. In addition, small theropod teeth were found around the pelvis block, possibly derived from a scavenging *Nanotyrannus lancensis* (Larson, pers. comm., 2014). Also, a hadrosaur bone fragment was found at the pelvis block which may suggest that the *T. rex* had eaten this duck-billed dinosaur.

High resolution LIDAR (Laser Imaging Detection and Ranging) scanning coupled with photogrammetry was performed at the dig site by a team from Manchester University to produce three-dimensional color images of the articulation of the bones (Fig. 1.21E). Black Hills Institute carried out a traditional method to record the locations of the bones using a grid. The result is illiustrated in Fig. 1.22 and clearly shows that the *T. rex* skeleton is disarticulated. Striking is that the skull was found upside down at the deepest part of the section whereas the pelvis and femur were located higher in the sequence and 10 to 8 m away from the skull, respectively. The elevation difference of 2 m between the skull and the right leg would assume an unexpected dipping of the sandstone layer of 5-10 degrees (Larson, pers. comm., 2014). After two weeks of digging, all bones were recovered and the large bones were covered with plaster jackets to ensure safe transport (Fig. 1.21F). The quality of the recovered bones is remarkable in such a way that they have maintained their original three-dimensional morphology (Fig. 1.21G). In other words, to quote Peter Larson, director of Black Hills Institute and experienced *T. rex* hunter, about this locality: "in more than 50 years of digging I had never seen a site where the bones could be uncovered with the aid of only a paintbrush. I must say that the preservation (of this specimen) is superior to any other Rex."

The specimen contains an articulated skull, left scapula with fused coracoid (left shoulder girdle), furcula (wishbone), much of the axial column, an extraordinarily complete rib cage, a nearly complete pelvis, right leg and a large part of the tail. The only elements that are missing comprises the left leg, both feet and arms, parts of the lower jaws and parts of the tail (Fig 1.22). Provisional bone count at the Black Hills Institute indicates that 53% of the skeleton has been recovered, which grants this discovery a position in the top three of most complete *Tyrannosaurus rex* specimens ever found (Larson, 2008; Appendix 6). First osteological analysis suggests that this *T. rex* specimen is approximately 12 m in length and is of a robust morphotype which represents a female (Schulp et al., 2015; Larson, 2008). In addition, the individual has many healed bone pathologies that may suggest inter-specific combat (Schulp et al., 2015). First insights from a thin section of the rib of this *T. rex* showed many growth lines, but also extensive remodeling. This should point towards a very mature animal, but more detailed histological analysis can provide the minimum age of this specimen in the near future. The skeleton is currently hosted at the Black Hills Institute for the final preparation work. In September 2016, the *T. rex* specimen, currently registered in Naturalis as RGM 792.000, will be transported to the museum in Leiden to form the centerpiece of a new dinosaur exhibition (Schulp et al., 2015).


**Fig. 1.21.** Impression of the activities before, during and after the excavation of the Naturalis *T. rex*. The initial situation on the Murray Ranch before the start of the excavation, with the position of the skull block, is shown in **(A)**. Approximately one week later, a large part of the overburden was removed and most of the bones were exposed **(B)**. To ensure no small bone fragments were lost, detailed seaving of the loose sandstone was performed **(C)** before the large bone and teeth could be uncovered using knife and paintbrush **(D)**. In addition, LIDAR-scanning was performed by the University of Manchester to study the 3D position and articulation of the bones **(E)**. Finally,

the large bones were 'mushroomed', covered with plaster jackets and strengthened with plywood to ensure safe transport, as can be seen with the skull block **(F).** After almost two years of preparation work at the Black Hills Institute, the unique 3D preservation of the bones is beautifully visible in the tail vertebrae **(G)**. Figures A and B were kindly provided by Peter and Tim Larson (Black Hills Institute) and photos D-F were made by Servaas Neijens.

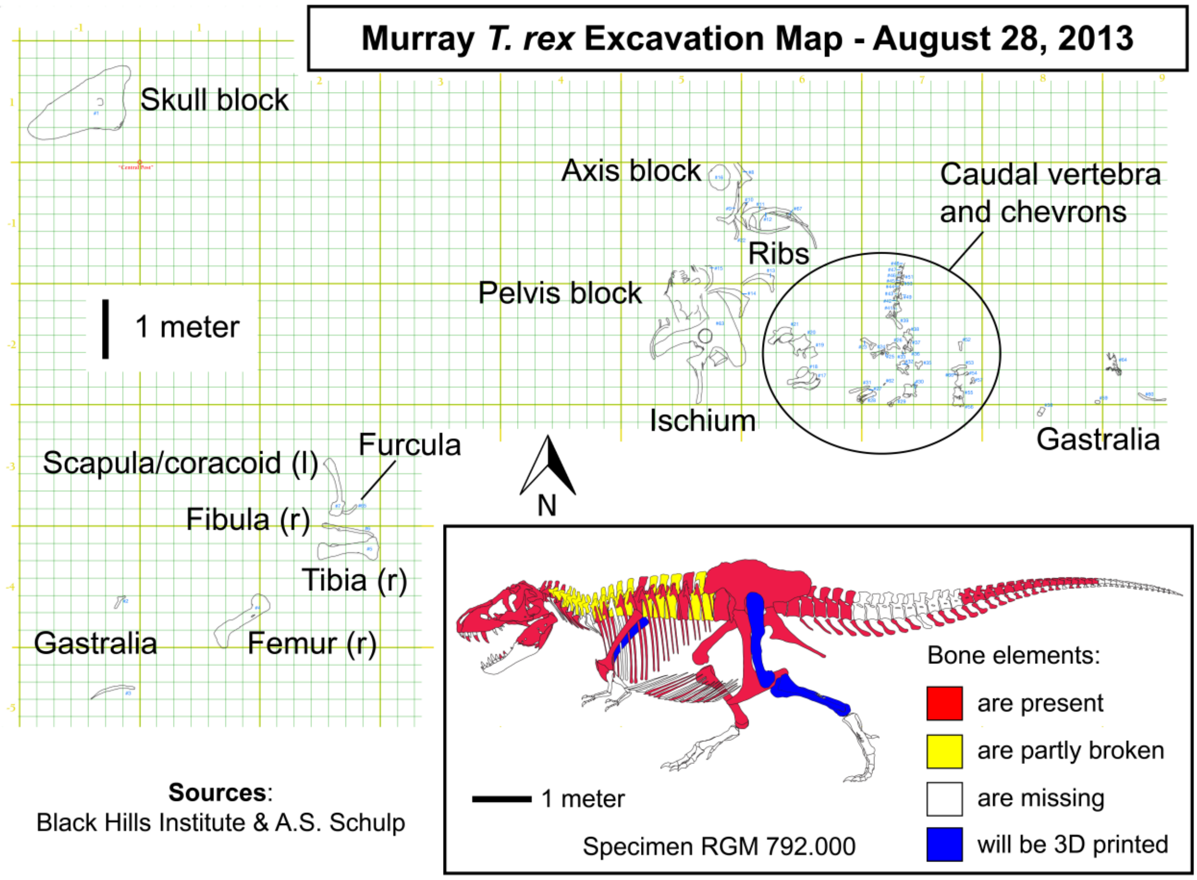


**Fig. 1.22.** The excavation map of the Naturalis *Tyrannosaurus rex* specimen on the Murray Ranch in Montana, created by the Black Hills Institute and shown here with the permission of Tim and Peter L. Larson. The 2D map shows a disarticulated skeleton with the right leg and pelvis block separated respectively 8 and 10 m from the skull block. The silhouette represents a preliminary inventory of the bone count and shows which bone elements are present, partly broken, totally missing or will be 3D printed in mirrored shape for display in the museum exhibition (shown with permission of Anne S. Schulp).

The study area (Fig. 1.23) is situated on the private ranch of Lige and Mary-Ann Murray, c. 50 km southwest from the town of Jordan, Garfield County, eastern Montana, USA. The study area comprises c. 44 km$^2$ of agricultural land and typical *badlands* characterized by shallow incising (dry) creeks, gentle sloping, grass-dominated hills and buttes covered with a hard sandstone cap. The highest morphological features are Emma Butte, Piney Ridge and School Butte (c. 1060-1090 m above sea level) in the southern part of the study area, whereas the Sand Creek in the northern part represents the topographically lowest area (c. 950 m above sea level). Appendix A.1.1-A.1.3 displays digital elevation models of the Murray Ranch. The exposure density throughout the study area is in general very low due to abundant prairie vegetation and recent hillslope processes. Furthermore, the rare rock outcrops show intense surface weathering caused by the extreme weather conditions in this part of the USA. In winter, temperatures can drop to -40°C or lower and the accompanied freeze and thaw cycle results in deep penetrating frost weathering in the subsurface. In summer, the conditions in Garfield County are semi-arid with average temperatures above the 30°C (NOAA). Appendix A.1.4 shows a coarse-scale geological map of the area based on the mapping of Vuke & Wilde (2004). In most of the area, the HCF is exposed, but it is interpreted by Vuke & Wilde (2004) that outcrops from the FUF are present in the high elevation area in the south. The Sand Creek area in the north is interpreted as alluvium from a Holocene river channel. In Fig. 1.23, the red square marks the actual study area (c. 4.8 km$^2$) with the location of the different sections, as described in Chapter 3.

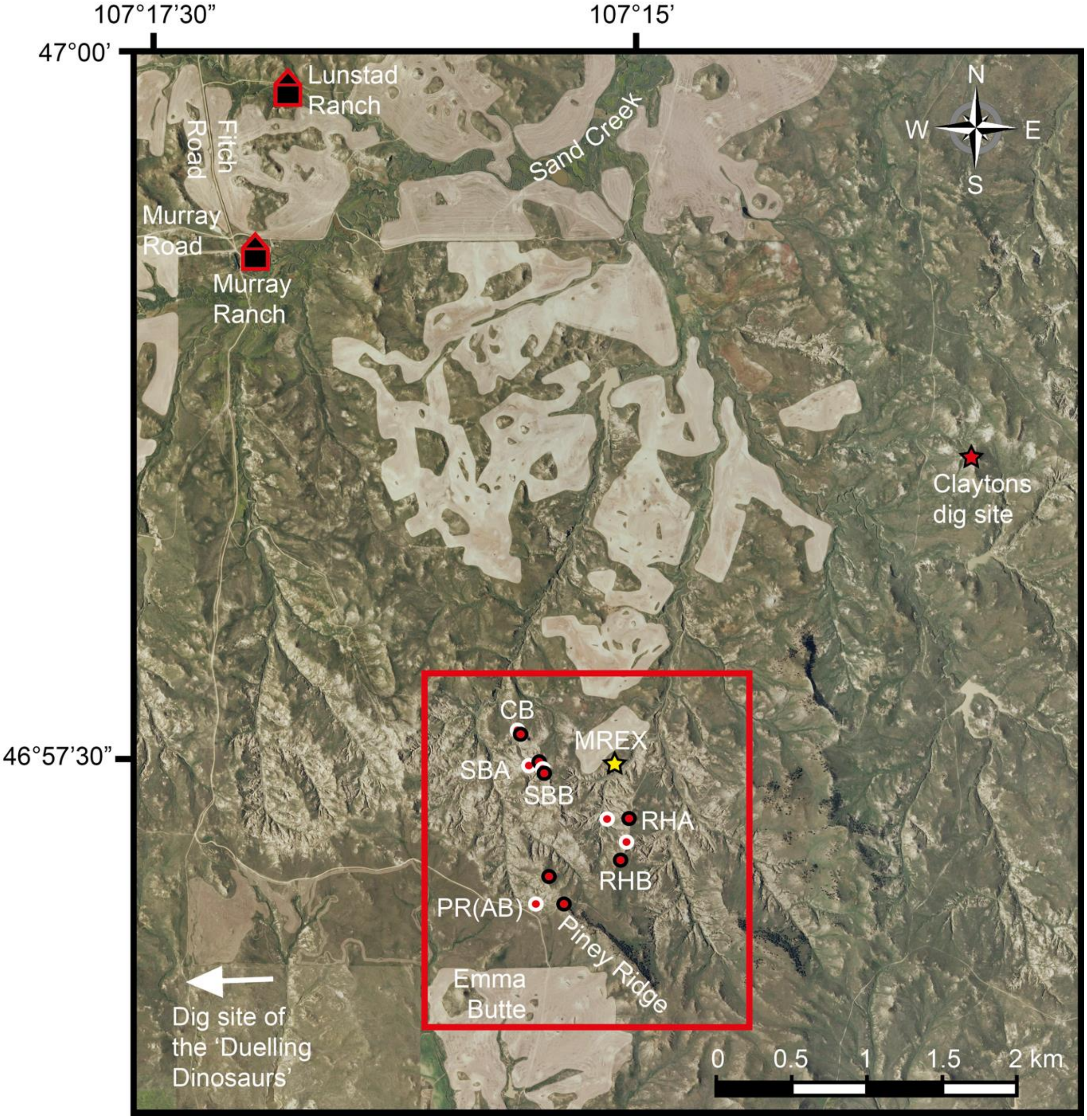


**Fig 1.23.** Aerial overview of the study area of the Naturalis *T. rex* on the Murray Ranch in eastern Montana, USA. The white-red circles mark the position of the base of every section whereas the black-red circles coincide with the top of every section. The orthophotographs used in this figure are produced by the USGS in 2014 (NAIP imagery) and are derived from the 7.5-minute series of the Emma Butte and School Butte Quadrangle, Garfield County, Montana. The red square indicates the actual study area (highlighted in chapter 3: Fig. 3.1) with the various sections indicated: MREX (Naturalis/Murray rex excavation site), CB (Cyclic Butte), SBA & B (Shelly Butte A & B), RHA & B (Rex Hills A & B) and PR(AB) (Piney Ridge A & B section). A digital elevation model (DEM), a 3D model and a geological map of the same area is shown in Appendix 1 (Fig A.1.1., A.1.3. and. A.1.4.).

## 1.5. Research aims and approach

This Master Thesis Report describes the geological setting of the Naturalis *Tyrannosaurus rex* specimen, from a small-scale, fossil site-specific perspective towards a large-scale, temporal and spatial contextual framework. My three main research questions are as follows:

1. How did this *Tyrannosaurus rex* specimen get so well-preserved?
2. What did its paleoenvironment look like?
3. How old are the *T. rex* bearing sediments?

In general, I use a multi-proxy approach combining the fields of vertebrate paleontology, palynology, sedimentology, geochemistry and integrated (litho-, magneto-, cyclo- and bio-) stratigraphy to resolve the three questions stated above. The following paragraphs will zoom in on these specific questions regarding previous work, the novelty of this research and the proposed approach.

### 1.5.1. Sedimentology and taphonomy

The Naturalis specimen is possibly the best preserved (!) *Tyrannosaurus rex* skeleton ever found (Larson, 2014, pers. comm.). It is not the best specimen in terms of amount of completeness, since the famous *T. rex* specimens nicknamed Sue (FMNH PR2081) and Stan (BHI 3033) yields 73% and 63% of the skeleton (by bone count), respectively. Although more complete, Sue shows clear indications of bone deformation. For instance, the skull is severely crushed toward the left side, the snout is compressed ventrally right in front of the orbits, the nasals have been pressed into the external naris and the left maxilla is heavily compressed and partly pulled away from the skull (Fig. 1.24A; Brochu, 2003). Some of the damage on the left side has been interpreted as evidence for a bite wound from another tyrannosaur (Larson & Donnan, 2002), but it is more likely that the depositional conditions responsible for the preservation of the animal played an important role in this. On the contrary, the Naturalis *T. rex* specimen displays no clear shearing in the skull (Fig. 1.24B), although the left jaw shows some compression due to the gliding of broken jaw shards. When the broken pieces are glued together, the skull will be straight and symmetrical again (Schulp, 2016, pers. comm.).

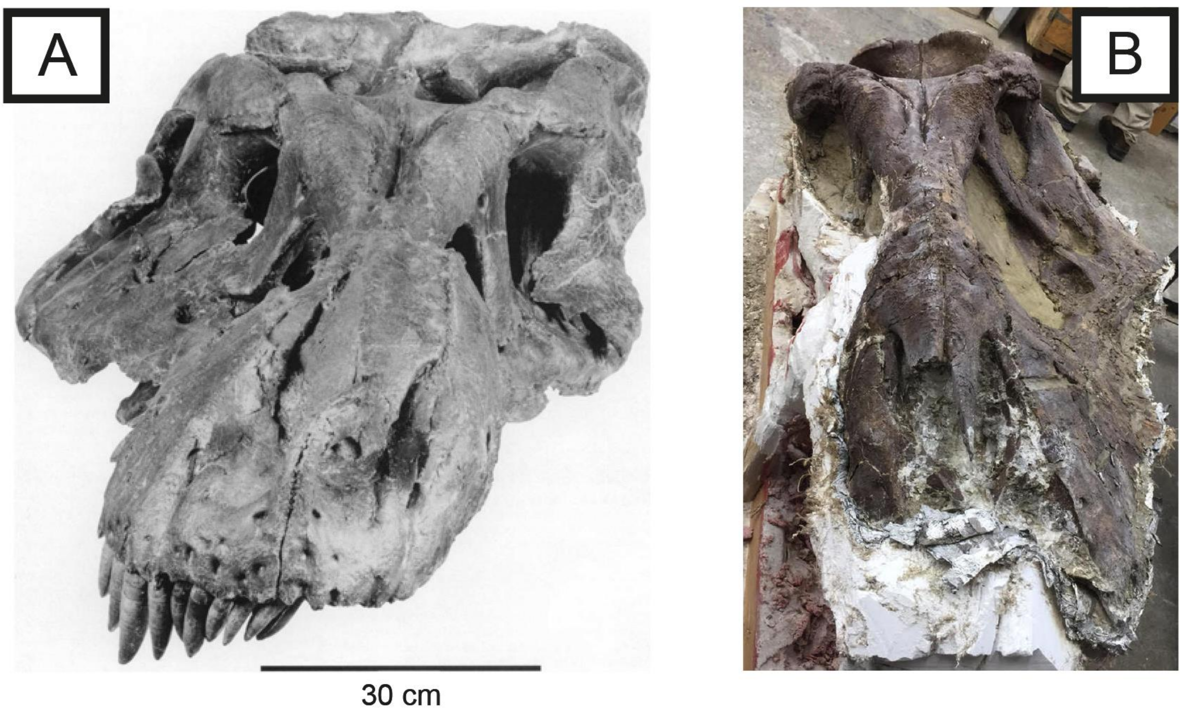

**Fig 1.24.** Anterior view of the skull of *Tyrannosaurus rex* specimen Sue (FMNH PR2081), which shows severe shearing towards the left side **(A)** (Brochu, 2003). On the other hand, the skull of the Naturalis specimen (RGM 792.000) shows no clear signs of post-mortem compression **(B)**.

Which series of events could lead up to the extraordinary preservation of the Naturalis *T. rex*? To unravel this mystery, a thorough understanding of its taphonomic history is needed. Taphonomy is the field of science that studies the transition of organic matter from the biosphere into the geological record (Lyman, 1994) and is thus influenced by both biotic and abiotic factors. Biotic, taphonomic aspects comprise for example the health of the animal before it died (and potential influence on rates of body decay), agents acting upon the carcass before burial (such as scavengers and bone swallowing carnivores) and biological agents acting upon the carcass immediately after burial (e.g. microbial decay that breaks down tissues, fats and bones). On the other hand, abiotic taphonomic factors include environmental agents (water, wind, ice, gravity) as forces that can bury the fossil, but also transport, rework or erode (parts of) the fossil remains causing removal, disarticulation or exposure. Furthermore, formation of concretions, diagenesis (permineralization and replacement) of bone and surrounding sediment and the influence of groundwater movement and composition on bone chemistry can play an important role in the fossilization process and the ultimate preservation (Behrensmeyer et al., 2000).

When new dinosaur discoveries are made, scenarios are often developed on how the particular animal died and what happened between the moment of its death and its ultimate discovery. However, these taphonomic hypotheses are rarely tested and supported with quantitative evidence related to the encasing sedimentary rock. Numerous taphonomic studies have been performed on dinosaur sites within the Campanian Two Medicine Formation in northern Montana (e.g. Rogers, 1990; Rogers & Kidwell, 2000) and the coeval Dinosaur Park Formation in Alberta (e.g. Eberth, 2015), but detailed publications about the vertebrate taphonomy within the Hell Creek Formation are less common (mainly based on the work of White et al., 1998). To my knowledge, detailed taphonomic analysis of *in situ* skeletons of *Tyrannosaurus rex* are only available for the specimen Peck's rex (MOR 980; Derstler and Myers, 2008 b) and Jane (BMR P2002.4.1; Henderson & Harrison, 2008) and only two conference posters deal with the excavation of F-2 Rex (MOR 2925; Hall & Keenan, 2010) and Celeste or C-rex (MOR 1126; Cooley, 2001).

This scarcity of taphonomic studies might be explained by the assumption that *T. rex* (along with other dinosaurs) has suffered from a 'showmanship syndrome' since its first discovery in 1902. Due to its immense popularity, *T. rex* fossils were historically excavated rapidly for display in museums or private collections, especially between the mid 1960s until the mid 1990s (Hall & Keenan, 2010). Once the skeletons were removed from the field, any data not directly recorded during the excavation in association with the bones complicates an accurate taphonomic interpretation. Although for the present study I went back one year after the excavation of the Naturalis specimen, the initial documentation of the bones performed by the Black Hills Institute was relatively complete. In addition, the LIDAR images produced by the Manchester University can give additional information regarding the 3D orientation of the bone elements and sedimentary horizons.

In this Master Thesis Report, I present the first taphonomic study of a *Tyrannosaurus* rex specimen which is combined with a detailed, quantitatively supported, sedimentological analysis. The content and sedimentary structures of the rocks at the excavating site were described at a very high (c. 2 cm) resolution. In addition to qualitative techniques in the field, the sediment characteristics were also identified using thin section microscopy and by means of quantitative techniques such as laser-diffraction grain-size and thermogravimetric (loss-on-ignition) analysis. Using these sophisticated techniques in combination with paleontological data (for instance the articulation and orientations of the bones), it is possible to provide a basic reconstruction of what happened after the *T. rex* of Naturalis died and thereby also elucidate its unique preservation (see Chapter 4).

### 1.5.2. Paleoenvironment

The Hell Creek Formation is widely regarded as a lowland fluvial system fed by erosional sediments from the Rocky Mountains (Fastovsky & Bercovici, 2016). However, detailed paleoenvironmental analysis applied on vertebrate localities within the formation is not often published. The presence of the vertebrate fossil site within the HCF itself offered most scientists enough certainty to give it the label 'fluvial depositional environment'. Unfortunately, by doing so different sub-environments within this sedimentary system can not be identified, such as river channel deposits (thalweg), pointbar, toe-of-point bar, distal levee, crevasse splay, floodplain, marsh, shallow (oxbow) lake and abandoned channel facies (e.g. Kroeger et al., 2002; White et al., 1998). Fastovsky (1987) identified five distinct fluvial facies within the HCF and concluded that the floral and faunal changes seen at the K-Pg boundary are partly artefacts of the depositional system. The different fluvial architectures and associated paleoenvironments from Fastovsky (1987) are applied on the sedimentary strata seen in the study area and described in Chapter 4.

In case of *Tyrannosaurus rex*, despite its popularity, few papers report on the Upper Cretaceous landscape it lived in. Retallack (1994) defined several Late Cretaceous pedotypes from the Bug Creek area and correlated associated ancient climate, vegetation, fauna, topography, (sediment) matrix and the duration of formation. Retallack stated that remains of *T. rex* have been found in so-called Sapakot, Maka and Spatsiko paleosols, but with no clear pattern of preference. McIver (2002) carried out the first thorough paleoenvironmental and paleobotanical reconstruction on a *Tyrannosaurus rex* specimen (named Scotty, RSM 2523.8) from the Frenchman River Formation in Saskatchewan, as she studied the sediments together with the fossil plant remains (including numerous identifiable leaves, seed and fruits) that are preserved in intimate association with the remains of the dinosaur. Derstler and Meyers (2008) and Henderson & Harrison (2008) performed a qualitative examination (based on lithology, sedimentary structures and macroflora only) of the depositional environment of 'Pecks rex' and 'Jane', finding an oxbow lake filling and a typical floodplain sequence, respectively. Lyson & Longrich (2011) executed a broader study testing the patterns of occurrence of the Upper Maastrichtian (dominantly HCF) dinosaur fossils in association with the lithology in which they got preserved (sandstone versus mudstone). They found that *Tyrannosaurus rex* (based on 45 specimens containing at least 2 associated bone elements) shows no preferred association for sandstone or mudstone deposits and hence occupied both river and floodplain environments.

In Chapter 4, I present a possible reconstruction of the habitat of the Naturalis' *Tyrannosaurus rex* and will compare it to the study of Lyson & Longrich (2011) and other *T. rex* specimens of which the paleoenvironment was analysed. Besides a qualitative study of the variations in lithology, sedimentary structures and macrofossils throughout the sequence, I also used quantitative grain-size and loss-on-ignition data to infer paleostream velocity and redox conditions (such as anoxia) before, during and after the burial. Furthermore, I performed a palynological pilot-study of clay-rich sediments just below the *T. rex* specimen and higher up in the sequence to interpret the past vegetation. Since taxonomy of pollen and spores is very time-consuming, I used predominantly the general approach of Vajda et al. (2013) to subdivide the palynomorph taxa into 4 distinct groups: land-ferns, aquatic ferns, gymnosperms and angiosperms. Combining the qualitative and quantitative sedimentary and geochemical data together with the palynological results, I provide the reader with a snapshot into the terrestrial ecosystem of the *Tyrannosaurus rex* of Naturalis.

### 1.5.3. Integrated stratigraphy

Unfortunately, fossil bone material older than c. 0.5 Myr can not be dated by radio-isotopic techniques such as $^{14}C$ or U-Th dating (e.g. Van der Plicht et al., 1989). Attempts for direct U-Pb dating of dinosaur bones were performed (e.g. Fassett et al., 2011), but the validity of these dates is heavily questioned since bone recrystallization and the not-closed nature of the associated U-Pb system may have obscured the data (e.g. Koenig et al., 2012). In order to constrain the geological age of the Naturalis *T. rex* site, I had to focus on a long sequence of Hell Creek rock layers including the *T. rex* bearing horizon. As already extensively described in paragraph 1.3.6, chronostratigraphy within the HCF has always been its 'Achilles heel' due to the lenticular behavior of the fluvial deposits and the lack of 'tonsteins' in coal layers for constraining reliable absolute age control. Much research has been done regarding the stratigraphy surrounding the K-Pg boundary which allow fairly detailed 'top to bottom' stratigraphic placement of fossils in the upper third of the Hell Creek strata. However, Johnson (2008) stated correctly that more radio isotope dates near the base of the HCF are needed to refine the age models for Maastrichtian terrestrial fossils. The spatial and temporal extent of the suggested unconformity between the HCF and underlying FHF is still unknown and this hampers 'bottom-up' stratigraphic placement of fossils from the *Triceratops* fauna within the lower two-third of the HCF.

Despite all these challenges, I tried to pinpoint the Naturalis' *Tyrannosaurus rex* as accurately as possible in time by using an integrated stratigraphic approach similar to the methodology of Harrison et al. (2013). They tried to date *T. rex* specimen 'Jane' using pollen, leaves and paleomagnetism and ended up with an estimated age with an accuracy of c. 100 kyr. I carried out a magnetostratigraphic study at the burial site including upward extension in nearby sections and I performed a palynostratigraphic pilot-study using the biostratigraphic age model of Nichols (2002). Due to the scarcity of fossil leaves in the study area, a paleobotanical examination was not possible.

Instead, a novel stratigraphic approach was tested in the study area that is known as cyclostratigraphy. This method uses the Milankovitch theory of climate change and the registration of astronomically induced climate forcing within the stratigraphic record (e.g. Hilgen et al., 2015). The Milankovitch parameters eccentricity (with a duration of c. 405 and 100 kyr), obliquity (c. 41 kyr) and precession (c. 21 kyr) causes cyclic variations in solar insolation on the Earth surface on (so-called orbital) time scales of $10^4$ to $10^6$ years and their periodicities can be used to constrain an accurate geological timescale. The fluctuations in received solar energy through time resulted in climate changes that can be recorded in distinct regular alternating layers of sedimentary rock. Cyclostratigraphy in marine deposits (for instance sapropel-marl or limestone-marl alternations) have proven its reliability over the past decades, since especially the deep marine realm is not prone to intense erosion and large changes in sedimentation rates (Hilgen et al., 2015). Cyclostratigraphy in terrestrial strata was for a long time restricted to lacustrine successions, but since the pioneering work of Abels et al. (2013) in the Bighorn Basin in Wyoming, it has been suggested that cyclostratigraphy is applicable on fluvial deposits as old as the Eocene. With a possible precision of 20 kyr or even less, cyclostratigraphy is the dating technique with the highest resolution so far on geological time scales, but only when this method is coupled to techniques that ensure reliable absolute age control, such as $^{40}Ar/^{39}Ar$ dating.

A short field expedition on the Murray Ranch during the excavation in 2013 suggested the sedimentary horizons surrounding the *T. rex* burial site could potentially be influenced by Milankovitch cyclicity (Abels, 2014, pers. comm.). High resolution lithostratigraphic logging and grain-size and thermogravimetric analysis can identify the characteristics of the different sedimentary variations throughout the section. This way, I try to understand the phase relationship between the cycles of solar insolation intensity (e.g. precession) and its climate response in the sedimentary record in terms of different paleoenvironmental end-members. By determining and counting the repetitive layers of these paleoenvironmental end-members, I can hopefully place the sedimentary record of the *T. rex* in an astronomically tuned geological time scale, constrained with a first order age model based on bio-magnetostratigraphy.

Moreover, the Naturalis *T. rex* site is located in a relatively unexplored part of the HCF. Most, if not all, publications on the formation in Garfield County concerns the outcrops on the southern shore of the Fort Peck Reservoir, north of Jordan, in the so-called Hell Creek type locality. These exposures contain a long record of the FHF, HCF and FUF, since (fluvio)glacial and fluvial erosion during the Quaternary have created deep incisions in the badlands. The less incised Hell Creek outcrops in Garfield County situated south of Jordan, on the southern flank of the Blood Creek Syncline, have not got much scientific attention although interesting discoveries (e.g. the Dueling Dinosaurs) have been made in this region. The Naturalis specimen is the only known *Tyrannosaurus rex*, to my knowledge, that has been discovered in Garfield County south of Jordan. Therefore, the challenge is to place this specimen in a regional stratigraphic framework based on composite studies from northern Garfield County and southwestern North Dakota which are separated from the study area by c. 70 km and c. 280 km, respectively. In Chapter 4 of this thesis, the Naturalis *Tyrannosaurus rex* site is correlated with a new chronostratigraphic framework (covering the most recent ages of all known geochronologic tie-points) of both the Flag Butte lectostratotype in Montana and the Mud Buttes composite section in North Dakota. By doing so, I put this fossil locality in the most accurate temporal framework currently possible which can serve as a pilot study to add more *T. rex* specimens within this age-constrained database. Ultimately, this temporal context gives much more scientific value to these dinosaur specimens, since it can aid in testing important ecological and evolutionary hypotheses.

In the end, this Master Thesis report on the geological context of this dinosaur specimen may serve as a starting point for further research, education and exposition purposes regarding the *Tyrannosaurus rex* of Naturalis Biodiversity Center. Ongoing and/or future research plans concern for instance CT-scanning, paleopathology, biomechanics, soft-tissue studies, isotope geochemistry and histological analysis of the specimen. These modern techniques, combined with the essential geological information, can help to infer the ancient life-style, locomotion, diet and habitat of this *Tyrannosaurus rex*. Furthermore, using this multidisciplinary approach, we can make an as accurately as possible reconstruction of the life, death and post-mortem history of this iconic dinosaur during the Late Cretaceous all up to the moment it was discovered in 2012 by Michele and Blaine Lunstad.

# 2. Methods

In this chapter, the applied methodologies and the materials used in this Master Thesis project are listed. Firstly, the various geological field methods carried out at the study area in eastern Montana are explained in detail. The sediment samples collected in the USA are used in the Sediment Analysis Laboratory and Geotechnical Laboratory at the VU to perform grain-size and thermogravimetric analysis and to make rock thin sections and pollen slides. These techniques are described in this order in paragraph 2.2 to 2.5. In paragraph 2.6, the paleomagnetic methods are described ranging from coring in the field to magnetic susceptibility, thermal demagnetization and alternating field demagnetization at the Paleomagnetic Laboratory Fort Hoofddijk, Faculty of Geosciences, Utrecht University. The combined field and laboratory sampling strategy of this Master Thesis yielded in total 103 grain-size samples, 104 thermogravimetric samples, 22 pollen slides, 6 rock thin sections and 80 analyzed paleomagnetic cores where 50% were measured with thermal demagnetization and 50% with the alternating field technique.

## 2.1. Fieldwork

Geological fieldwork was conducted at the Murray Ranch in eastern Montana from 22 September until 12 October 2014. The field campaign consisted of a detailed sedimentologic analysis and the making of a lacquer peel at the Naturalis *Tyrannosaurus rex* excavation site, the construction of a lithostratigraphic framework of in total 7 different sections and geological mapping of the surrounding area using Differential GPS and GIS data.

### 2.1.1. Lacquer peel

One of the first activities at the study area included the creation of a sedimentary lacquer peel at the dig site of the pelvis of the Naturalis *T. rex* specimen, using standard techniques described in detail by Voigt (1949), Maarse & Terwindt (1964) and Van Baren & Bomer (1979). This lacquer peel will be displayed in the new *T. rex* exhibition in Naturalis from September 2016 showing internal sedimentary structures in the unconsolidated sandstone that may give clues about possible burial scenarios for the dinosaur.

First of all, a trench of c. 80 cm wide and 1.80 m high was dug with pickaxe and shovel (Fig 2.1.A) at the location of the pelvis block and a smooth inclined surface of c. 60 – 70 degrees was created with a machete. A horizontal surface at the top of the peel was created for pouring the lacquer solution as a front over the sediments (Fig 2.1.B). Several chemicals can be used as a high viscosity lacquer. In the Netherlands, a cellulose nitrate lacquer with thinner is commonly used (Van Baren & Bomer, 1979). During this fieldwork Vinac was used, these polyvinyl acetate beads are dissolved in acetone and were kindly provided by P. Larson of the Black Hills Institute. After the first lacquer coating has dried for approximately a day, a fine cheesecloth is attached on the peel surface (Fig 2.1.C) and again the lacquer solution was applied liberally to the cloth with a paint brush. After another day of drying, the peel was ready to be removed using a plywood board of c. 65 cm and 165 cm. The wooden board was glued on one side and this sticky side was leaned against the cheesecloth (Fig 2.1.D). By careful pulling the cheesecloth back onto the board and rotating everything horizontal, the lacquer peel is completed and can be transported and studied in detail (Fig 2.1.E).


A
B
C
D
E

**Fig. 2.1.** The field method of making lacquer peels of sedimentary structures includes the digging of a trench **(A)** and the pouring of a lacquer solution over a smoothened inclined surface **(B)**. After drying, a fine cheesecloth is attached on the peel surface and glued again **(C)**. Subsequently, a glued plywood board is leaned on the cheesecloth and finally this cheesecloth containing the sediments is pulled back onto the board **(D and E)**.

### 2.1.2. Lithostratigraphic logging

To ensure accurate stratigraphic logging and good quality sediment samples, a fresh, unweathered rock surface should be reached. Therefore, c. 1 m wide trenches are dug using pick-axe and shovel (Fig 2.2.A) at selected sections in the study area. A Precision Jacob's Staff of 1.6 m with an 8047-15 Abney Level (both from ASC Scientific) is used to accurately measure stratigraphic heights in the field within and between sections (Fig 2.2.B). Lithological field descriptions of the outcrops include qualitative data on sediment grain size, color, content of organic (e.g. fossil plant remains, roots, amber, shell fragments) and inorganic (e.g. Fe or Mn nodules) components, sedimentary structures and fossil bone remains. Color classification of sediments is performed using the Munsell Standard Soil Color Chart (1995 edition, from Eijkelkamp Agrisearch Equipment) (Fig 2.2.C). Hand sampling and field descriptions are based on the methods described in the Soil Survey Manual (Soil Survey Division Staff, 1993). Sediment samples are taken at a regular interval (Fig 2.2.D), ranging from a 2 cm resolution at the Naturalis *T. rex* site (MREX) to 10 cm resolution at the Cyclic Butte section (CB) and at different lithological units (and thus irregular resolution) at Shelly Butte B Section (SBB). The procedure for collecting paleomagnetic samples is described in section 2.6.1.

### 2.1.3. Geological mapping

Mapping of the area was carried out using an iPad Air 2 equipped with a GPS receiver and the software GIS Pro (Garafa, LLC). Detailed topographic, ortho- and geological maps of the regional study area in Garfield County were available from the online databases of the US Geological Survey (USGS) and Montana Bureau of Mines and Geology (MBMG). The geological maps of the Melstone and Sand Springs 30' x 60' Quadrangle (MBMG, Vuke & Wilde, 2004) and the ortho and topographic data of the Emma Butte Quadrangle (USGS 7.5 minute series) were mostly used. Furthermore, a portable Trimble Differential GPS (DGPS) (Fig 2.2.E) was used in the field to accurately measure the altitude up to c. 1 m precision. The focus was on tracing characteristic marker beds (e.g. distinct calcrete, carbonaceous shale or shell horizons) (Fig 2.2.F), because these strata are in general visible over relatively large distances. In addition, the elevation of the base and top of every section was measured to verify the correlations made in the lithostratigraphic framework presented in Chapter 3. However, caution should be taken because the exposure density in the study area is low, Hell Creek sediments are often lenticular in geometry and a small dip in strata over a long distance could influence the correlations.

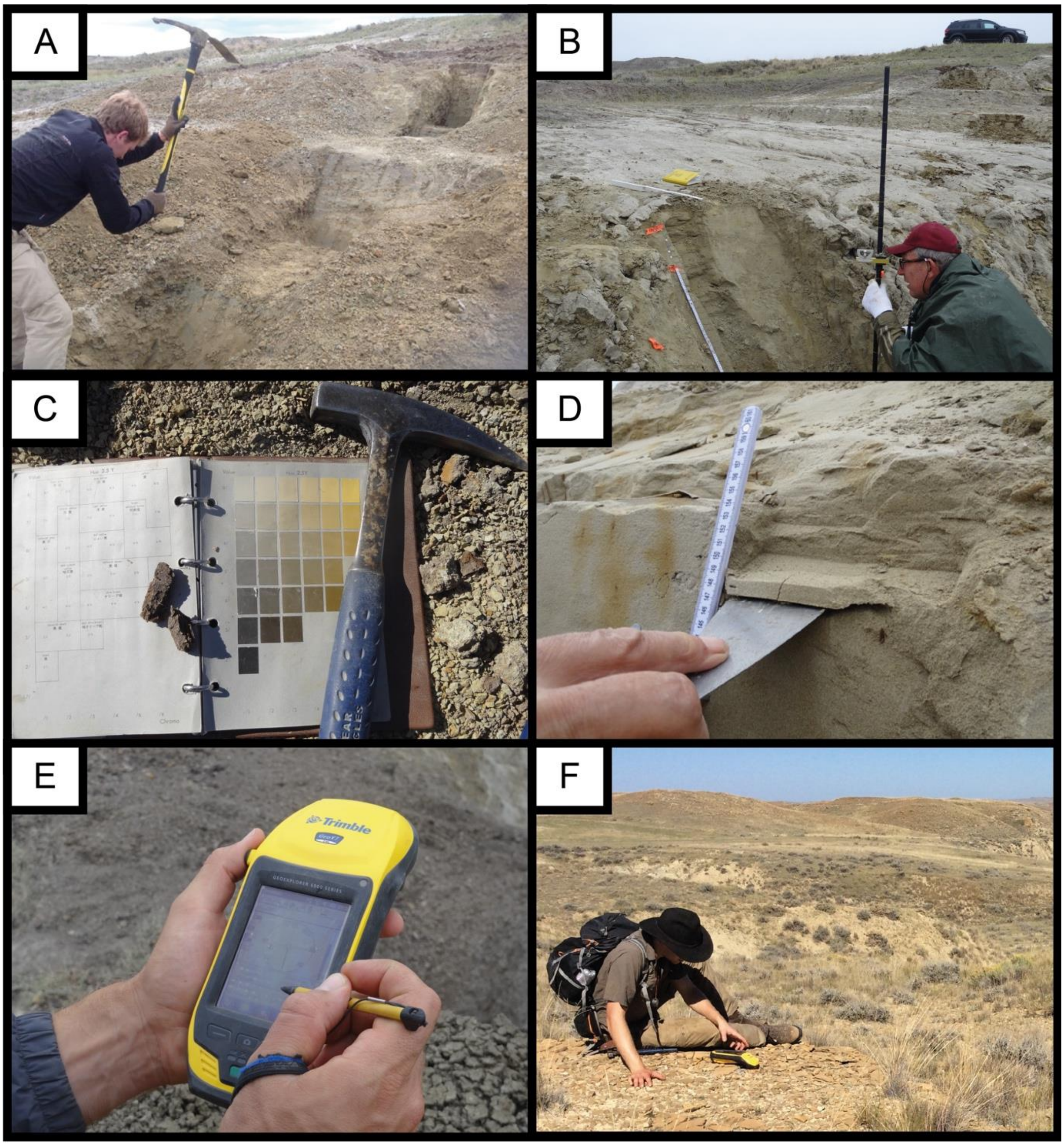


**Fig 2.2.** An overview of the field methods used during the Montana field campaign in 2014. Trenches were dug in the subsurface using pick-axe and shovel to make sure fresh rocks are described and sampled **(A)**. A Jacob's Staff with Abney Level is used for accurate stratigraphic height measurements within and between sections **(B)**. Qualitative lithological descriptions of the trenches are made focusing on grain-size, sedimentary structures, organic and inorganic features and Munsell soil color **(C)**. Sediment samples are taken at a high resolution **(D)** (ranging from 2 to 10 cm) for grain-size and thermogravimetric analysis at the VU. The geological mapping of the study area is possible using a Trimble Differential GPS receiver **(E)**, which is used in such a way that accurate elevation measurements are conducted on distinct topographic or sedimentary levels to help the correlation of the poorly exposed strata in this region **(F)**.

## 2.2. Grain-size analysis

Grain-size or particle size is one of the most important physical characteristics of sediments and sedimentary rock. It refers to the diameter of individual grains of sediment and the primary classification of sediments is based on this feature. Siliciclastic sediments can be classified using the Wentworth scale into clay (< 8 µm), silt (8 - 63 µm), sand (63 - 2000 µm) and gravel (> 2000 µm) (Table 2.1). Grain-size data are distributions and they offer powerful proxies of past environmental and climatic conditions that are related to sediment sorting processes such as entrainment, transport and deposition (e.g. Visher, 1979). Grain-size distributions are often multimodal and asymmetrical in character, because sediments get mixed during deposition. Traditional statistical techniques (e.g. described by Folk, 1966), such as the mean, median, standard deviation, percentage of the clay, silt or sand fraction, kurtosis, and skewness of grain-size distributions, are unable to address all the complexity.

Unmixing grain-size distributions into several dominant components, known as grain-size end-members, can help to solve this complexity. Using an End-Member Analysis, which statistically fits a finite number of end-members to a given dataset, is a powerful method to decompose grain-size distributions into geologically meaningful parts to better understand sediment provenance and distinguish different depositional processes. Over the past two decades, several end-member modelling techniques have been developed ranging from FORTRAN codes (Prins & Weltje, 1999; Weltje, 1997), Matlab scripts (Dietze et al., 2012; Paterson & Heslop, 2015), R-packages (Dietze & Dietze, 2013) and an alternative hierarchial Bayesian statistical approach (Yu et al., 2015). These techniques all show their value in unraveling modern and past depositional dynamics in a variety of sedimentary systems, ranging from marine (e.g. Prins & Weltje, 1999; Prins et al., 2002; Van der Lubbe et al., 2014), aeolian (e.g. Prins & Vriend, 2007) and fluviatile (e.g. Toonen, 2013) to lacustrine environments (e.g. Dietze et al., 2014).

**Table 2.1.** Grain-size classes used in this study and the associated size range in µm.

| Class | Grain-size (µm) | Class | Grain-size (µm) | Class | Grain-size (µm) |
|---|---|---|---|---|---|
| **Clay** | < 8 | **Silt** | 8 – 63 | **Sand** | 63 – 2000 |
| | | Very fine silt | 8 – 16 | Very fine sand | 63 – 125 |
| | | Fine silt | 16 – 32 | Fine sand | 125 – 250 |
| | | Coarse silt | 32 – 63 | Middle coarse sand | 250 – 500 |
| | | | | Coarse sand | 500 – 1000 |
| | | | | Very coarse sand | 1000 – 2000 |

### 2.2.1. HELOS Laser Diffraction

The grain-size distributions of selected field samples are measured using the Sympatec HELOS/KR laser diffraction particle-size analyser of the Sediment Analysis Laboratory at the VU. The HELOS (Helium-Neon Laser Optical System) is accommodated with an advanced wet dispersing system (known as QUIXEL) suitable for grain-size analysis on all kind of suspensions and emulsions in the size range of 0.12 µm to 2000 µm (Sympatec www.sympatec.com/EN/LaserDiffraction/LaserDiffraction.html). Although the entire MREX section was sampled at a vertical resolution of c. 2 cm, it was decided that the samples were measured at a regular interval of 10 cm due to sample costs. The CB section was also analysed at a 10 cm resolution, whereas the SB section was measured on basis of lithological units instead of a regular stratigraphic interval.

Prior to laser diffraction, the sediment samples had to be prepared following the procedure of Konert & Vandenberghe (1997) to ensure solely the lithogenic fraction is measured (Fig. 2.3). Approximately 200 mg of pure clay samples and 10 g of pure sand samples are added to graduated beakers of 800 ml to attain a beam obscuration of 15 to 25% on the HELOS device.

The samples are treated with 5 - 10 ml of 30% hydrogen peroxide ($H_2O_2$) (Fig 2.3.A) and are subsequently heated to boiling point (Fig. 2.3.B) to accelerate the chemical process and to make sure all organic matter is oxidized. After boiling, the walls of the beakers are cleaned to ensure all sediment is at the bottom of the cups before the beakers are filled up to the top with water. After leaving the suspension standing overnight and decantating down to c. 50 ml, the next step is to remove all carbonate material by adding 5 - 10 ml of 10% hydrochloric acid (HCl) and subsequent heating to boiling point (Fig. 2.3.B). To prevent clumping of clay minerals to agglomerates and thereby biased laser diffraction results, 300 mg of sodium pyrophosphate ($Na_4P_2O_7 \cdot 10H_2O$) is added to the suspension, followed again by heating it until the boiling point. After cooling, the samples in suspension can be measured in the HELOS Laser Diffraction sensor device (Fig 2.3.C), with the resulting pure lithogenic grain-size distribution data expressed in volume percentage (vol %). The best results are received when the samples are diluted in such a way that a concentration between 25% and 15% is achieved.

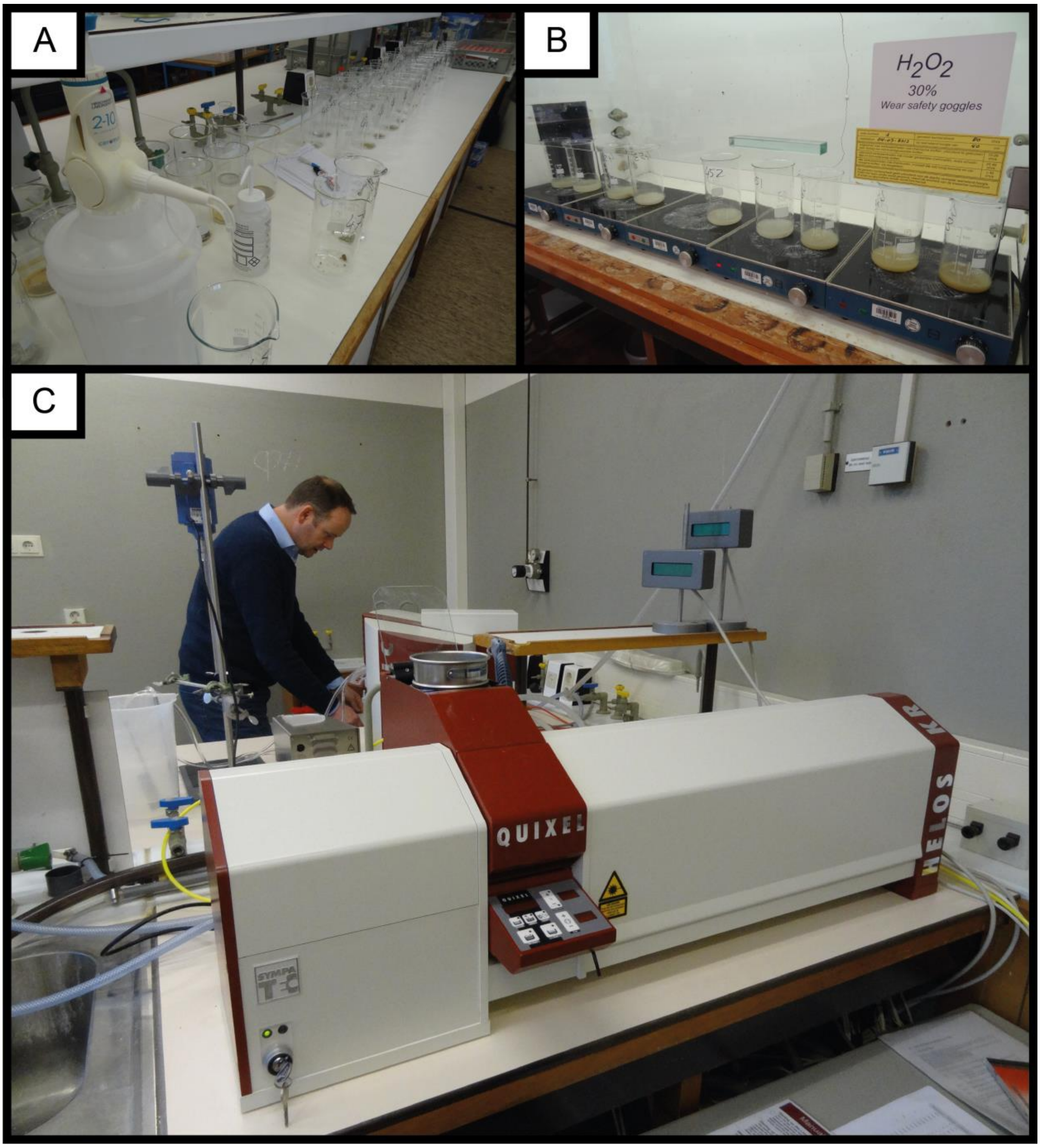

**Fig. 2.3.** The procedure for grain-size analysis at the VU. Sediment samples are treated with $H_2O_2$ and HCl **(A)** and subsequently heated to the boiling point **(B)** to remove organic and carbonate material. Between the $H_2O_2$ and HCl treatment, the samples have to be filled to the top with water, left standing overnight and decantated the next day. $Na_4P_2O_7 \cdot 10H_2O$ is added to prevent clay-clumping before the solutions, with a residue of the lithogenic fraction, can be measured in the HELOS/KR QUIXEL laser diffraction particle-size analyser **(C)**.

### 2.2.2. End-member Modelling Algorithm

The complete lithogenic grain-size distribution dataset (n = 103) is used as input for the End-Member Modelling Algorithm (EMMA). All data from the MREX, CB and SB sections were used in EMMA to cover the full variation in grain-size distributions of the Hell Creek deposits on the Murray Ranch. The specific EMMA-technique of Weltje (1997) and Prins & Weltje (1999) was used in this study, mainly because of practical reasons, since Dr. Maarten Prins kindly performed the end-membering using the DRS-Unmixer Software of Heslop (2008).

The EMMA technique of Weltje (1997) and Prins & Weltje (1999) was the first mathematical method that resulted in a numerically stable and statistically rigorous solution for the complex mixing problem in sedimentary geology. EMMA has been designed to provide the simplest possible explanation of the observed variation among a set of composition in terms of (un)mixing (Weltje & Prins, 2003; 2007). An advantage of EMMA compared to traditional curve-fitting algorithms is that the number of grain-size distribution end-members and the shapes of their curves do not have to be specified within EMMA. Some of the new developed EMMA-techniques (e.g. from Dietze et al., 2014) resulted in end-members with an unrealistic bimodal grain-size distribution (Prins, 2016, pers. comm.). The EMMA-technique of Weltje (1997) and Prins & Weltje (1999) has proven its reliability when applied to large data sets of complex polymodal grain-size distributions, because it commonly results in unimodal endmembers which are expected when considering the fractionation during production or dispersal of sediments (Weltje & Prins, 2007).

## 2.3. Thermogravimetric analysis

Organic and carbonate content are important characteristics of soils and sediments and can be used to study soil quality, to distinguish and quantify various plant, animal and mineralogical material within the matrix and to infer modern and past environmental and depositional conditions. A traditional technique to determine the amount of organic matter and carbonate minerals in sediments includes sequential loss-on-ignition (LOI) using step-wise heating. This method is based on differential thermal analysis: organic matter begins to ignite at about 200 °C and is completely depleted at about 550 °C, and most carbonate minerals are destroyed at higher temperatures (between 800 and 1000 °C) (Santisteban et al., 2004). The weight loss during these chemical reactions is easily measured by weighing the samples before and after heating and is closely linked to the organic and carbonate content of the sediment (Heiri et al., 2001).

However, this conventional technique has some disadvantages. Difficulties with accurate temperature control of the furnace, the lack of a standard method used resulting in time-consuming corrections and the complexity of distinguishing different clay and carbonate minerals are some of the major drawbacks (Konert & Beets, unpublished). At the Sediment Analysis Laboratory of the VU a novel technique is developed to overcome these problems by performing thermogravimetric analysis (TGA) (Fig 2.4) with a device that measures weight loss as a function of temperature in a controlled environment and with a precise internal balance (Konert & Beets, unpublished). This instrument, the LECO TGA701, is connected to a computer and consists of a multiple sample furnace that allows up to 19 samples to be analyzed simultaneously. Each sample in the rotating carousel has a weighting moment of 2 minutes per temperature step. The furnace temperature is step-wise increased from 25 °C to 1000 °C during a run of approximately 3 to 4 hours. In addition, the TGA device uses a continuous flow of different gasses such as compressed air, pure oxygen, carbon dioxide or nitrogen which allows different analysis to be used (see Table 2.1 for a summary of the different analyses).

Before TGA can be performed, the sediment samples have to be crushed with a mortar to a homogeneous mixture (Fig 2.4.A) to make sure the exposure surface of the material during heating is very small. Subsequently, the samples are dried overnight in an oven with a constant temperature of 50 °C to remove most of the moisture (Fig 2.4.B). One teaspoon (c. 1 to 2 grams) of sample powder is suggested to add to the ceramic crucibles that are put into the carousel of the TGA device (Fig 2.4.C). The first program step is always the drying step until 105 °C, which releases the adsorbed water, to secure all calculations are performed with an oven dried initial weight (Konert & Beets, unpublished). The resulting carbonate and organic matter content of the samples are both expressed in weight percentage (wt%) of dry mass. By studying the raw TGA data (including the first derivative of weight loss per temperature step per sample), a discrimination between different clay minerals (e.g. montmorillonite, kaolinite, illite and muscovite) and carbonate minerals (aragonite, siderite, dolomite, calcite and aragonite) is possible and provides useful information since these minerals are formed under different (paleo)environmental conditions (Konert & Beets, unpublished).

**Table 2.2.** Scheme of TGA-steps commonly used at the VU with a ramp rate of 10 °C/min (Konert & Beets, unpublished).

| Step name | Start/end temp. (°C) | Atmo-sphere | Equation | Information |
|---|---|---|---|---|
| Moisture | 25 – 105 | Air | ((W[Initial]-W[Moisture])/W[Initial])*100 | Water in the sample evaporates providing the moisture content |
| LOI-330 | 105 – 330 | $O_2$ | ((W[Moisture]-W[OM-330])/W[Moisture])*100 | The easily burned organic matter (OM) is combusted, this is called LOI-330 |
| LOI-550 | 330 – 550 | Air | ((W[Moisture]-W[LOI-550])/W[Moisture])*100 | The tougher to burn humus is burned, known as LOI-550 |
| $CaCO_3$ | 550 - 1000 | $CO_2$ | ((W[RestLOI]-W[CaCO3])/W[Moisture])*10000/44 | The inorganic carbonate ($CaCO_3$) is burned at high temp. |

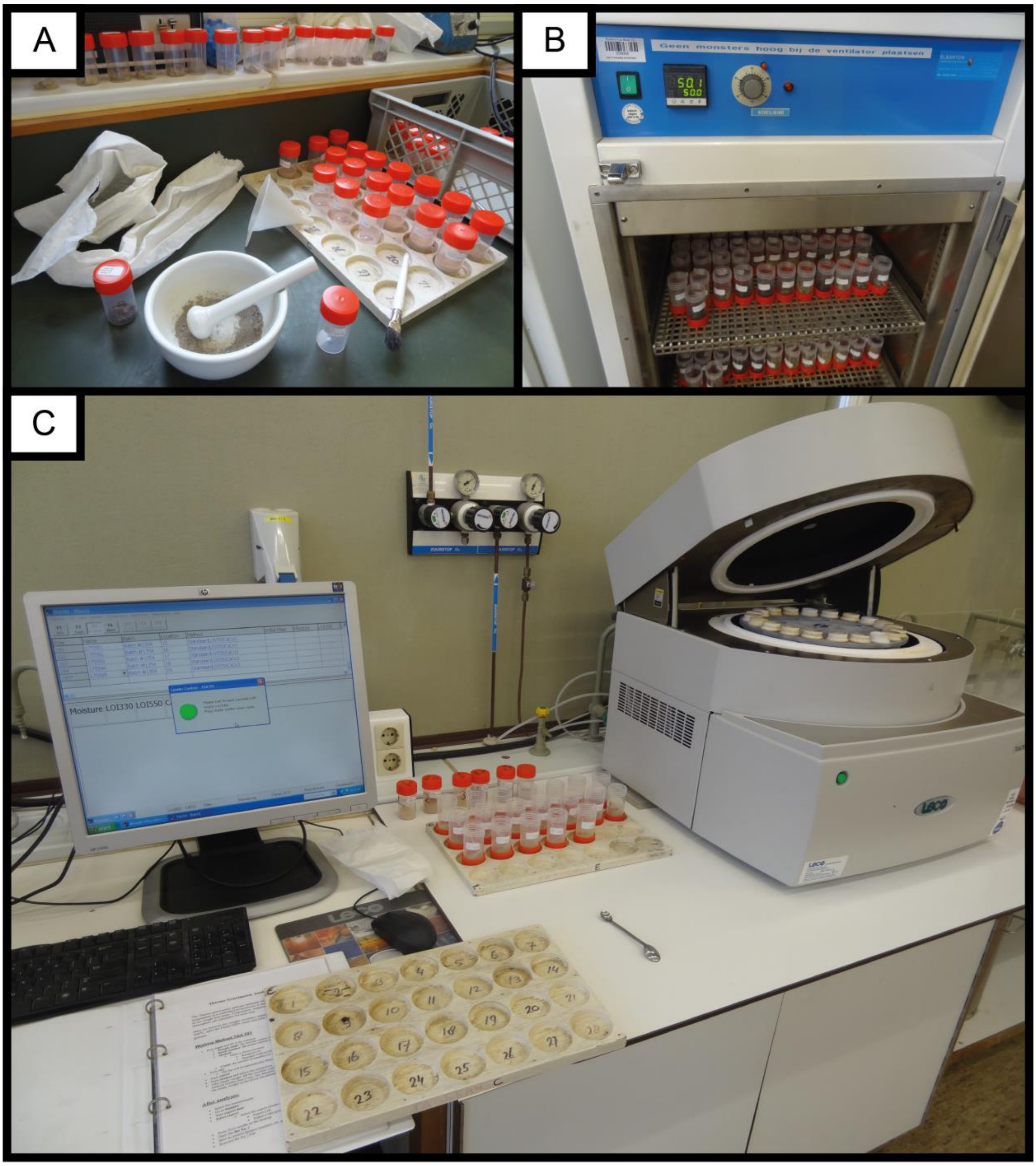


**Fig. 2.4.** The procedure for thermogravimetric analysis at the VU. Sediment samples are grinded with a mortar into a homogeneous mixture **(A)** and subsequently dried overnight at a temperature of 50 °C to remove most of the moisture **(B)**. A total amount of 19 samples can be heated per run in the LECO TGA701 device **(C)**. The associated weight loss per temperature step is automatically calculated per sample and thereby quantifies the organic and carbonate content within the sediment.

## 2.4. Petrography

At the Geotechnical Laboratory at the VU, several thin sections (28 x 48 mm and with a thickness of c. 30 μm) were kindly produced by Bouke Lacet to use for optical microscopy. The selected samples are a loose sandstone derived from the *T. rex* pelvis block located in the Black Hills Institute (BHI LB2), an unionid bivalve concretion from Shelly Butte (Shell) and the samples from the stratigraphic intervals BHI P1.2., MREX16, MREX81 and MREX116. The thin sections are studied using the Nikon Eclipse 500i Polarizing microscope and photographs are taken using associated NIS-Elements Microscope Imaging Software.

## 2.5. Palynology

Palynology is the microscopic study of fossil pollen grains and spores to reconstruct past vegetation, environments and climate. The pollen preparation at the Laboratory of Sediment Analysis at the VU begins with the extraction of c. 2 to 3 $cm^3$ organic rich material from selected sediment samples and the adding of a 2 ml suspension with a known quantity of Lycopodium marker spores to allow absolute pollen analysis. The subsequent preparation follows the standard techniques described by Faegri and Iversen (1989) and includes (in correct order) removal of clay, leaching, acetolysis, separation of pollen using heavy liquids and the creation of the pollen slides (Fig 2.5).

To soak off (most of) the clay and organic material, the pollen samples are treated with c. 500 mg sodium pyrophosphate ($Na_4P_2O_7 \cdot 10H_2O$) and 25 ml of 10% potassium hydroxide (KOH) (Fig 2.5.A). The samples are subsequently heated to 90 °C in a 100 ml beaker followed by sieving through a 200 μm mesh (Fig 2.5.B), washing with distilled water and 1 minute centrifuging at 2000 rotations per minute (rpm) (Fig 2.5.C). To remove all organic material, the samples are washed with acetic acid ($CH_3COOH$) (Fig 2.5.D)., followed by adding 3.5 ml of an acetolyse mixture (composed of 9 parts of acetic anhydride ($C_4H_6O_3$) and 1 part sulfuric acid ($H_2SO_4$)) and subsequent heating to 100 °C (Fig 2.5.E) and vortexing. To separate the pollen from the solution, in total 7 ml of the heavy liquid sodiumpolytungstate ($3Na_2WO_4 \cdot 9WO_3 \cdot H_2O$ with a specific density of 2 $g/cm^3$) is added (Fig 2.5.F) and centrifuged at 2000 rpm for 15 min. The samples are washed with water and possibly further vortexed to make sure all sediment and fine plant remains are gone. After adding 1.5 ml 96% ethanol, glycerine jelly (Fig 2.5.G.) and stove drying for 24 h at a maximum temperature of 70 °C, the residues are transferred to pollen glass slides by sealing the material with paraffin wax on a heated plate (Fig 2.5.H).

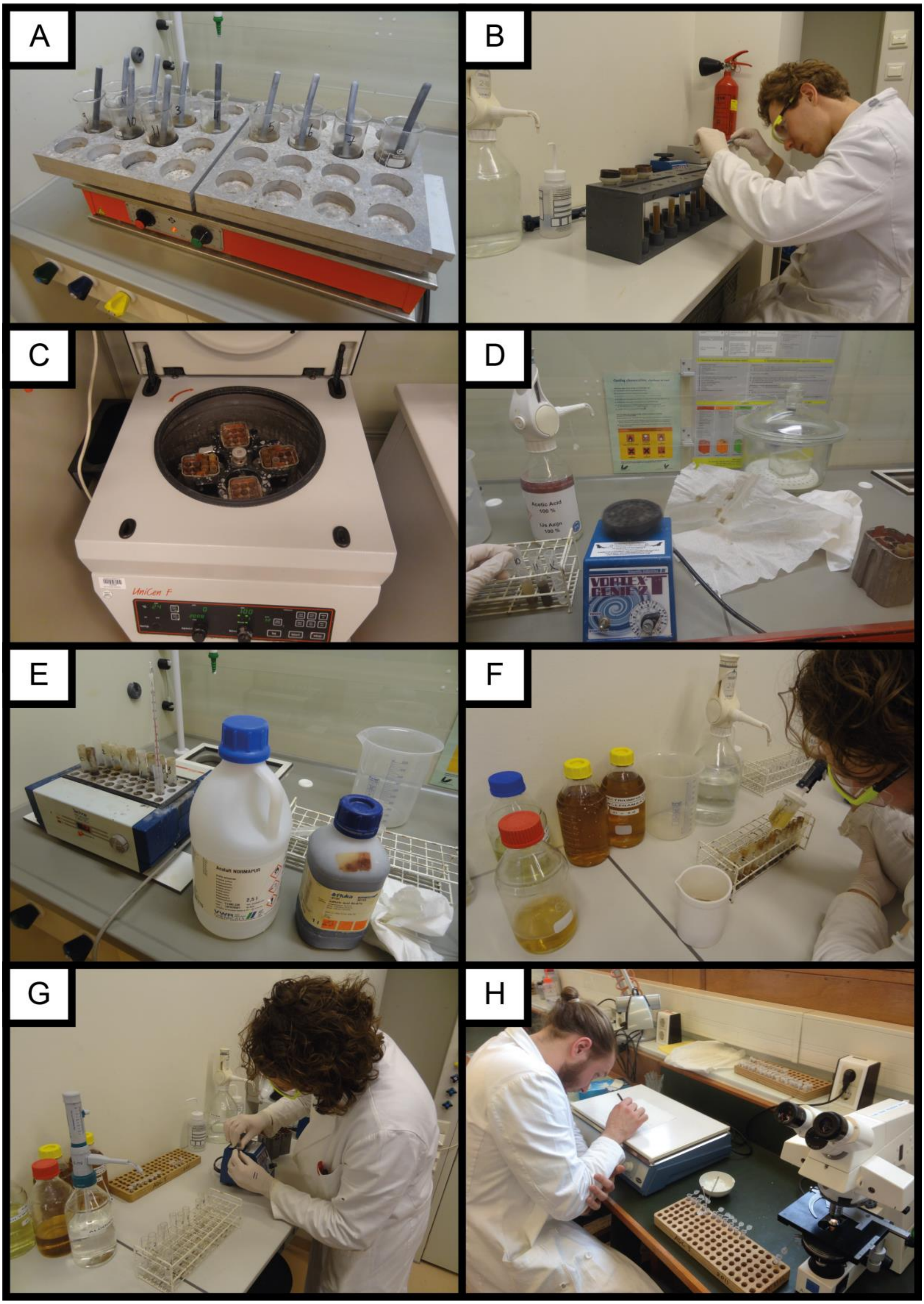
A
B
C
D
E
F
G
H

**Fig. 2.5.** The pollen slides preparation at the VU involves - after adding of a known amount of *Lycopodium* marker spores - the removal of organic and clay material using potassium hydroxide, sodium pyrophosphate, subsequent heating **(A)**, sieving over 200 µm **(B)** and regular centrifuge vortexing **(C)**. The next step involves acetolyse by adding and heating acetic acid **(D)**, acetic anhydride and sulphuric acid **(E)**. Furthermore, the heavy liquid sodiumpolytungstate is added to separate the pollen **(F)**. Subsequently, ethanol and glycerine jelly is added before the pollen solution is transferred in small sample cups **(G)**. After an overnight drying in the oven, the glass pollen slides can be produced using glycerine and paraffin wax on a heated plate **(H)**.

The identifying and counting of the pollen occurred with the help of a Carl Zeiss Axioskop light microscope (Fig 2.6) with magnifications of 400x, 630x and 1000x and oil immersion if necessary. In each sample a total sum of 100 pollen/spore grains is counted and the Hell Creek pollen taxa are morphologically identified using reference literature of Nichols (2002), Bercovici et al. (2009), Vajda et al. (2013), Tschudy & Leopold (1970) and Funkhouser (1961). Photographs of the different palynomorphs are taken using a Leica DFC420 Camera supported by the Leica Application Suite program of Leica DFC Twain software.

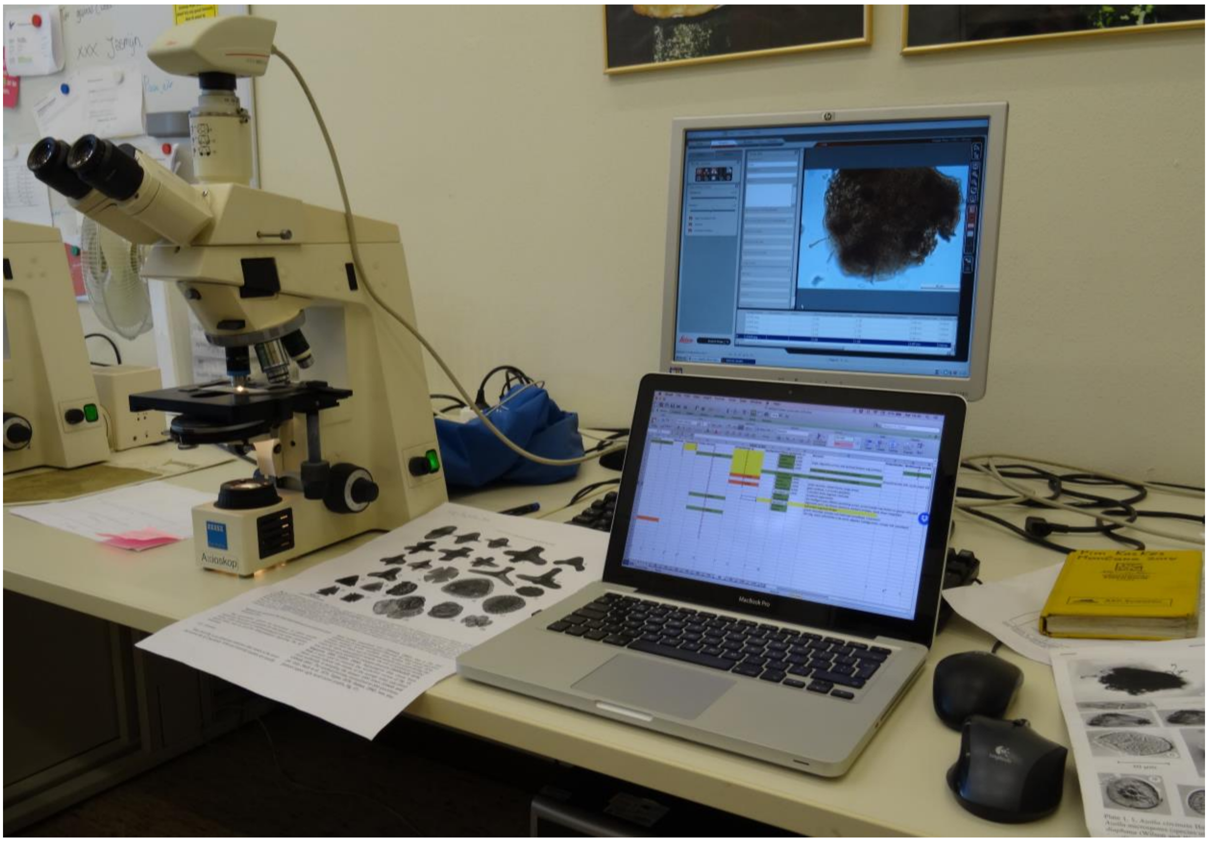

**Fig. 2.6.** The identifying and counting of the pollen occurs with the help of a Zeiss light microscope with magnifications of 400x, 630x and 1000x. Photos of various palynomorphs are taken using a Leica DFC420 Camera and associated software. In this figure, a spore of the aquatic fern *Azolla cretacea* is lying under the microscope and is displayed on the computer screen.

## 2.6. Paleomagnetism

### 2.6.1. Paleomagnetic sampling

For constructing an accurate age model of the fossil locality, it was necessary to take paleomagnetic samples at several fine-grained horizons throughout the study area to use for a magnetostratigraphic study. Deep trenches are dug until solid sedimentary rocks are reached that are large and consolidated enough to collect cores (of c. 2.5 cm in diameter and 6 - 12 cm long) with an electric powered portable drilling apparatus that is equipped with a water-cooled diamond bit (Fig 2.7.A). After drilling into the outcrop, a non-magnetic slotted tube with an adjustable platform (Pomeroy Orienting Fixture) is inserted around the sample (Fig 2.7.B). Using a magnetic compass attached to the platform, the azimuth (strike) and plunge (dip) of the drill direction (into the outcrop) is noted (Fig 2.7.C) and marked on the sample through the slotted tube. After extraction, the sample is labeled and a permanent arrow is marked on the upper side of the core that indicates the drilling direction. Subsequently, the sample is covered in aluminum foil for safe 'non-magnetic' transport and the name, orientation of the arrow and location of the sample are written down in a fieldbook (Fig 2.7.D) (Tauxe, 2010)

At some locations, it was not possible to drill cores with the electric powered drill due to the fragility of the sedimentary rock. Instead, block samples were taken by rasping off a flat surface in an outcrop and marking the strike and dip on the sample. The extracted and labelled samples are later drilled in the lab with compressed air into suitable cores, but these blocks are often more weathered and show lower accuracy of orientation compared to cores of the classical field-drilling procedure. A minimum of three cores per stratigraphic level was collected to ensure good results. The sedimentary layers of the study area show in outcrop no clear inclined bedding so horizontal layering is assumed and thus no tectonic conversion had to be performed.

To establish when a magnetization was recorded in a rock unit and identify possible remagnetization events it is suggested to perform field tests based on geometric relationships such as the fold test, the baked contact test and the conglomerate test (Tauxe, 2010). The fold test and baked test were not possible due to a lack of tectonic folding of strata and the absence of intrusions in the study area. The conglomerate test is based on the fact that when the magnetization vectors of the sampled conglomerate clasts are not randomly oriented, a remagnetization event must have occurred in a later stage after the formation of the clasts. Unfortunately, no suitable conglomerate beds have been found in the study area to perform this test. Back at the Paleomagnetic Laboratory Fort Hoofddijk in Utrecht, the obtained cores were cut into several useful samples, accurately weighed using a Mettler P1210 Weighing Instrument, measured on magnetic susceptibility and stepwise demagnetized using two different methods.

### 2.6.2. Magnetic susceptibility

One of the most important rock magnetic characteristics is the magnetic susceptibility (MS). This is a measure of the degree of magnetization of a material in response to an applied magnetic field. MS is a dimensionless number, because it is defined as the proportionality between induced magnetization and the applied field, which both are expressed as amperes per meter. MS can give vital information about the composition of a rock sample and thereby can reveal the potential magnetic carriers. MS can easily be measured in the lab by using the AGICO Kappabridge KLY-2 (Fig 2.7.E). When a specimen is placed in the coil of this device, the alternating current within the coil induces a small alternating magnetic field in the sample. This causes an offset in the alternating current of the Kappabridge which is proportional to the induced magnetization. After calibration, this offset can then be calculated in terms of the room-temperature MS (Tauxe, 2010). In order to correct the susceptibility for the sample's mass, the measured susceptibility values were divided by sample weight yielding the specific MS.

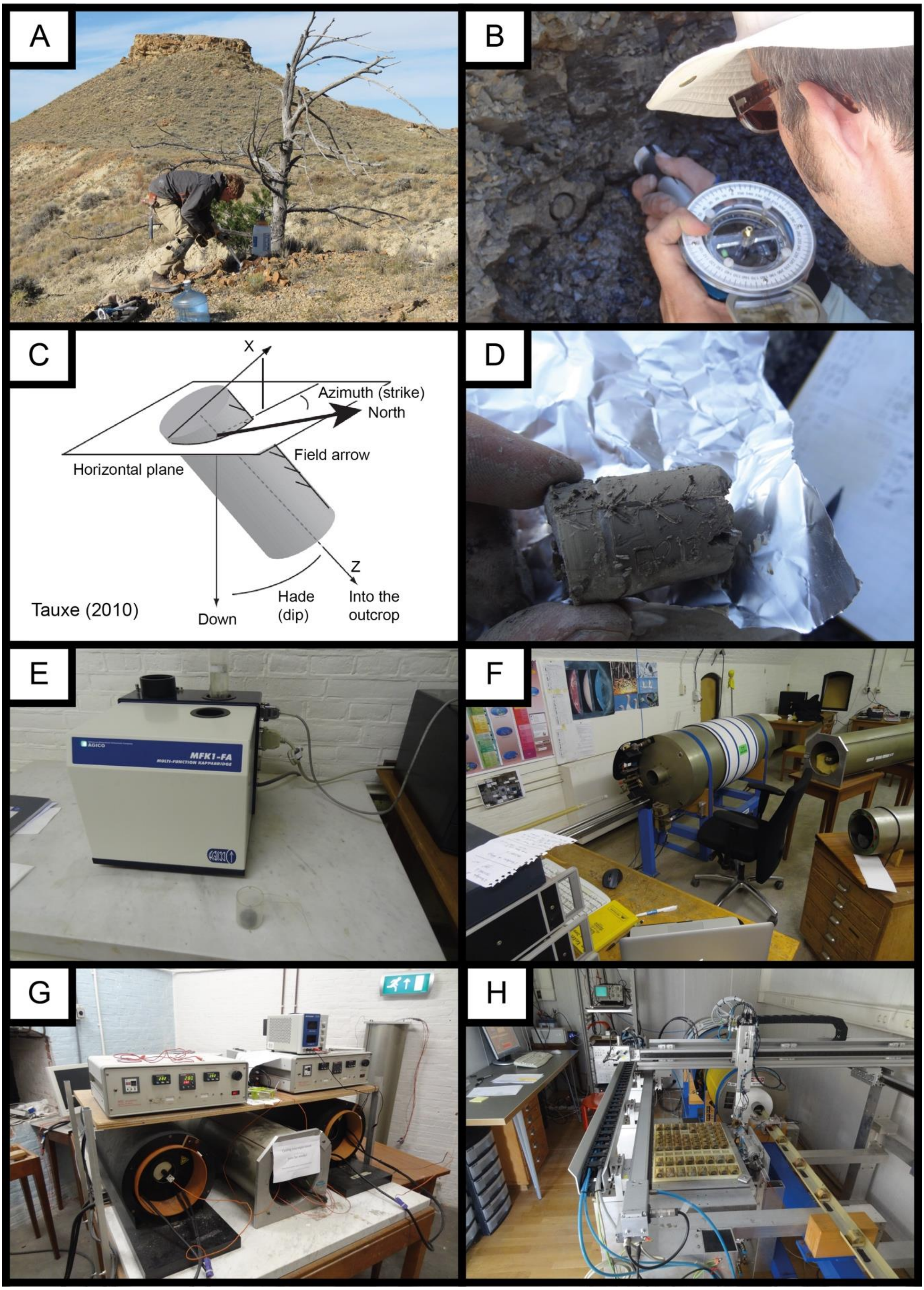


**Fig 2.7.** Paleomagnetic methods used in the field (A-D) and at Paleomagnetic Laboratory Fort Hoofddijk in Utrecht (E-H). Cores are drilled at selected intervals of solid fine-grained sediments using an electric powered drill that could be cooled with water **(A)**. Cores are oriented using a magnetic compass attached to an adjustable platform **(B)** using standard techniques described

by Tauxe (2010). In **(C)** a schematic representation of the orientation angles for core samples is shown where the hade (also known as plunge or dip) is the angle of the Z-axis (pointed into the outcrop) from the vertical and the azimuth (or strike) is represented as the horizontal projection of the X-axis measured clockwise from the geographic north. Strike and dip is noted in a fieldbook and the cores are labeled and wrapped in aluminium foil for transport **(D)**. After cutting the cores in useful sized specimens, they are weighed in the lab with a Mettler P1210 Weighing Instrument and subsequently measured for specific magnetic susceptibility in the AGICO Kappabridge KLY-2 **(E)**. 40 cores are thermally demagnetized using the DC Squid cryogenic magnetometer **(F)** and heating of the samples occurred in a magnetically shielded furnace **(G)**. 40 other cores were automatically demagnetized using the alternating field method on the ROBOT magnetometer of Fort Hoofddijk **(H)**.

### 2.6.3. Thermal demagnetization (TH)

The permanent magnetism of a rock or sediment that may preserve a record of Earth's magnetic field is known as the natural remanent magnetization (NRM). In case of sedimentary rock, clay-rich intervals are most suitable for paleomagnetic studies, because they contain many iron minerals (e.g. magnetite, titanite, greigite) and therefore consists of millions of small magnets. However, not all of these tiny magnets carry their original remanent vector anymore and have acquired new components of magnetization during their existence. Recognition and removal of this so-called secondary NRM or overprint is achieved with rock magnetic experiments and demagnetization in the lab. Thermal demagnetization is based on the relationship between relaxation time and (unblocking) temperature of the samples.

At Fort Hoofddijk, the NRM of two sample batches is measured on an in-house built robotized sample handler controller attached to a horizontal 2G Enterprises DC SQUID cryogenic magnetometer (with a noise level of 3 x $10^{-12}$ $Am^2$) (Fig 2.7.F). This magnetometer (nicknamed CRYO) operates using so-called superconducting quantum interference devices (SQUIDs), see for details about this technique Tauxe (2010). Thermal demagnetization (TH) is carried out in a magnetically shielded, laboratory-built, furnace (Fig 2.7.G) using the following temperature increment schedule: 20 – 100 – 120 – 150 – 180 – 210 – 240 – 260 – 280 – 300 – 320 – 340 – 360 – 380 - 400 °C.

### 2.6.4. Alternating field demagnetization (AF)

Another method for demagnetizing a sample is by means of an alternating field (AF) coil interfaced with a magnetometer. In other words, an oscillating field is applied to a paleomagnetic specimen in a null magnetic field environment to remove the low stability remanence components. At Fort Hoofddijk, a laboratory-built automated measuring device was used known as the ROBOT (Fig 2.7.H). For this study 15 AF increments were used: 0 – 5 – 10 – 15 – 20 – 25 – 30 – 35 – 40 – 45 – 50 – 60 – 70 – 80 – 90 - 100 mT (milli Tesla). Magnetometers such as the CRYO or the ROBOT are used to measure the three components of the magnetization necessary to define a vector (e.g. x,y,z). This data can be converted to the more common form of declination and inclination using Zijderveld diagrams (Tauxe, 2010)

### 2.6.5. Zijderveld diagrams and magnetostratigraphy

Magnetostratigraphy is a sub-discipline of stratigraphy that studies the variations of Earth's magnetic field through time. The direction, also known as the polarity of the magnetic field, switched irregularly throughout Earth's history from a 'normal' polarity (where the geomagnetic North Pole is directed towards the geographic North Pole) to a 'reversed' polarity (Fig. 2.7.A). Determining the accurate stratigraphic position of the geomagnetic reversals serves as a relative dating tool for the fossil rock record. These 'paleomagnetic bar codes' are created by using the TH and AF demagnetization data as input values for so-called 'Zijderveld diagrams' (Fig 2.7.B).

For interpreting the demagnetization data, the new online and user-friendly portal paleomagnetism.org was used (Koymans et al., 2015). The criteria for selecting specific TH or AF increments in Zijderveld diagrams is based on a minimum of 5 selected increments, a preference for steps with a maximum angle of deviation (MAD) lower than 20 and a common rule that often the first 2 or 3 and last 2 or 3 steps should be erased because they show signs of a modern overprint or a remagnetization event. Zijderveld diagrams are orthogonal vector diagrams that consists of a set of two projections of the vectors, one on the horizontal plane and one on the vertical plane. For details about visualizing this demagnetization data, see Zijderveld (1967).

During demagnetization, the remanent magnetization vector will change until the most stable component has been isolated, at which point the vector decays in a straight line to the origin. This final component is called the characteristic remanent magnetization (ChRM) and its directions (and thus declination and inclination) are calculated using principal component analysis (Kirschvink, 1980). At last, the obtained declinations (0 – 360 °) and inclinations (-90 – 90 °) are plotted versus stratigraphic height to interpret the timing of normal and reversed chrons and thereby providing an accurate age model (Tauxe, 2010).

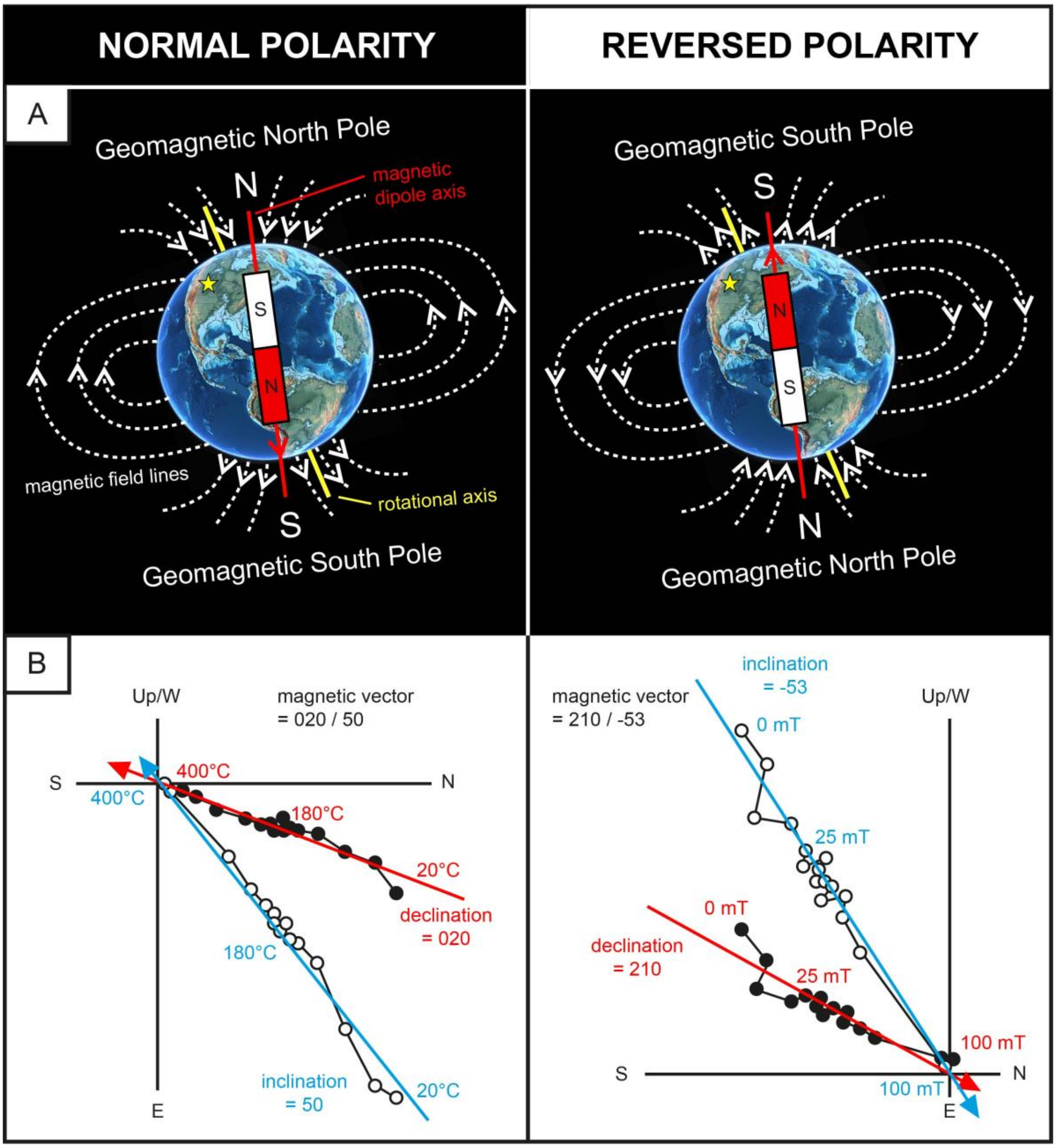

**Fig 2.8.** Schematic representation of Earth's magnetic field with the source of the field lines displayed as a magnet in the interior of the planet **(A)**. The sketch also shows the difference between Earth's magnetic dipole axis and its rotational axis. The magnetic field has switched its polarity from normal (left picture) to reversed (sketch on the right side) irregularly through Earth's history. The normal polarity is characterized with the geomagnetic North Pole pointed towards the geographic North Pole, whereas during a reversal chron this is opposite. The geomagnetic field vector consists of two important components, namely the inclination (the angle downwards from the horizontal) and the declination (the angle in a horizontal plane between the geographic and magnetic north). These two features can be calculated using so-called Zijderveld diagrams. These diagrams of two hypothetical samples are shown in **(B)** to illustrate the difference between normal and reversal intervals in terms of demagnetization pattern. In the left graph, the dots indicate x,y,z measurements per thermal steps in °C while the Zijderveld diagram on the right shows the alternating field increments in mT. A rock sample with remanent magnetization from the Northern Hemisphere should hold, during a normal polarity, a declination directed to the North and a positive inclination. This is the case for the Naturalis Montana site, as indicated with a yellow asterisk at approximately the correct Northern Hemisphere latitude on a paleogeographic Google Earth map of the Late Cretaceous (derived from globalgeology.com from C. R. Scotese).

# 3. Results

In this chapter, the results of my Master Thesis project are presented, subdivided in paragraphs covering my three main research questions concerning the taphonomy/sedimentology, paleoenvironmental reconstruction and integrated stratigraphic framework of the Naturalis *T. rex*. The first paragraph is dedicated to a general description of all the sections used in this study.

## 3.1. Description of the sections

Eight different sections are examined in this research project, of which seven are projected on the map of Fig. 3.1 and in the general lithostratigraphic framework of Fig. 3.2. Photo-overviews, field-correlations and graphs of all sections are shown in Appendix 2. In Table 3.1, the latitude/longitude, stratigraphic height, degree of detail in lithostratigraphic logging and the applied methodologies on the samples of the sections are listed. Due to the limited time of the field campaign, the low exposure density and the main aims of this project (listed in paragraph 1.5), it was decided to perform different log and sample resolutions throughout the study area. Especially regarding the taphonomic research question (paragraph 3.2 and 4.1), the focus lies on the MREX section (excavation site of the Murray *T. rex* = Naturalis *T. rex*), which is described, sampled and measured at a very high resolution.

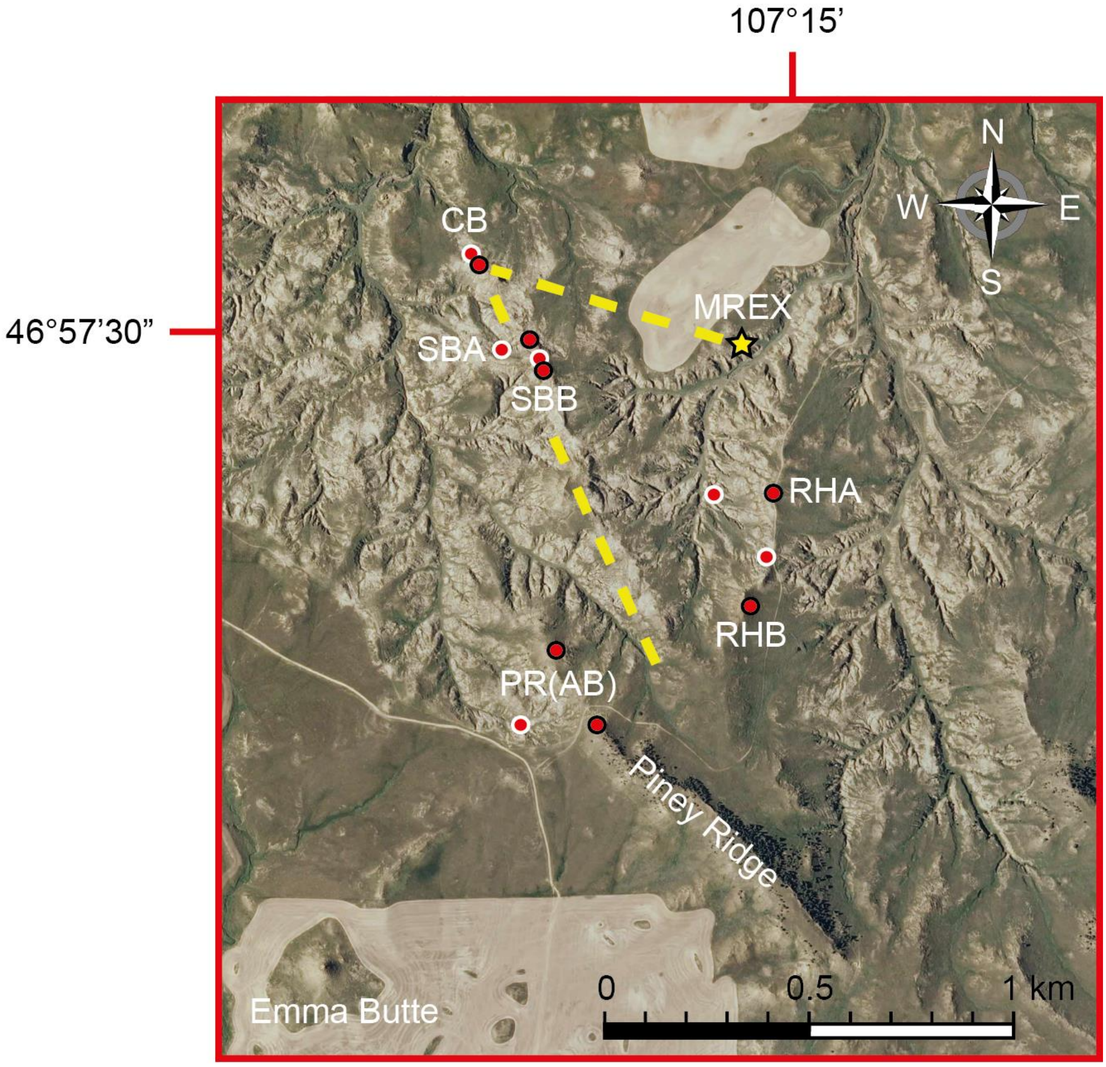

**Fig. 3.1.** Aerial overview of a zoom-in of the study area of the Naturalis *T. rex* on the Murray Ranch with the various sections indicated. The white-red circles mark the position of the base of every section whereas the black-red circles coincide with the top of every section. The location of this map is indicated with a red square in Fig. 1.23. The orthophotographs used in this figure are produced by the USGS in 2014 (NAIP imagery) and are derived from the 7.5-minute series of the Emma Butte and School Butte Quadrangle, Garfield County, Montana. A digital elevation model (DEM) of the same area is displayed in Appendix 1 (Fig. A1.2) and shows that the MREX section corresponds to the topographically lowest section whereas the Piney Ridge section is located at the highest elevations. The yellow dashed line marks the approximate position of the correlation line which was used to place the different sections into a lithostratigraphic framework with a composite stratigraphic height of in total 65 m (Fig. 3.2 and Fig. 3.17). Due to the scattered pattern of the sections and their variable elevations, it was decided to split the correlation line in an E-W portion and a NW-SE part to plot the different sections in a realistic way on this correlation line.

**'Section' BHI-P1** represents a small block of only 17.5 cm within the rock matrix encasing the pelvis bones of the Naturalis *Tyrannosaurus rex* specimen. This sandstone block is situated in the Black Hills Institute (BHI) in Hill City, South Dakota, USA. All geological methods were applied on this section, excluding paleomagnetism (see Table 3.1), since this large sediment block is extracted from the field and the exact stratigraphic position and original orientation is not known. A simplified lithostratigraphic log and the grain-size and thermogravimetric data of BHI-P1 is shown in Fig. A2.2 and a photo-overview with close-ups of the section are visible in Fig. A2.1. Note that the upper part of BHI-P1 coincides with the lower portion of the MREX section, since the rip-up clasts at the base of the lacquer peel show similarities with the clay/silt pebbles at the top of BHI-P1. This means that the pelvis block is sampled upside-down in comparison with the real stratigraphic sequence.

**Stratigraphic section MREX** is the most important section of this study and comprises a 582 cm long sequence at the dig site that is characterized by a sharp boundary between a basal clay layer and a ~3 m thick (partly cross-bedded), poorly consolidated sandstone. This sandy interval gradually fines upwards and is overlain with an alternation of siltstone, carbonaceous shale and very fine sand. The MREX section stands for 'Murray rex section' and is the topographically lowest studied section on the Murray Ranch. The section is located at the excavation site of the Naturalis *T. rex* and is a composite log consisting of in total 8 trenches that are described and sampled at a very high resolution of ~2 cm. The sediment samples were measured at a 10 cm resolution for grain-size and thermogravimetry (e.g. Fig. A2.4). In addition, sampling for magnetostratigraphy and palynology was carried out on sediments from the basal clay layer (see Fig. 3.22). The lacquer peel of Fig. 3.3 and 3.4 coincides with stratigraphic (vertical) interval 9 - 157 cm in the MREX section. The dinosaur bones are situated in the ~3 m thick sandstone interval. The LIDAR scans made by Manchester University can provide the exact positions of the different bone elements, but these scans are not yet processed. In Fig. A2.3, a photo-overview of the MREX section is given showing all the trenches and associated sample numbers.

**Stratigraphic section CB** is an abbreviation for Cyclic Butte and this 14.3 m long section is located in the western part of the study area. As the name already suggests, the outcrop is characterized by well-exposed, regular alternating layers (see paragraph 1.5.3). To study this pattern, the entire butte was logged for cyclostratigraphy at a high resolution, but it was decided to perform sampling (and measuring for grain-size, thermogravimetry and pollen, see Fig. A2.6) only on one well-developed 'cycle' between 13.9 and 16.5 m stratigraphic height. In Fig. A2.5, photos of the entire CB section are shown together with the location of the sampled interval and the interpreted field correlations. These correlations are mainly based on the rhythmic appearance of a number of carbonaceous shale horizons (CS). These dark, organic rich layers are bounded by yellow-grey colored sandstone intervals which evolve into olive-grey siltstones and again in carbonaceous shales. Fig. A2.5C also shows the interpreted correlation between Cyclic Butte, Cricket Butte and the neighboring section of Shelly Butte.

**Stratigraphic section SBA&B** are two sections in the western part of the study area that are part of the informally called Shelly Butte. As the name already suggests, this section is marked by the presence of a 0.5 m thick 'lumachelle', a shell horizon composed mainly of unionid bivalves. Section SBA can be correlated with Cyclic Butte using some carbonaceous shale levels and a distinct calcrete horizon (calcrete 4), as shown in Fig. A2.7A. These hard, orange colored calcretes are not (iron-rich) concretions, but are interpreted as calcium rich, hardened layers in or on a paleosol due to water table fluctuations. Section SBA was more badly exposed than SBB and only sampled for paleomagnetism, whereas in SBB also grain-size, TGA and pollen samples were taken at stratigraphic height 0.2 – 6.1 m (see Fig. A2.8). This interval of SBB shows a leaf horizon on top of the shell bed overlain by a clear inclined, fining upward sequence bounded by a sandstone.

**Stratigraphic section RHA&B** stands for Rex Hills section A & B, which are two poorly exposed sections in the eastern part of the study area covering 11.7 and 15.7 m stratigraphy, respectively. These sections are logged at a low resolution and are not sampled for analysis, but since they include several shell horizons and two prominent, persistent calcrete levels (4 and 6) RHA&B can be used as a useful marker to correlate Shelly Butte with Piney Ridge (see Fig. A2.9).

**Stratigraphic section PRA&B** is one combined section in the southeastern part of the study area comprising a long sequence (~38 m) with two tops, one is the megacrossbedded sandstone cap of the SE-NW oriented Piney Ridge and one is the isolated butte ~200 m NW of Piney Ridge. As can be seen in Fig. A2.10, the exposure density in especially the upper part of PR(AB) is very low, so logging was performed at a low resolution and samples were only taken for paleomagnetism since this section represents the stratigraphically highest part (Fig. 3.2).

**Table 3.1.** Location (latitude/longitude of the base and top), estimation of the total stratigraphic height and the degree of detail of stratigraphic logging of the 8 sections described in this thesis. These sections are Black Hills Institute Pelvis Block #1 (BHI-P1, a loose block holding the pelvis bones of the Naturalis *T. rex*, so no coordinates can be given), Murray (Naturalis) rex section (MREX), Cyclic Butte section (CB), Shelly Butte A & B section (SBA & SBB), Rex Hills A & B section (RHA & RHB) and the combined Piney Ridge A & B section (PR(AB)). Furthermore, if determination of color in the field is carried out using a Munsell Soil Color Chart, this is indicated. Finally, all the performed sampling for lab analyses of the sections are given, namely grain-size (GS), thermogravimetry (TGA), slides for palynology (Pollen; pollen slide numbers are indicated) and paleomagnetic drilling and subsequent analyses at Fort Hoofddijk (Pmag). 'Part' means that only a selected part of the section is color coded or sampled for grain-size and thermogravimetry.

| Name section | Coordinates base section | Coordinates top section | Strat. height | Detail of logging | Munsell | GS | TGA | Pollen | Pmag |
|---|---|---|---|---|---|---|---|---|---|
| **BHI-P1** | - | - | 17.5 cm | Very high (2.5 cm) | X | X | X | X (1) | |
| **MREX** | 46.958170° -107.252664° | 46.958126° -107.253131° | 582 cm | Very high (2 cm) | X | X | X | X (2-4) | X |
| **CB** | 46.960198° -107.261555° | 46.959995° -107.261434° | 1430 cm | High (10 cm) | X part | X part | X part | X (5-8) | X |
| **SBA** | 46.958228° -107.260155° | 46.958381° -107.259743° | 870 cm | Moderate (~25 cm) | | | | | X |
| **SBB** | 46.958243° -107.259645° | 46.957760° -107.259191° | 1540 cm | Moderate (~25 cm) | X part | X part | X part | X (9-11) | X |
| **RHA** | 46.955005° -107.253145° | 46.954992° -107.251888° | 1170 cm | Low (~50 cm) | | | | | |
| **RHB** | 46.953503° -107.252116° | 46.952689° -107.252810° | 1750 cm | Low (~50 cm) | | | | | |
| **PR(AB)** | 46.949869° -107.259484° | 46.951495° -107.258903° | 3800 cm | Low (~50 cm) | | | | | X |

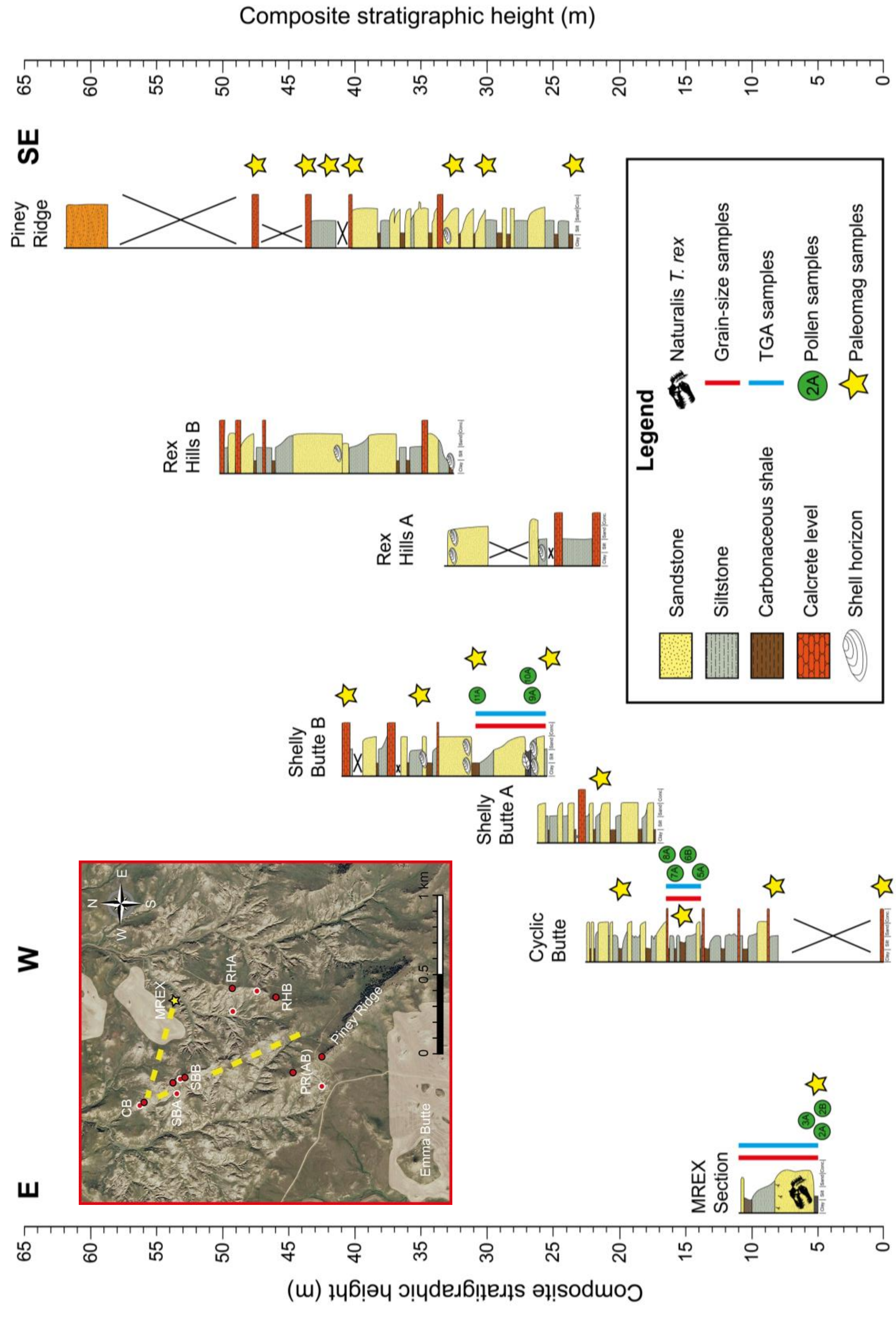


**Fig. 3.2.** Lithostratigraphy of all individual sections marking the position of the samples used for the different lab analyses (grain-size, thermogravimetry, pollen and paleomagnetic analysis). Since not all sections in the study area were Munsell color coded, the different lithological units (sandstone, siltstone, carbonaceous shale and calcrete) are displayed in a simplified fashion. The inset shows the map view of the various sections and also the approximate position of a profile line (in yellow) for the stratigraphic correlations (see paragraph 3.4.1 for the correlations itself).

## 3.2. Sedimentology and taphonomy

In this paragraph, the data of the first research question regarding the unique preservation of the Naturalis *Tyrannosaurus rex* specimen are presented and the focus lies predominantly on the MREX section. The other sections (BHI-P1, CB and SB) are described in less detail, but their complete graphs (the lithostratigraphic column and the associated grain-size and thermogravimetric data) can be found in Appendix 2. This part of the chapter is subdivided into subparagraphs concerning descriptions of the observed sedimentary structures in the field, the grain-size data, the thermogravimetric data and the microscopic observations of thin sections.

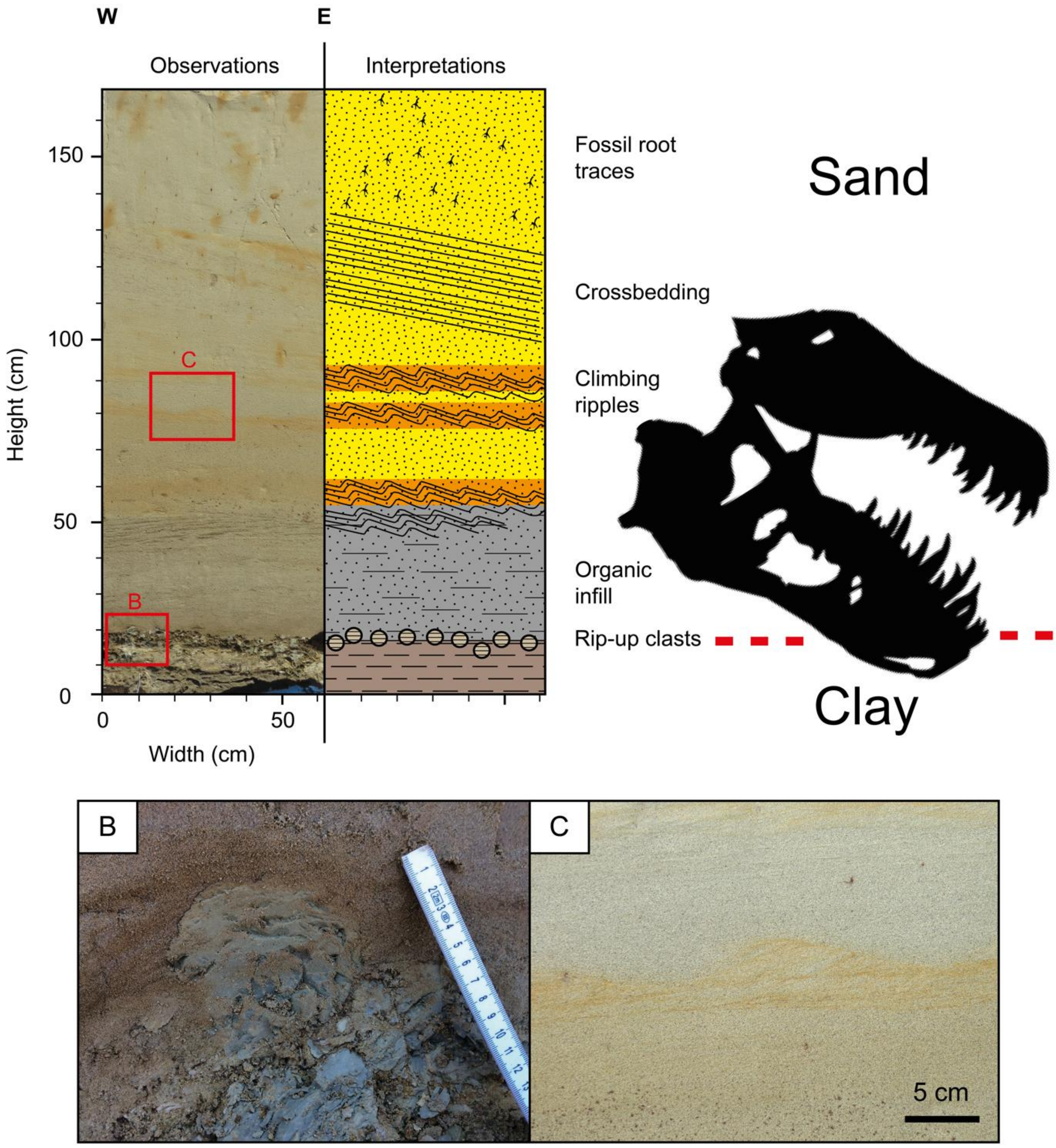


**Fig. 3.3.** Photo of the lacquer peel made at the location of the pelvis block of the Naturalis *T. rex* and the associated sedimentary structures and the approximate position of the *T. rex* pelvis **(A)**. Close-ups are shown from the rip-up clasts at the boundary of the basal clay layer with the massive sand package **(B)** and the climbing ripples in the rusty sandy interval **(C)**.

### 3.2.1. Sedimentary structures

One of the first activities carried out at the dig site of the Naturalis *T. rex* was the creation of a lacquer peel of ~170 cm long and ~60 cm wide (see also 2.1.1). This peel showed the most prominent sedimentary structures at the excavation site that can give vital information about the depositional conditions before, during and after burial. In Fig. 3.3A a photograph of the lacquer peel and a description of its observed sedimentary characteristics is shown. The base of the lacquer peel consists of a brown-grey clay layer that shows a sharp, erosive boundary with the overlying yellow-grey sand package. This boundary is characterized by the presence of rip-up clasts (Fig. 3.3B), which are rounded clay pebbles that are eroded by force and reworked from the underlying mudstone interval. Clear sedimentary structures (e.g. bioturbation) appear to be absent in this basal clay layer and also in the other mudstone intervals of the MREX section. Noteworthy is the presence of an organic rich layer around 5 m stratigraphic height with coaly, poorly determinable fossil leaf and root fragments.

The skull of the Naturalis *T. rex* specimen was found upside-down in the hill on the Murray Ranch 'with its snout still sticking in the basal clay layer' (Farrar, 2015, pers. comm.), as indicated in Fig. 3.3A. The lower sand sequence on the lacquer peel is dominated by organic infill layers and climbing ripple laminations in the orange-brown intervals (Fig. 3.3C). Subsequently, the upper sand level within the lacquer peel displays clear trough cross-stratification (visible due to the concentration of plant detritus or charcoal fragments inside these crossbed sets) and some rusty traces of fossil roots. Other evidence for floral (and faunal) remains in this sand layer is rare. The angle of dip of the foresets of the unidirectional crossbeds in the upper part was measured at 16° and the lee-side of these foresets is directed towards the east. However, since the peel surface was created under an angle of 65°, the angle of the foresets should be corrected towards a vertical plane. Using goniometric relationships, the corrected foreset angle was calculated at 15° (Fig 3.4).

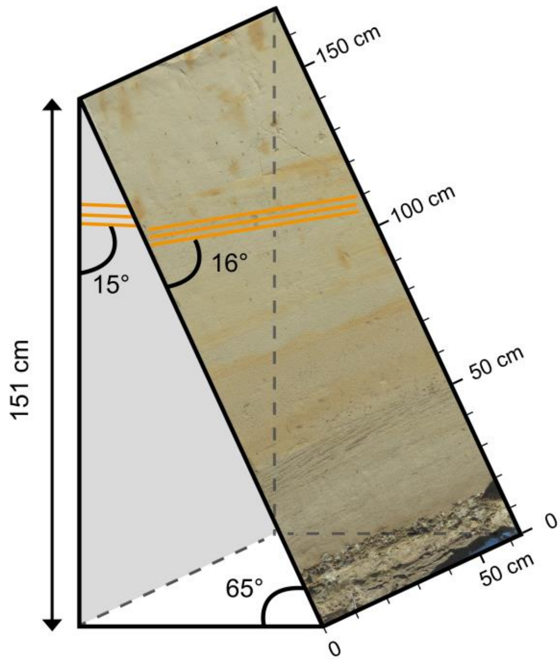


**Fig. 3.4.** Schematic overview of the inclined lacquer peel surface that was created under an angle of approximately 65°. The cross-stratification found in the upper part of the peel shows an angle of 16°. Using goniometric calculations, the real inclination angle of the foresets is 15°.

### 3.2.2. Grain-size analysis

As described in paragraph 2.2.1, the grain-size distributions of the lithogenic fraction of selected sediment samples were measured using the HELOS laser diffraction device with a size range of 0.12 to 2000 µm. All raw grain-size data of the sections BHI-P1, MREX, CB and SB (n = 103) can be found in Appendix 4 and the associated Excel-file. Here, the focus lies on the MREX section (see Fig. 3.5) and the other sections are described briefly, since their graphs are shown in Appendix 2.

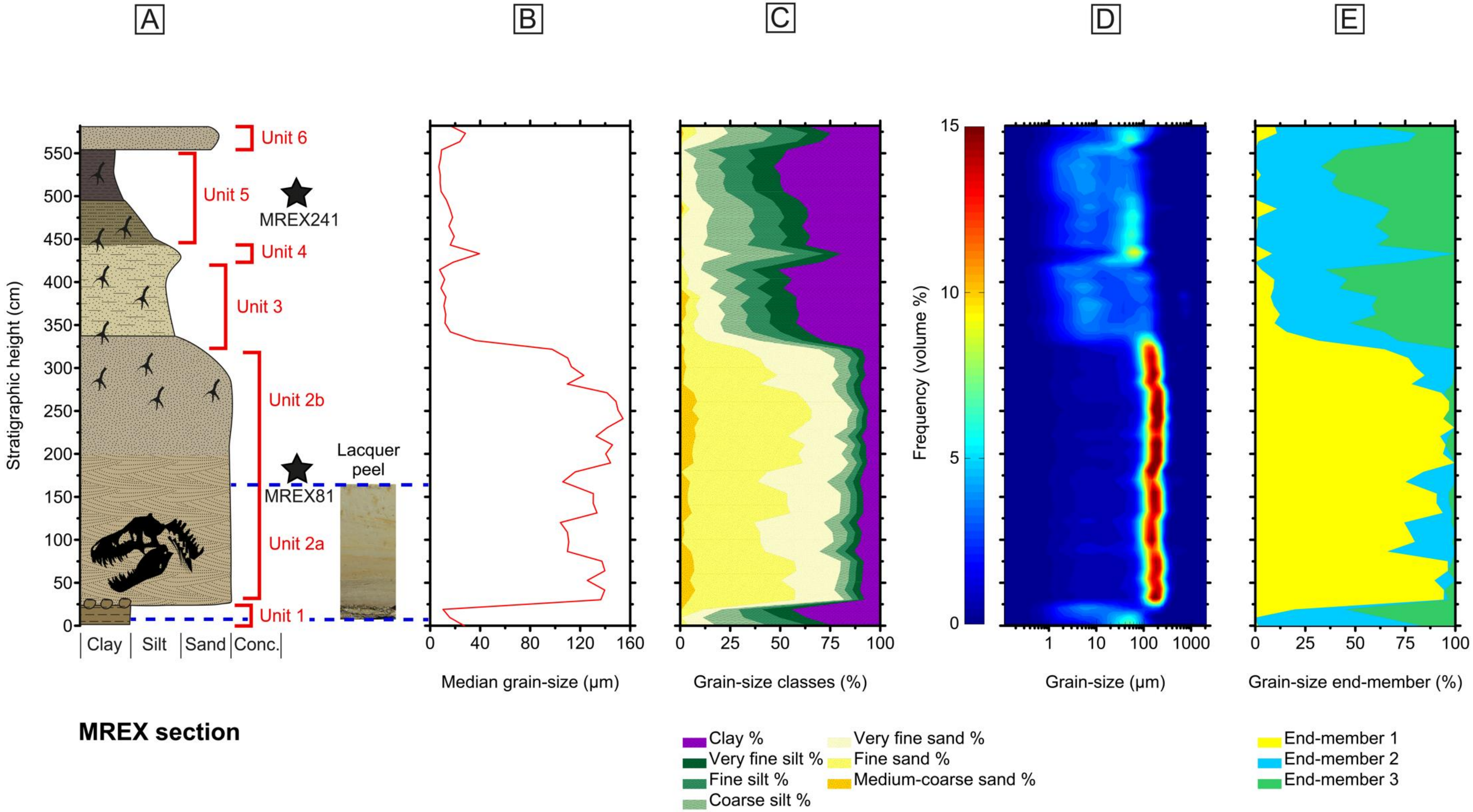
A
B
C
D
E
Stratigraphic height (cm)
Unit 6
Unit 5
Unit 4
Unit 3
Unit 2b
Unit 2a
Unit 1
MREX241
MREX81
Lacquer peel
Clay
Silt
Sand
Conc.
Median grain-size (µm)
Grain-size classes (%)
Frequency (volume %)
Grain-size (µm)
Grain-size end-member (%)
MREX section
Clay %
Very fine silt %
Fine silt %
Coarse silt %
Very fine sand %
Fine sand %
Medium-coarse sand %
End-member 1
End-member 2
End-member 3

**Fig. 3.5.** Graph of the MREX section summarizing all grain-size data. Firstly, the lithostratigraphic log and weathering profile of the section is shown with the associated Munsell soil colors and the stratigraphic position of the six sedimentary units, lacquer peel and the selected samples MRXEX81 and MREX241 **(A)**. In the second graph, the median grain-size (in μm) is plotted in red versus the stratigraphic height, together with the volume % of seven different grain-size classes, namely clay (purple), silt (greenish colors) and sand (yellowish colors) **(B)**. See Table 2.1. for the associated grain-size ranges for the different size classes. When the different grain-size distribution curves of all the samples are plotted versus stratigraphic height, the contourplot of **(C)** is created with the use of Matlab. In this graph, the z-axis represents the frequency (in volume %) and the high frequency interval between 0.2 and 3.2 m is striking and indicates a thick fine sand package with a very good sorting. Finally, the graph of **(D)** presents the contributions of the three grain-size end-members (see Fig. 3.5) over the stratigraphic interval. The high abundance of end-member 1 (EM1) within the interval between 0.2 and 3.2 m is clearly visible. The other intervals are mixtures of EM2 and EM3.

All grain-size results of the MREX section are shown in Fig. 3.5 and plotted versus a lithological column and weathering profile, which is subdivided into six distinct sedimentary units (Fig. 3.5A) based on field observations and the quantitative grain-size dataset. The median grain-size record (Fig. 3.5B) shows the general fine to coarse grained trends and these correspond well with the lithological column produced in the field. In addition, the filled background of Fig. 3.5C displays the cumulative volume percentage of seven different grain-size classes which also fits the pattern of the six sedimentary units in the MREX section.

At the base of the section a fine-grained interval of ~20 cm is present with on average a median grain-size of 18 μm, 35% clay and 48% silt. **Unit 1** is rapidly changing in a large, sandy package of ~3 m with a coarse median grain-size of 128 μm that consists predominantly of very fine sand (28%) and fine sand (46%). **Unit 2** can be subdivided in two subunits with 2a differentiating from 2b by the presence of clear cross-stratification and climbing ripples. Unit 2 gradually fines upwards into **Unit 3**. This is a mudstone interval of c. 1 m between 330 and 430 cm stratigraphic height that has an average median grain-size of 15 μm, 40% clay and 39% silt. Subsequently, a very small (~15 cm) coarser unit (**Unit 4**) is present which has a median grain-size of 39 μm and contains 55% silt (32% coarse silt) and 26% sand (23% very fine sand). This 'sandy pulse' is followed by a clear fining and darkening upwards sequence which holds the smallest median grain-size (12 μm) and also the smallest percentage of the sand fraction (44% clay, 46% silt and only 10% sand). **Unit 5** is sharply bounded by a lighter coarser unit which forms the top of the 5.81 m long MREX section. **Unit 6** shows similarities with Unit 4 and is characterized by a median grain-size of 23 μm, 49% silt and 20% sand.

Besides descriptions based on the median grain-size and the volume % of different size-classes, it is possible to show grain-size records in a three-dimensional display as contour plots. Each sediment sample that is measured in the laser diffraction device is marked by a specific grain-size distribution, a curve that illustrates the grain-size pattern in μm versus the frequency in volume % (which is a measure of how many grains of a specific size are present within the sample), as can be seen for sample MREX81 and MREX241 in Fig. 3.6D. All these grain-size distributions are matrices and can be plotted versus stratigraphic height with the use of for instance the software Matlab. In the resulting color-filled contour plot, a z-axis is added that represents the frequency (in volume %), which can be seen in Fig. 3.5D. Median grain-size data only gives an 'averaged' value throughout the section which is useful to trace general fine/coarse trends. The volume % of the different size-classes provides a more detailed view in the contributions of clay, silt and sand through time, but still this data is based on a subdivision into only nine size-classes (see Table 2.1). Frequency contour plots give additional information to the above mentioned techniques, since they display the entire grain-size distributionary curve of each sample (based on 57 size classes instead of 9) and thereby can give vital insights in for instance the sorting of the sediments throughout the section.

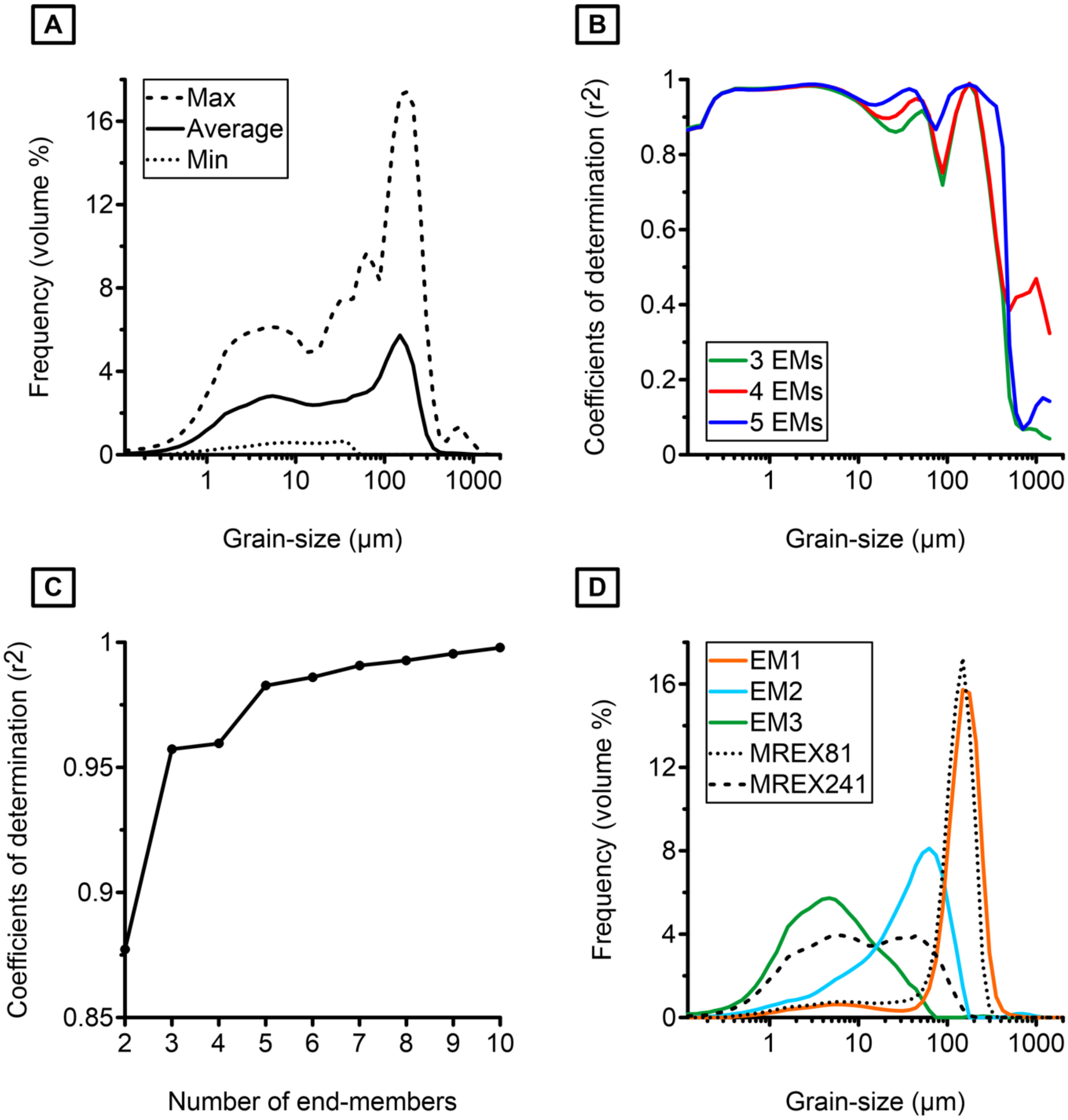


**Fig. 3.6.** End-member modelling results of the entire grain-size dataset (n = 103) of the Murray Ranch. Average grain-size distribution and minimum and maximum values are plotted to reveal the range of volume frequency (in %) for each size class (on a logarithmic axis in μm) **(A)**. The graph with coefficients of determination ($r^2$) versus grain-size shows at which size classes the different end-member models (with 3, 4 and 5 end-members, respectively) fits the best the observed variations **(B)**. A plot with the 'adjusted' (mean) $r^2$ across the full size range as a function of the number of end-members illustrates that a three-end-member model already explains 96% of the observed variance in the grain-size dataset **(C)**. Therefore, a three-end-member model was chosen and the modelled grain-size distribution curves of the three end-members are displayed in **(D)**. They represent a uniform fine sand deposit (EM1, modal size ~150 μm), a broad very fine sand to coarse silt distribution (EM2, modal size ~63 μm), and a background signal of fine silt and clay (EM3, modal size ~5 μm). The grain-size distributions of the measured sediment samples consist of portions of these three end-members. For instance, sample MREX81 shows large similarities with the curve-shape of EM1, in contrast to the totally different distribution of sample MREX241, which consists of large portions of EM2 and EM3.

In Fig. 3.5D, the variations in sorting of the different MREX samples (n = 57) are clearly visible with Unit 2 as most prominent interval. This unit is characterized by a very high frequency interval (on average 12.5 volume %) for a narrow size range (~125 – 225 μm) which is present throughout its entire stratigraphic range (0.2 – 3.2 m). This indicates a relatively homogeneous, 3 m thick, well-sorted sand interval that displays a totally different grain-size signature compared to the rest of the MREX section. For instance, Unit 3 and 5 show some similarities with each other in terms of that their grain-size distributions are dominated by a broad curve (~2.5 – 5.5 volume %) in the clay to (fine) silt interval (~5 – 50 μm), in large contrast with the uniform sand peak of Unit 2. Unit 4 and in a lesser extent parts of Unit 1 and 6 shows another distinct grain-size signature that is marked by a somewhat uniform peak around 60 μm (~5 – 9 volume %) combined with a 'tail' of fine silt and clay. These three distinct grain-size signatures discovered in the frequency contour plot of Fig. 3.5D show similarities with the so-called grain-size end-members of Fig. 3.6E, which are described below.

To disentangle the different transportation mechanisms within the grain-size distributions of the MREX section, it is important to also study the other grain-size records throughout the study area to produce a regional (and not outcrop-scaled) depositional model of the Hell Creek deposits on the Murray Ranch. Therefore, the entire grain-size dataset (n = 103, including BHI-P1, MREX, CB and SBB, see Fig. 3.7) was unmixed into several dominant components, known as end-members. To examine the possible end-members it is important to examine the average grain-size distribution curve and the maximal range of volume frequency for each size class. This graph is plotted in Fig 3.6A and hence provided the lower and upper boundary of the complete grain-size dataset. The end-member-modelling algorithm (EMMA) of Weltje (1997) and Prins & Weltje (1993) was applied to decompose all these grain-size distributions into genetically meaningful end-members. The minimum number of end-members that is required for a satisfying approximation of the data is determined by calculating the coefficients of determination ($r^2$) for scenarios with the number of end-members varying between 2 and 10 (Weltje, 1997).

The $r^2$ statistics indicate that the grain-size records on the Murray Ranch are adequately described as mixtures of three end-members. A three end-member solution produces a significant fit with a $r^2$ of >0.8 within the size range 0.12 – 250 μm, excluding the range ~70 - 100 μm which has a $r^2$ of ~0.7 (Fig. 3.6B). There are virtually no reliable measurements above 250 μm (see the maximal range in Fig. 3.6A), so the decrease in $r^2$ in this size range can be ignored. A higher number of end-members does slightly improve the statistical fit for the size-range 70 - 100 μm, but produces unrealistic new end-members. For instance, a four end-member solution consists of an extra end-member in between the coarsest end-members, but it creates a bimodal curve with an unlikely peak in the coarse sand fraction (see blue curve in Fig. 3.8A). A five end-member model introduces an additional end-member (see blue curve in Fig. 3.8B) with a uniform peak at ~250 μm and an extremely high frequency (~ 43 volume %), which is just not possible considering the maximum frequency in Fig. 3.6A is only 16 volume %. Furthermore, a three end-member model already explains 96% of the observed variance in the entire dataset (see the median 'adjusted' $r^2$ of 0.96 in Fig. 3.6C), and more end-members do not really improve this $r^2$ value significantly. Finally, a visual examination of all plotted distributions reveals three dominant curves in the measured grain-size (see all black curves in Fig. 3.7).

Hence, a three end-member model was chosen as the best solution to describe the grain-size variations in the total dataset of the Murray Ranch. The three modelled end-members are all categorized as unimodal, fine skewed grain-size distributions (Fig. 3.6D). The coarse-grained end-member (EM1) displays a distinct uniform peak at ~150 μm, which is in the fine sand fraction. The intermediate end-member (EM2) is marked by a broader distribution of coarse silt and very fine sand with a mode at ~63 μm. The fine-grained end-member (EM3) is characterized by a modal particle size near 5 μm and a broad curve within the very fine silt and clay fraction. Subsequently, it is possible to plot the proportional distributions of these three end-members versus stratigraphic height, since each measured sediment sample consists of a percentage of EM1, EM2 and EM3 (compare the grain-size curves of samples MREX81 and MREX241 with the three end-members in Fig. 3.6D).

The contribution of EM1, EM2 and EM3 within the MREX section is plotted in Fig. 3.5E. Unit 1 is marked by large proportions of EM2 and EM3 (~57% and 36%, respectively) in contrast to Unit 2 which is almost only composed of EM1 (~87%) and a small portion EM2 (~11%). Subsequently, Unit 3 and Unit 5 display nearly equal mixtures of both EM2 and EM3 with increasing portions of EM3 upwards in the sequence. In Unit 3, EM2 and EM3 both contribute ~45% to the total and in Unit 5 this pattern is ~49% for both end-members. Unit 4 represents a small pulse of solely EM2 (~92%) and Unit 6 is also dominated by EM2, but the contribution of EM3 increases towards the top. Using the proportions of these end-members, it is possible to display in a very simplified but correct way the role of different fluvial processes through time. These interpreted transport mechanisms within the Hell Creek Formation are discussed in Chapter 4.

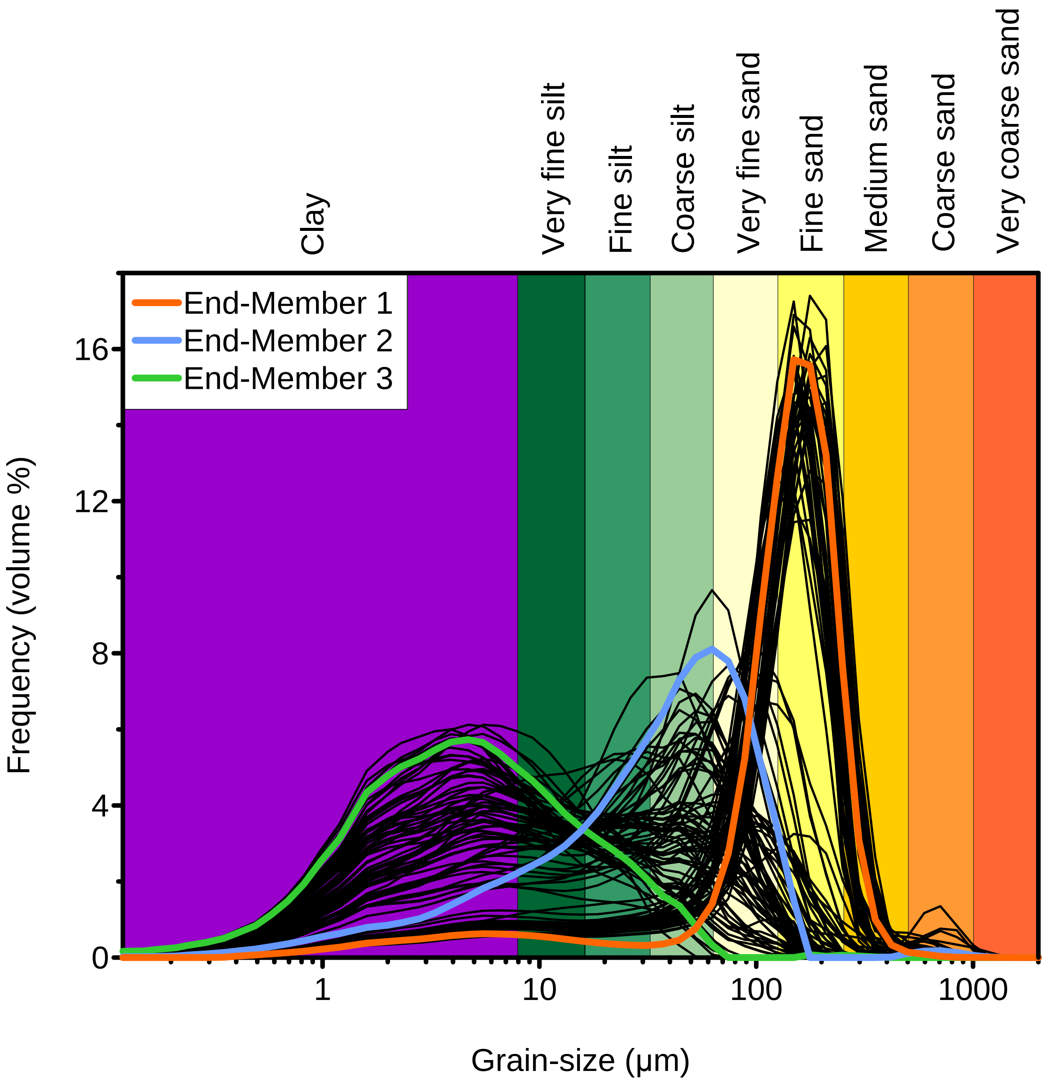


**Fig. 3.7.** All grain-size distributions of the Murray Ranch and the three calculated end-members plotted in one diagram, displaying also the size ranges of the associated grain-size classes (the same colors are chosen as in Fig. 3.5C).

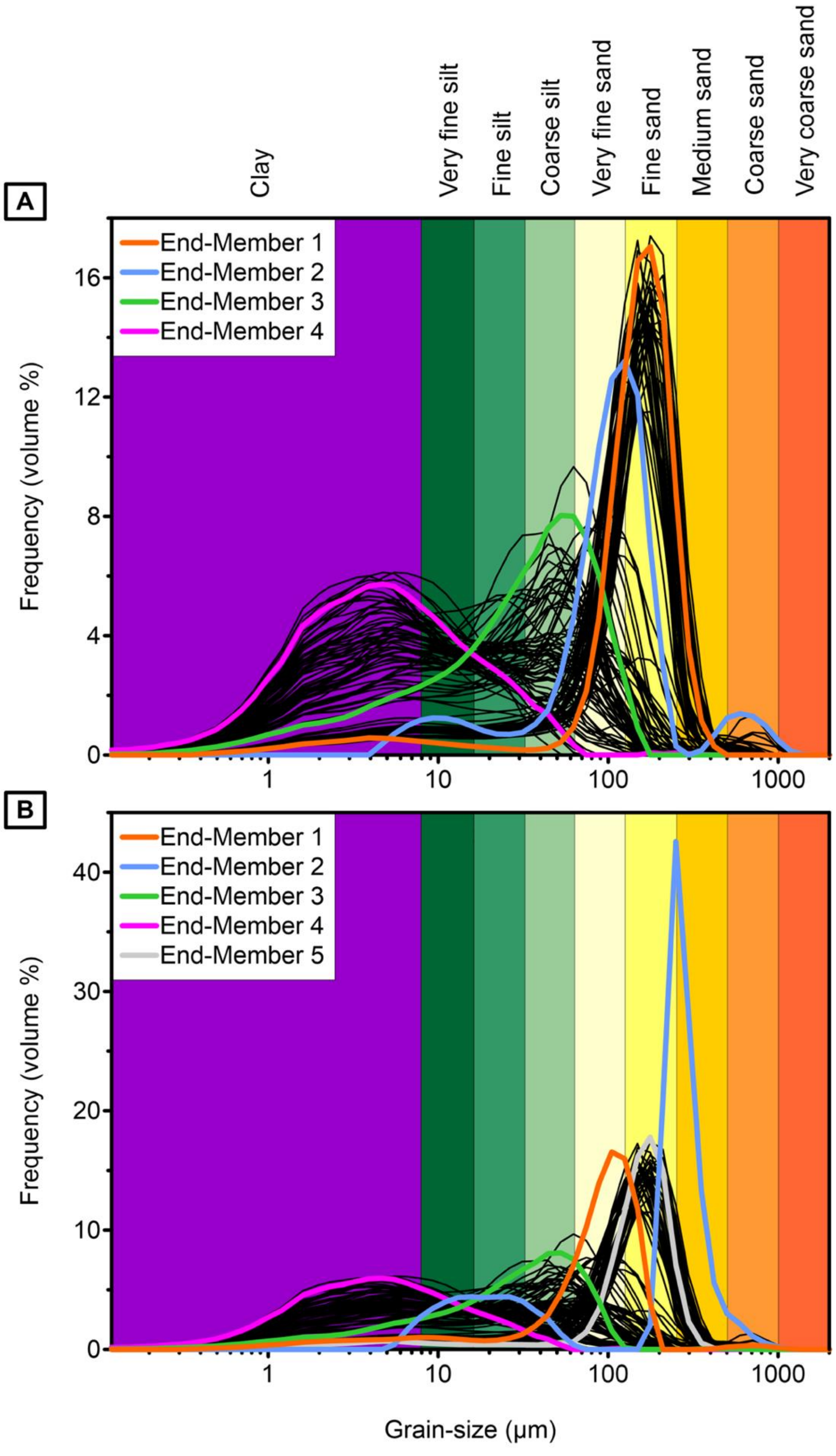


**Fig. 3.8.** A four **(A)** and five **(B)** end-member model of the entire grain-size dataset. The four end-member model creates a fourth end-member with an unrealistic bimodal peak in the coarse sand fraction. A five end-member model introduces an end-member which has a far too large frequency volume % and a strange bimodal peak in the silt fraction. Therefore, a three end-member model was chosen.

It is also possible to visualize the total grain-size dataset (n = 103) in a ternary mixing model to study spatial (and to a lesser extent temporal) variations in grain-size. In Fig. 3.9, the different sections on the Murray Ranch are plotted in two ternary diagrams covering the grain-size classes and end-members, which show a similar pattern. Sand% and EM1% of more than 60% are only found in section BHI-P1 and MREX. In contrast, the sediments from the CB and SB section are dominated by binary mixing of EM2 and EM3. CB and SB are the only two sections that hold clay% higher than 60% and EM3% of more than 70%. When looking in close detail to the MREX section, it becomes evident that the high EM1% is only present in Unit 2, illustrating the unique grain-size fingerprint of this part (which contains the *T. rex* skeleton) in comparison with the rest of the study area.

BHI-P1 shows very similar grain-size characteristics compared to Unit 2 of the MREX section, as can be seen clearly in Fig A2.2. BHI-P1 displays a uniform grain-size peak (with a distinct mode at ~150 μm) throughout its short sequence with only the uppermost sample that shows more similarities with Unit 1 of MREX. The CB section is marked by a clear fining-upward sequence of ~2 m and a gradually increase in EM3% until the 'cyclic' sequence is bounded by a calcrete and a sandy interval with a high EM2% (see Fig. A2.6). The SB section shows a similar fining upward trend that is bounded by a sandy pulse, but in this section the sequence is much longer (~5 m), as can be seen in Fig. A2.8.

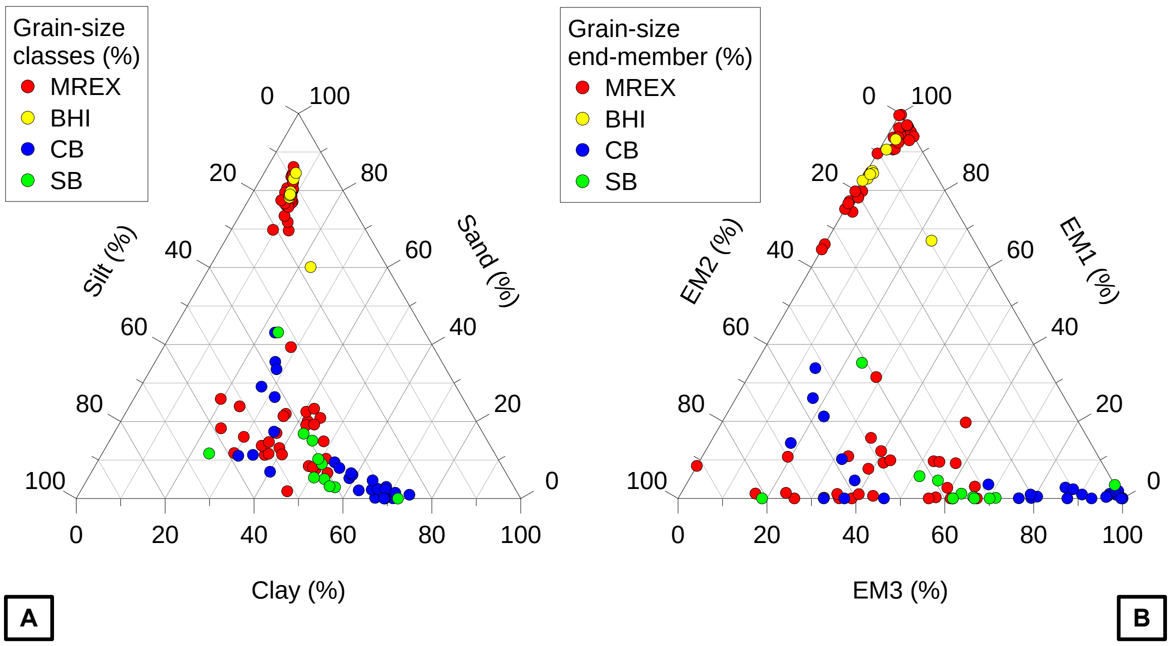


**Fig. 3.9.** Mixing model of the Hell Creek sediments (n = 103) on the Murray Ranch plotted in a ternary mixing space for grain-size classes (sand, silt and clay %) **(A)** and grain-size end-member (EM1, EM2 and EM3 %) **(B)**. Both ternary diagrams show a similar pattern in terms of the dominance of sand and EM1 in the BHI and the (lower) MREX section in contrast to the high % of clay and EM3 in the CB and SB section.

### 3.2.3. Thermogravimetric analysis

Besides studying the characteristics of the lithogenic fraction of the Hell Creek sediments, specific attention was paid on the geochemical properties of the deposits in the study area, by using thermogravimetric analysis (TGA). In Fig. 3.10A, it is apparent that sample MREX81 (from Unit 2) loses its weight predominantly at temperatures from 750°C and higher, whereas sample MREX241 (from Unit 5) displays most weight loss between 100 and 550°C. These two samples were chosen, because within the MREX section they hold the highest carbonate ($CaCO_3$ (wt%)) and organic (LOI550 (wt%)) values, respectively.

A different way to visualize the raw TGA data is based on the first derivative of the weight loss (Fig. 3.10B), which basically means how fast a sample loses its weight per temperature step. This technique allows for the separation of different clay and carbonate minerals, since each mineral is characterized by a specific dissociation signature versus temperature. For instance, sample MREX81 displays a prominent double weight-loss peak, one at ~830°C and a slighter higher peak at ~930°C. This double peak is attributed to the carbonate mineral dolomite, according to Konert & Beets (unpublished). This double peak is related to the decomposition of dolomite - during combustion under an atmosphere of pure $CO_2$ - into calcite ($CaCO_3$) and periclase ($MgO$), and the subsequent decomposition of this $CaCO_3$ into $CaO$ at a higher temperature. Hence, the following chemical reactions take place (from Valverde et al., 2015):

$$CaMg(CO_3)_2 \rightarrow CaCO_3 + MgO + CO_2 \text{ (at ~830°C)} \qquad \text{and} \qquad CaCO_3 \rightarrow CaO + CO_2 \text{ (at ~930°C)}$$

Dolomite can be separated from (limestone) calcite, because this original calcite is marked by a single peak at a slightly higher temperature of ~950°C. Dolomitic calcite (derived from the decomposition at ~830°C) is characterized by relatively low crystallinity compared to limestone $CaCO_3$ and therefore decomposes at lower temperatures around ~930°C (Valverde et al., 2015). So, possibly MREX81 also shows some inmix of original calcite, since the peak is broader and also includes temperature around 950°C.

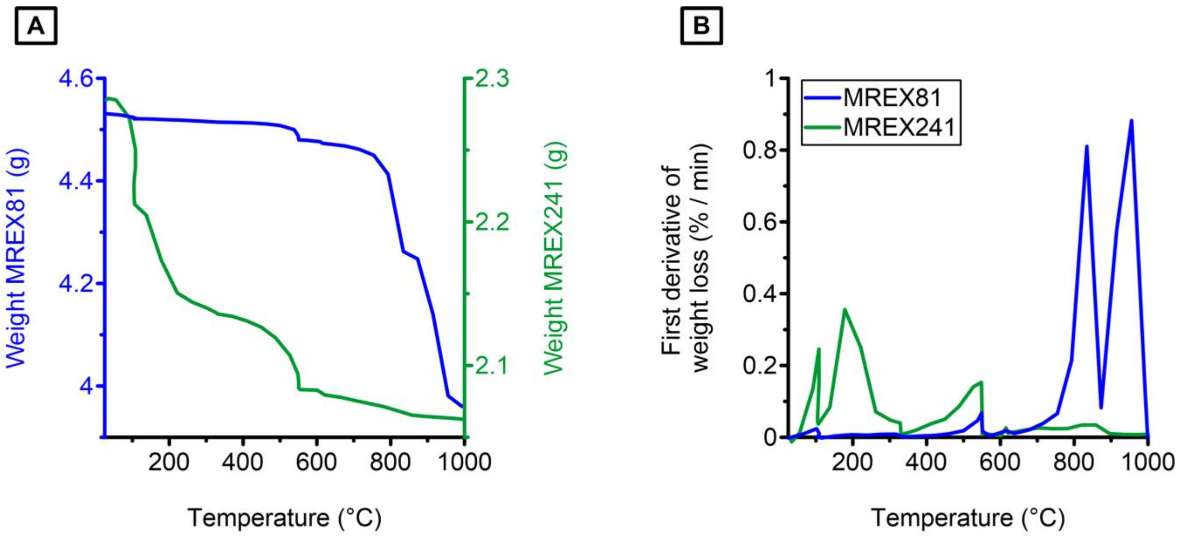


**Fig. 3.10.** Raw TGA data per temperature step of two selected samples, namely MREX81 and MREX241, showing two totally different thermogravimetric fingerprints. The first graph shows the weight of both samples as a function of temperature **(A)**, the second curve illustrates the first derivative of the weight loss, which is a measure of how quickly the sediment samples loses their weight per temperature step **(B)**.

Sample MREX241 shows a clear weight loss peak at 100°C (related to moisture content), at 550°C (linked to combustion of all the organic matter) and a broad peak at ~200°C which might be related to the presence of the clay mineral montmorillonite or is just easily to burn organic matter (Konert & Beets, unpublished).

The same batch of samples (n = 104) was chosen for TGA as the one that was measured for grain-size analysis, including one extra sample in the SB section. In Fig. 3.11, all the TGA data of the MREX section is shown versus stratigraphic height. Firstly, the total organic content (LOI550) illustrates low organic values in the sandy intervals (Unit 2, 4 and 6 display an average LOI550 value of 1.4%) compared to high values in the mudstone intervals (Unit 1, 3 and 5 shows a mean value of 2.8%). Unit 3 and Unit 5 are characterized by a fining upward and increasing organic trend resulting in a maximum value of almost 6% (sample MREX241). The high LOI550 value in the top of Unit 6 might be explained by distortion of modern-day plants, since this part is almost at the surface.

On the other hand, the total carbonate data of the MREX section show in general an opposite signal with sharp boundaries at the base and the top of the section. The sandy units 2 and 6 hold high $CaCO_3$ values with an average of 15% and a maximum value of 26% (sample MREX81). The mudstone Units 1, 3 and 5 are low in carbonate content and have an average value of 2.6%. Unit 4 shows a small decrease in organic content, but no change in carbonate % and hence displays the same trend as in Unit 3 and 5.

It is also possible to plot the individual thermogravimetric signatures from Fig. 1.10B versus stratigraphic height in a similar way as the grain-size contourplot of Fig. 3.5D, but this time the z-axis represents the first derivative of weight loss. In Fig. 3.11D, this TGA contour plot is shown and it is marked by two intervals (unit 2 and 6) with a prominent double peak between 800 and 850°C and between 900 and 950°C. This is probably related to the abundant presence of the carbonate mineral dolomite, but high values around 950°C may also suggest some influence of the mineral calcite within the sandstone matrix. These carbonate minerals are clearly absent in Unit 3, 4 and 5, because this large interval is characterized by enhanced weight loss values at 550°C and in the temperature range 150 - 330°C indicating the presence of much organic matter and possibly the clay mineral montmorrilonite. In nearly all samples, a small peak at 100°C is visible due to the evaporation of the moisture in the sediment.

All TGA data of the BHI-P1, CB and SBB section is shown in Appendix 2. The BHI-P1 section shows clear similarities with Unit 2 of MREX with $CaCO_3$ values between 16 and 25%, LOI550 values between 0.9 and 2.4% and a double weight loss peak signature with a high second peak around 930°C (Fig. A2.1). Cyclic Butte is marked by high dolomite values (~17%) at the base and top of the section, whereas the middle part displays an upward trend of increasing organic %. Shelly Butte reveals also this more organic upward trend (at a maximum of 7%), but lacks high dolomite values at the base, but this may be related to a low sample resolution. Finally, it might also be possible to perform an end-member modelling algorithm on the TGA dataset, but this technique is currently under development and its benefits should still be studied. One of the complexities of the raw dataset is that every TGA-sample is measured at slightly different temperature steps and this hampers quick end-membering.

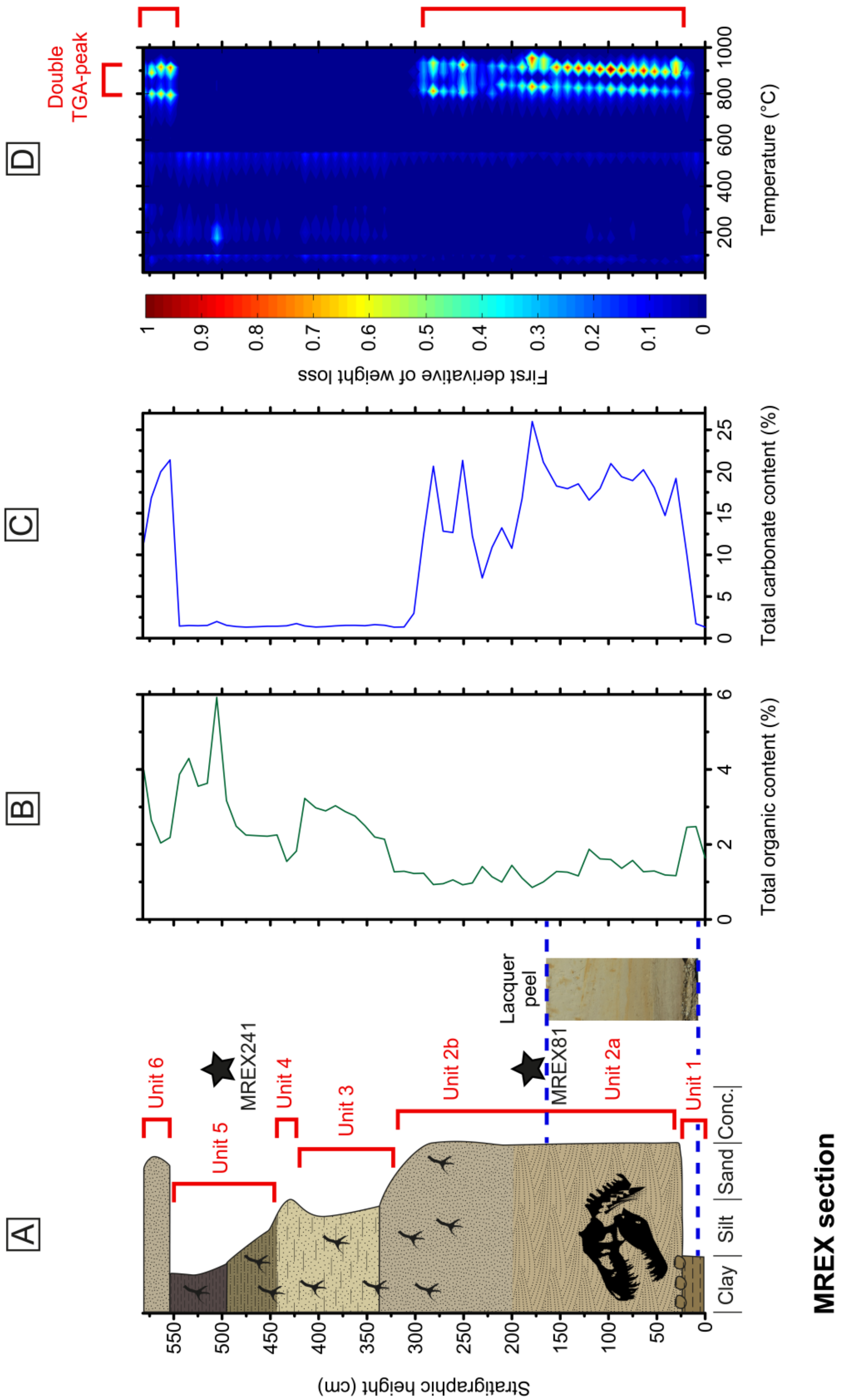


**Fig. 3.11.** TGA data of the MREX section showing the stratigraphic position of the six sedimentary units and the two samples of Fig 3.10 **(A)**. The graphs with the total organic content **(B)** and total carbonate content **(C)** are roughly opposite of each other. The TGA contourplot **(D)** confirms this pattern and shows double dissociation peaks in Unit 2 and 6 (indicated in red), suggesting the presence of the carbonate mineral dolomite (Konert & Beets, unpublished).

### 3.2.4. Petrography

Detailed microscopic examination of thin sections of sediment samples surrounding the *T. rex* fossil (sample MREX16, MREX81, MREX116, LB2 and BHI P1.2) revealed that the rock is mainly matrix-supported, because the matrix (defined as detrital material with a mean diameter of <30μm) comprises more than 15% of the rock volume (Dott, 1964).

The mineral grains in Unit 2 of the MREX section are predominantly quartz (~ 70%) and carbonate (~ 25%) and a very small fraction of amorphous organic matter and rare feldspar and mica grains (~ 5%). Quartz is recognized by its colorless appearance in PPL (Fig. 3.12A), low relief, absence of cleavage, undulose extinction in XPL (Fig. 3.12B) and low birefringence (resulting in pink and orange colors when a gypsum plate is inserted in the microscope, such as in Fig. 3.12C). Using optical microscopy, it is very difficult to distinguish calcite from dolomite, since both carbonate minerals are characterized by very high relief, perfect rhombohedral cleavage, high birefringence, pearly appearance with tiny patches of color and lamellar twins on some crystal faces (Fig. 3.12D&E). Therefore, the generalized term 'carbonate mineral' is used in Fig. 3.12. An additional thin section was made of the shellbed of section SBB to test if microscopic structures of the aragonitic bivalve shell (for instance the nacreous layer or wavy growth laminations) are visible in the sediments surrounding the *T. rex* fossil. However, no such shell structures were observed in Unit 2 of the MREX section.

There are also no clear signs of a secondary matrix produced by diagenesis, because no calcite cement structures are visible. This confirms the observation in the field that the sandstone was poorly consolidated and therefore it was possible to make a lacquer peel in this deposit. Furthermore, all grains are more or less of the same size, so a good sorting is present, as confirmed also by the data derived from the grain-size analysis. Finally, the grains of quartz and carbonate have a subangular to very angular shape. Hence, based on the thin sections of Unit 2 of the MREX section, it is concluded that the rock entombing the Naturalis *Tyrannosaurus rex* can be classified as an immature, well-sorted, poorly consolidated, matrix-supported, calcareous, arenitic sandstone (Dott, 1964).

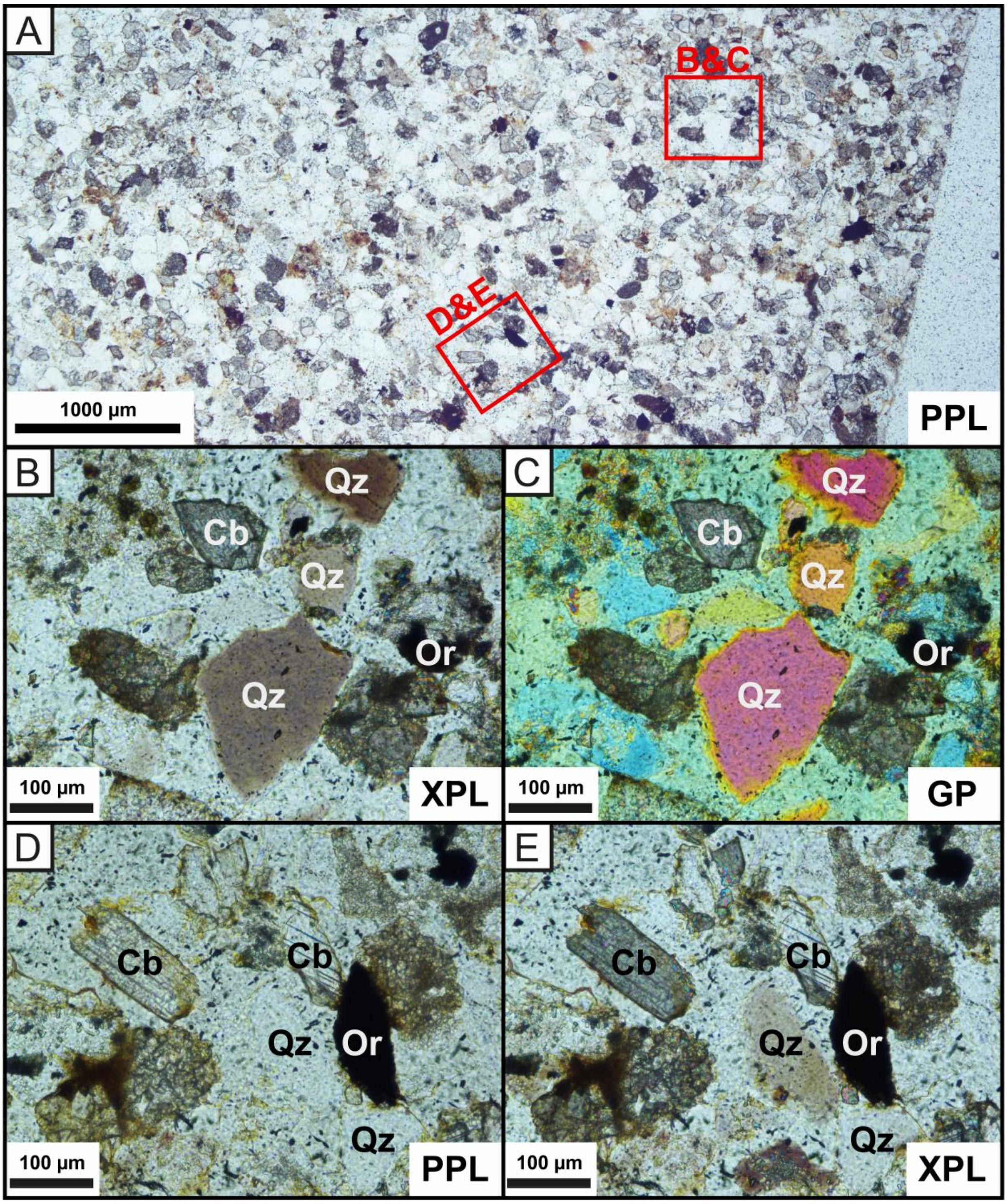


**Fig. 3.12.** Selected close-ups of the thin section of sample MREX81 showing a well-sorted lithology with mainly subangular to very angular quartz (~ 75%) and carbonate (~ 25%) grains. Abbreviations: PPL = plane polarized light, XPL = cross polarized light, GP = gypsum plate, Qz = quartz, Cb = carbonate, Or = amorphous organic matter.

## 3.3. Paleoenvironment

In this paragraph, results are presented which can help to reconstruct the ancient habitat of the Naturalis *Tyrannosaurus rex*. The sedimentological and geochemical data shown in paragraph 3.2 already give some clues about the paleoenvironment, but in this section specific faunal and macrofloral evidence from the field and a palynological pilot-study is reported to answer the second research question.

### 3.3.1. Field evidence

During the field campaign on the Murray Ranch, besides sampling of the Hell Creek sediments for grain-size analysis and TGA, extra attention was paid for paleoenvironmental indicators. An overview of this field evidence can be found in Fig. 3.13.

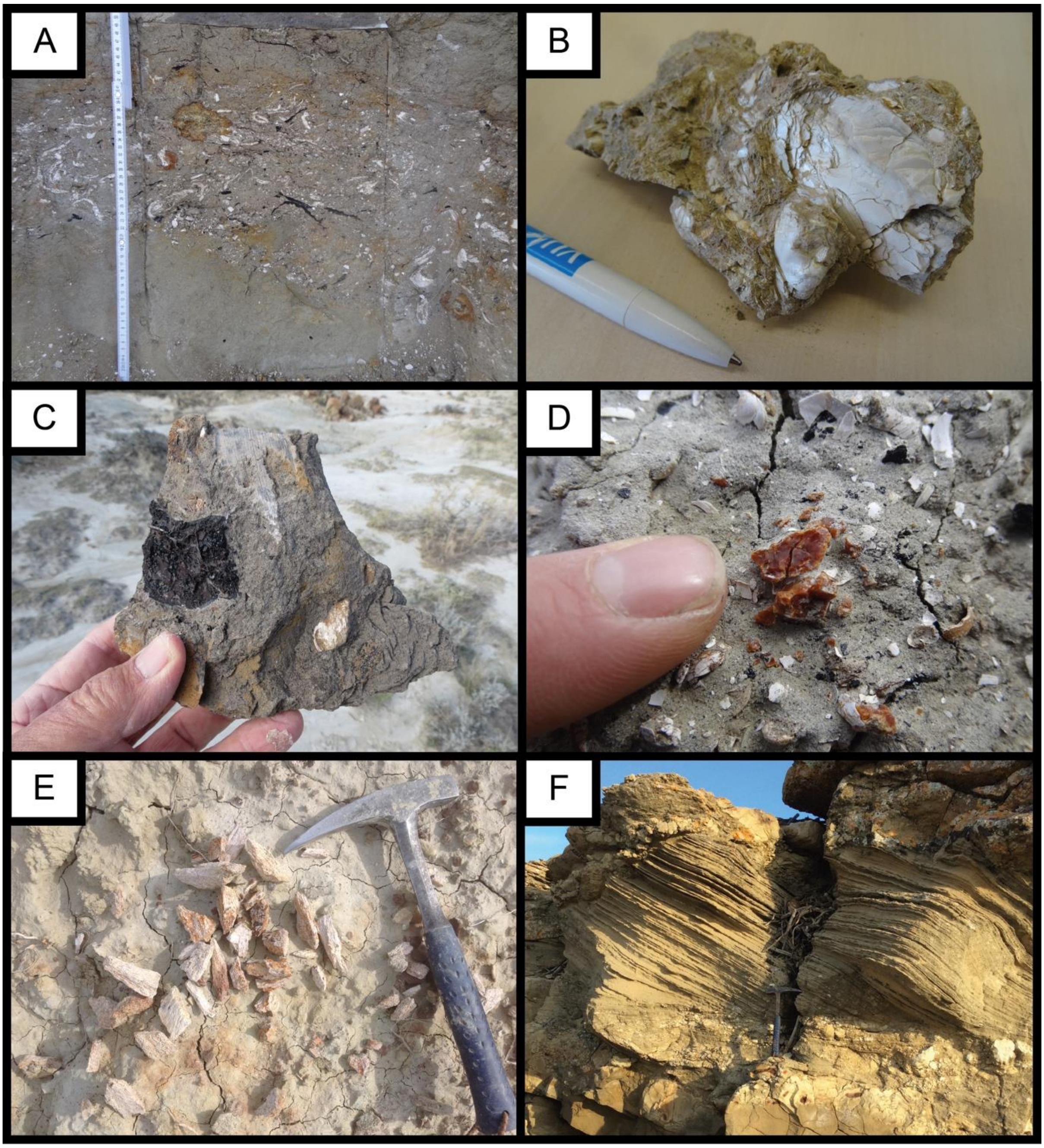

**Fig. 3.13.** Paleoenvironmental field evidence from the Murray Ranch, ranging from a prominent shell layer **(A&B)**, coalified leaf horizon **(C)**, microsites with amber **(D)** and dinosaur bone fragments (in this case *Triceratops*) **(E)** and large rip-up clasts overlain by megacrossbedding **(F)**.

For instance, the ~0.5 m thick shell bed at Shelly Butte is one of the most prominent features in the study area. A small lacquer peel (Fig. 3.13A) was made at this location to study these sedimentary structures and revealed the presence of charcoal seams, siderite nodules and well-preserved aragonitic bivalves. These shells were identified as members of the family of Unionidae which represents freshwater mussels (Fig. 3.13B). The shell bed is overlain by a leaf horizon which holds numerous coalified and fragmented leaves from angiosperms (Fig. 3.13C), but the coaly preservation inhibited accurate identification. All these findings suggest quiet water conditions in which bivalve fauna could live and leaves could settle and preserve. Shell layers were also found higher up in the SBB section and in both Rex Hills sections (Fig. 3.2).

On the contrary, leaves and shells were not found at the MREX section, so a different depositional setting is favored at the dig site. The rip-up clasts, climbing ripples and crossbeds (Fig. 3.3) point towards high energetic conditions. Rip-up clasts and crossbeds are also observed elsewhere in the study area, for example at the top of the Piney Ridge section. However, here these structures are much larger and therefore indicate even higher flow velocities and erosive forces (Fig. 3.13F).

Furthermore, multiple microvertebrate accumulations (abbreviated as microsites) were found throughout the study area and contained many pieces of amber and charcoal (Fig. 3.13D), shell fragments, (gar) fish scales and vertebrae, egg shell fragments, coprolites, and tooth and bone shards of numerous vertebrates such as turtles, crocodiles, champsosaurs and dinosaurs (Fig. 3.13E. These isolated dinosaur finds were identified by Peter Larson and included *Triceratops* sp., *Edmontosaurus annectens, Pachycephalosaurus wyomingensis*, *Nanoyrannus lancensis* and *Tyrannosaurus rex*.

### 3.3.2. Palynology

To examine the ancient vegetation associated with the Naturalis *Tyrannosaurus* rex, a pilot-study was carried out on the microfossil flora of pollen and spores of the Hell Creek deposits on the Murray Ranch. The objective of this palynological analysis was three-fold. Firstly, it was tested if the same preparation technique used for Holocene pollen samples in the Sediment Laboratory at the VU could be applied for Cretaceous pollen. Secondly, the general trends in vegetation and therefore paleoenvironment of the Naturalis *T. rex* was assessed by counting and subdividing the pollen assemblage into ferns, gymnosperms and angiosperms (Fig. 3.14) according to the methodology of Vajda et al. (2013). Thirdly, biostratigraphy was carried out over a composite stratigraphic log of ~32 m by examining specific marker species and their ranges of first and last occurrences based on the palynostratigraphic model from the Hell Creek Formation by Nichols (2002). A detailed pollen count table and the raw palynological data can be found in Appendix 4.

Regarding the first objective, the preparation technique as described in paragraph 2.5 was succesfully applied on the pollen samples from the Murray Ranch. The preservation of most pollen slides was fairly good despite their geological age. However, more added organic material would have been better, because in most cases a minimal amount of 100 pollen grains was just reached. Two samples were not suitable for counting, namely sample 1 (BHI-P1.8) and 4 (MREX16). These sediment samples consist of clay-pebbles in a sandstone matrix, but unfortunately did not yield enough pollen material. It is important to note that the pollen samples from the MREX section (#2-4) are not from the immediate sediments enclosing the fossil, but from the clay layer beneath the pelvis block. So to be precise, the paleoenvironment just before the burial of the Naturalis *T. rex* is examined and not the time of the burial itself, since pollen are rarely preserved in a sandstone matrix (Kroeger et al., 2002).

Ten pollen slides contained enough pollen material and were counted for this study to determine the general vegetational trends. In this study, the pollen and spores were subdivided in three main groups, the ferns (which in this case include both bryophytes (mosses, hornworts and liverworts) and pteridophytes (true ferns, horsetails, clubmosses, spikemosses and quillworts), gymnosperms and angiosperms, as can be seen in the microscopic photo-overview of Fig. 3.14. A fourth group was added, namely the '*Azolla* sp. and *Ghosispora bella*'. These taxa are ferns, but have a distinct paleoenvironmental signature and are therefore considered to be a different classified group in this study. In addition, the presence of algal cysts was noted in the pollen slides, but they were not counted in percentage abundance calculations. On average, the palynofloral assemblage of the ten counted samples consists of 55% angiosperm pollen, 29% fern spores, 9% gymnosperm pollen and 7% spores from *Azolla* sp. or *Ghosispora bella*. Throughout the sequence this pattern does not really change, as can be seen in the circle diagrams of Fig. 3.15.

An exception is sample 2A (MREX1), which holds much more ferns than the other samples. However, this may be related to the fact that this sample was the first one I examined and at that moment I was in the beginning of the process of getting a solid taxonomic understanding of the Hell Creek pollen assemblage. Especially, because sample 2B (from the same stratigraphic level and studied in a later stage) displays similar percentages of the four groups as in the average composition. Furthermore, sample 11 (SBB6.1) is marked by a low relative abundance of angiosperms, but this may be linked to the fact that this specific sample is derived from the most organic-rich part of the study area (LOI550 of ~7 wt %). Therefore, sample 11 was very rich in pollen grains and only a fraction of the pollen slide was examined, because it was decided to count a number of 100 pollen/spores per slide. Overall, the Hell Creek palynoflora is relatively homogeneous throughout the studied sections and is dominated by angiosperms.

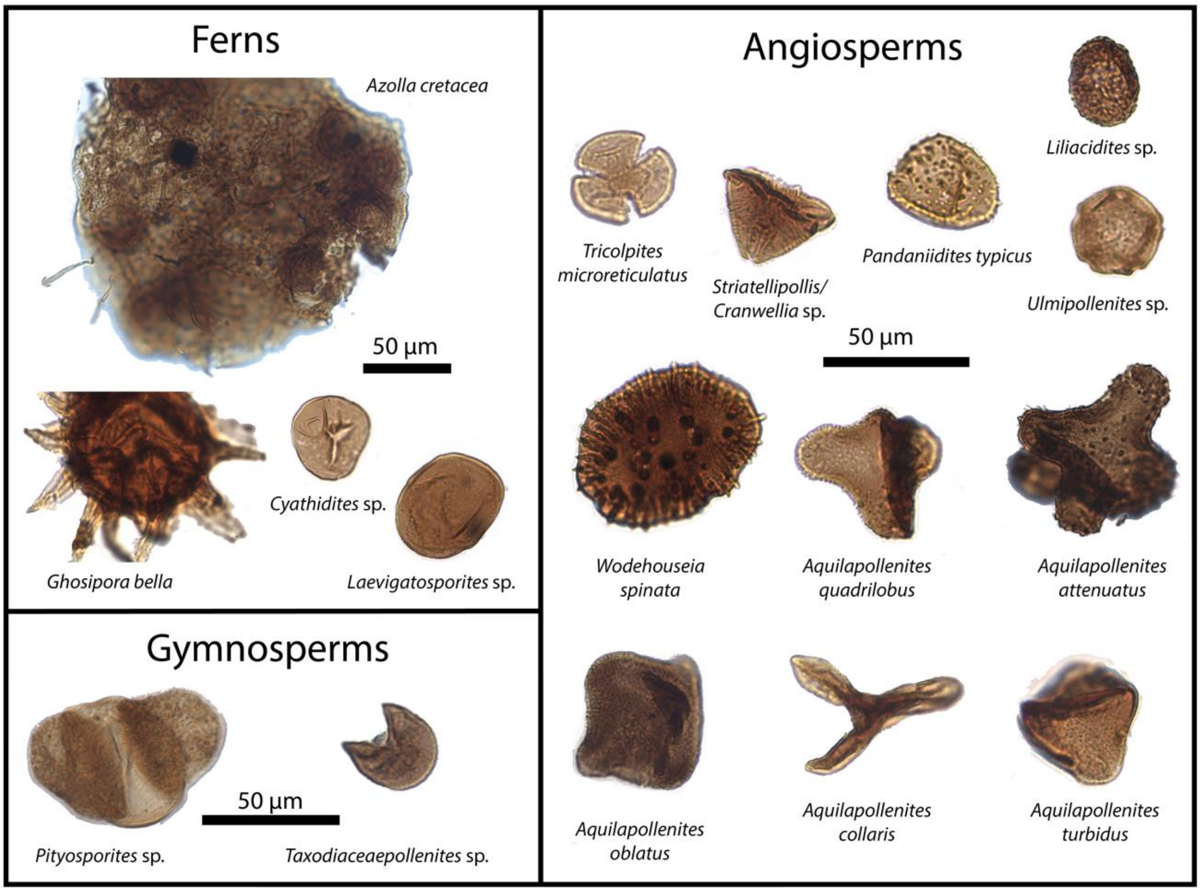


**Fig 3.14.** Microscopic photographs of a number of characteristic and important palynomorph taxa found in rocks of the HCF in the study area. The pollen and spores are subdivided here in three groups: the ferns (land and aquatic), gymnosperms and angiosperms. The taxa shown here are all described in Nichols (2002) in terms of morphological characteristics, occurrences (in the Mud Buttes area in North Dakota) and paleoecological and biostratigraphic significance.

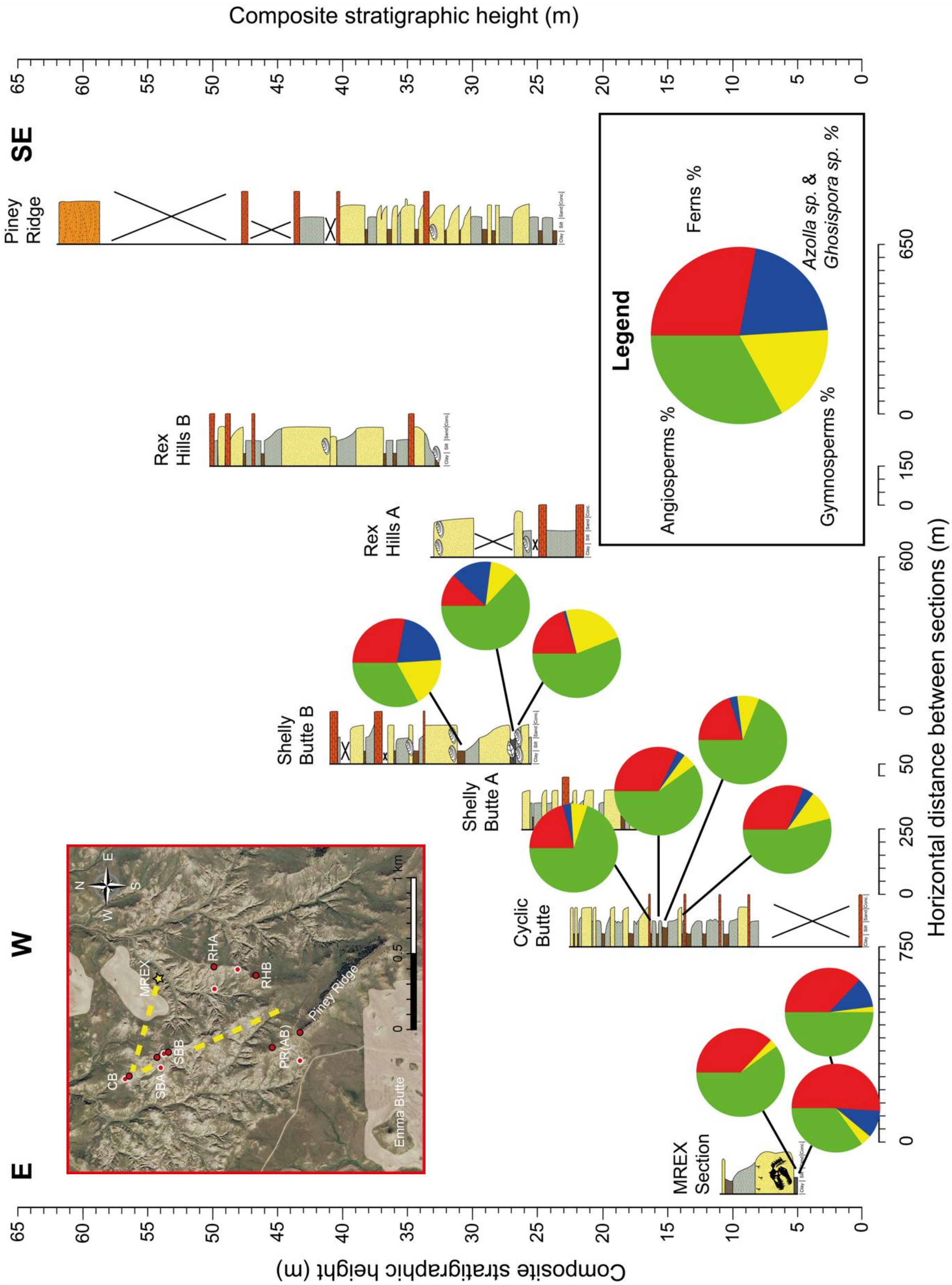


**Fig. 3.15.** Pollen circle diagrams plotted on top of the lithostratigraphic framework of the Murray Ranch of Fig 3.2. This figure shows a relatively homogenous palynoflora, since the variations of the contribution of the four palynomorph groups does not dramatically change throughout the stratigraphic sequence.

Besides the general vegetational trends, specific attention was paid to a number of marker species and genera of the Hell Creek Formation that have characteristic paleoenvironmental and biostratigraphic significance. In Fig. 3.16, a total number of 25 different pollen and spore taxa (or group of taxa) is shown with their stratigraphic ranges (not their relative abundance, but solely their presence or not). First of all, a composite log was necessary to place all these pollen samples in one biostratigraphic framework. This composite log is ~32 m thick and involves the entire stratigraphy of the MREX section, the lowermost calcrete level of the CB section, the middle and upper part of the CB section (~3 – 14.3 m), a portion of the upper part of the SBA section (~5.5 – ~8.5 m) and the entire lower part of the SBB section (0 - ~7 m). The pollen and spores were mostly identified using photos and descriptions from Nichols (2002) and subsequently classified into the botanical and morphological categories of Table 4 and 5 of Nichols (2002). The most important outcomes of this study are listed below per major botanical group.

The major botanical group of ferns is morphologically subdivided into monolete and trilete spores. The monolete spores are dominated by *Laevigatosporites* spp. (Fig. 3.14) and this genus encompasses an elongated, simple morphology lacking sculpture and within the size range 25 – 60 µm. It is the most common and abundant taxon in the Hell Creek palynoflora (Nichols, 2002) and also in the study area, as can be clearly seen from count table in Appendix 4. The trilete spores are more diverse, with *Cyathidites* spp., *Stereisporites* spp. and *Gleichenites* spp. as most important genera. These relatively small ferns are characterized by a triradiate mark in the center, have in general a smooth surface that lacks ornamentation and varies in shape from triangular to slightly circular. Similar to their monolete relatives, the trilete spores are present through the entire sequence, but they are in general ~50% less common than monolete spores.

A distinct group of trilete spores are *Azolla* spp. and *Ghosispora bella* and they are considered as a separated major group. In this study, *Azolla* spp. encompasses two species; *Azolla circinata* and *Azolla cretacea* (Stanley, 1965), of which the latter is far more abundant. They can be recognized by their large size and their massulae (coherent mass) of microspores. *Azolla cretacea* has anchor-like projections (glochidia), whereas *Azolla circinata* displays more rounded or fiddlehead-shaped glochidia. Notable is the widespread occurrence of *Azolla* spp. in Fig. 3.16 (indicated in blue) , these aquatic ferns have been found in all but one sample (#3 = MREX11). *Ghosispora bella*, recognized by its spine-like appearance, is less common.

The gymnosperms are subdivided into two distinct morphological groups: the large bisaccate pollen ('double air-sacs shape', e.g. *Pityosporites* spp.) and the smaller inaperturate pollen ('pacman shape', such as *Taxodiaceaepollenites hiatus*). Both pollen types are present throughout the entire stratigraphic range, with a clear increase in inaperturate pollen towards the top of the sequence. However, the contribution of gymnosperm taxa within the total Hell Creek palynoflora of the study area is limited.

The angiosperms are by far the most abundant and most diverse floral group on the Murray Ranch and they are botanically subdivided into a small group of monocots and a more diverse group of dicots. The monocots are represented by three dominant genera, namely *Pandaniidites*, *Arecipites* and *Liliacidites*. The latter two genera were combined in one group, since they are somewhat difficult to distinguish because they are both characterized by a monosulcate structure (with one elongated aperture (colpus or sulcus)). Pollen of the genus *Pandaniidites* also show one pore, but they have a typical echinate sculpture, meaning covered with small spines.

The dicot taxa *Ulmipollenites* spp. / *Alnipollenties* spp. and *Striatopollenites* spp. / *Cranwellia* spp. were also combined to categories of convenience when scanning the slides, because these are morphologically difficult to distinguish. The most abundant angiosperm species found was *Tricolpites microreticulatus* (see Table A4.1), easy to identify because of its small size (>30 µm), 'clover three'-like appearance with three colpi and microreticulate sculpture. Since the angiosperms show a high biodiversity, are often not completely preserved, but are characterized by colpi and reticulate structures, I categorized unidentifiable angiosperms in the informal group 'other angiosperms'. An important biostratigraphic dicot species is *Wodehouseia spinata,* which is easy to recognize by its unique ovate lenticular shape with four colpi and echinate sculpture. Because this species is found in nearly all samples from top to bottom (indicated in green in Fig. 3.16), the palynoflora of the study area can be classified into the Late

Maastrichtian *Wodehouseia spinata* Assemblage Zone. Another relevant biostratigraphic marker taxon is *Aquilapollenites* spp. (Tschudy & Leopold, 1970). In this study, 13 different species of *Aquilapollenites* were recognized, which are all characterized by a reticulate sculpture, but differ enormously in shape. Specific attention was paid to the presence of *Aquilapollenites collaris*, (indicated in green in Fig. 3.16), a species which differs from the rest of its relatives by a long slender body and a distinctive collar like zone of finely reticulate sculpture separating coarser reticulate sculpture on the major pole. It was only found in three of the four uppermost samples and thereby might give some age constraints (see paragraph 4.3.2).

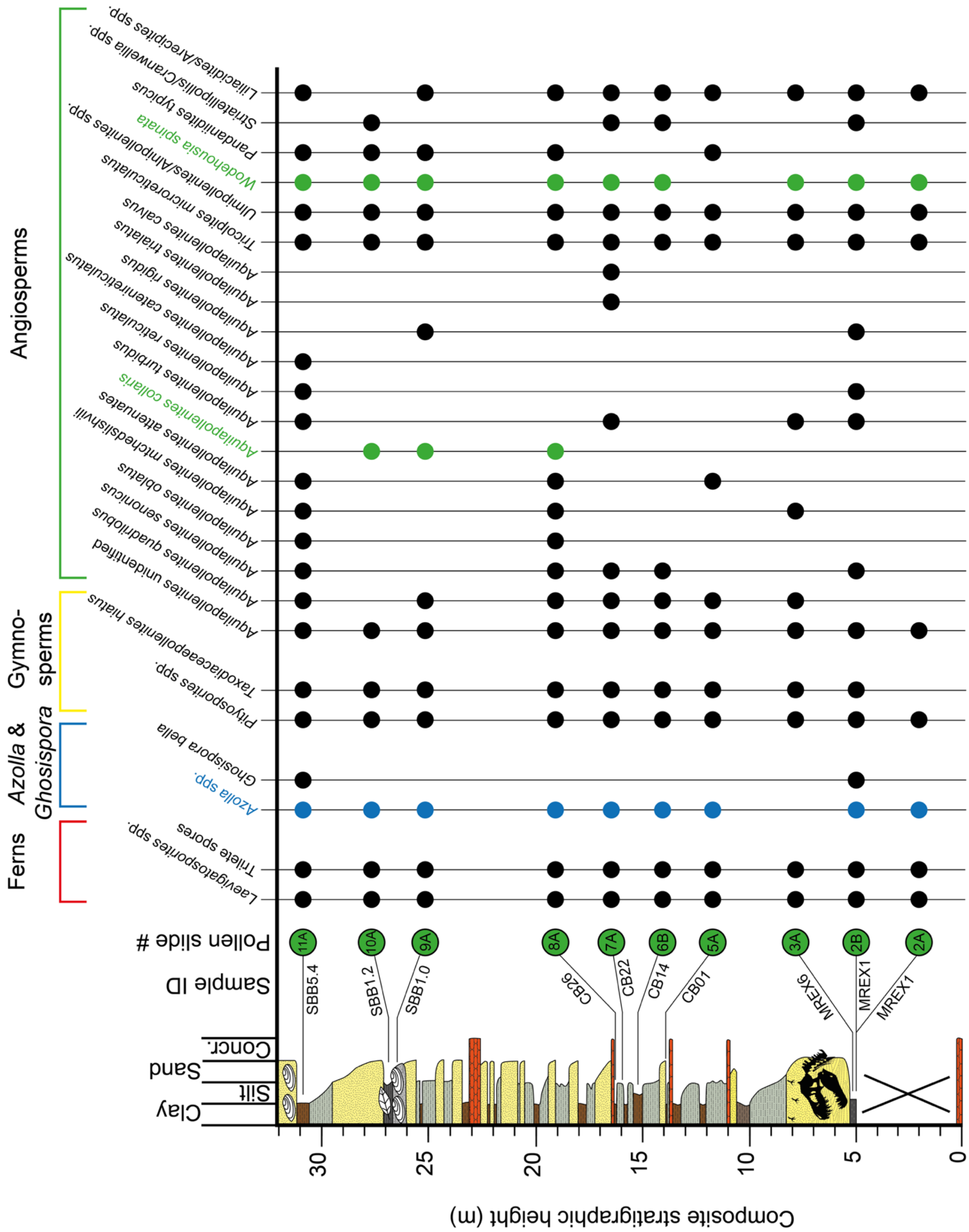


**Fig. 3.16.** Distribution of 25 different spore and pollen taxa in the Hell Creek Formation on the Murray Ranch, three taxa are color-indicated since they are discussed in detail in the text. A composite stratigraphic log was made from the MREX, CB and SB sections to place all samples in one biostratigraphic framework.

## 3.4. Integrated stratigraphy

In this paragraph, the results of the stratigraphic study are presented. To place the fossil locality accurately in time, it was necessary to examine also the exposures in the neighborhood of the dig site. A local, temporal framework was produced by correlating the different successions of sediments throughout the study area into a composite log. Subsequently, integrated (litho-, bio-, magneto- and cyclo-) stratigraphy was applied on the sections to date the *T. rex* bearing strata. Biostratigraphy is already described in the previous chapter, so in this part the focus lies on magneto- and cyclostratigraphy.

### 3.4.1. Field correlations

As already shown in Fig. 3.2 and Table 3.1, seven sections were used to produce a regional correlated lithostratigraphic framework of the study area. To produce such a framework was not an easy task, for several reasons. First of all, the exposure density on the Murray Ranch is very limited due to an extensive cover of prairie vegetation, recent hill-slope processes resulting in abundant alluvium and the presence of only shallow incisions in the landscape. Moreover, as mentioned before, the fluvial deposits of the Hell Creek Formation are by nature lenticular and the large variations in sedimentation rate between different lithologies (e.g. sandstone versus mudstone) inhibits accurate lateral correlations and challenges the dating of specific horizons. Finally, there is a small tectonic dip of ~1.3° towards the northwest, based on the interpretation that the crossbedded sandstone top of Piney Ridge (PRB) correlates with the 5 m lower positioned hard sandstone cover of the isolated butte 220 m to the NW (PRA). This small dip might not seem much, but can clearly obscure correlation of thin beds over long distances.

To overcome these problems, a number of techniques were applied. Elevation measurements were performed on specific stratigraphic levels using a Differential GPS (Fig. 2.2E&F) and prominent and persistent horizons were traced with this DGPS and also with an iPad equipped with GIS-PRO software. Furthermore, Google Earth was used to check the topographic relationships between the sections and the elevation tool in this software was used to verify the DGPS measurements. As a prominent layer throughout the study area, the shell bed of section Shelly Butte A was chosen as a base level. On basis of DGPS measurements, the base of the MREX section was set on ~1015 m above sea level and the top of the section (Piney Ridge B) was set on ~1083 m above sea level, so a height difference of ~68 m was established. However, the resulting correlated stratigraphic log (visible in Fig. 3.17) shows a total composite stratigraphic height of only ~62 m. Especially the Rex Hills and the Piney Ridge sections were 'lowered' in their height to compensate for the tectonic dip by placing their shell layers at the same stratigraphic height as the shell beds of SBB. These shell layers are interpreted as lake bottoms and are therefore assumed as originally horizontal throughout the study area.

Some of the field correlations should be discussed here and are visible in Appendix 2. Although some 750 m apart, it was interpreted that the base of Unit 2 of the MREX section is correlated to the top of a distinct calcrete level below Cyclic Butte. On top of this calcrete level is an 8 m thick poorly exposed, but very sandy interval which is interpreted as a lateral and thicker component of the channel sandstone of the MREX section. The top of this poorly exposed channel body is a flat plain which resembles the base of the main CB section (Fig. A2.5B). The overlying silt and mudstones correspond fairly well with Unit 3 and 5 of MREX. The carbonaceous shales of CB can be correlated within one point of view with the strata of Cricket Butte and Shelly Butte, together with the help of calcrete horizon 4 just above CB (Fig. A2.5C). Calcrete 4 and the shell beds of SBB can be linked to the layers of section Rex Hills A (Fig A2.7A and A2.9A). The top of SBB is another calcrete level (Fig A2.7A) which can be correlated with the second calcrete in the Piney Ridge section (visible in the middle of the photo of Fig. A2.10B).

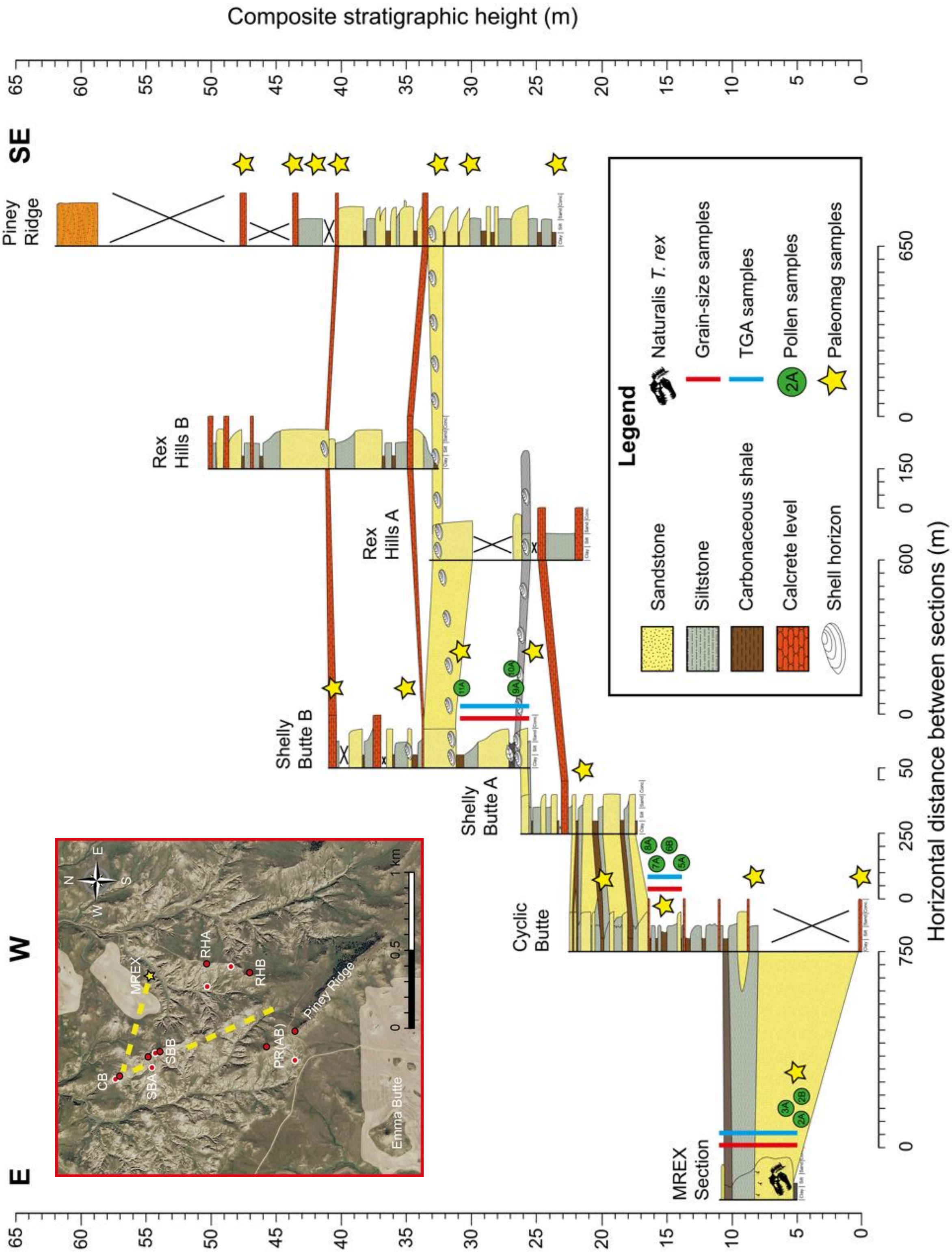


**Fig. 3.17.** Lithostratigraphic framework of the study area showing all the field correlations and consisting of ~62 m of stratigraphy. Some of these correlations are visible in the photo-overviews of Appendix 2. As correlative horizons various distinct and persistent shell beds, carbonaceous shales and calcrete levels were chosen.

Ideally, a stratigraphic fence diagram was made of the study area, since the placement of the different sections within the 'average correlation line' (see Fig. 3.1) introduces some additional errors. However, the number of sections and the overlap in elevations between the sites was not sufficient enough to create a meaningful fence diagram. On basis of the geological map of Vuke and Wilde (2004), it was decided to work from the bottom to the top of the Hell Creek Formation, so from the MREX section upwards. From Fig. A.1.4, it was interpreted that the Paleocene Fort Union Formation should be present in the southeastern part of the study area. However, the K-Pg boundary claystone (as described in paragraph 1.3.6) was not recognized in the field. This does not definitely mean the Paleocene Fort Union is not present on the Murray Ranch, because the K-Pg boundary markers are often eroded (Smit, 2014, pers. comm.). To verify if the study area comprises solely Cretaceous or also Paleogene deposits, a detailed magnetostratigraphic study is needed, which is described below.

### 3.4.2. Magnetostratigraphy

Oriented paleomagnetic samples were collected from the study area at a series of different elevations to ensure a close spacing and a large stratigraphic range which provided the basis for a long time record with a high resolution. All paleomagnetic results (MS, TH and AF) versus a composite stratigraphic log are shown in Fig. 3.18. The composite log of ~62 m thickness was created by extending the log used for palynology (Fig. 3.16) and assuming the calcrete top of the SBB section correlates with the second calcrete level of the PR(AB) section. The Rex Hills sections were not incorporated in this log since no paleomagnetic samples were taken at these sections.

In general, the paleomagnetic results were of intermediate quality. In total, 104 samples were demagnetized, but after careful statistical analysis using the online portal paleomagnetism.org, only 40 were selected to use in Fig 3.18. These 40 samples are listed in Table A5.1 and all 104 samples can be found in the associated Excel file of Appendix 5. The magnetic susceptibility data shows some variations per lithology. The siltstone intervals display an average magnetic susceptibility of 8.4E-8 (max = 9.04E-8 and min = 7.07E-8), whereas the calcrete levels hold in general quite low values (on average 5.5E-8), except for one sample at 40.5 m stratigraphic height (9.66E-8). The samples all but one displays positive inclination and only five samples show a declination towards 180°. MAD stands for the maximum average deviation of the interpreted characteristic remanent magnetization (ChRM) direction and a cut-off with a MAD of 20 was chosen to select the most reliable samples. The intensities of the natural remanent magnetization (NRM) show a wide range from 26 μA/m towards 2621 μA/m within the calcrete levels, whereas the siltstones are more constant and display an average value of 411 μA/m.

Rock magnetic analysis performed by Lars Noorbergen on fluvial deposits from the Fort Union Formation suggested that magnetite ($Fe_3O_4$) was the most dominant magnetic carrier and this would probably also be the case for the Hell Creek Formation (Noorbergen, 2015, pers. comm.). Due to the very low intensities of the Fort Union samples, a TH incremental heating profile from 20 to 400°C was chosen also in this study and an AF range of 5 – 100 mT, to be able to isolate stable components and detect overprints. In Fig. 3.19 – 3.21, three paleomagnetic samples are shown with a distinct signature consisting of a Zijderveld diagram, an equal area plot and an intensity curve, as derived from paleomagnetism.org. Sample TRX7 (in the clayey siltstone Unit 1 of the MREX section) was picked (Fig. 3.19), because this calcrete sample was located in a fine-grained interval as close as possible to the Naturalis *T. rex* skeleton (Fig. 3.22). Sample PRB1.1 B+C on Piney Ridge (Fig. A2.10A) was chosen as the stratigraphically highest position (at a composite height of 47.5 m) of the section and thereby providing the upper range of the magnetostratigraphic framework (Fig. 3.20). Sample SB1.1 AB represents the calcrete top of the Shelly Butte B section (composite height of 40.5 m) and was chosen because of its reversed signature in contrast to the rest of the samples.

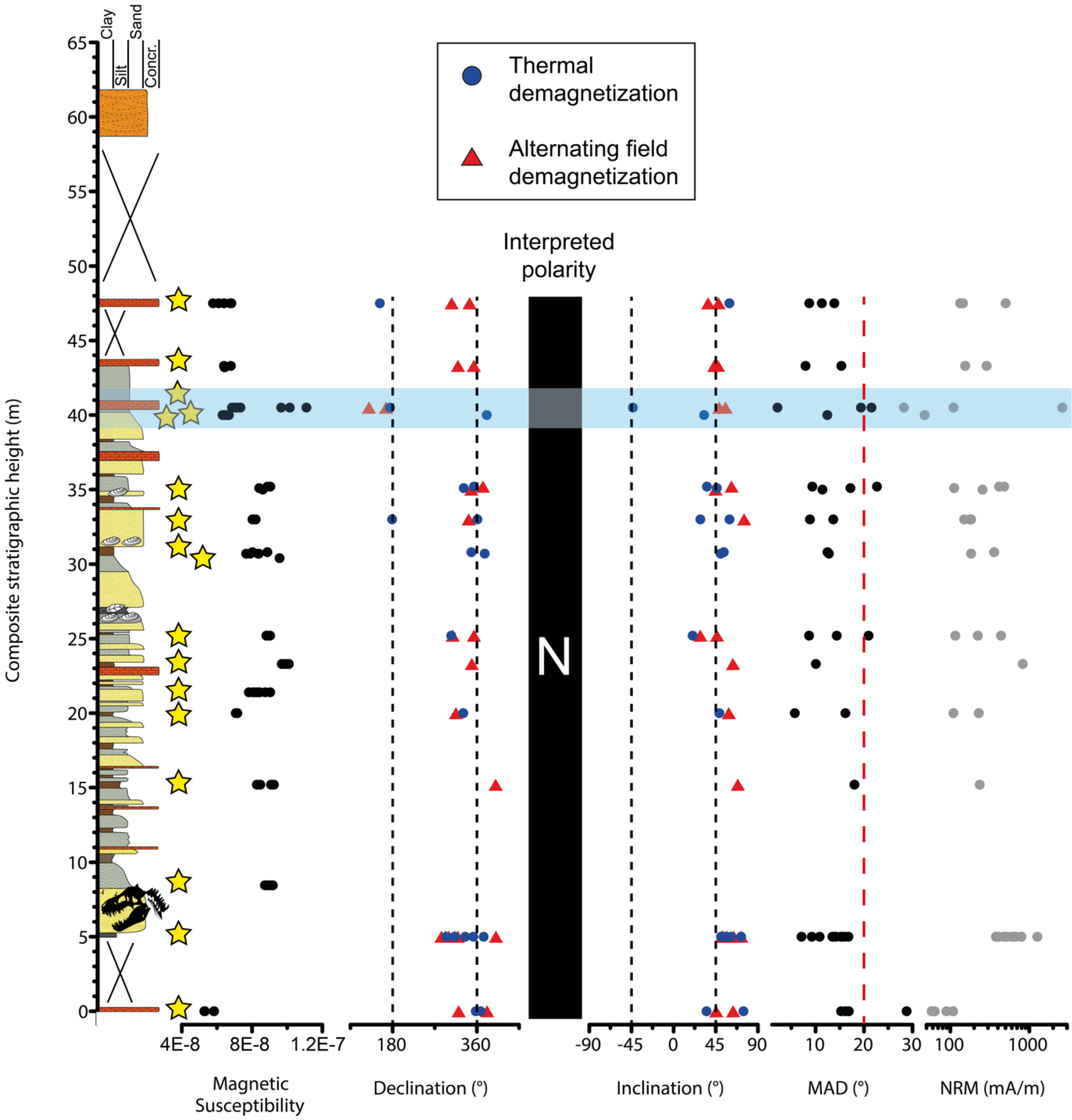


**Fig. 3.18.** Magnetostratigraphic framework of the study area. A composite lithostratigraphic log is displayed with the position of the paleomagnetic samples and the related lithology. Magnetic susceptibility data, declination, inclination (both TH and AF) and the interpreted polarity are shown together with the maximum angular deviation (MAD, higher than 20 is assumed to be unsuitable for interpretation) and the natural remanent magnetization (NRM). The blue shaded rectangle indicates the interval of a deviated declination and inclination pattern, which is explained in the text.

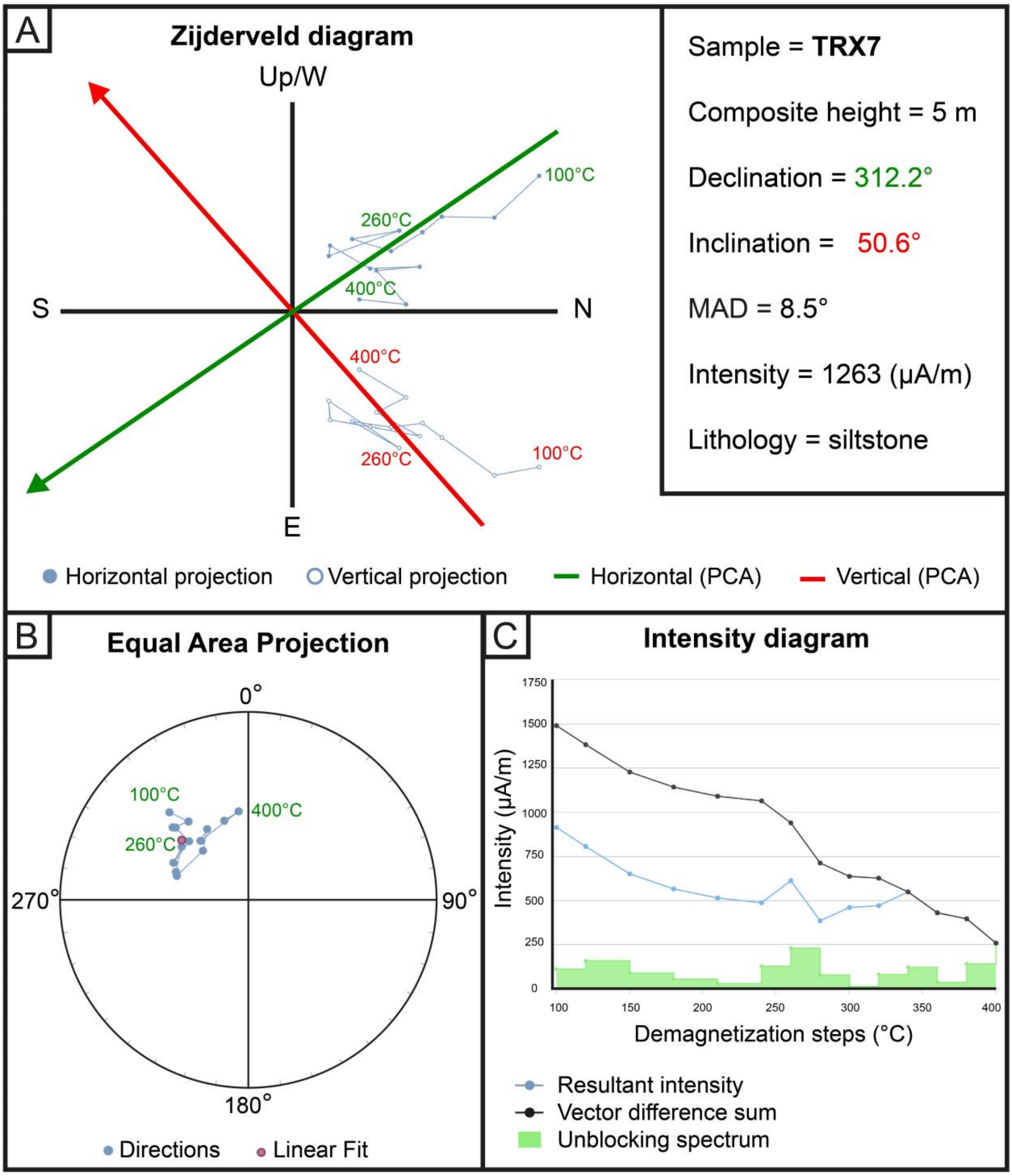


**Fig. 3.19.** Paleomagnetic signature of sample TRX7, which is located at the basal clay layer of the MREX section and hence very close to the stratigraphic position of the Naturalis *Tyrannosaurus rex*. The orthogonal vector diagram or Zijderveld diagram of the sample is displayed in **A**, which shows the interpreted declination and inclination lines (which are forced through the origin) of the characteristic remanent magnetization and the thermal steps. A different way of plotting the 3D directions is by means of an equal area projection **(B)**. This sample clearly shows a normal polarity, since the inclination is positive and the declination is pointed towards the north/northwest and is clustered on the lower hemisphere (solid circles) in the equal area plot. In **C**, the intensity diagram is shown resulting in a gradual decrease of the natural remanent magnetization (NRM) without major remagnetization events.

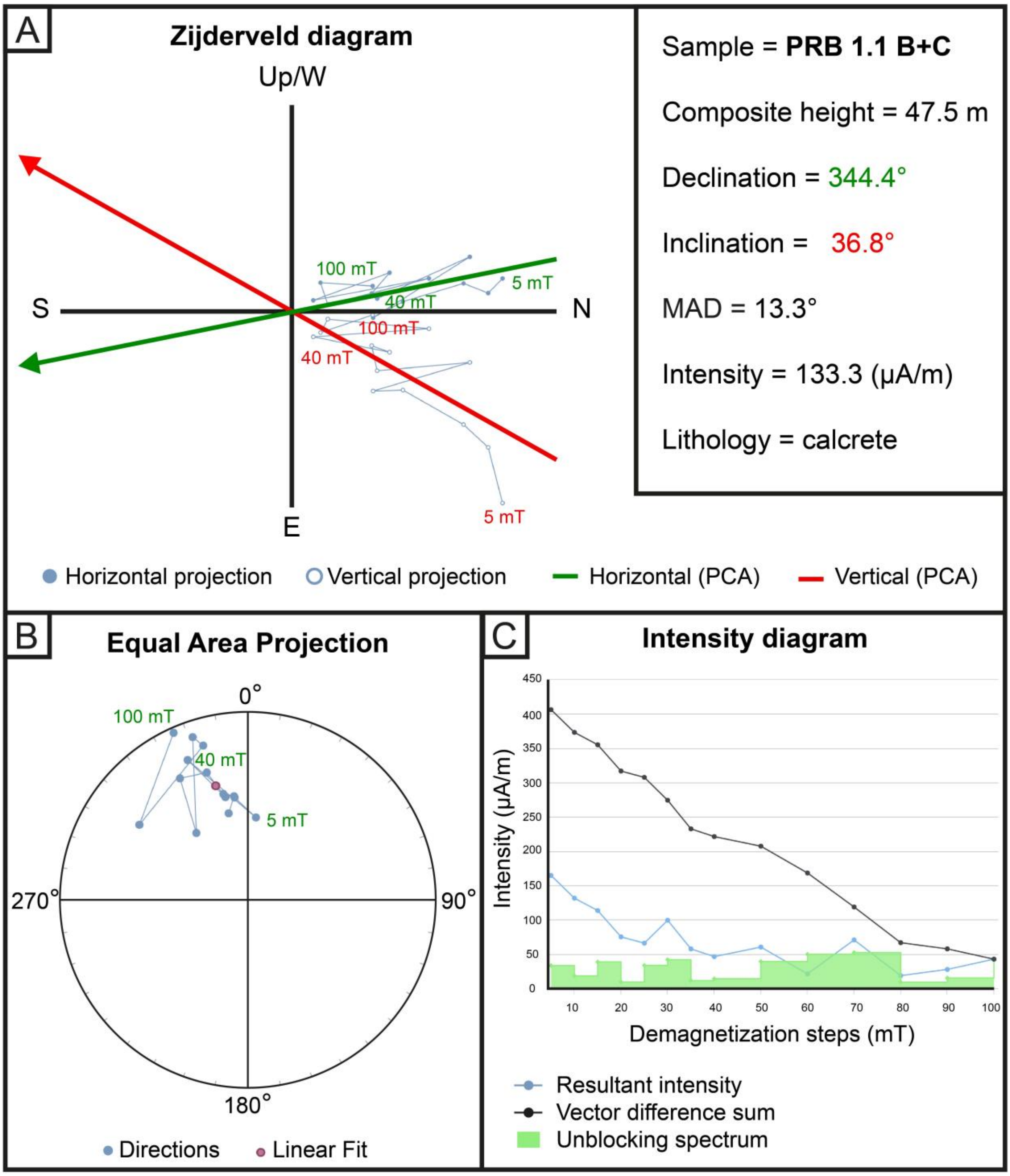


**Fig. 3.20.** Paleomagnetic signature of sample PRB 1.1 B+C, which is from the Piney Ridge section and derived from the stratigraphically highest position. The orthogonal vector diagram or Zijderveld diagram of the sample is displayed in **A**, which shows the interpreted declination and inclination lines (which are forced through the origin) of the characteristic remanent magnetization and the alternating field steps. A different way of plotting the 3D directions is by means of an equal area projection **(B)**. This sample clearly shows a normal polarity, since the inclination is positive and the declination is pointed towards the north/northwest. Although the inclination is somewhat shallow. In **C**, the intensity diagram is shown resulting in a gradual decrease of the natural remanent magnetization (NRM) without major remagnetization events.

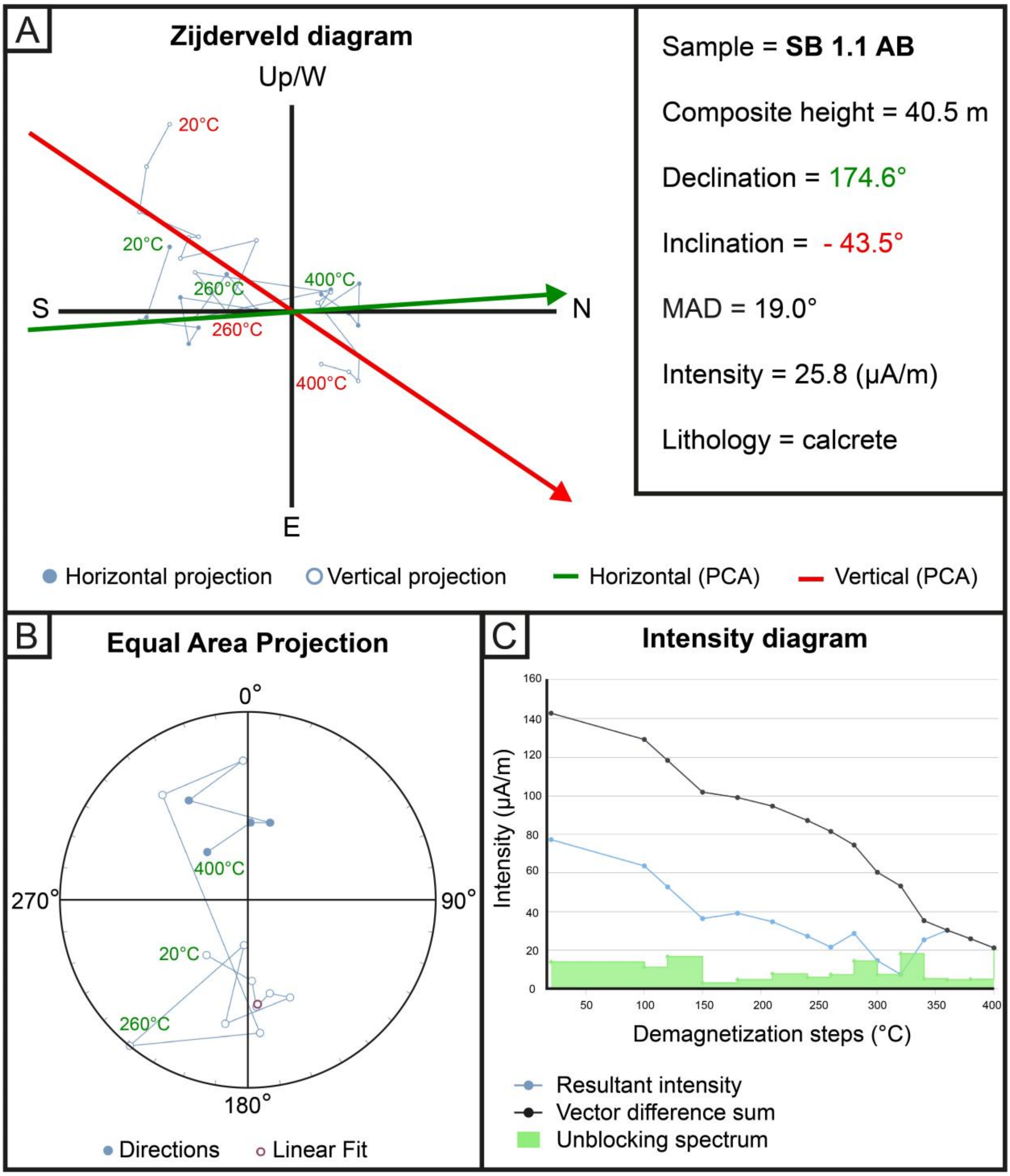


**Fig. 3.21.** Paleomagnetic signature of sample SB 1.1 AB, which is from the top of the Shelly Butte B section and is marked by a significantly different signal than the other samples. The orthogonal vector diagram or Zijderveld diagram of the sample is displayed in **A**, which shows the interpreted declination and inclination lines (which are forced through the origin) and the alternating field steps. A different way of plotting the 3D directions is by means of an equal area projection (B), which shows a large spreading of the TH steps. This sample shows a reversed polarity, since the inclination is negative and the declination is pointed towards the south. In **C**, the intensity diagram is shown resulting in a gradual decrease of the natural remanent magnetization (NRM) without major remagnetization events, but the intensity itself is very low.

In all samples, the first magnetic component represents a present-day induced magnetization and is a randomly oriented component that is removed below a temperature of 120°C. That is why the first two to three incremental heating (or AF) steps should be ignored in interpretation of the magnetic vector data. Since no set of clear reversed samples was found and the samples display in general low intensities (Fig. 3.18), it was difficult to detect the temperature boundaries for the two other different magnetic components. In most cases, the second component is removed between 200 and 270°C, has a normal polarity and is interpreted to represent a viscous overprint by the present-day Earth's magnetic (e.g. Abels, 2008). The third component is mostly interpreted as the characteristic remanent magnetization of the sediment, but the unblocking temperature for this component could not be established because it was not reached below 400°C. The blue shaded rectangle in Fig. 3.18 indicates the only interval with a reversed signature. However, as can be seen from Fig. 3.21, the intensity is very low of this sample and samples in close proximity above and below show clear normal polarity. Two other samples from this interval display positive inclination and a 180° declination, which is not possible since Montana was located on the Northern Hemisphere during the Late Cretaceous. These samples were probably oriented wrong in the field.

Excluding sample SB1.1-AB (at a composite stratigraphic height of 40.5 m and holding the only negative inclination), the average inclination using TH is ~45.9° and with the AF technique the mean is 53.9°. Especially the AF-values fairly matches the interpreted paleolatitude (Fig. 3.23), as collected from the online portal paleolatitude.org (Van Hinsbergen et. al., 2015).

In conclusion, despite the intermediate quality of the paleomagnetic samples, we can say that no geomagnetic reversal could be identified based on this data. Only one sample displayed a reversed polarity, but this sample hold a very low intensity and showed in a different part of the same core traces of an iron rich vein which may have remagnetized the sample at a later stage into a reversed signature. Hence, a normal polarity is present within the entire sampled composite section of 47.5 m.

**Fig. 3.22.** Jan Smit (VU) in front of the basal outcrops of the channel deposit in which the Naturalis *T. rex* was found, approximately at the location of the lacquer peel. Below the sandy interval, oriented paleomagnetic test samples were taken for age dating in clay-rich material in September 2013. After analysis at the UU, these samples all indicate a normal polarity (photo: Hemmo Abels).

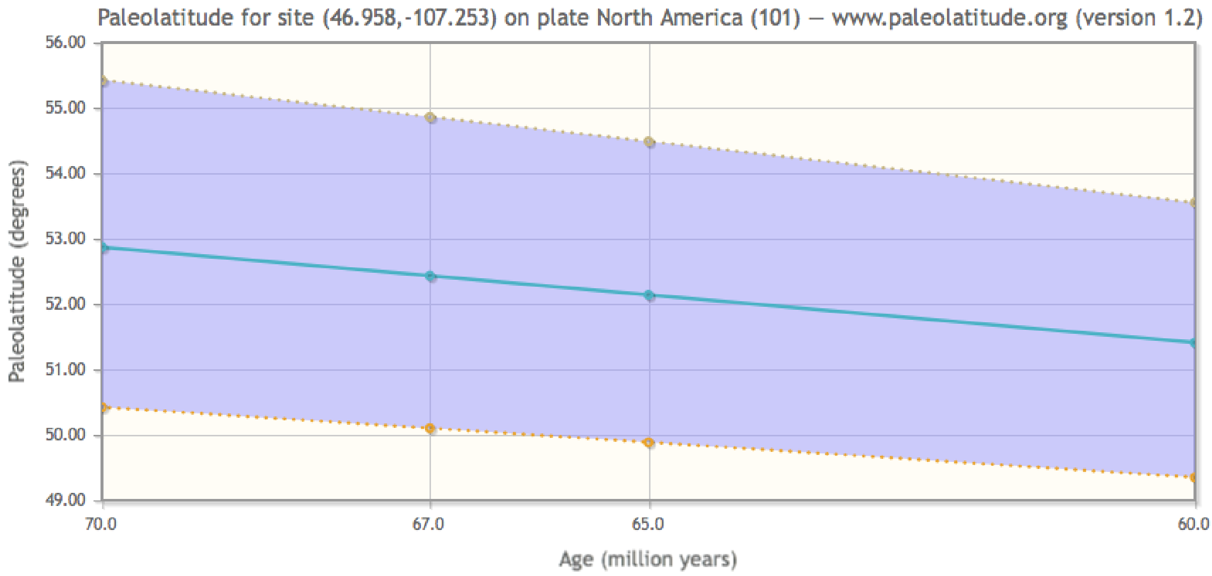


**Fig. 3.23.** The paleolatitude of the Naturalis *T. rex* site was at 67.0 Ma around 52.5°N. This is derived from the online portal Paleolatitude.org (Van Hinsbergen et al., 2015) and fairly matches the average inclinations found in the rock record of the study area.

### 3.4.3. Cyclostratigraphy

Since no magnetic reversal was found in the rock record of the study area, the use of cyclostratigraphy is limited. Nonetheless, an attempt was made to identify the specific sedimentary cycles in the field by means of a detailed lithostratigraphic description. One of the properties that is often used in cyclostratigraphic studies is matrix color. For instance, from a photo-overview of Cyclic Butte (e.g. Fig. A2.5), regular alternating layers can be observed characterized by a sequence of yellow colored sandstones, olive grey siltstones and dark brown carbonaceous shales which are bounded again by a yellow colored sandstone unit that resembles the base of the new 'cycle'.

The color was qualitatively derived from selected intervals in the field using a Soil Munsell Color Chart. Using the software Wallkill Color, these Munsell colors were converted into RGB values (for digital imaging the lithological logs) and into lightness (L*), redness (a*) and yellowness (b*), which can be used in pedogenic and also cyclostratigraphic studies. For example, Abels et al. (2013) performed time-series analysis of color records from fluvial deposits in the Bighorn Basin in Wyoming using the Analyseries 1-1 Program of Paillard et al. (1996) and identified a distinct cyclic pattern.

The color data of the MREX section and the Cyclic Butte section are shown in Fig 3.24 and 3.25, respectively. The yellowness of the MREX section resembles fairly good its six sedimentary units described in paragraph 3.2. The pattern of redness and yellowness is less pronounced, but the dark and organic rich Unit 5 displays the higher redness and lowest yellowness value. The CB section shows a fining upward sequence with also a decreasing lightness trend. The redness values increase from 1 m onwards whereas the yellowness values decrease from that stratigraphic height, but the pattern is quite blocky.

This blocky appearance is based on the fact that the angle, hue, value and chroma from the Munsell Soil Color Chart are converted into only a limited number of lightness, redness and yellowness values. Due to the lack of intermediate values and the lack of a long stratigraphic record, no spectral analysis was performed on this color data. Next time, it is recommended to use a portable photospectrometer to quantitavily measure the matrix color. Moreover, the entire Cyclic Butte section (and ideally also other sections) should be measured and not just one 'cycle'.

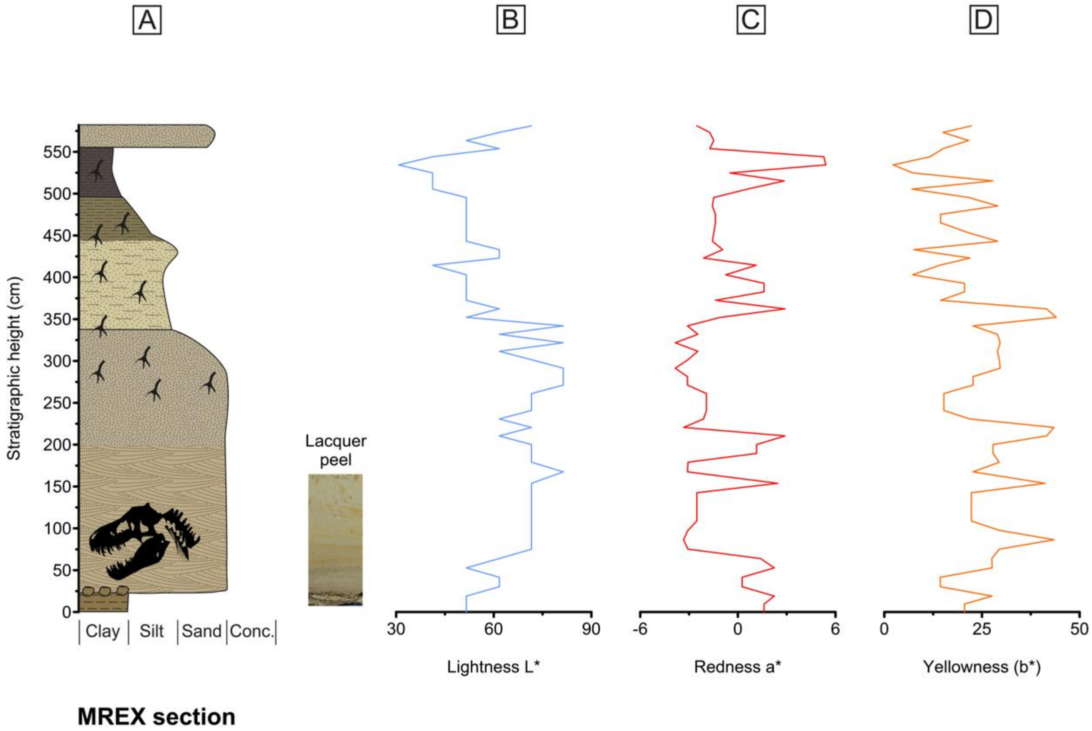


**Fig. 3.24.** Color data from the MREX section **(A)**, showing the variations in lightness L* **(B)**, redness a* **(C)** and yellowness b* **(D)**, based on the Munsell Soil Color observation in the field.

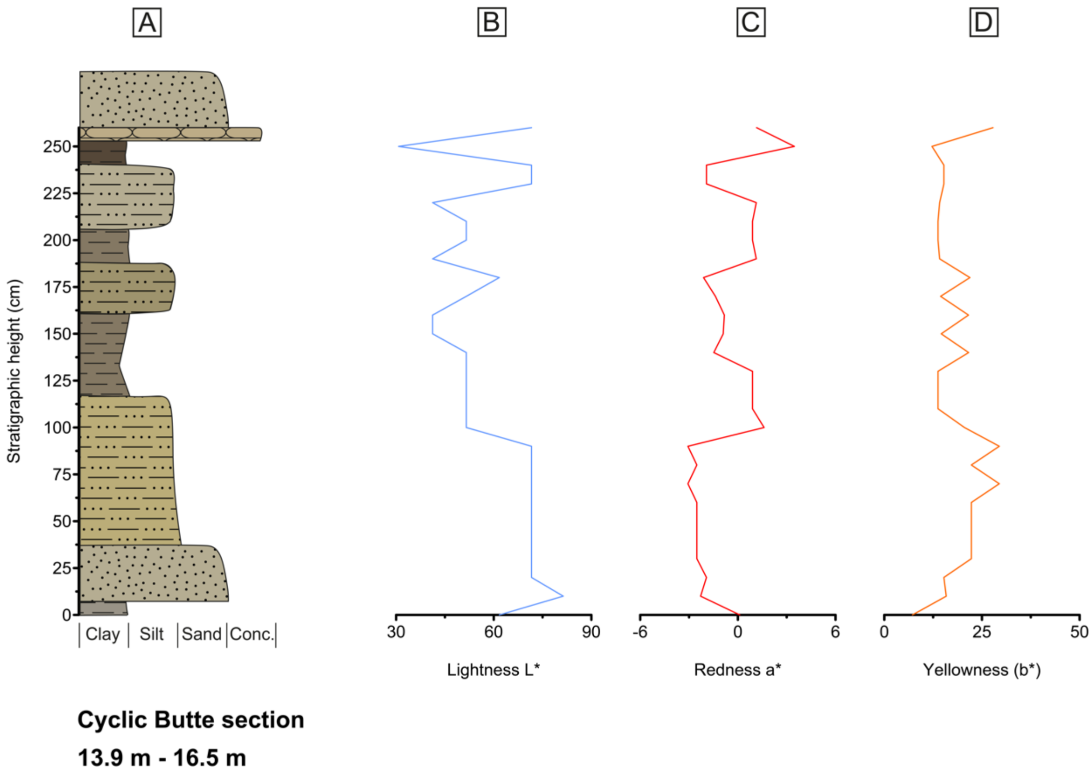


**Fig. 3.25.** Color data from the CB section **(A)**, showing the variations in lightness L* **(B)**, redness a* **(C)** and yellowness b* **(D)**, based on the Munsell Soil Color observation in the field.

# 4. Discussion

What do the results, described in the previous chapter, mean for answering the three research questions about the Naturalis *Tyrannosaurus rex* specimen? In this chapter, the results of my Master Thesis project are interpreted from a site-specific scale (the taphonomy and sedimentology of the excavation site) towards a local scale (a paleoenvironmental reconstruction based on the deposits on the Murray Ranch) and finally a regional scale (placing this fossil site in a regional stratigraphic framework of the Hell Creek Formation in the Williston Basin of Montana, North Dakota and South Dakota). In all paragraphs, a thorough comparison is made with other *T. rex* specimens (of which taphonomic, paleoenvironmental and/or stratigraphic data is known) to illustrate the uniqueness of this specimen within the entire *T. rex* database.

## 4.1. Sedimentology and taphonomy

From the previous chapter it became clear that Unit 2 of the MREX section and to a lesser extent section BHI-P1 (which shares almost all sedimentological characteristics of Unit 2) are the most important sedimentary units to understand the series of events before, during and after burial that lead to the extraordinary preservation and high completeness of the Naturalis *T. rex* skeleton. Unit 2 holds the bones of this dinosaur and clearly stands out from the rest of the sequence in a number of characteristics that is described below. To simplify, Unit 1 of the MREX section represents the pre-burial conditions whereas Unit 3-6 of the MREX section and all other sections in the study area (CB, SB, RHAB and PRAB) are considered to be post-burial. In this paragraph, several post-mortem scenarios are discussed, a realistic estimation is provided for the burial rate, the high carbonate content and its source is elucidated and finally the taphonomy of this *T. rex* is compared with other well-known specimens.

### 4.1.1. Sedimentary properties and post-mortem scenarios

How can we explain the unique preservation of the Naturalis *Tyrannosaurus rex*? To answer this question, it is necessary to use both paleontological and geological information to make an accurately as possible reconstruction of what happened after the dinosaur died. First of all, a careful examination of the excavation map was carried out to investigate the vertebrate elements that were discovered (Fig. 1.22). There is evidence for minor scavenging of the *T. rex* carcass, since some shed theropod teeth were found near the pelvis (Fig. A2.1B), probably attributed to *Nanotyrannus lancensis* (Larson, 2016, pers. comm.). So, after the *Tyrannosaurus rex* died (probably due to its high age or as a result of one of its many pathologies) it probably came to rest on a bank of a meandering river and these scavengers feasted on the carcass. This may explain some of the missing bone elements, for instance the arms, feet and outer tail vertebrae. These relatively small, protruding and vulnerable bones and muscles are easy to rip apart from a cadaver by medium-sized scavenging animals. In addition, it is known from calcium isotope data on *T. rex* teeth (Schaeffer, 2016) and from bone-bearing coprolites (Chin et al., 1998) that *T. rex* was able to crush and digest bones. So, this is also a way to remove some of the skeletal remains, but this possibility is unlikely since only the small, outer parts are missing and another *T. rex* would probably also scavenge the central body of its dead congener.

A third explanation for the missing elements is transport by a medium, in this case most certainly by means of running water because of the weight of the skeletal remains. The 2D excavation map clearly shows a disarticulated and scattered pattern of the skeleton (Fig. 1.22). The articulated skull is separated 10 m from the pelvis block and 8 m from the shoulder girdle and femur. Besides this scattered horizontal distribution, there was also a clear difference in elevation, since the skull was situated approximately 2 m below the shoulder girdle/femur and 1 m below the pelvis block (Farrar, 2015, pers. comm.).

A fourth possibility for the missing elements is by means of natural erosion. However, by the time of the discovery of the *T. rex* on the Murray Ranch by Michele and Blaine Lunstad, only a small part of the skull was sticking out of the ground on a so-called cow trail (Lunstad, 2014, pers. comm.). Some cows damaged parts of the skull and frost-weathering caused the breaking of the lower jaw in numerous sharp pieces, but overall the skull was in good condition. The rest of the skeleton was unharmed in the subsurface and waiting to be excavated a couple of months later. A detailed taphonomic study should still be performed on the abrasion and weathering marks on the bones. However, we can already say that the overall pristine appearance of the bones suggests a short time period of aerial exposure of certainly less than a year (Behrensmeyer, 1978). The traces of scavenging are present but are minor and thus there was not a lot of time for the cadaver to rot away on the river banks. It probably was caught by fast flowing water, was transported (together with the shed teeth) and buried in such a fast way that scavenging could not occur after the burial event.

Besides paleontological information, the geological record can be used to establish different post-mortem scenarios. The sediments surrounding the fossil yield valuable information which can help to reconstruct the depositional conditions upon burial, fossilization and ultimate preservation of this dinosaur. All characteristics of Unit 2 of the MREX section point towards a very rapid burial of the *T. rex* specimen shortly after its death. The distinct sediment properties revealing this fast entombing are listed in three categories (sedimentary structures, grain-size and geometry) and explained below.

1. **The sedimentary structures** visible in the MREX section and especially at the lacquer peel (Fig. 3.3) point towards running water under high energetic conditions. The presence of rip-up clasts at the scoured base of Unit 2 suggests a large erosive force that caused incising in the underlying mudstone interval and produced reworked clay pebbles that rounded due to the vortex movement underwater (Fig. 3.3B). The basal part of Unit 2 is also marked by extensive organic infill layers and climbing ripples, which are sets of asymmetric ripples that are superimposed on each other and seem to 'climb upslope'.

   To produce climbing ripples, a combination of aggradation (vertical) and migration (lateral) of the bedform is needed to create the diagonal pattern of Fig. 3.3C. Sediment is transported in running water by suspension load and bedload in such a way that some grains fall out of suspension (aggrading the bed) whereas other grains are transported as bedload and cause migration of the bed. Different angles of climb represent different ratios of aggradation and migration, as studied in high detail by Allen (1970). He defined a relationship between the angle of climb $\zeta$ to the rate of deposition M (in units of mass per units time and area), the bedload sediment transport rate j and the ripple height H, as is illustrated in Fig. 4.1A. Allen (1970) showed that when the angle of climb is smaller than the angle of the stoss-side, there is no stoss side preservation and climbing ripples of type A (erosional-stoss or subcritically) are formed (Fig. 4.1B). The morphology of the climbing ripples discovered on the MREX lacquer peel (Fig. 4.1C) is quite similar to this type and not so much to the aggradational pattern of 'Type S' (depositional-stoss or supercritically) climbing ripples (Fig. 4.1D). The angles of the climbing ripples were not measured in the field, because they were not always clearly visible in the homogeneous sand package. Nonetheless, the presence of these climbing ripples is unmistakable and indicates that sediment fluxes in the water flow were very high at the time of the burial of the *T. rex.* The preliminary classification of these climbing ripples in Type A suggests relatively low aggradation rate versus high ripple migration rate (Ashley et al, 1982).

   The climbing ripples are overlain by an interval dominated by medium scale cross stratification. These sets of cross beds are clear visible due to the influx of plant detritus. Sand grains are normally transported as bedload and can be deposited when stream velocity drops such as at the steep slope of a ripple-mark, facing downstream. A succession of these 'ripple front's is preserved as a series of cross-beds. The steep front faces tilt down-current and hence indicate current flow direction. On the lacquer peel this steep front is clearly facing to the east (Fig. 3.3A) and thus indicate a paleocurrent direction towards the east. This is in good agreement with the large paleogeographic and tectonic setting of the Williston Basin, since in general the rivers during the Late Maastrichtian flowed from the Rocky Mountains in the west towards the remains of the Western Interior Seaway in the east (e.g. Fastovsky, 1987).

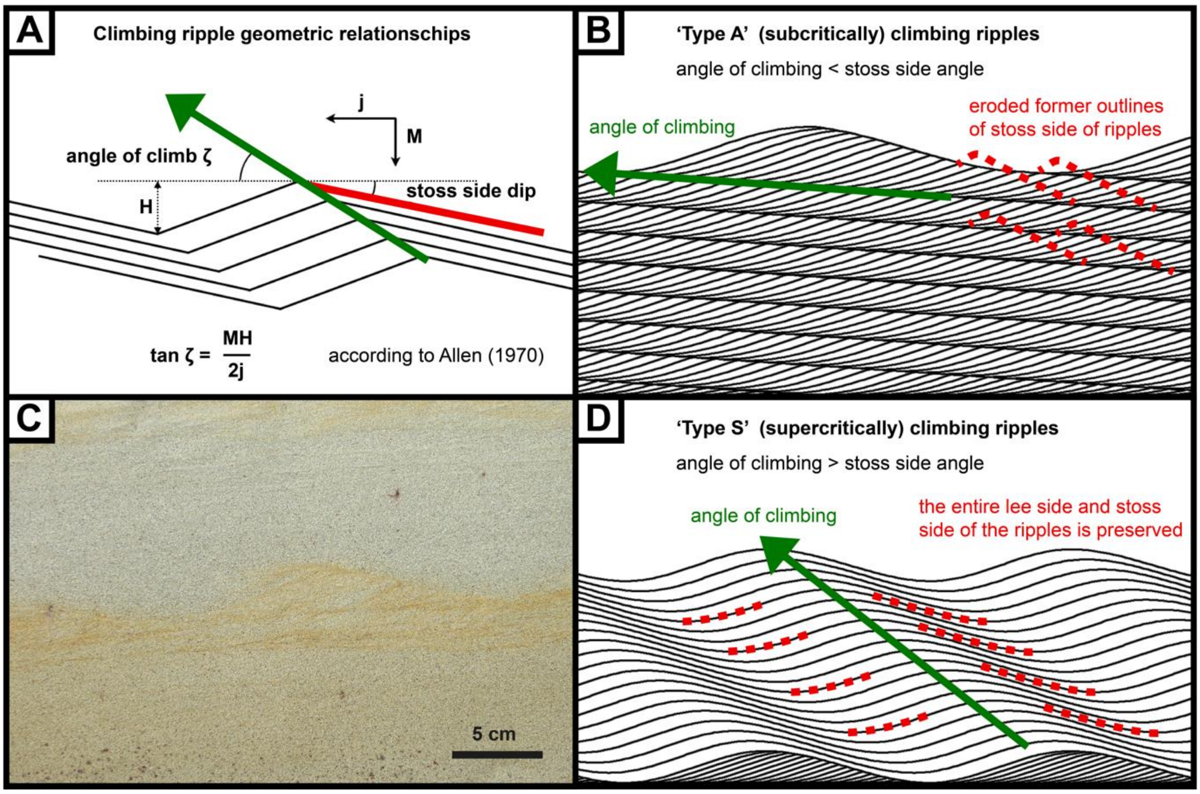


**Fig. 4.1.** Schematic representation of a set of climbing ripples showing the geometric relationships between the angle of climb, the angle of the stoss side, the height of the ripple (H) and the rate of deposition (M) and the rate of bedload sediment transport (j) (Allen, 1970) **(A)**. The 'Type A' climbing ripples **(B)** show clear similarities with the observed ripples in the field **(C)**, which do not display an aggradational pattern such as in the 'Type S' climbing ripples **(D)**.

2. **The grain-size properties** of the MREX section quantitatively showed that Unit 2 stands out and was formed by a high energy water flow of approximately a constant velocity. The relatively coarse median grain-size of Unit 2 is quite homogeneous with an average of 128 µm, a maximum of 150 µm and a minimum value of 97 µm (Fig. 3.5B). This median grain-size range, which falls around the size range boundary between very fine sand and fine sand (Fig. 3.5C), is clearly different than the rest of the units in the MREX section. Unit 1 and 3-6 display on average a median grain-size of 16 µm in the clay to fine silt fraction range (maximum of 39 µm and a minimum of 7 µm) and hence must be deposited under lower flow velocities.

   In addition, the sorting of Unit 2 is extremely good in comparison with the rest of the MREX section (Fig. 3.5D) and together with the absence of clay and silt intercalations, this supports the constant water velocity hypothesis. This pattern is illustrated by the high contribution of grain-size end-member #1 (EM1, see Fig. 3.5E)., which is a unimodal grain-size distribution marked by a uniform peak around 150 µm (Fig. 3.6D). EM 1 also consists of a small clay and silt tail, which represents the fine grains in suspension of running water (Prins, 2015, pers. comm.) The virtually absence of EM1 in the rest of the MREX section and also in the rest of the examined sections in the study area (Fig. 3.9B) illustrates its unique grain-size fingerprint. This observation point towards the idea that Unit 2 is an event bed that is probably created by a single flood event. To strengthen this statement, a literature comparison is performed which studies the relationship between grain-size and paleodischarge and an estimation of the water flow and settling velocity is also recommended (see paragraph 4.1.2)

As a comparison for paleodischarge, the grain-size dataset of Toonen (2013) was examined which focused on the Holocene flood history of the Lower Rhine river in the border region of the Netherlands and Germany. In a study of the last 450 years, the authors demonstrated that their end-member modelling data correlated well with discharge and turned out to be a sensitive proxy for inferring flood magnitudes (Toonen et al., 2014). They found a thin, relatively coarse sedimentary unit with a median grain-size of 70 μm at 6.5 m depth within the infilled oxbow lake Bienerer Altrhein, which was abandoned around AD 1550 according to historical sources. Toonen et al. (2014) correlated this thin layer, that showed high percentages of especially the coarse end-member 2, with the historical flooding of AD 1648 and estimated that the paleodischarge of the Lower Rhine was 16.800 $m^3$/s. This is even larger than the AD 1926 flood of the Lower Rhine region, which is the largest discharge record in modern observational data, namely 12.600 $m^3$/s. Therefore, Toonen et al. (2014) interpreted the coarse layer as an extreme flood deposit, as can be seen in Fig. 4.2C.

Of course, to compare a temperate, combined melt- and rainwater river from northwestern Europe with a record from the last c. 500 years with a subtropical, rain-driven river from the Late Cretaceous of North America is not an easy task. In addition, the proximity of the site to the active river channel, the provenance and maturity of the sediment and the stability of the river banks is important to consider when an accurate comparison can be made between the grain-size datasets and interpreted transport mechanisms of these two studies. Regarding the Lower Rhine river on the Dutch-German border, the general, recent provenance of the sediments can be assumed as the Swiss Alps and the Rhenish Massif at a distance of c. 550 km and c. 200 km, respectively (e.g. Westerhoff, 2008). The Bienerer Altrhein (Fig. 4.2B) is an infilled oxbow lake situated c. 3.3 km from the active river channel. Toonen et al. (2014) mentioned also that ice jamming occured during the AD 1648 flood that locally raised water levels and caused bed instability and levee breaches.

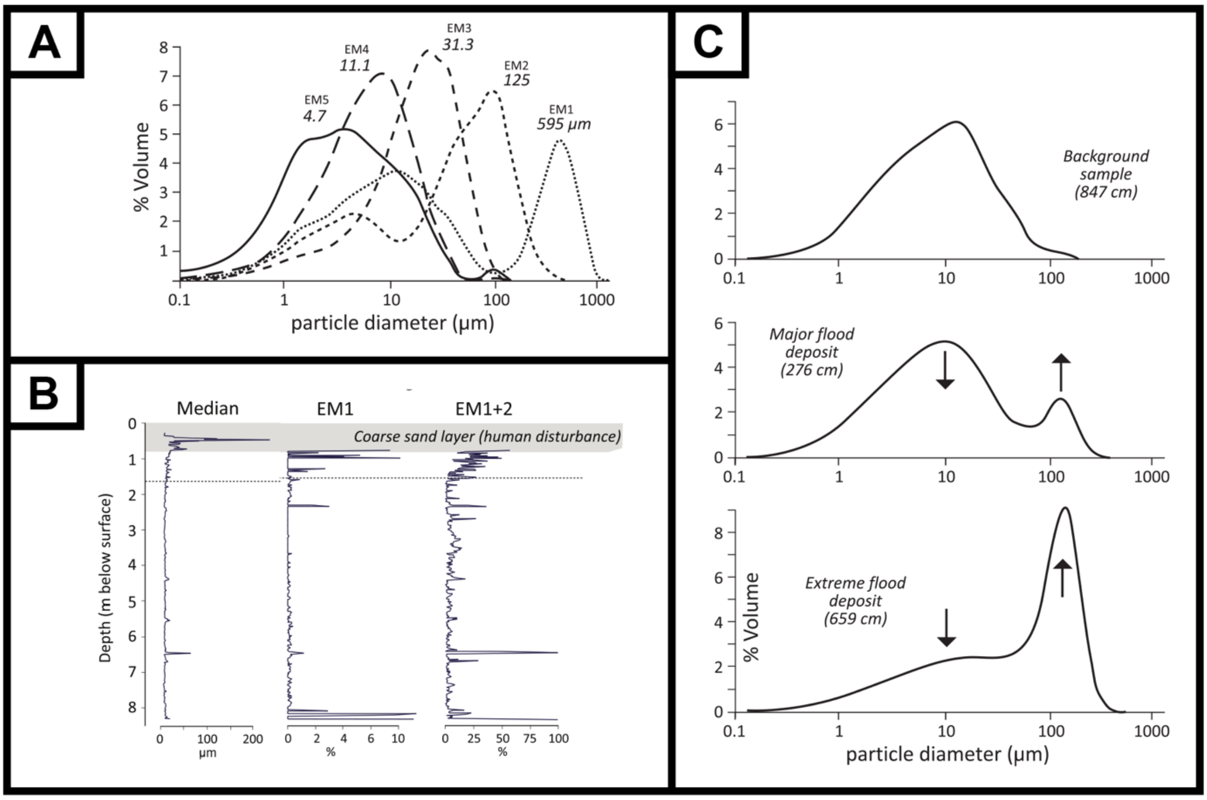


**Fig. 4.2.** Grain-size data of Toonen et al. (2014) for comparison with this study, showing the curves of their five end-member model (A), the data versus depth (B) and 3 selected samples (C).

Regarding the *T. rex* site, no ice jamming took place, but the levees of the lowland Hell Creek rivers consisted in general of poorly drained, soft sediment. These sediments were only stable enough to permit incipient pedogenesis and this implies that the levees were susceptible for floodings (Fastovsky & McSweeney, 1987). Provenance studies of the Hell Creek Formation in eastern Montana are limited. However, analysis of paleocurrent directions in the Early Paleocene suggest that sediment was transported in general to the east from central Montana into the Williston Basin (Cherven and Jacob, 1985). This trend is in agreement with sandstone compositions that indicates a dominantly volcanic-metamorphic provenance for Late Cretaceous sediments, associated with Laramide magmatic arc volcanism to the west (Sprain et al., 2016). Two possible source areas are the calcalkaline silicic to intermediate lavas and tuffs of the Elkhorn Mountains (southwestern Montana) and the sedimentary-type granites of the Bitteroot Lobe (of the Idaho Batholith, located in eastern Idaho), both dated to the Early Campanian (c. 80 Ma) and situated c. 400 and 600 km of the *T. rex* site.

Despite all the differences between the two studies, it is interesting to see that Toonen et al. (2014) interpreted a grain-size distribution curve similar to the EM1 in this study (with a uniform peak around 150 µm, but with a lower volume %, see Fig. 4.2C and Fig. 3.6D) as an extreme flood deposit. Although the provenance and river type is definitely different, the interpretation of Toonen et al. (2014) may suggest that the unique grain-size fingerprint of Unit 2 in this study is indeed linked to a flood event of a significant magnitude. To verify this massive flood hypothesis, it is also important to study which part of the fluvial environment is represented by the dig site, as is described below.

3. **The geometry** of the succession of sediments at the excavation site itself and the opposing valley suggests an asymmetric channel morphology of a bend in a meandering river, as can be seen in Fig. 4.3. On the opposite side of the valley near the dig site, a hard sandstone body is exposed (Fig. 4.3C) which can be linked to Unit 2 of the MREX section.

   This hard sandstone body of c. 3 m thick shows rip-up clasts at the clayey base and unidirectional cross beds pointing towards the east. This outcrop is interpreted as the thalweg, the deepest part of the river channel, and the deposit at the base can be classified as a fossil lag deposit. Since this outcrop is located c. 70 m to the east of the MREX section at the same elevation and in the same direction of the inferred paleocurrent orientation, it was interpreted that they belong to the same river channel. Using the information of both exposures, a fluvial architecture of the dig site could be designed showing the morphology and sedimentary sequences (Fig. 4.4). This architecture is based on a north-south cross section of 15 m wide and 6 m height covering some of the details of the excavation map of Fig 1.22.

   The cross section clearly shows an asymmetric geometry and an infill of this channel-shape with the sedimentary units of the MREX section as described in paragraph 3.2.2. The *T. rex* skull was found in the deepest part of the channel, the thalweg such as in Fig. 4.3C, and the other bone elements higher up in the sequence and a couple of meters to the south. Unit 2 and 3 of the MREX section probably show a lateral relative horizontally layering, with the first infill in the thalweg. Unit 4 and 6 are interpreted as crevasse splay deposits and show a lateral thinning towards the north, this is based on a field observation of these white-colored planar beds as seen in Fig. 4.3A. On the contrary, Unit 5 resembles remnants of a marsh deposit which thickens in the opposite direction of the crevasse splays.

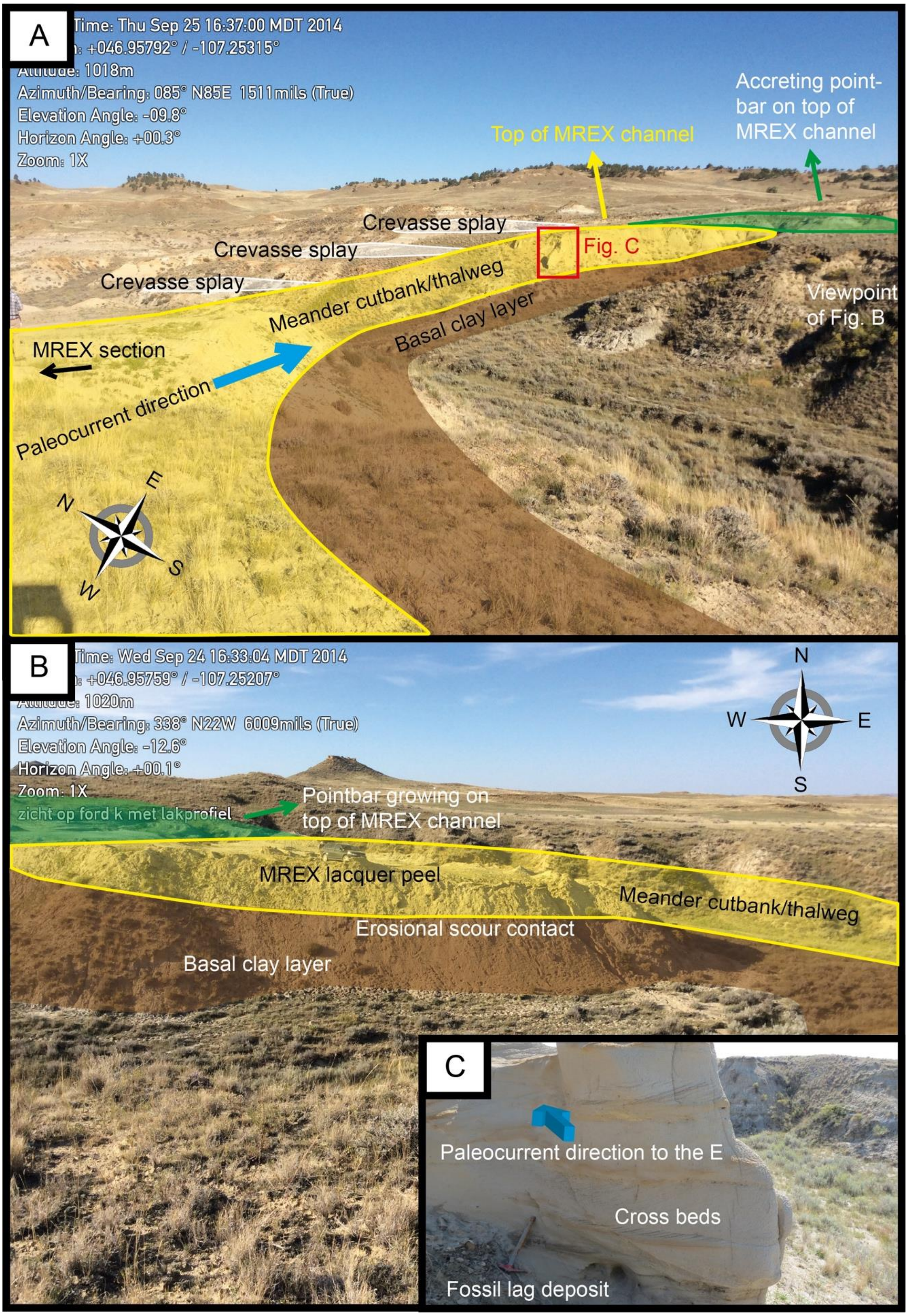


**Fig. 4.3.** Interpretation of the sedimentary units exposed and non-exposed near the MREX section with a view towards the east from the dig site itself **(A)**, a view on the dig site from the opposite side of the valley **(B)** and a close-up of a cross-stratified sandstone body resembling the thalweg (deepest part) of the *T. rex* channel and indicating a paleocurrent direction towards the east **(C)**.

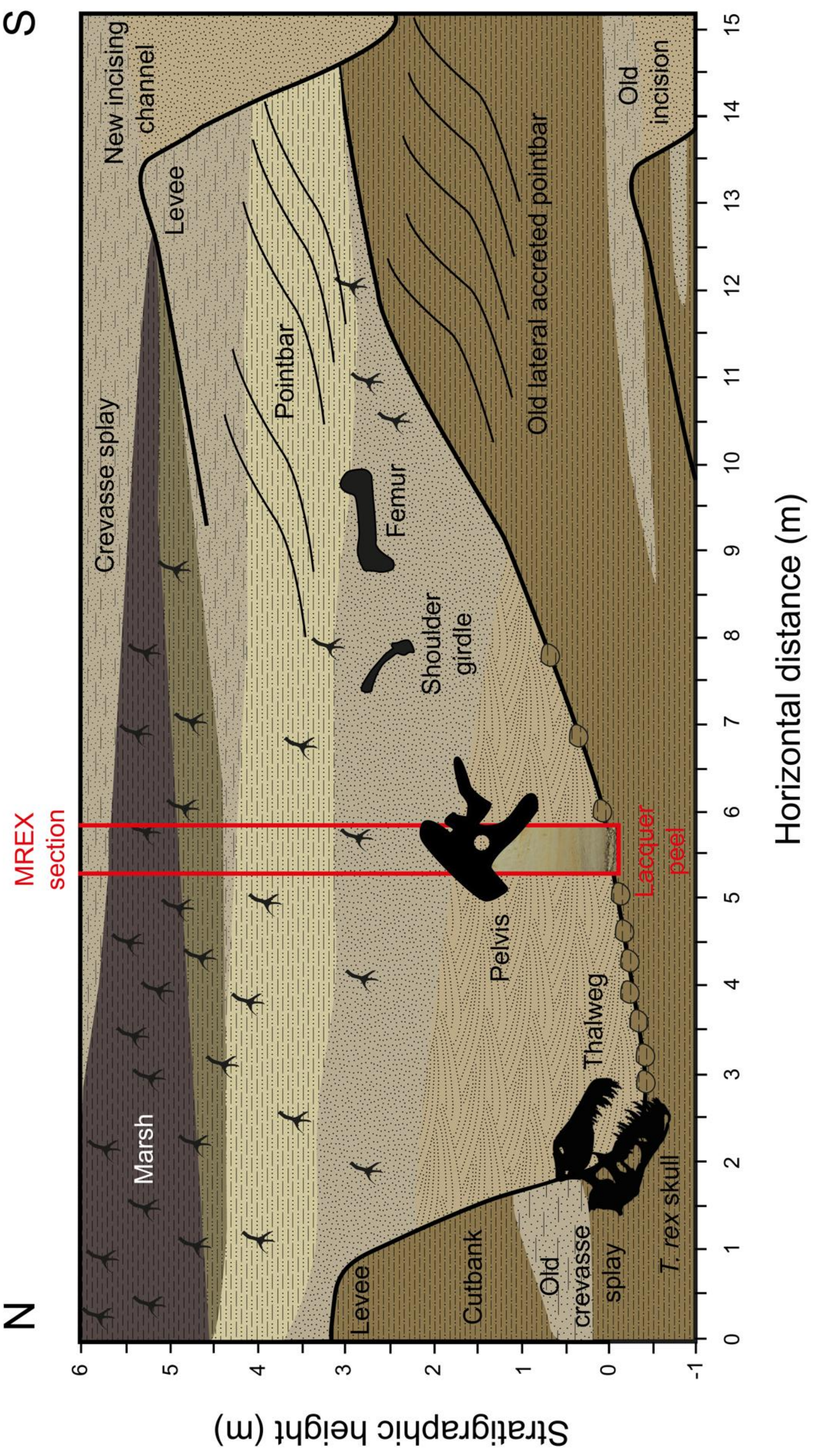


**Fig. 4.4.** Interpreted N-S cross section of the ancient fluvial architecture at the excavation site. It shows the lateral extent of several fluvial, sedimentary units and the approximate stratigraphic and horizontal position of the MREX section, the lacquer peel, and four different bone elements: skull, pelvis, shoulder girdle and femur.

What kind of river channel does Fig. 4.4 resemble? It probably was not an active, main river channel because the dimensions (depth and width) are not large enough for being a main meandering river in the paleocatchment. During deposition of the Hell Creek Formation in a virtually flat landscape, it was expected that the meandering rivers incised large floodplains and displayed a channel width of less than 300 m (e.g. Johnson, 2002). Probably, the channel of Fig. 4.4 was a tributary of a larger one and it could have been abandoned during the dry season before it was partly incised (as can be seen from the rip-up clasts) and filled up very rapidly at the beginning of the wet season after a large thunderstorm or prolonged precipitation related to the summer monsoon.

Toonen et al. (2012) categorized two different abandoned channel fills in Holocene river system of the Netherlands' Rhine delta, namely oxbow (meander neck) cutoffs and avulsion-abandoned channels (Fig. 4.5). Proximal oxbow lake fills are characterized by plug bars, which are sandy units that fill the channel entrances once the meander bend is cut off and subsequently hinders flow into the channel causing ponding water in the distal oxbow. Avulsion-abandoned channels are caused by an avulsion event (e.g. by a chute cut-off on a swale on the pointbar) that causes inactive channels over multiple meander lengths. At this moment, both options (proximal oxbow fill or avulsion-abandoned channel) are plausible, since a flood event from the active river may have breeched in one of these abandoned channels. A preservation of a channel geometry and a well-sorted sandy infill can be find in both scenarios.

The influence of a possible monsoonality within the study area is discussed in paragraph 4.2.3 and 4.3.1. The associated flooding was probably not a *flash flood event*, because during such a happening an entire floodplain is influenced and large objects (pebbles, tree trunks etc.) are transported. These objects have not been found and also due to the uniform grain-size of Unit 2, such a scenario is not favored. Once the depression was filled, the channel probably avulsed and started to incise in a different location. At the dig site itself a pointbar deposition started that showed a fining and organic upward trend related to a more distal position from the river bed through time. This overgrown pointbar sedimentation was interrupted by crevasse splay deposits derived from minor floodings from a channel close by (Fig. 4.4). This clastic influx prevented further accumulation of plant material and thus inhibited large marshes to grow.

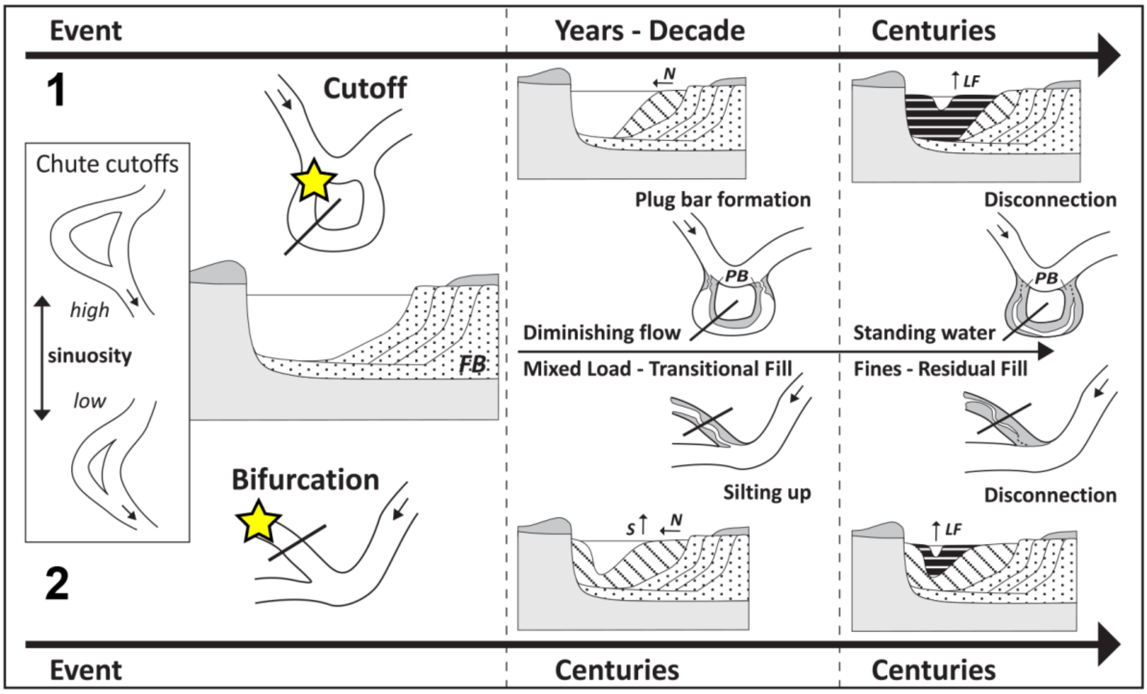


**Fig. 4.5.** Conceptional sedimentary model for two types of channel fills: individually meander neck cutoffs (1) and avulsion-abandoned channels (2) (from Toonen et al., 2012). The astrix indicates the possible position of the MREX site within these two ancient fluvial subenvironments.

In conclusion, the most parsimonious post-mortem scenario at this moment can be summarized as follows: an adult, female *Tyrannosaurus rex* died on a river bank in the dry season. A few theropods (probably *Nanotyrannus lancensis*) scavenged the carcass, but this did not last long. The wet season of the Hell Creek time started and prolonged rainfall caused water levels to rise in the main meandering river channel in the area. One of the levees of the active channel breached and a former shallow channel, which was abandoned during an earlier avulsion traject and lacked any water during the dry season, was filled in very rapidly with water and sand. Due to the force of the flood event, the partly disarticulated decaying *T. rex* carcass was transported into this tributary channel. The skull was slammed into the cutbank of this former meander curve and formed a flow obstacle leading to even a more rapid burial. The rest of the bone elements were laid down somewhat higher in the channel. Once the *T. rex* was completely buried by sand, quiet conditions prevailed that shielded of the dinosaur skeleton and protected it from further decay. After millions of years of limited sedimentation on top, minor tectonic uplift and intense fluvioglacial erosion, the modern-day climate of Montana caused exposure of a part of the skull, just enough for Michele and Blaine Lunstad to discover this ancient carnivore in the spring of 2013 and remove it from its Cretaceous sandy grave.

### 4.1.2. Burial rate

How fast did the burial of the *T. rex* carcass take place? Because the sedimentary unit encasing the fossil is quite homogenous, it can be considered as a simplified block of 3 m thick with an average median grain-size of 128 μm. To make a realistic estimation of the burial rate, a couple of hydraulic calculations are needed to apply on this "simplified block", as discussed extensively in Van Rijn (2007 a, b) and Soulsby (1997). These calculations include simple expressions of initiation of motion (movement of particles along the bed), initiating of suspension (particles moving in suspension), the resulting critical depth-averaged velocity, the bed load transport, the suspended load transport, the concentration and the settling velocity (for laminar and turbulent flow). To make these calculations more efficient, a Matlab script was written which is attached to this thesis report (Burialrate.m).

The following initial parameters were used in the calculation.

| | | |
|---|---|---|
| $D_{50}$ | = 128e-6 | Median grain-size (m) |
| U | = 0.5 | Water flow velocity (m/s) |
| h | = 1.5 | Water depth (upper boundary) (m) |
| s | = 2.65 | Relative density (ρ_sand/ρ_water) (-) |
| g | = 9.81 | Gravitational acceleration ($m/s^2$) |
| v | = 1e-6; | Kinematic viscosity ($m^2/s$) |
| $\rho_s$ | = 2650; | Density sand ($kg/m^3$) |
| $\rho_w$ | = 1000; | Density water ($kg/m^3$) |

A water flow velocity of 50 cm/s was chosen, based on the bedform stability diagram of Fig. 4.6A, because climbing ripples were discovered and the grain-size was 128 μm. The Hjulström diagram (Fig. 4.6B) shows that at this velocity both erosion and transport occurs and deposition is mainly in the form of suspended load. The cross-sectional area is estimated at ~22 $m^2$, using two simple rectangles (0.5*(3*2) and 0.5*(3*12.5)) as analogue for an asymmetric channel with a width of ~15 m and a height of 3 m (see Fig. 4.4). To simplify, in terms of cross-sectional area, the channel can also be assumed as a rectangle with a width of ~15 m and a height of 1.5 m, resulting in an area of 22.5 $m^2$. The step-wise calculations are shown on the next pages.

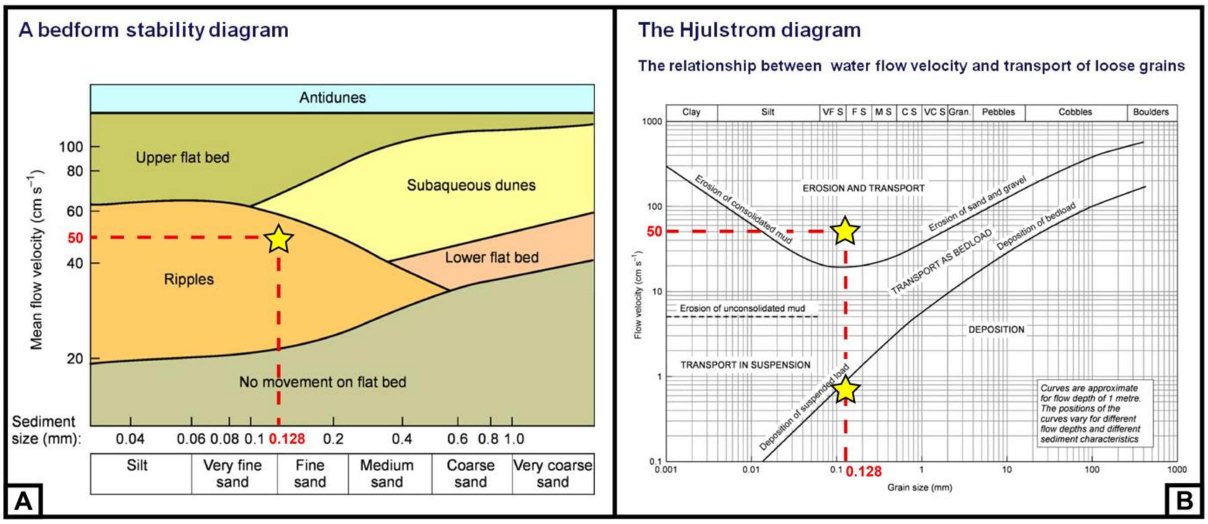


**Fig. 4.6.** A bedform stability diagram showing the grain-size (mm) versus mean flow velocity **(A)** and the Hjulström diagram **(B)** to determine at which grain-size and flow velocity the river will erode, transport or deposit sediment (Nichols, 2009).

1. The first two equations that are used display simple expressions for initiation of motion (1a) and initiation of suspension (1b) (Soulsby, 1997).

$\theta_{cr,motion} = 0.3/(1+1.2\ D^*) + 0.055\ [1-\exp(-0.02D^*)]$ = **0.0649** (1a)

$\theta_{cr,suspension} = 0.3/(1+ D^*) + 0.1\ [1-\exp(-0.05D^*)]$ = **0.0857** (1b)

with:
$D^*$ = $D_{50}\ [(s-1)\ g/v^2]^{1/3}$ = dimensionless sediment size (m),
$\theta$ = $\tau_b/[(\rho_s - \rho_w)g\ D_{50}]$ = Shields parameter (-),
$D_{50}$ = median grain-size (m),
$g$ = acceleration of gravity (m/s$^2$),
$v$ = kinematic viscosity coefficient (m$^2$/s),
$s$ = $\rho_s / \rho_w$ = relative density (-),
$\rho_s$ = sand density (kg/m$^3$),
$\rho_w$ = water density (kg/m$^3$),

2. Both these equations can be used to calculate the critical depth-averaged velocity of initiation of motion and suspension, as shown below (2a & 2b):

$U_{critical,\ motion} = 5.75\ [\log(12h/(6D_{50}))]\ [\theta_{cr,motion}\ (s-1)\ g\ D_{50}]^{0.5}$ = **0.2913 m/s** (2a)

$U_{critical,\ suspension} = 5.75\ [\log(12h/(6D_{50}))]\ [\theta_{cr,suspension}\ (s-1)\ g\ D_{50}]^{0.5}$ = **0.3349 m/s** (2b)

with:
$\theta$ = $\tau_b/[(\rho_s - \rho_w)g\ D_{50}]$ = Shields parameter (-),
$\tau_b$ = $\rho_w\ g\ U^2/C^2$ = bed-shear stress (N/m$^2$),
$U$ = depth-averaged velocity (m/s),
$C$ = $5.75\ g^{0.5} \log(12h/(3d90))$ = Chézy coefficient (m$^{0.5}$/s),
$h$ = water depth (m),
$s$ = $\rho_s / \rho_w$ = relative density (-),
$D_{50}$ = median grain-size (m),
$d_{90}$ = $2d_{50}$ = 90% particle size (m).

**3.** Now that we know the depth-averaged velocity, a third set of equations is needed to calculate the amount of material within the channel in kg/s/m. To infer the depth-integrated transport of both bed load (3a) and suspended load (3b), the following formulas are needed:

$q_b = \alpha_b \rho_s U h (D_{50}/h)^{1.2} (M_e)^{\eta}$ = **2.7044 kg/s/m** (3a)

with:

$q_{b,c}$ = depth-integrated bed-load transport (kg/s/m),
$M_e$ = $(U-U_{cr})/[(s-1)g D_{50}]^{0.5}$ (-),
$U$ = depth-averaged velocity (m/s),
$U_{cr}$ = critical depth-averaged velocity for initiation of motion (m/s),
$D_{50}$ = median grain-size (m),
$h$ = water depth (m),
$\alpha_b$ = coefficient (-) = 0.015 (Van Rijn, 2007 a),
$\eta$ = exponent (-) = 1.5 (Van Rijn, 2007 a),
$\rho_s$ = sediment density ($kg/m^3$),
$S$ = $\rho_s / \rho_w$ = specific density (-),

$q_s = 0.015 \rho_s U D_{50} M_e^2 (D^*)^{-0.6}$ = **0.0165 kg/s/m** (3b)

with:

$q_s$ = suspended load transport (kg/s/m);
$h$ = water depth (m),
$D_{50}$ = median grain-size (m),
$D^*$ = $D_{50}[(s-1)g/v^2]$= dimensionless particle size (m),
$s$ = $\rho_s / \rho_w$ = relative density (-),
$v$ = kinematic viscosity ($m^2/s$),
$M_e$ = $(U_e-U_{cr,suspension})/[(s-1)g D_{50}]^{0.5}$= mobility parameter (-),
$U_e$ = effective velocity (m/s) including effect of waves
$U_{cr,suspension}$ = critical depth-averaged velocity (m/s) for initiation of suspension

4. From these outcomes, it is obvious that the bedload transport is much larger than the suspended load transport. Assuming that the water flow velocity is constant over the entire length of the channel, the transport capacity of the bedload ($q_b$) is also constant (Fig. 4.7). Therefore, all sediment which enters the channel through suspension can be seen as an excess and thereby growth of Unit 2. The volumetric concentration (C) can be calculated by dividing the sediment discharge ($q_s$) by the water discharge (q, which is the water flow velocity times the water depth). Subsequently, the vertical sediment flux (and thus infill of the channel) can be derived by multiplying the settling velocity ($W_s$) with the concentration and finally the duration can be calculated of infill of the cross-sectional area. See all the equations below.

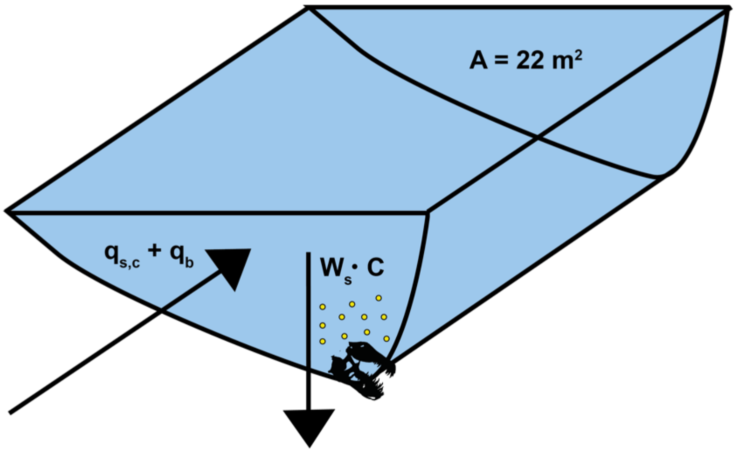


**Fig. 4.7.** Schematic geometry of the *T. rex* channel showing the most important parameters for the calculation of the burial rate. The transport of sediment through the channel consists of bedload ($q_b$) and suspended load ($q_s$). The settling velocity ($W_s$) and the concentration (C) of these suspended particles determine the vertical flux. The cross-sectional area of the channel is 22 m² and this results in an (average) water depth of 1.5 m.

Firstly, the fall or settling velocity of a particle need to be calculated, which is a function of grain-size, sediment density and the drag force coefficient, related to the Reynolds number (Re). The two equations below are used, focusing on the two extremes in flow regime, namely pure laminar and pure turbulent flow.

$$W_{s\ laminar} = \frac{0.8 * (\rho s - \rho w) * g * {D_{50}}^2}{18\mu} = \mathbf{0.0122\ m/s} \tag{4a}$$

$$W_{s\ turbulent} = \sqrt{3.3 * g * (\rho s - \rho w) * D_{50}} = \mathbf{0.0833\ m/s} \tag{4b}$$

with:

$W_{s\ laminar}$ = settling velocity of a particle under a pure laminar flow (m/s)
$W_{s\ turbulent}$ = settling velocity under a pure turbulent flow (m/s)
$D_{50}$ = median grain-size (m),
g = acceleration of gravity (m/s²),
$\rho_s$ = sand density (kg/m³),
$\rho_w$ = water density (kg/m³),

As an average value 0.05 m/s is chosen to use in the following formulas, since most natural water flow are a mixture of both flow regimes. Using all the parameters above we can calculate the volumetric concentration (of pure suspended particles), the vertical sediment flux and finally the time it takes to produce the 3 m high MREX section.

$C_{vol} = (q_s / (U\ h\ \rho_s)$ = **0.0165 kg/s/m** (4c)

$C_{flux} = C_{vol}\ W_s$ = **0.0165 kg/s/m** (4d)

Timescale = h / $C_{flux}$ = **3.605 *10⁶ s** (4e)

with:
$C_{vol}$ = volumetric concentration of suspended particles (%)
$q_s$ = critical depth-averaged suspended load transport (kg/s/m);
U = water flow velocity (m/s)
h = water depth (m),
$\rho_s$ = sand density (kg/m$^3$),
$C_{flux}$ = vertical sediment flux (m/s)
$W_s$ = average settling velocity of a particle under a mixed laminar flow (m/s)
Timescale = duration of the infill of the channel (s),

When the duration in seconds is divided by 86400, a timescale of **c. 41 days** is the result. This means a timespan of **c. 6 weeks or 1.5 month** before the MREX channel is filled with sediments.

Of course, many uncertainties still remain. Flow velocity decreases when a depression is filling, so this would imply a slower burial rate. On the other hand, the skeletal elements could have served as a flow obstacle and thereby increasing the burial rate. Assuming a full-grown *Tyrannosaurus rex*, its length must have been in the order of 12 - 13 m and its weight should be similar to Sue, so around 6000 kg. Interestingly, the skull was apparently the heaviest part, because that was deposited in the deepest part of the river channel. Using the Matlab script, it is easy to vary some of the parameters. For example, when the settling velocity is increased to a complete turbulent value of 8.33 cm/s (and the rest remains constant), the burial rate is only 25 days. Also, the water flow velocity is assumed to be 50 cm/s, but an increase to 60 cm/s speeds up the burial to only 16 days. The same holds for changing the (average) water depth to for example, only 1 m.

So, despite all uncertainties, the order of magnitude for the burial duration remains more or less the same when using realistic hydraulic and geometric parameters, namely in the order of days to weeks or (in one of the slowest scenarios) a couple of months. When we compare this burial rate with the average sedimentation rate of the Hell Creek Formation, based on the most recent age model derived from Hicks et al. (2002) and shown in paragraph 4.3, we can conclude that the *T. rex* burial event can be assumed as geologically instantaneous. The background depositional rate of the HCF is c. 14.000 year/m and thus 42.000 year / 3 m, which is 2 to 3 *10$^5$ slower than the *T. rex* burial (assume a duration of 0.1 to 0.2 year), making this burial event indeed remarkable.

### 4.1.3. Source of carbonate

The TGA results and the petrography evidently showed that Unit 2 of the MREX section can be classified as a highly calcareous arenitic sandstone. The maximum $CaCO_3$ values reach even 26%, which is certainly a lot for a fluvial sandstone. In comparison, shallow marine and coastal sandstones are mostly rich in carbonate (cement), since recrystallization of (fragments of) calcareous organisms is quite common. Less carbonate is found in fluvial sandstones because of the lower biogenic carbonate production in freshwater (Bjørlykke and Jahren, 2010). Apparently, this anomalous peak in carbonate in this fluvial sandstone contributed to the remarkable preservation of this dinosaur, but in what way? And what is the source of this carbonate?

To answer these questions, a more detailed examination of the geochemical data and the thin sections is needed. The raw TGA results of Unit 2 of the MREX section (Fig. 3.10 and 3.11D) showed a characteristic fingerprint dominated by a double peak, one at 830 °C and one at 930 °C, which is associated with the mineral dolomite ($CaMg(CO_3)_2$) and possibly a very small influx of calcite. In thin sections, this dolomite is visible as angular grains and not as carbonate cement (e.g. Fig. 3.12C). This angularity point towards an immature sandstone and a proximal source for the quartz and the dolomite. It seems like the dolomite grains are primary and just like the quartz minerals of detrital origin and not – as is often the case – secondary due to in situ diagenetic alteration. The lack in cementation is key in this, which is also visible in the unconsolidated texture of Unit 2. It was quite remarkable that it was possible to make a lacquer peel in these Upper Cretaceous rocks. However, it might also be possible that the dolomite is authigenic (and therefore angular) and formed due to degradation of organic matter at the burial site (C. Meyer, 2016, pers. comm.). A detailed petrographic study is needed to test this hypothesis.

The high dolomite content within Unit 2 probably functioned as some kind of carbonate shield which protected the skeleton against later soil leeching. Together with the rapid burial within a uniform sand package, this carbonate buffering provided the perfect recipe for the preservation of this *T. rex*. In addition, sandstone has the property that it is uncompressible compared to for instance claystone. This characteristic probably contributed to the absent or diminutive bone deformation and therefore the original 3D preservation.

What were the geochemical conditions in the subsurface that made this high carbonate content and bone preservation possible? Retallack (1994; 1997) carried out extensive research on the paleosols of the Hell Creek and Fort Union Formation and tried to explain the high abundance of vertebrate bone material in the Hell Creek deposits in contrast to the few bones but wealth of fossil plant material in the earliest Paleocene. Retallack stated that conditions required for good preservation of plant remains and bones are typically mutually exclusive. He explained this in his 1984-paper by means of a Pourbaix diagram or Eh–pH diagram (Fig. 4.8), which illustrates the fields of stability of minerals in terms of the activity of electrons (reduction potential or Eh) and the activity of hydrogen ions (acidity or pH) (Retallack, 1984). This makes it possible to determine whether a mineral or a geochemical component is in equilibrium with its surroundings or subject to chemical transformation by means of oxidation/reduction or hydrolysis. In natural environments, Eh values extend in general from -400 to +800 millivolts and pH values from 1 to 10.

Plants are best preserved under reducing conditions with a low to negative Eh and low pH, where microbial activity is reduced. Such low oxygen conditions are commonly associated with waterlogged habitats, such as swamps and marshes, that are rich in organic acids from plant decay or with saturated soils low in calcium carbonate (McIver, 2002). This is in good agreement with the overall ponded and swampy deposits of the Fort Union Formation. On the contrary, bones and shells are best preserved in environments of high to positive Eh and high pH, or in other words, under oxidizing and alkaline conditions. These are commonly found in well-drained soils or sediments, or if in saturated sediments where permeability is high and the sediments are flushed with oxygen-rich water. Such deposits commonly appear yellow, brown, or red in color (McIver, 2002). Unit 2 is also marked by a yellowish color.

Regarding the Naturalis *T. rex* site, Unit 2 is probably located in the red stability field in Fig. 4.8, in (highly) calcareous, intermittently wet conditions. Since no macrofloral remains were found in Unit 2, we can exclude anoxic conditions upon burial and severe leeching due to later acidic groundwater movement. However, using CT-scanning, a pyrite nodule was found inside a cavity of the 20th caudal vertebra of this *T. rex* (Bastiaans, 2016). This shows that groundwater seepage caused some bone permineralization and replacement after the burial. Nevertheless, the skeletal remains are in general in extremely good geochemical conditions, which suggests that the river water transporting the bones was also rich in calcium carbonate. According to Fig. 4.8, shells are preserved in the red stability field. No shells were discovered in Unit 2, but this may be related to the high paleocurrent strengths resulting in the burial event.

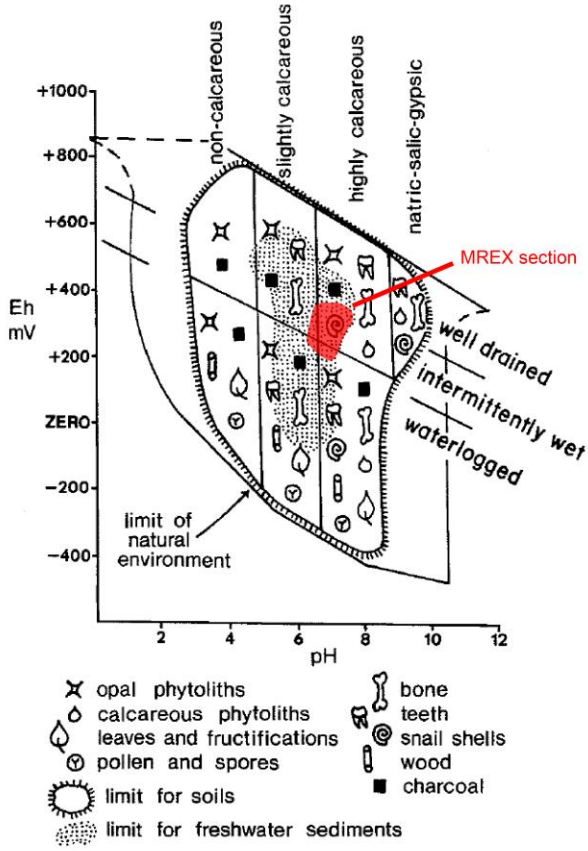


**Fig. 4.8.** Theoretical Pourbaix diagram showing the Eh-pH stability (equilibrium) fields for common kinds of terrestrial fossils preserved in fossil soils (from Retallack, 1984). The interpreted stability field of (Unit 2 of) the Naturalis *T. rex* locality is highlighted, which falls mainly within the highly calcareous – intermittently wet field.

Retallack (1994; 1997) stated that the entire Hell Creek Formation was alkaline and therefore hold so much fossil bone material. To examine if the high dolomite values at the Murray Ranch are a local phenomenon or indeed a general characteristic of the entire HCF throughout the Williston Basin, some channel sandstones from the Bug Creek area were kindly sampled by Hemmo Abels and Lars Noorbergen in 2015 and subsequently analysed by Leonie Portanger. The grain-size and thermogravimetric signatures are shown in Fig. 4.9.

The three samples (BCAS1, BCRB and SA) are all very different, with nearly no carbonate in BCAS1, a dolomite peak with some inmix of calcite in sample BCRB and SA displays a high broad calcite peak. Based on only these samples, it can not be concluded if the HCF sandstones are dominated by dolomite. The local source of carbonate for the Murray Ranch could be the uplifted carbonate plateau of the Porcupine Dome, which comprises predominantly Cenomanian to Campanian limestones from a former transgressive phase of the Western Interior Seaway (see paragraph 1.2.2 and Condon, 2002), located c. 50 km to the south of the study area (Fig. 4.10).

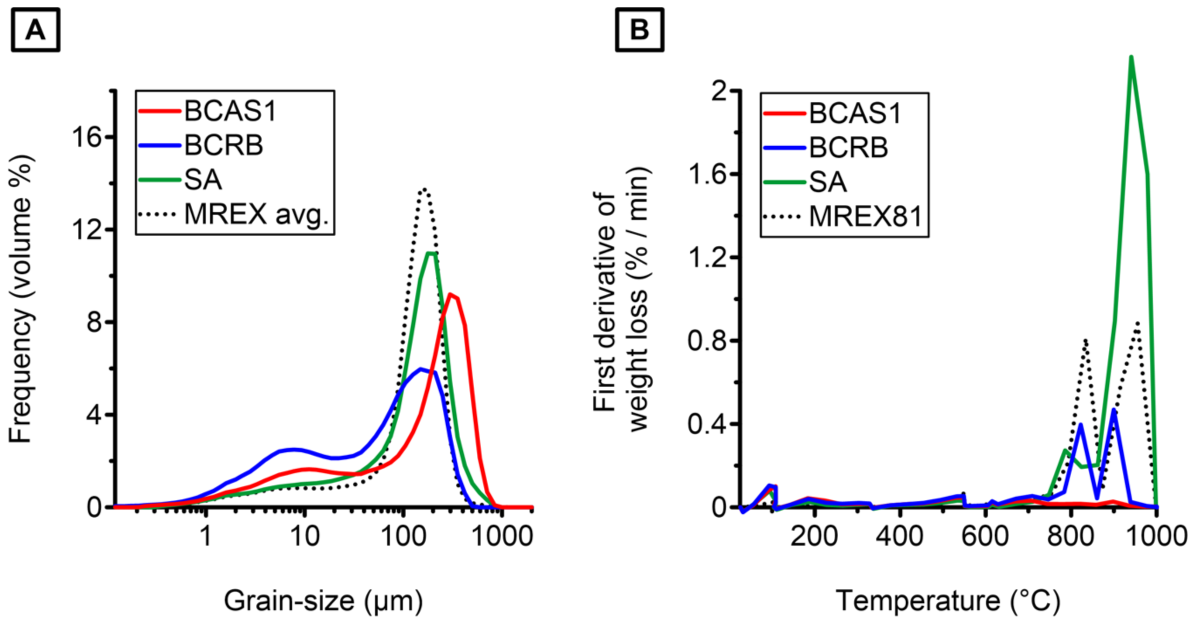


**Fig. 4.9.** Grain-size and TGA data of the samples derived from the Bug Creek area, and compared with the average grain-size distribution of MREX Unit 2 **(A)** and the TGA curve of MREX81 **(B)**.

However, the age of the uplift of the Porcupine Dome is interpreted later or partly during the deposition of the Paleocene Tongue River member of the Fort Union Formation (c. 62 Ma, according to Peppe et al., 2011), because these strata are involved in the deformation of the Porcupine Dome (Rennick & Riffenburg, 1929). Basic dikes have been documented in and near the Porcupine Dome, which indicates that this dome, similar to the Big Snowy and Judith Mountains, was created due to the intrusion of igneous masses. Simultaneously with the creation of the Porcupine Dome, its related minor folds, the Ingomar Dome and Antwerp anticline, were formed. At the same time, the rocks throughout Montana were very slightly wrinkled, and a large syncline oriented in a northwest-southeast developed, known as the Blood Creek Syncline (see Fig. 1.7). Nevertheless, it could be that some deposits in the pre-Porcupine Dome region were already somewhat higher in the landscape or that the Hell Creek rivers incised these old carbonate rocks and thereby bringing the dolomite grains into the study area (Fig. 4.10).

How thick was the maximum overburden on top of the Naturalis *T. rex*? This might explain partly the purity in geochemical and geometric sense of the *T. rex* skeleton. In paragraph 1.2.3, an estimation of the amount of erosion since the deposition of the HCF was calculated based on borehole data from the Poplar Dome area in easternmost Montana. However, this post-Cretaceous erosion was difficult to assess for the study area. It is interpreted that the HCF and the Tullock and Lebo member of the Fort Union Formation was once present throughout the study area, since widespread tectonic uplift did not occur before late Paleocene times (Rennick & Riffenburg, 1929). Stratigraphic thickness measurements are scarce in this region, but based on thickness measurements in the northwestern part of the Powder River Basin (c. 150 km apart from the Murray Ranch) from Brown (1993) an estimation of the thickness of the Tullock member and Lebo member (100 and 150 m, respectively) was possible. Adding up to the general assumed thickness of the HCF (c. 100 m), we end up with a minimum amount of erosion of c. 350 m. In paragraph 1.2.3, a maximum erosion of c. 730 m was established, because it is interpreted that the study area experienced less erosion than the by Pleistocene glaciers covered Poplar Dome area. This range of erosion (350-730 m) and thus overburden thickness would probably not have caused severe temperature and diagenetic modification of the host rock, which is indeed visible by the lack of diagenetic minerals and cementation in Unit 2.

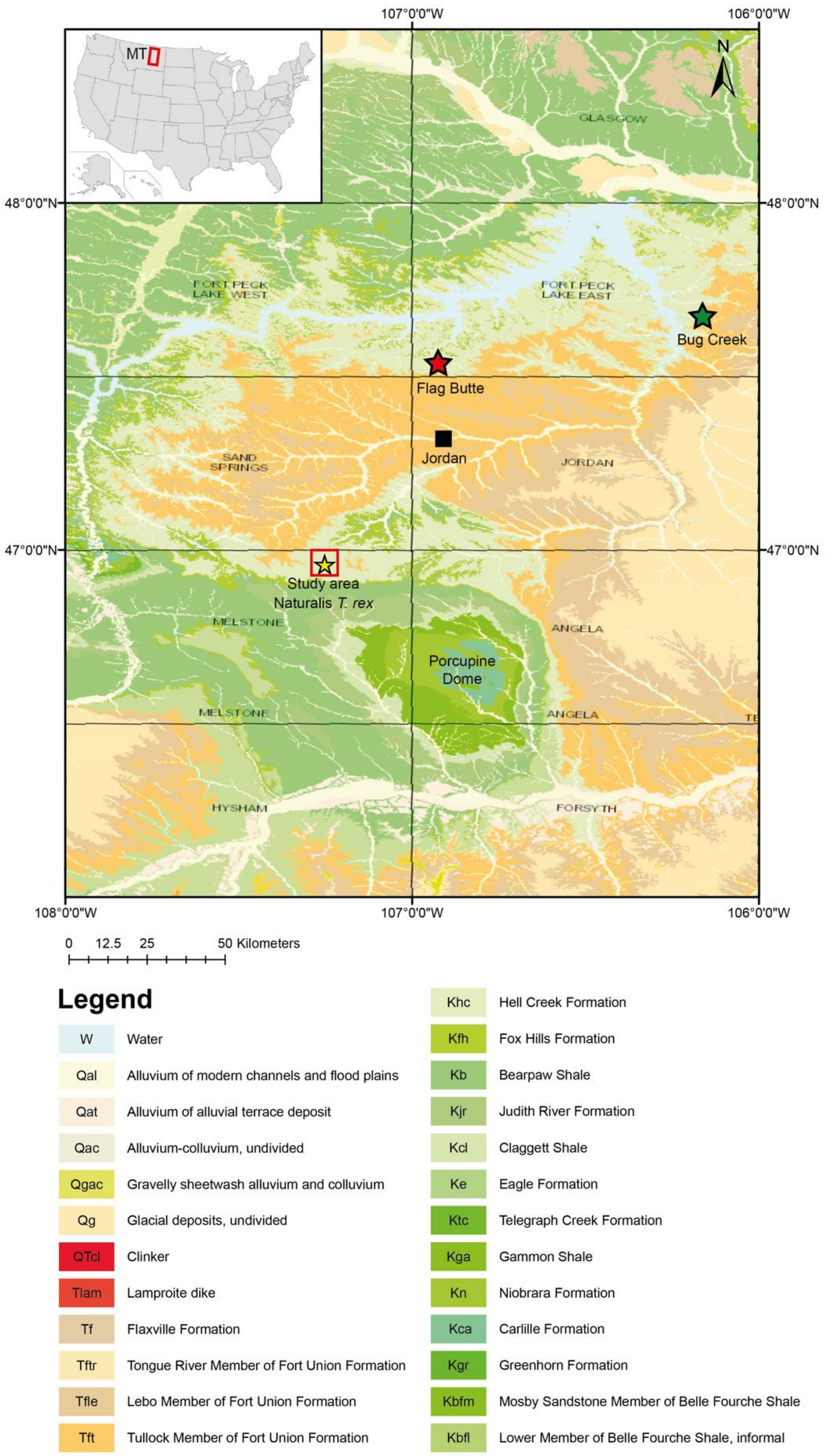


**Fig. 4.10.** Detailed geological map of eastern Montana showing the distributions of Cretaceous (all greenish colors), Tertiary and Quaternary deposits. The town of Jordan is marked together with the Naturalis *T. rex* site, the Flag Butte lectostratotype locality and the Bug Creek area in which the samples of Fig. 4.9 were collected. The proposed interpreted source area for the carbonate is the Porcupine uplift, c. 50 km towards the southeast of the study area.

### 4.1.4. Comparison with other *T. rex* specimens

To place the Naturalis *Tyrannosaurus rex* in a broader context, a thorough comparison is necessary with other well-studied specimens. In Appendix 6 (Table A6), a revised *T. rex* database is presented with details of all known 70 specimens (up to May 2016). In Table 4.1, a selection of this database is made and specimens are chosen where specific literature is available that studied their taphonomic and paleoenvironmental conditions.

The lithology database of Lyson & Longrich (2011) showed that *Tyrannosaurus rex* specimens were discovered in both sandstones as mudstones and thereby it is concluded that *T. rex* could be preserved by a range of many different taphonomic scenarios. Table 4.1 reveals that this *T. rex* shows most similarities with Pete, the specimen that was collected from a channel sandstone deposit in Wyoming. All the other specimens in Table 4.1. are characterized by more fine-grained deposits that suggest a less rapid burial, such as the 'bloat and float hypothesis' of Peck's Rex and C-rex with a deposition within a stagnant (oxbow) lake. Such a bloat and float post-mortem scenario might also be possible

Regarding the geochemical conditions of the bones, an interesting comparison can be made with specimens Tristan and Black Beauty. As the name already suggests, the ink-black color of these two skeleton can be explained by the inclusion of dark pigment. This pigment results from anaerobic decaying processes and the penetration of clay minerals and manganese within the bones. Such anoxic conditions may be possible due to the influx of acidic groundwater and/or deposition on the bottom of a stagnant lake or swamp.

The Canadian *T. rexes* (Black Beauty, Huxley Rex and Scotty) and Stan are all preserved in hard ironstone in contrast to the loose and soft sandstone of the Naturalis *T. rex*. This unconsolidated structure is remarkable, since sandstone is normally uncompressible and thereby protects the bones from overlying strata. However, this soft sandstone apparently can aid to a superb preservation.

The final interesting comparison I would like to make is with the Dueling Dinosaurs, also located on the Murray Ranch, c. 8 km away from the MREX section. This spectacular discovery is a fossilized battle scene containing a very complete and beautifully preserved ceratopsian (possibly a new species) and a theropod identified as *Nanotyrannus lancensis* (Larson, 2013). The encasing matrix of these fossils is also a homogenous looking thick sandstone bed that is most probably deposited by a major flood event, similar to the one that covered the Naturalis *T. rex.*

**Table 4.1.** See next page: an overview of characteristics of eight selected *Tyrannosaurus rex* specimens of which a (somewhat) detailed taphonomic and paleoenvironmental analysis is published. This overview is used in paragraph 4.1.4 and 4.2.4 to compare the depositional context of Trix with other relevant specimens.

| Specimen information | | | | Geometry | Sedimentary characteristics | | | | Fossil characteristics | | | Interpretations | |
|---|---|---|---|---|---|---|---|---|---|---|---|---|---|
| Specimen ID + ref. | Nickname | State - County | % of skeleton | 3D burial geometry | Lithology (grain-size) | Sedim. structures | Color | Nodules | Pattern of articulation | Floral remains | Faunal remains | Taphonomic scenario | Depositional setting |
| MOR 980 (Derstler & Meyers, 2008b) | Peck's Rex | MT - McCone | 40+% | Not clear, but looks like Rex Sand is deposited in a symmetric depression | 0.1-1.8 m thick loose silty sand unit (Rex Sand) above the BBQ-sand | Erosional base, bioturbated top, weak currents | Orange brown | Siderite, pyritic & limestone nodules | Disarticulated, but caudal vertebrae are still articulated no scavenging | Many carbo-nized wood, seeds, amber, dicot, palm & conifer leaves | Rare snails, crocodile, gar fish, turtle, hadrosaur & Triceratops | Bloated carcass moved into an oxbow lake, dropped & rotted at lake bottom. | Stagnant, anoxic oxbow lake |
| MOR 2925 (Hall & Keenan, 2010) | F2-rex | MT – Garfield | 10% | ? | At the base of a 2 m organic-rich mudstone | Isolated vf sand lenses, rhyzolites & slicken-slides | Dark purple | No, but gypsum coat present | Disarticulated vertebrae, rib cage & lower hindlimb. No scavenging. | Abundant fig seeds & plant fragments | Only a single shed theropod tooth, not more | Less than 2 years of subaerial exposure before burial & little fluvial transport | Pedogenically modified floodplain environment |
| MOR 1126 (Cooley, 2003) | C-rex | MT - Garfield | 9% | ? | Coarsening upward, organic rich mudstone | Bioturbated mudstone | ? | No (?) | Partially articulated T. rex lying on its left side | Abundant fragmentary and complete leaves | Only fresh-water clams & gastropods: Sphaerium & Campaloma sp | Bloat and float of a carcass into a lake (?) | Lake setting with quiet water |
| BMR P2002.4.1 (Henderson & Harrison, 2008) | Jane | MT - Carter | 52% | Not clear, but the clay-ball unit is lenticular and skeleton is found in the lower part | At the contact of a sst & a poorly sorted sand, silt & clay-ball conglomerate | X-bedding in basal sandstone & laminations in siltstone | Tan-brown sst & green clay-balls | Many siderite nodules that encases bones | Disarticulated, but hips, base of the tail and feet are kept in place. Looks like death-pose | Abundant wood, leaves (e.g. Pistia sp.), seeds, cones & 51 pollen genera | Many bivalves, gastropods, lizards, fish, crocodiles, champsosaurs & turtles | Death on a pointbar sand, followed by a rapid burial of a viscous mudflow & capping by silt. | Typical flood-plain sequence: Pointbar → mudflow → development of an oxbow lake |
| LDP 997-2 (Derstler & Meyers, 2008a) | Pete | WY – Niobrara | 12+% | Looks like channel geometry, but outcrop is small | Soft, medium-grained sandstone capped by a concreted sst | Large (30-80 cm) X-bed sets | Light brown | No (?) | Widely spread out in a debris field, 2 semi-articulated vertebrae | Only scattered pieces of carbonized wood | No (?) | Not certain if bones came to rest on a pointbar or in a channel | Point bar and meandering channel deposits followed by braided streams |
| RSM 2523.8 (McIver, 2002; Tokaryk & Bryant, 2004) | Scotty | SK | 40+% | ? | A 2 m thick sandstone unit with thin silt & clay lenses that preserve many plant remains | X-bedding at the base overlain by silts & clays. No rooting | Light olive-grey to dark green-grey | Degraded bones are encased in thick ironstone | Disarticulated | Abundant deciduous leaves, logs, fruits of e.g. palms. nuts & seeds | Abundant, e.g. gastropods, clams, turtle, fish, mammal, theropod & hadrosaur | The carcass was exposed over a long period of time and slowly buried on a pointbar | Pointbar: low energy section of a meandering river system |
| FMNH PR2081 (Larson & Donnan, 2002) | Sue | SD - Ziebach | 73% | A well-developed meandering curve that is covered by a prograding pointbar | Mosty fine sandstone and some siltstone | Some (minor?) crossbedding | ? | Some ironstone concre-tions | Semi-articulated, in a death pose, tail articulated to the pelvis | Leaves and interbedded plant layers | Freshwater clams, turtle, crocodile, fish, thescelosaur, hadrosaur, theropods | Relatively slow burial? | Pointbar: low energy section of a meandering river system |
| RGM 792.000 (this study, Naturalis) | Trix | MT - Garfield | 50+% | An asymmetric river channel geometry with the skull at the cutbank-base | 3 m vf-f, loose, well-sorted sandstone, avg. median GS = 128 µm | X-bedding, climbing ripples & rip-up clasts | Light brown-yellow | 1 siderite nodule, (average $CaCO_3$ % = 15.2%) | Disarticulated very scattered, but skull & pelvis itself are articulated | Very few fossil roots imprints, avg. organic % = only 1.2% | Very little! Only a few theropod teeth & a bone of a hadrosaur | Very rapid burial and significant transport by a massive flood event | Abandoned river channel lag deposit filled after a flood event |

## 4.2. Paleoenvironment

While in the previous paragraph the emphasis was on Unit 2 of the MREX section, in this part the other sections on the Murray Ranch are also examined to produce a local paleoenvironmental analysis. Firstly, a relationship between the geochemical and sedimentological characteristics is determined and this way it was possible to define so-called paleoenvironmental end-members for the study area. Subsequently, the palynological results are discussed to provide insights in the ancient vegetation. In addition, some remarks are made regarding the importance of the position of the shoreline of the Western Interior Seaway for the different landscapes of Hell Creek time. Finally, the interpreted depositional environments of selected *T. rex* specimens are compared with this discovery.

### 4.2.1. Paleoenvironmental end-members

In this study, it was decided to perform both grain-size analysis and TGA on every sediment sample (n = 103). Therefore, it is possible to create cross-plots of these two independent datasets to examine if there is a relationship or not. In Fig. 4.11 the complete median grain-size dataset is plotted versus the organic and carbonate data and shows a negative correlation and no clear correlation, respectively. Subsequently, it was decided to compare the three grain-size end-members with the LOI550 and $CaCO_3$ dataset (Fig. 4.12) since these end-members show a less-averaged pattern (compared to the median grain-size) and they are related to specific transport mechanisms. From 4.11, it is visible that high percentages of EM3 coincides with high LOI550 values whereas a high contribution of EM1 is linked to in general a high $CaCO_3$ value.

This opposite relationship for $CaCO_3$ and LOI550 was also recognized by Jelle Wiersma in his Bachelor Thesis at the VU about the taphonomy and sedimentology of a Tyrannosaurid from the Campanian Kaiporowits Formation in Utah. His coarsest grain-size end-member (with a mode of 500 µm, medium sand) showed $CaCO_3$ fluctuations of 35% and 55%. He explained this by the fact that siliciclastic grains form more porous deposits and are commonly cemented by silica or carbonate due to diagenetic processes steered by groundwater. Also reworked or fragmentary shell particles might play a role in the elevated $CaCO_3$ values in the sand facies (Wiersma, 2013).

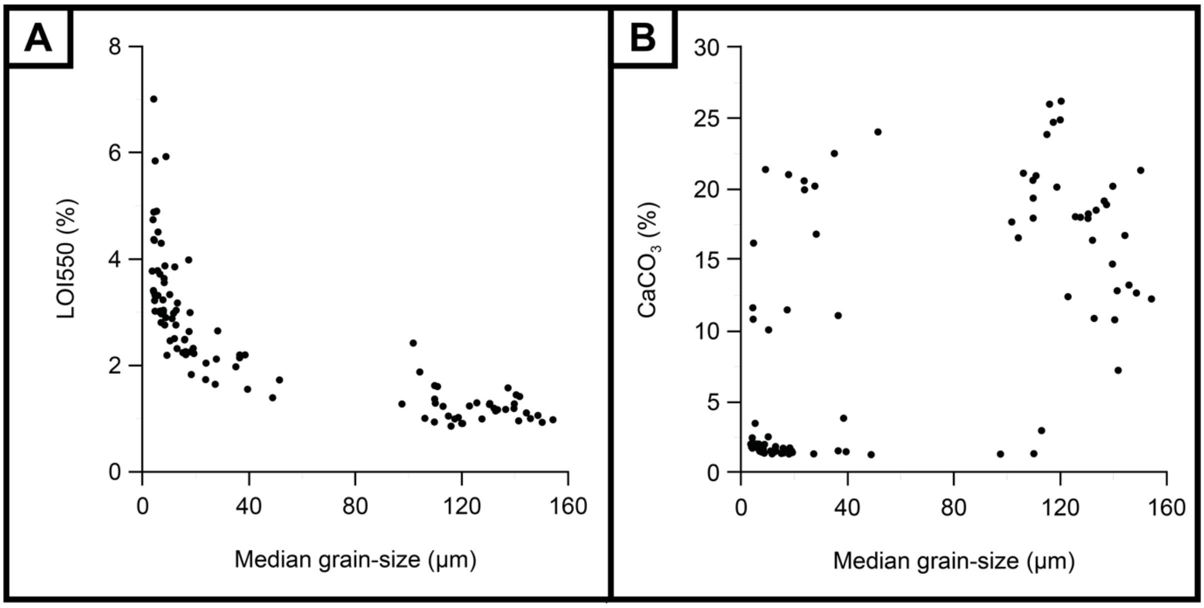


**Fig. 4.11.** Cross plots of the entire grain-size dataset versus the TGA dataset, showing a negative correlation between median grain-size and LOI550 **(A)** with (an exponential) $r^2$ value of 0.78. No clear correlation between median grain-size and $CaCO_3$ is observed **(B)**.

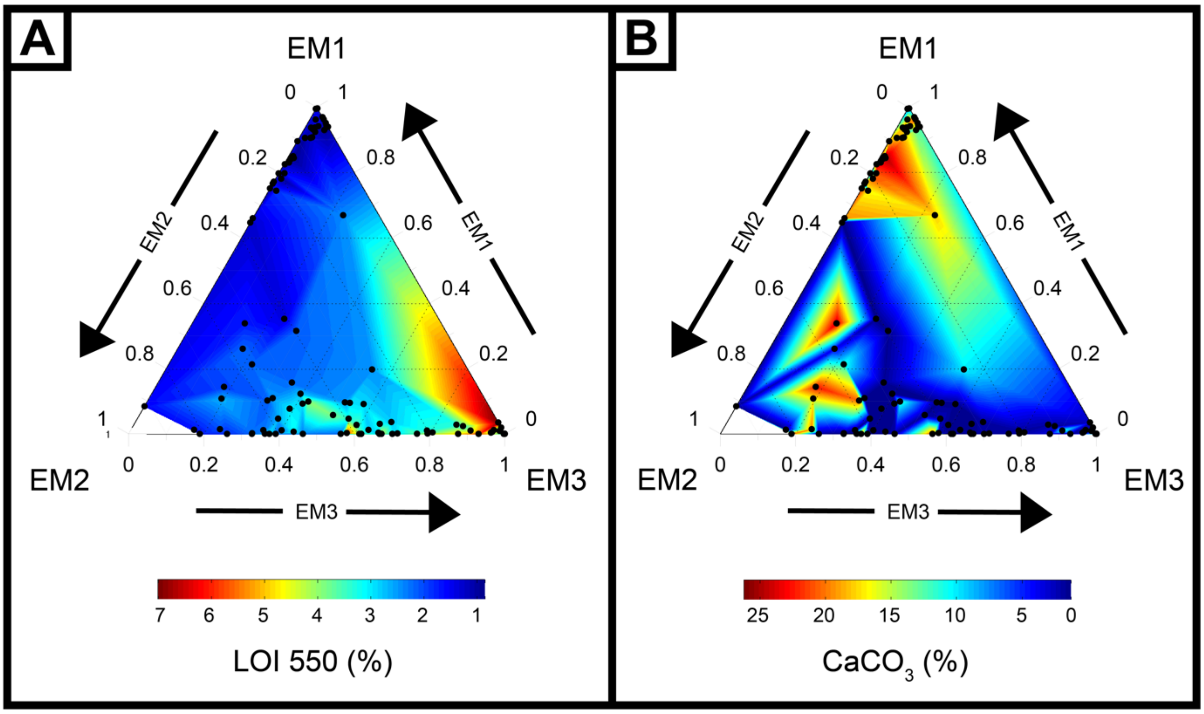


**Fig. 4.12.** Ternary mixing diagram showing within each sample the contributions of every grain-size end-member together with an extrapolated color-fill overlay of LOI550 **(A)** and $CaCO_3$ **(B)**. The extrapolation pattern is somewhat distorted due to the unequal distribution of the samples within the ternary diagram and the applied triangular extrapolation technique in Matlab.

On the contrary, the organic content is high in the fine-grained intervals. This can be explained by the fact that small particles are deposited under low flow velocities, low pH and low oxygen % and plant material can easily settle and get preserved in such conditions.

Based on the correlation between the grain-size end-members and the TGA data, it is possible to construct so-called paleoenvironment end-members of the Hell Creek Formation within the study area. This is possible, because the combination of two independent datasets both point towards specific geological conditions. A modern analogue of these paleoenvironmental end-members is shown in Fig. 4.13 and the stratigraphic and lateral extent of the three en-members within the channel fill of the Naturalis *T. rex* is shown in Fig. 4.15. The three paleoenvironmental end-members (PEM) are described below:

- **Paleoenvironmental end-member 1 (PEM1):**

PEM1 is clearly different from the other end-members in terms of a uniform peak in grain-size with a mode within the fine sand fraction around 150 µm. This coarse end-member resembles relative high water flow velocities that are also quite constant and therefore causes good sorting of the sediment. The $CaCO_3$ values are high due to oxygen-rich an alkaline water. The LOI550 values are low due to these oxic conditions and because of the high water flow velocities that destroy or transport organic particles quite easily. PEM1 is interpreted as (the thalweg of) a fluvial channel deposit (Fig. 4.13), it could both be an active river channel or an abandoned channel (meander scar) that was filled in during a flooding.

PEM2 and PEM3 are both interpreted as overbank deposits, so laid down outside the active river bed and hence associated with lower paleocurrent strengths. These overbank sediments are subdivided in very fine sand to coarse silt 'crevasse splay' and proximal pointbar deposits (PEM2) and fine silt to clay 'floodplain' deposits (PEM3).

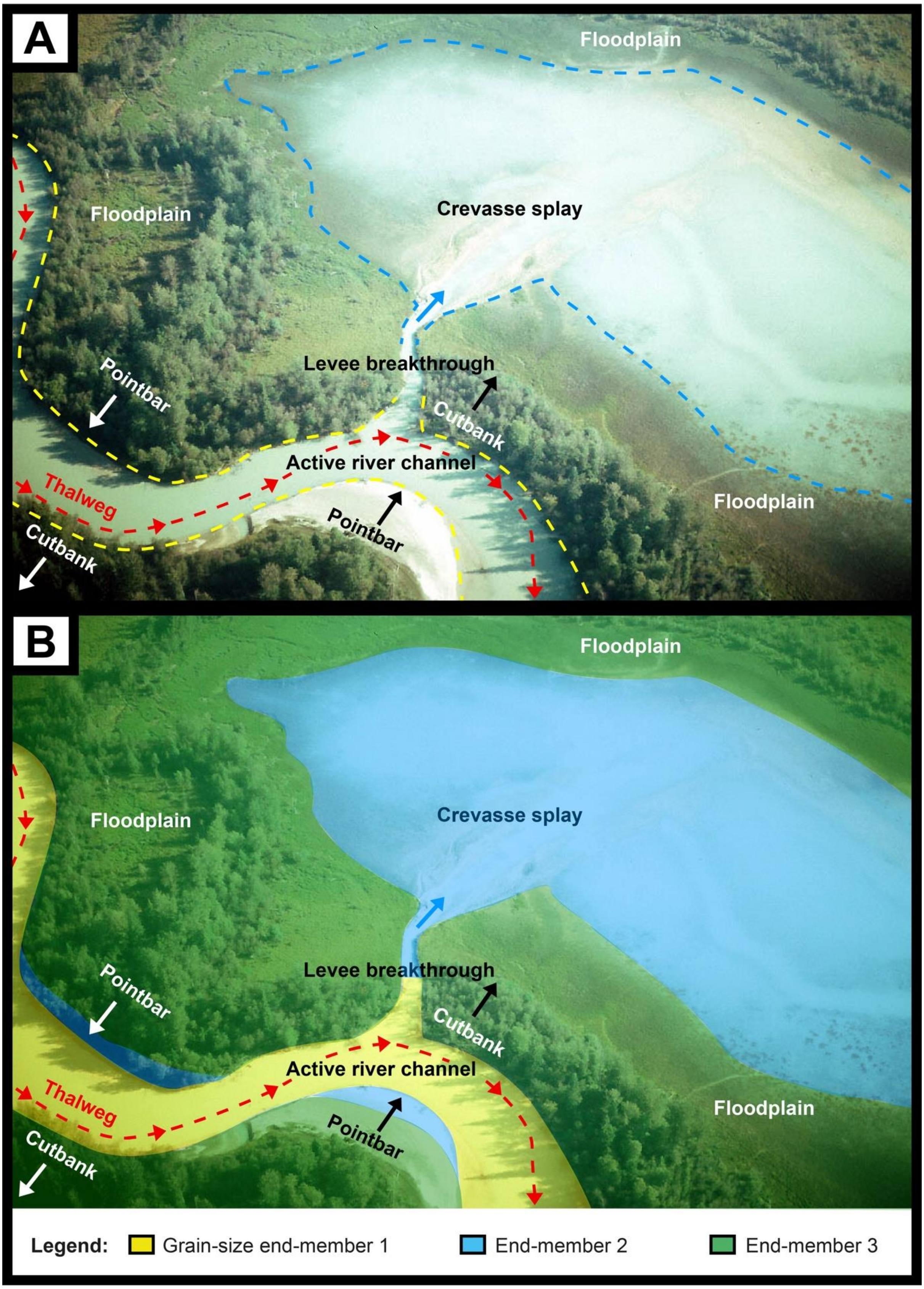


**Fig. 4.13.** Aerial view of a modern-day crevasse splay deposit following a levee breakthrough in the Columbia River of Alaska (photograph by H. J. A. Berendsen, Utrecht University). The different fluvial subenvironments are shown, the position of the thalweg and the direction of migration of the pointbars and cutbanks of the meandering river **(A)**. This meandering river system can be

interpreted as a general modern analogue for the fluvial Hell Creek Formation. The second photo shows an interpretation of the lateral extent of the three grain-size (and hence also paleoenvironmental) end-members in this study within such a modern-day meandering river system **(B)**.

- **Paleoenvironmental end-member 2 (PEM2):**

The crevasse-splay deposits have been identified many times in the field as planar-shaped, white-yellow colored sands, sometimes associated with the presence of shell fragments. These minor floodings must have been a common sight within the HCF, since the natural levees consisted of unconsolidated fine-grained sediments that could easily be removed by erosional water force. By contrast, it was observed in the field in Montana that the paleoriver channels of the Fort Union Formation rarely broke through their levees. This can be explained by the widespread presence of strong coal layers which forces the anastomosed rivers to stay within their own channel (Noorbergen, 2015, pers. comm).

PEM2 is marked by a wide range in both carbonate as organic values. This can be explained by the fact that a crevasse splay originated from an active channel and brings in carbonate-rich waters that are dropped on a floodplain. Here, the crevasse splay is quickly overgrown by vegetation that brings in a considerable amount of organic particles. These crevasse splays could evolve into shallow lakes, as can be seen from Fig. 4.13 and Fig. 4.14 and thereby provided habitats for unionid bivalves.

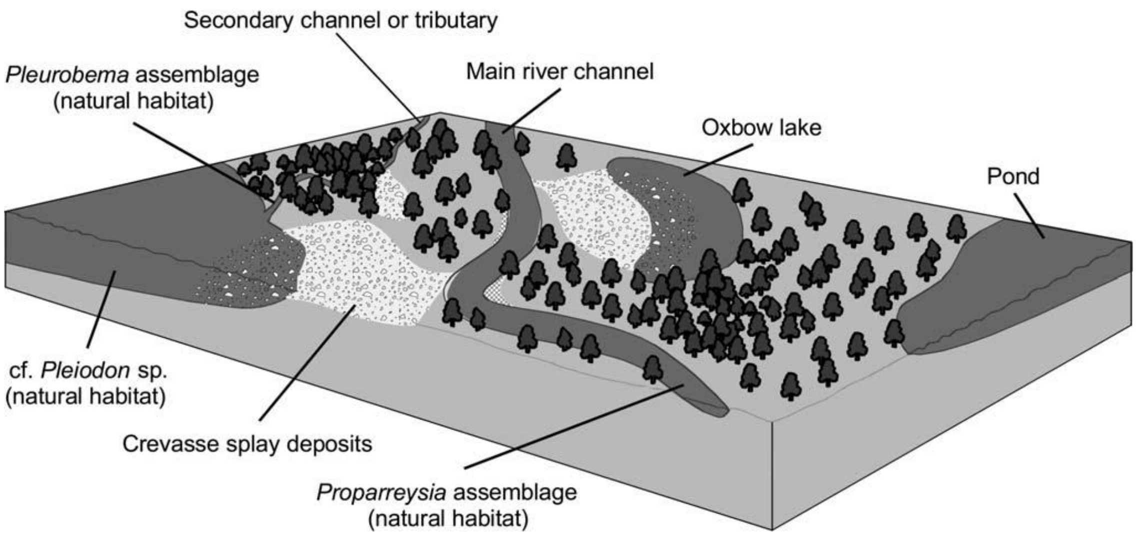


**Fig. 4.14.** Reconstruction of a Hell Creek landscape illustrating main types of water bodies in floodplain and natural habitats of two unionoid assemblages and cf. *Pleiodon* sp. Some crevasse splays are shown that are responsible for transport of bivalves out of river channels during flood events (from Scholz & Hartman, 2007).

- **Paleoenvironmental end-member 3 (PEM3):**

PEM 3 could comprise a range of different subenvironments, e.g. distal pointbar deposits, natural levees, paleosols on top of the floodplain, swales, oxbow or shallow lakes and marshes. Based on solely grain-size and TGA data it is difficult to distinguish these different subenvironments, because they are all more or less characterized by fine-grained and organic-rich deposits. Associated sedimentary structures (e.g. clay drapes, vertical root traces, coal seams) or the presence of specific fauna and flora may distinguish between these deposits. The carbonaceous shales of the HCF record sediment-dead areas in backswamps where plant debris was not diluted by influx of terrigenous sediments (Rigby & Rigby, 1990; Smit et al., 1987).

Fastovsky (1987) identified five major sedimentary facies within the HCF and the Fort Union Formation and these can be compared with our paleoonvironmental end-members.

- Cross-stratified sandstone = PEM1
- Siltstone facies = PEM2 and PEM3
- Facies of epsilon cross-stratification = PEM2
- Facies of organic accumulation = PEM3
- Variegated facies, not really found in the study area.

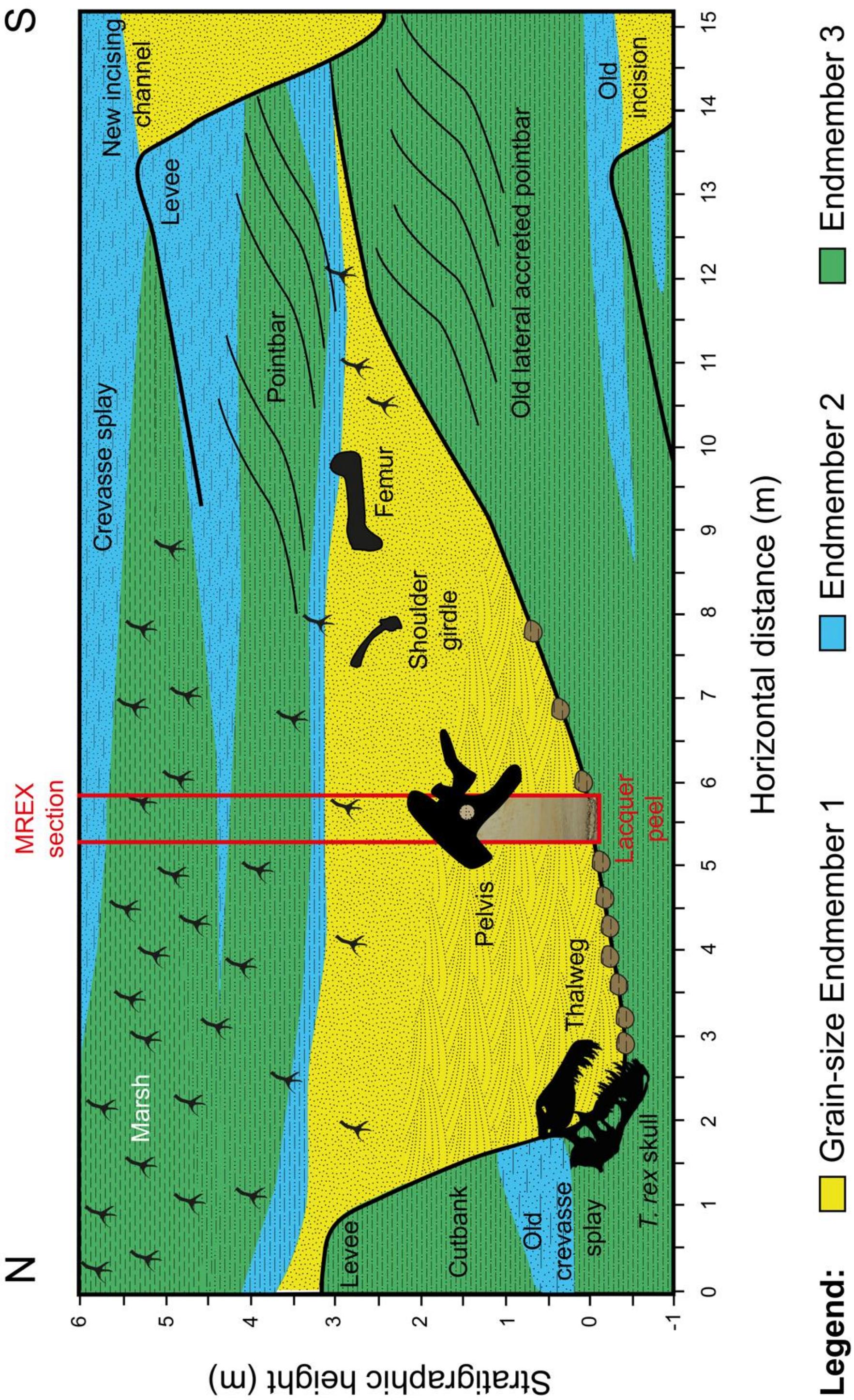


**Fig. 4.15.** The fluvial architecture of Fig 4.4 with interpreted lateral and vertical extent of the different grain-size and thus paleoenvironmental end-members.

### 4.2.2. Vegetational reconstruction

The present-day arid prairie landscape of eastern Montana was once a lush, forested environment during the Late Maastrichtian. From the results of the palynological pilot-study it became evident that the palynofloral assemblage of the Hell Creek deposits is dominated by angiosperms with an average contribution of 55%. The ferns contribute for 29% to the total, the gymnosperms 9% and the group '*Azolla* spp. and *Ghosispora bella*' for 7% (Fig. 3.15). This vegetational pattern does not change much throughout the stratigraphy, hence indicating the presence of a relatively homogeneous, highly biodiverse subtropical forest of deep time. The assumed botanical affinities and paleoenvironmental implications of different palynomorph taxa are described below.

According to Nichols (2002), the monolete fern genus *Laevigatosporites* spp. is the most common and abundant taxon within the Hell Creek palynofloral assemblage. In this study, this genus, which shows close resemblance with the living species of the fern family Polypodiacea (Tyron & Tyron, 1982), was also the most common and abundant palynomorph (see Table A4.1). This indicates that ferns were a major component of the Maastrichtian vegetation of North America. In addition, several species of trilete ferns were identified which reveals these fern types show more diversity than their monolete relatives. The common genera *Cyathidites* and *Gleichenites* could not be attributed to modern-day fern families, whereas there is evidence that the spores of the genus *Stereisporites* were produced by a Cretaceous species of *Sphagnum* (commonly known as peat moss) that probably lived in mires of the HCF.

Two specific taxa of trilete ferns (*Azolla* spp. and *Ghosipora bella*) were classified as a separate major palynological group, because they resemble characteristic paleoenvironmental conditions. Modern-day species of *Azolla* (family of Salviniaceae) are floating aquatic ferns that rapidly grow on the water surface of for instance ponds. The anchor-like projections (glochidia) of the dominant species found in the study area, *Azolla cretacea*, are quite similar to those of the living species *Azolla filiculoides* (Tryon and Tryon, 1982). *Azolla* spp. was found in all but one sample (Fig. 3.16) and thereby clearly shows the widespread occurrence of open, stagnant water in the Hell Creek depositional environment. *Ghosispora bella* also is a marker species for quiet water conditions. The presence of these two spore taxa, together with the presence of unionid bivalves and leaves in the study area, independently confirms the hypothesis of many shallow lakes in the habitat of *Tyrannosaurus rex*.

The gymnosperms are dominated by two morphologically different types of pollen, the bisaccate and inaperturate pollen. The bisaccate pollen in the study area are all attributed to the family of Pinaceae including *Pinus* (pine), *Picea* (spruce) and *Abies* (fir). Since living species of Pinaceae produce large quantities of pollen that can easily be transported by wind and may be found far from the original source area. Besides these pinaceous conifers, traces of *Taxodium* and *Glyptostrobus* have been found, which are arboraeal species that inhabited forested swamps and are characterized by inaperturate pollen. These gymnosperms probably formed the upper canopy of the Hell Creek forests. The increase of *Taxodium* pollen in the stratigraphically highest sample might indicate swampier conditions in the study area (Fig. 3.15).

The angiosperms are most abundant and most diverse in the pollen assemblage. The monocots (e.g. *Arecipites* and *Pandaniidites*, see Fig. 3.14) are predominantly palm trees. Clearly, the palms were a major component of the Hell Creek flora, being nearly ubiquitous. These palm trees, together with for instance the presence of crocodilians, suggests a mild, sub-tropical climate, with no prolonged annual cold and probably ample precipitation. Most dicot angiosperms pollen are herbaceous, but botanical affinity is difficult to asses since many taxa went extinct at the K-Pg boundary (Nichols, 2002). The botanical affinity of e.g. *Wodehouseia spinata* and *Aquilapollenites* sp., the marker taxa for the Hell Creek palynoflora, remains unknown.

Combining these pollen data, it is concluded that the habitat of the Naturalis *T. rex* was a meandering river like environment with a dense riparian forest with a canopy of metasequoias and conifer, a middle zone of cycads, palms and some broadleaf plants such as magnolia and juglans and an undercover of ferns, horsetails and moss. Many shallow lakes were present on the floodplain covered with aquatic ferns and inhabited by unionid bivalves, gar fish, turtles and crocodiles. A first scientific reconstruction of this decribed landscape is shown in Fig. 4.16.

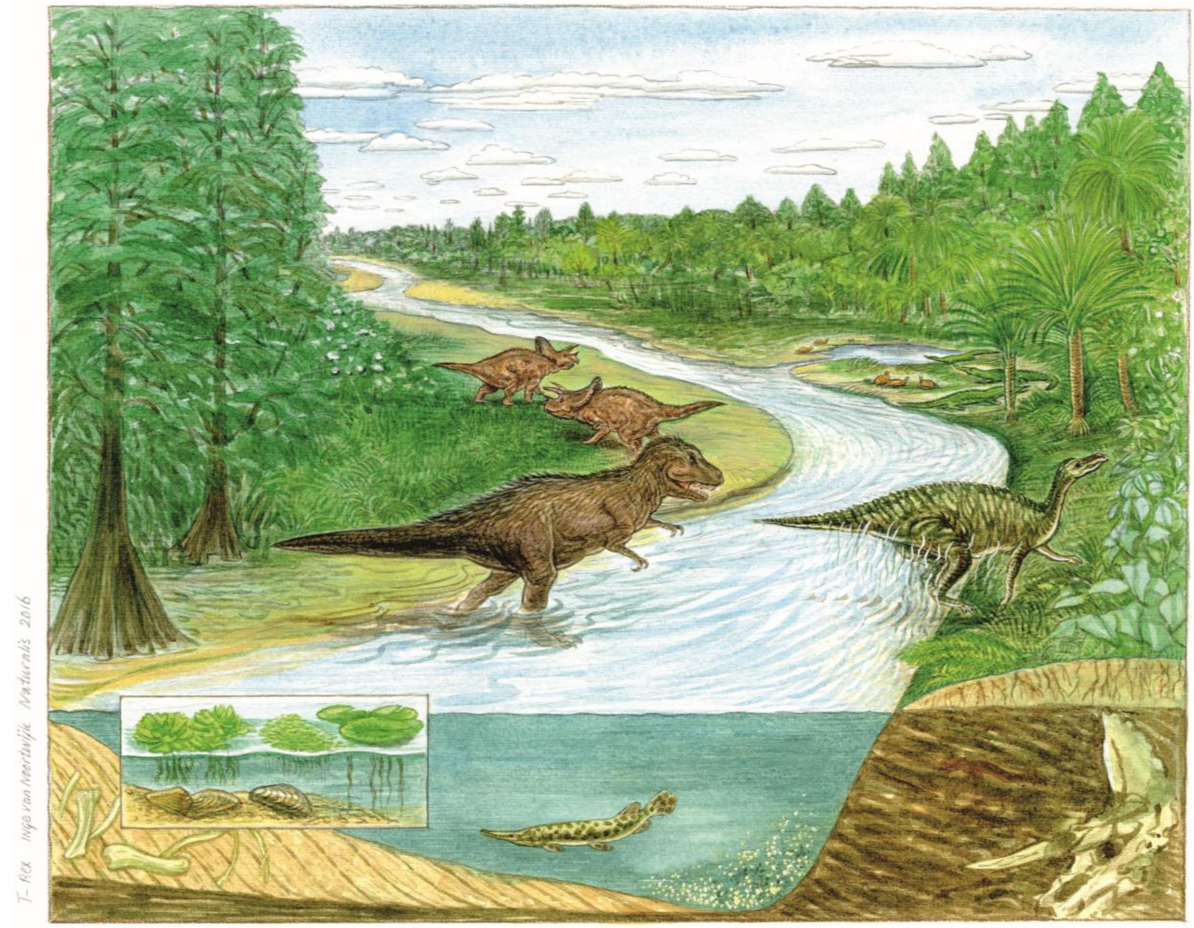


**Fig. 4.16.** A scientific artist's impression of the fluvial paleoenvironment of the Naturalis *Tyrannosaurus rex* showing an *Edmontosaurus*, *Triceratops* and a canopy of gymnosperms, a middle vegetative cover of deciduous trees and palms, and an undercover of land ferns, horsetails and aquatic ferns. This reconstruction of the landscape during deposition of the HCF was made by Inge van Noortwijk, scientific illustrator of Naturalis Biodiversity Center.

### 4.2.3. Position of the paleoshoreline

For a long time, it was believed that the HCF was deposited as a regressional sequence as a result of the retreat of the Western Interior Seaway in the Late Maastrichtian. However, recent findings of the marine Breien Member and Cantapeta Tongue in North Dakota (Murphy et al., 2002) suggest that the HCF might be a transgressive unit that was the precursor of the Early Paleocene Cannonball Sea, the final marine unit of the Northern Great Plains.

A good understanding of the position of the paleoshoreline is important, because this influences the lateral extent of the different fluvial subenvironments (near shore, tidal influenced delta, and upland meandering rivers) and thereby also controls the floral and faunal regimes of the HCF. Several aspects can influence the pattern of these fluvial subenvironments, such as large scale tectonic or climatic changes, variations in base level and accommodation space, but also compaction of different lithological units can play a role.

In Fig. 4.17 a recent regional paleogeographic map of the Williston Basin is shown that is totally different than the map of Fig. 1.5B, since in Fig. 4.17 a much larger Western Interior Seaway is displayed. This has some important consequences, because the gradient of the rivers will decline even more resulting in wettening of the hinterland and for instance more carbonaceous shale deposits are expected. In addition, this figure is important because it shows large lateral variations throughout the Williston Basin and it is not easy to compare the sedimentary trends of for instance the Flag Butte section in Montana with the Sunset Butte in North Dakota due to possible differences in time of proximity to the Western Interior Seaway.

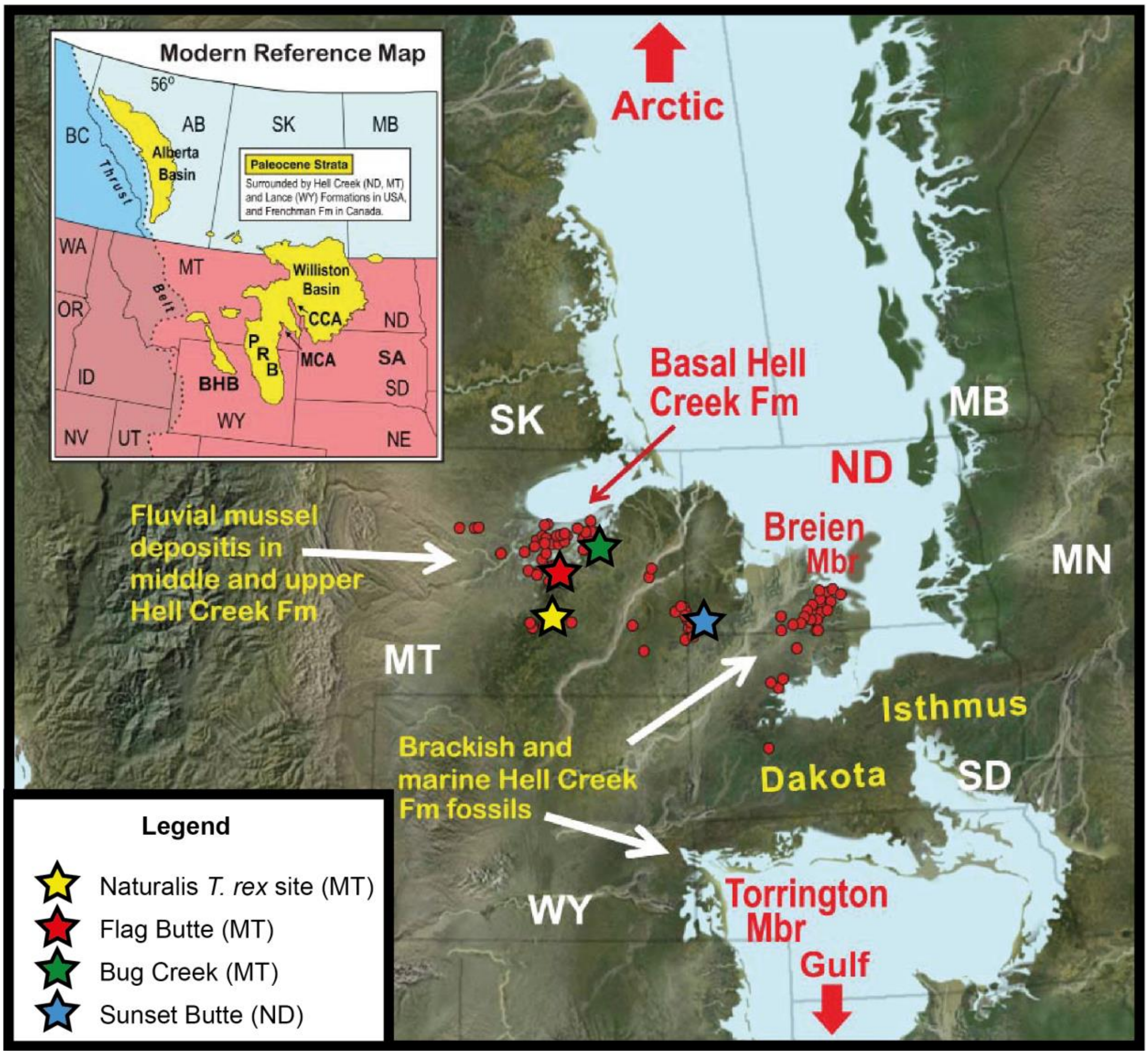


**Fig. 4.17.** A regional paleogeographical map of the Northern Great Plains around 67 Ma showing a restoration of the Hell Creek landscape and time-equivalent environments according to the interpretations of Hartman et al. (2014; supplementary information). The approximate location of the Naturalis *T. rex* site in Garfield County in Montana and the three lithostratigraphic reference sites of Fig 1.18 (Flag Butte in Garfield County, Bug Creek in McCone County and Sunset Butte in Slope County, North Dakota) are shown. Abbreviations: PRB and BHB refer to the Powder River and Bighorn Basins, respectively; BH, CCA, MCA, SA refer to the Black Hills, Cedar Creek Anticline, Miles City Arch, and Sioux Arch, respectively. The restoration is based on Western Interior Seaway coastlines interpreted from the time of the Linton Member of the Fox Hills Formation. The Linton Member, the uppermost and youngest unit of the Fox Hills, is approximately equivalent to the mid to late part of the late Maastrichtian interpreted to be about 66.5 to 67 Ma. Several major delta lobes of Hell Creek sediments are indicated. Islands are emergent remnant Fox Hills Formation features. The Linton Member is mostly at sea level or just above with higher ground along the center of the Sioux Arch and towards the Cedar Creek Anticline (inset map). The Black Hills had influence on sedimentation patterns to some extent as another high ground (at least on the western side). Several large estuaries are shown. The Linton Member landscape reconstruction is modified in Montana to represent a coastline that includes effectively all continental fossils in the Garfield and McCone County area. Drainage patterns developed for the Lancian in Wyoming have also been added to this preliminary model. Red dots are continental and brackish molluscan localities (Hartman et al., 2014).

### 4.2.4. Comparison with other *T. rex* specimens

Rigby (1987) interpreted that the HCF was deposited in an environment similar to the present-day Fitzroy River catchment in northwestern Australia. There, a riparian zone of a dense, tropical vegetation borders the rivers in a belt only a few hundred meters wide, but with an interriver area characterized by an open canopy and black soils. The ancient rivers that carved channels into the Hell Creek beds appear to have dried up during part of the year, similar to the Fitzroy River today. The only exception are isolated pools on the floodplains where animals like fish, amphibians, crocodiles and turtles survived the dry season. In such an environment giant dinosaurs such as *Tyrannosaurus rex* must have roamed. Lyson & Longrich (2011) added associated lithology to their Maastrichtian dinosaur database and found out that *T. rex* inhabited both proximal (river banks, indicated by sandstones) and distal (floodplain, marked by mudstones) fluvial environments. Of course, it should be taken in account that *T. rex* and other dinosaurs also lived in environments without active sedimentation resulting in no skeletal preservation.

However, despite its popularity, not many scientific accurate reconstructions are made of *T. rex* in its landscape that pays specific attention to the associated flora and fluvial subenvironments. Fig. 4.16 is one of the exceptions. In Table 4.1, some other studies are shown that examined the depositional environment of the associated *T. rex* discovery.

## 4.3. Integrated stratigraphy

In this paragraph, the focus is on the third research question concerning the dating of the *T. rex* bearing sediments. As already extensively explained in paragraph 1.3.6 and 1.5.1, an accurate chronostratigraphic model of the HCF is not available at the moment. Here, a new age model of the HCF is proposed based on values from the most recent geological time scale of Gradstein et al. (2012). Using cyclostratigraphy and biomagnetostratigraphy, an attempt was made to plot the Naturalis *T. rex* within this revised age model, as decribed in the paragraphs below.

### 4.3.1. Milankovitch forcing

The Hell Creek Formation is interpreted as an ancient fluvial sedimentary system. Fluvial systems can be forced by autogenic (intrinsic variations of the behavior of the river itself, see Fig. 4.18) and allogenic processes (external variations that control e.g. the rate of avulsion), as stated by Allen (1974). These allogenic processes might be related to Milankovitch-scale climatic fluctuations, as briefly described in paragraph 1.5.3.

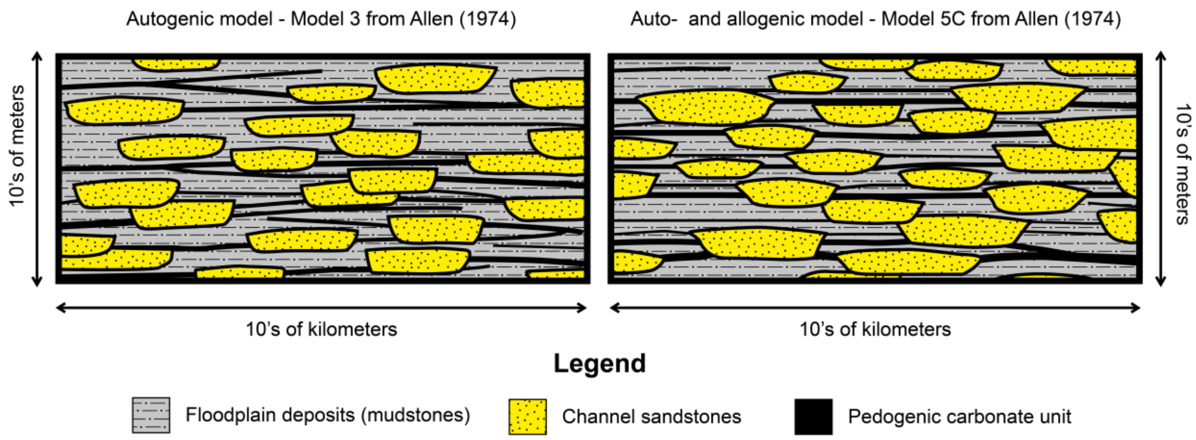


**Fig. 4.18.** Autogenic forcing in rivers causes irregular patterns of pedogenic carbonate levels (or lignites or carbonaceous shales) that are related to the intrinsic 'behavior' of the fluvial system. On the other hand, a combination of autogenic and allogenic forcing results into more horizontal, isochronous layers of pedogenic carbonate since climate (Milankovitch forcing) is dominating the fluvial system and may cause avulsion at regular timescales (modified from Allen, 1974).

Disentangling autogenic from allogenic forcing within fluvial deposits is complex and requires an integrated stratigraphic approach and high resolution sampling of regular alternating layers. Few studies have followed this approach. Abels et al. (2013) discovered precession-scale cyclicity in overbank deposits of the Eocene Willwood Formation in the Bighorn Basin Wyoming. The cycle defined by Abels et al. (2013) is 7-8 m thick and consists of a light colored fine sandy avulsion body overlain by a dark colored paleosol. Foreman (2014) found also in the Bighorn Basin in the post-PETM strata characteristic sand bodies with an average thickness of 7 m. This might imply that both the overbank deposits and the fluvial channels respond in the same way and therefore are orbitally forced in terms of rainfall and discharge fluctuations at regular time intervals.

What about older deposits? Jerret et al. (2015) talks about cyclic facies concerning peat accumulation in the Paleocene Willow Creek Formation in Canada and explains these as regional fluctuations in wildfire and oxidation. Eberth (2015) mentioned allogenic cycles within meandering river systems of the Campanian Dinosaur Park Fm in Alberta, interpreted as variations due to floodings and with the bone beds as fossil lag deposits at the base of a cycle.

Concerning the Hell Creek Formation, no significant attempt was made to understand and quantify these sedimentary cycles. Fastovsky (1987) identified five characteristic paleoenvironments, but he did not study their transitions and succession in detail. Interestingly, Rigby and Rigby (1990) mentioned the cyclic appearance of the Tullock beds just above the Hell

Creek deposits, but did not come up with an explanation for this pattern. On the Murray Ranch, specifically at the location Cyclic Butte, regular alternating layers are visible (Fig. 4.19).

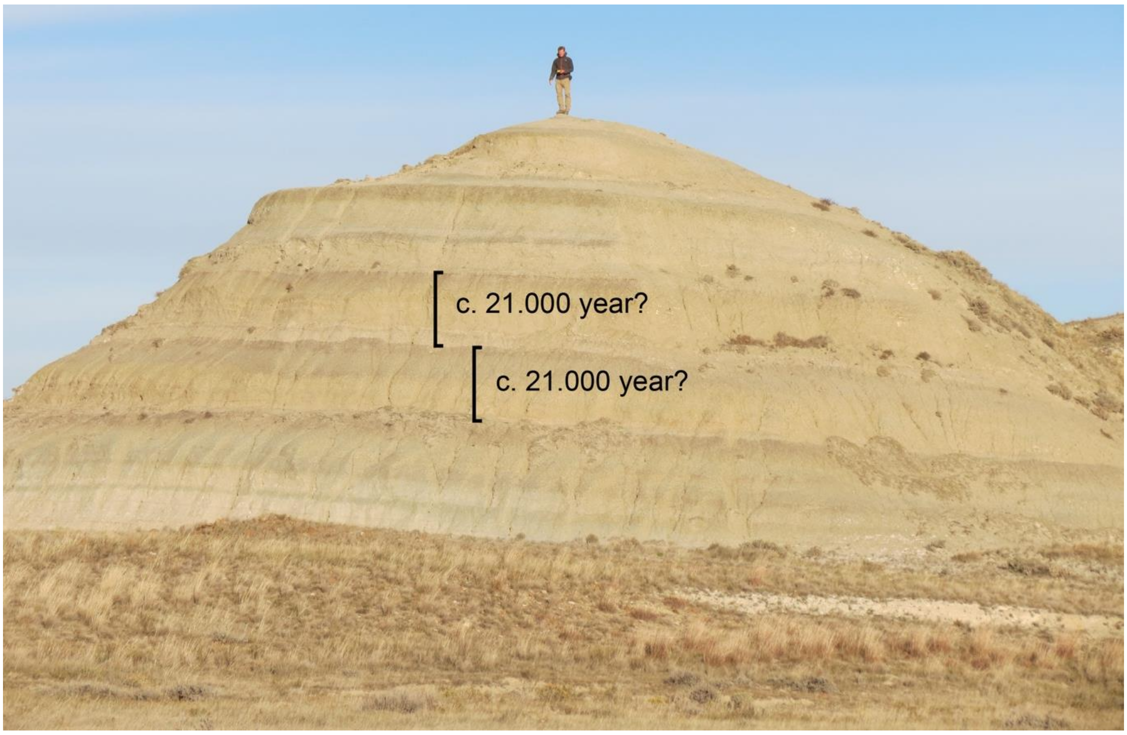


**Fig. 4.19.** Photo overview of Cyclic Butte on the Murray Ranch showing the typical rhythmic appearance of a yellowish sandstone, olive grey siltstone and a darkbrown carbonaceous shale unit overlain again with a yellowish sandstone. The author (1.82 m) for scale.

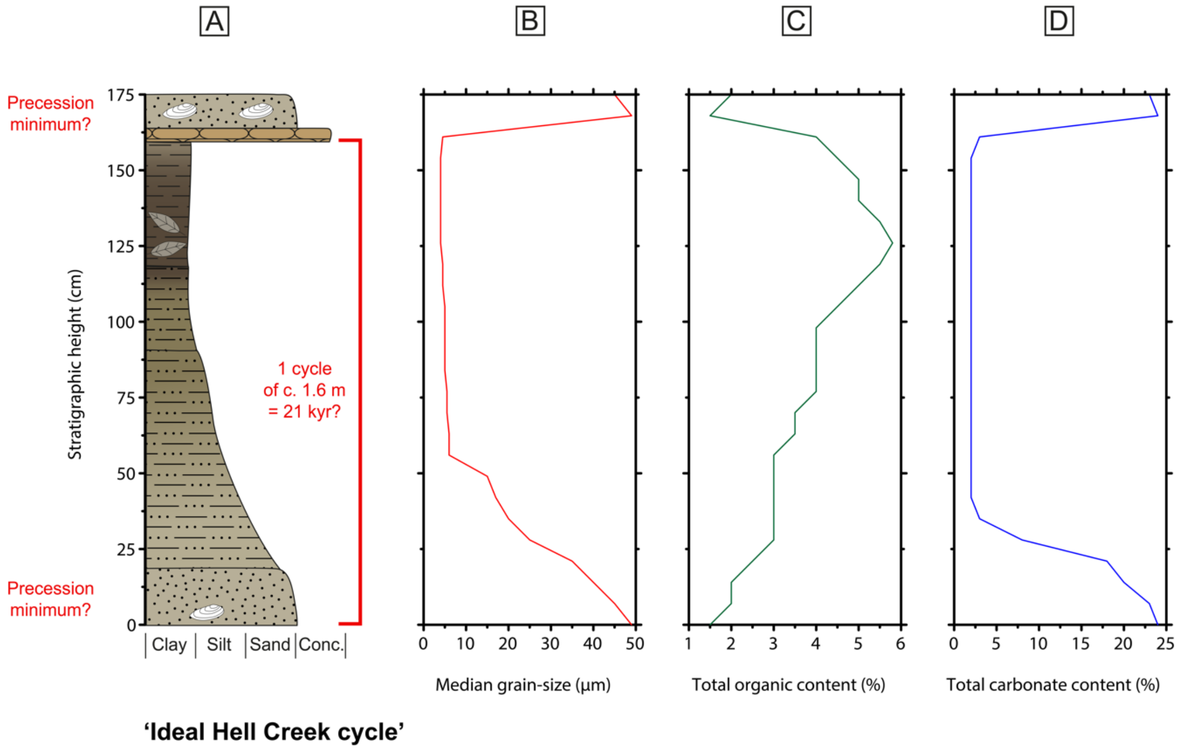


**Fig. 4.20.** Schematic representation of a hypothetical 'ideal overbank cycle' within the Hell Creek deposits of the study area. It consists of a relatively coarse and carbonate rich base of coarse silt to very fine sand and it gradually fines upwards and increases its organic content.

A schematic representation of a typical fining upwards Hell Creek cycle is seen in Fig. 4.20. Which phase relationships are present within this interpreted cycle? The basal sandy unit is interpreted as a crevasse splay deposit (PEM2) and can show some shell fragments. This must have been a (minor) flood event related to increased rainfall. Higher up in the sequence, the floodplain is still under water and can preserve a lot of organic material and leaves in a paleosol environment (PEM3). Near the top of the sequence, a calcrete level is identified which formed on top of this paleosol. A calcrete is a hardened, calcium-rich crust that normally forms in arid and semi-arid regions. Calcite is dissolved in groundwater and, under drying conditions, is precipitated as the water evaporates at the surface. Rainwater saturated with carbon dioxide acts as an acid and also dissolves calcite and then redeposits it as a precipitate on the surfaces of the soil particles; as the interstitial soil spaces are filled, an impermeable crust is formed. So, this calcrete level probably resembles a dry period and is covered again with a crevasse splay marking wet conditions. Also a regional hiatus can be present at the height of the calcrete level.

These precipitation changes are probably linked to monsoonality of the sedimentary system. Fricke et al. (2009) carried out a climate modelling coupled to oxygen isotope data of bivalves to study the Upper Cretaceous climate of North America. Aragonite secretion in freshwater unionid bivalves takes place in isotopic equilibrium with ambient river water, so the shell chemistry can be used in paleoclimate studies (Versteegh et al., 2009). Model simulations of Campanian wind directions and precipitation over North America indicate that a strong monsoon likely existed because of the close association of the Sevier highlands and the Western Interior Seaway (Fricke et al., 2009). Oxygen isotope data from unionid bivalves and paleosol carbonates recovered from a $\sim 10°$ latitude-wide section of the foreland basin reveal a spatial pattern that is consistent with such east to west movement of water vapor from low to high elevations, and subsequent recharge of foreland basin rivers by high-elevation precipitation.

So, a monsoonal influence was likely present in the Campanian and also in the Maastrichtian, because the Western Interior Seaway was still present at that time responsible for a necessary temperature and pressure gradient. In the Mediterranean region, rhythmic organic-rich sapropel layers have been identified in Plio-Pleistocene marine deposits and they have been attributed to enhanced summer monsoons. This caused intense rainfall, high river influx, a fresh water lens on top of the ocean, therefore reduced mixing and hence anoxic sea bottom conditions and the preservation of large amounts of organic material (Hilgen, et al., 2015).

These enhanced summer monsoons are interpreted to be caused by a precession minimum, or in other words: periods of intensified solar insolation on the Northern Hemisphere. This is also interpreted to be the main driving mechanism for the Hell Creek cycles and the phase relationship is probably that the crevasse splay deposits are caused by a precession minimum, since more rainfall causes flooding and the clastic influx stops the carbonaceous floodplain deposits to grow any further. The floodplain paleosol (PEM3) deposits are probably linked to a precession maximum, which indicates more dry conditions. Eccentricity modulates precession, so the thick crevasse splay deposits or the thick carbonaceous shale and calcrete levels (e.g. calcrete 4?) might also be explained by Milankovitch forcing. When precession is indeed the main driver of the regular alternating layers, a cycle of 1.6 m would resemble c. 21 kyr. When we assume the revised age model of paragraph 4.3.2 is correct, the average sedimentation rate (c. 14.000 year per 1 m, hence 22.400 year per 1.6 m) fairly matches the observed, 'orbital' sedimentation rate of the Hell Creek strata on the Murray Ranch. However, as can be seen in the next paragraph, no absolute ages were retrieved using magnetobiostratigraphy and without such a first-order age model, it is not possible to quantitatively test the Milankovitch forcing.

Speaking of seasonality, isotope geochemistry has also been performed on one of the teeth of the Naturalis *T. rex* that can be considered the proverbial tape-recorder covering approximately one year (Fig. 4.21). Fluctuations in oxygen isotopes resemble most probably the amount-effect, so more negative values coincide with the wet season. Hence, a clear wet and dry season is recorded in the tooth. The variations in the strontium isotope data might be related to this climatic seasonality, because the strontium isotope data show that some faunal migration (only the prey or both predator and prey) must have occurred (Schaeffer, 2016).

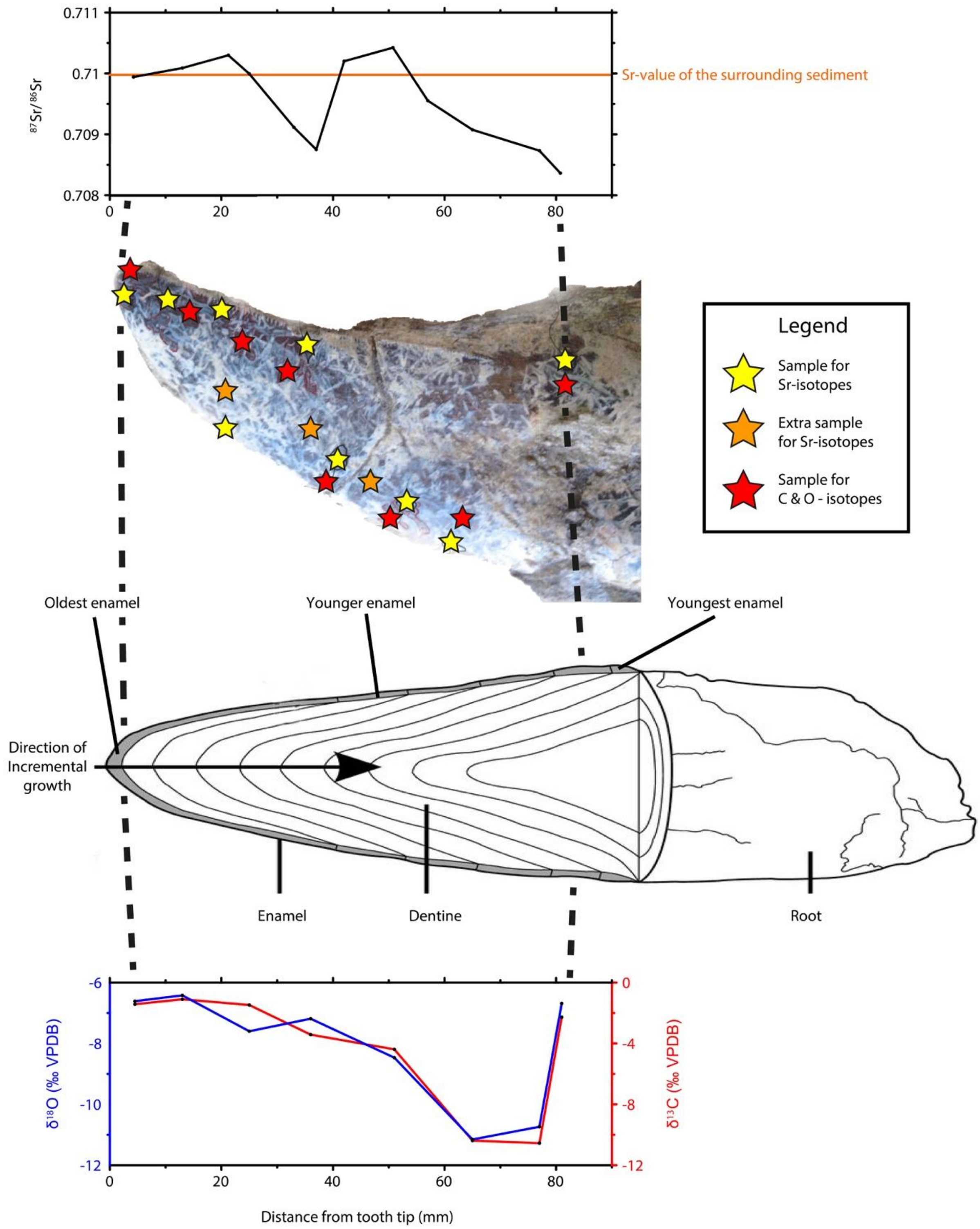


**Fig. 4.21.** Strontium, carbon and oxygen isotope data derived from the enamel of one of the teeth of the Naturalis *T. rex,* kindly provided by Joep Schaeffer, Vanessa Hausegger, Reneé Janssen and Jeroen van der Lubbe. The tooth resembles c. one year. Tooth cross section is derived from Goedert et al. (2016).

### 4.3.2. Refined age model and sedimentation rates

Age models of the HCF have not used the most recent age constraints from Gradstein et al. (2012). Therefore, I produced a revised age model of the HCF using the magnetochron durations and reversal ages of Ogg (2012) and the recent dating of the K-Pg Boundary by Renne et al. (2013). I apply this on an existing model of Hicks et al. (2002) based on a composite log of Sunset Butte in North Dakota, see Fig. 4.22. It should be noted that comparing ages from different studies must be performed with caution, since they may have used different standards.

Ogg (2012) uses the ages from Husson et al. (2011) and Thibault et al. (2012) to constrain the duration of chron c29r and c30n. This is based entirely on cyclostratigraphy. Hence, choosing between the absolute age of the K-Pg boundary by Kuiper et al. (2008) or Renne et al. (2013) does not influence the tuning.

Using this data, a chronostratigraphic framework of Sunset Butte (Fig. 4.23) and the lectostratotype of Flag Butte (Fig. 4.24) are created and an attempt is made to place the composite (magneto and bio-) stratigraphic log of the Murray Ranch (Fig. 3.16 and 3.18) within these temporal frameworks to constrain a geological age for the Naturalis *T. rex* locality.

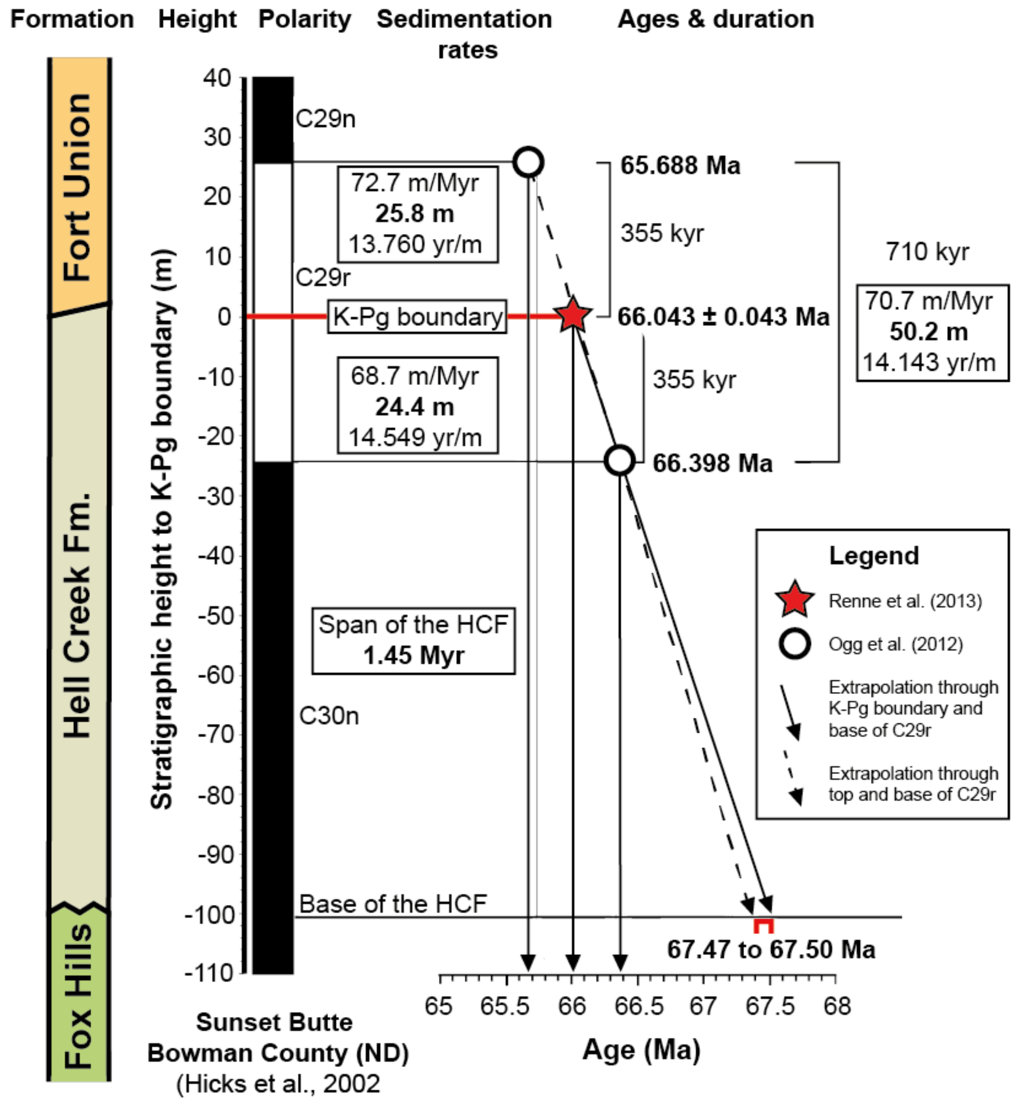


**Fig. 4.22.** Composite age correlation diagram constructed from the Sunset Butte composite log of Hicks et al (2002) using new parameters from Ogg (2012). Extrapolation from K-Pg boundary through C30n-C29r reversal yields age duration for Hell Creek Formation of 1.45 Myr (instead of the previous 1.36 Myr). Calculated sedimentation rates for each interval are shown.

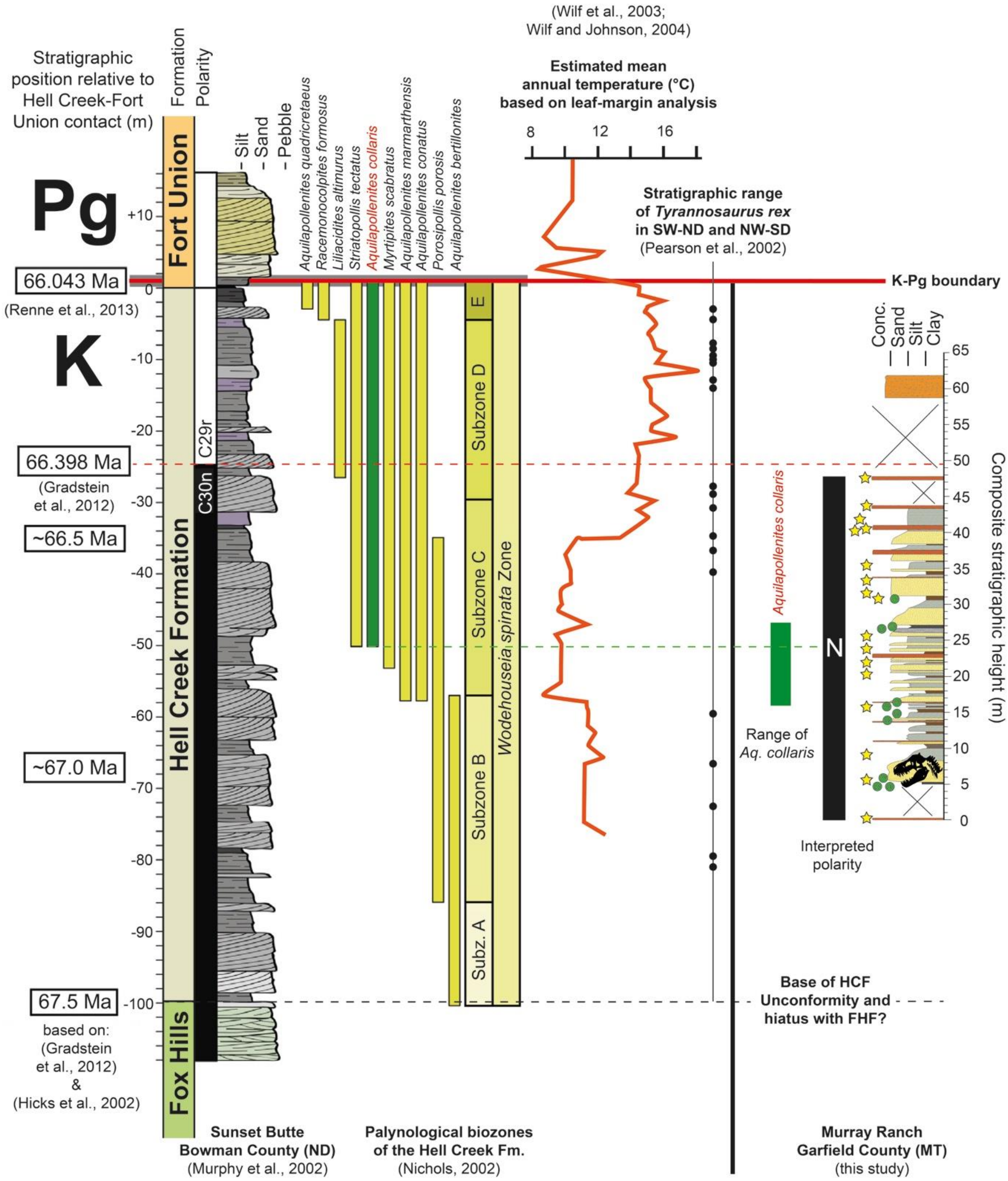


**Fig. 4.23.** Composite log of Sunset Butte (North Dakota) showing known absolute ages, polarities, lithostratigraphy and thickness, the palynological biozonation model of Nichols (2002), paleotemperatures derived from leaf margin analysis, stratigraphic ranges of *T. rex* remains combined with the stratigraphic data from this study. In this situation, the minimum age of the *T. rex* fossil site is indicated, because the top of the paleomagnetic sample range is correlated just below the real geomagnetic reversal. However, the position of the stratigraphic column of this study remains uncertain, because the paleomagnetic signal and the biostratigraphic data does not correspond to the 'expected pattern' observed in Sunset Butte. This discrepancy can be caused by many factors, which are explained in the text.

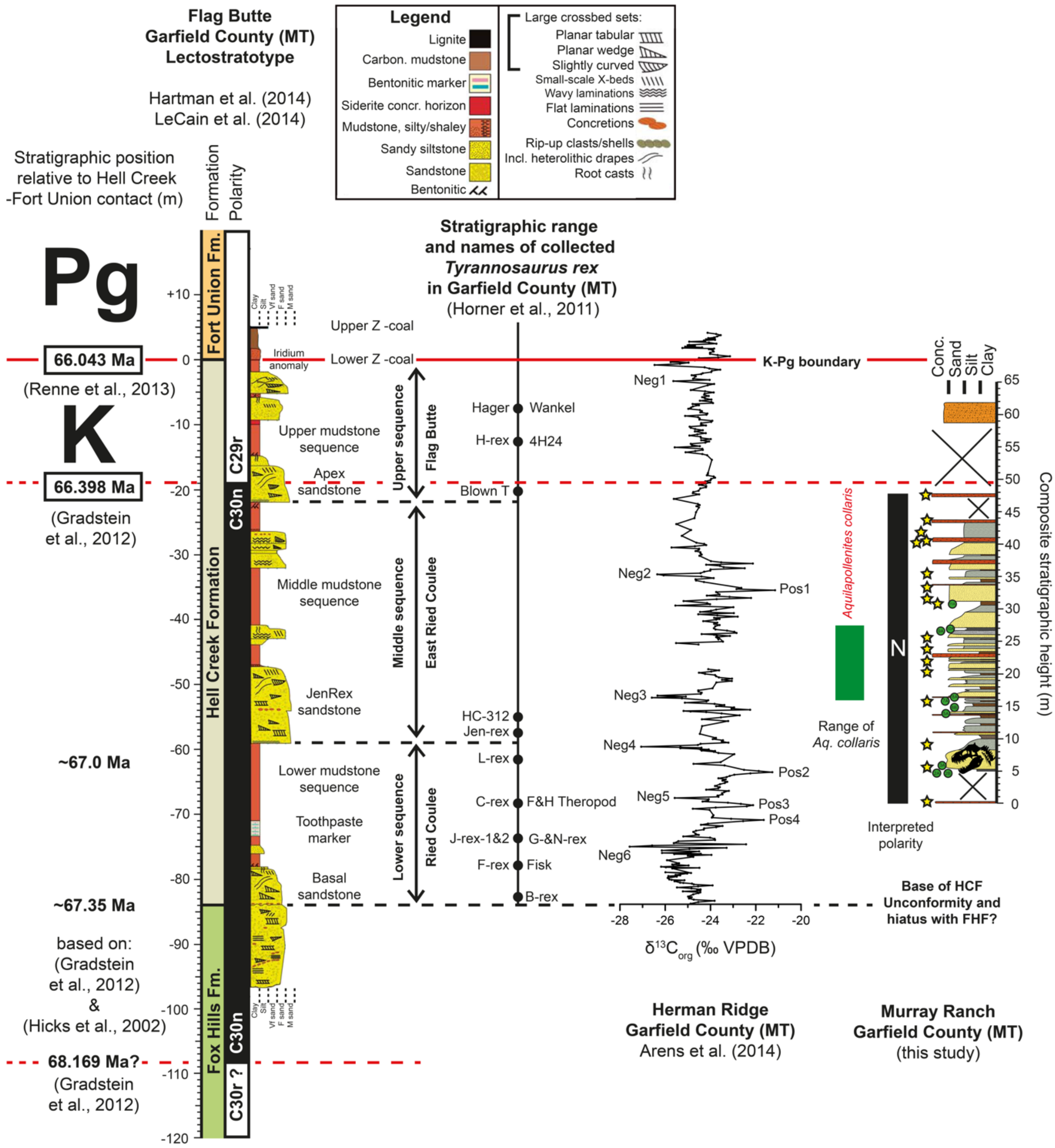


**Fig. 4.24.** Composite log of Flag Butte (Montana) showing known absolute ages, polarities, lithostratigraphy with units and thickness, stratigraphic ranges of *T. rex* skeletons, a composite carbon isotope curve combined with the stratigraphic data from this study. In this situation, the minimum age of the *T. rex* fossil site is indicated, because the top of the paleomagnetic sample range is correlated just below the real geomagnetic reversal. The real position of the stratigraphic column of this study within the lectostratotype remains uncertain,

As can be seen from Fig. 4.23 and Fig 4.24, it is difficult to place the Murray Ranch within the composite logs. Since only normal pola.rities have been measured, the sample paleomagnetic horizons must be located below the reversal c30n-c29r. However, it is difficult to then fit the *Aquilapollenites colaris* biozonation range, so a middle way is chosen and this results in a preliminary geological age of 67.0 Ma for the Naturalis *T. rex* site.

Unfortunately, there are many uncertainties and at this moment we end up with so-called 'floating stratigraphy', so there are some limitations of these two refined age models. Why does the Murray Ranch not fit into the Flag Butte and Sunset Butte composite age model? A couple of explanation are listed below:

- **Thickness variations of the HCF*:*** the HCF is assumed to be around 100 m thick in North Dakota and c.90 m in northern Garfield County. In southern Garfield County, virtually no studies of the Hell Creek Formation are reported and hence formational thickness determinations are lacking. Since the Murray Ranch is located on the westernmost margin of the Williston Basin, it is a good possibility the Hell Creek deposits are thinner than in the rest of Montana

- **The calculated duration of the HCF is not correct:** there is no absolute age for the base of the HCF and its age is estimated using extrapolation from the nearest reversal. However, previous paleomagnetic studies used very little samples and the depth of e.g. the c30n-c29r reversal within the HCF is not well-constrained.

- **Differential compaction** may obscure the sedimentation rates, because calcrete and sandstone bodies do not compress whereas mudstone intervals do and therefore comprises more time within a thinner package.

- **Paleomagnetic results are not reliable:** this is certainly an option, because the intensity within the paleomagnetic samples was in general very low. It might be possible that the characteristic remanent magnetization (the Cretaceous magnetic signal, based on the mineral magnetite) is only visible after 400 degrees Celsius. However, most of the samples lost already most - if not all - of their magnetization at this temperature.

- **The field correlations are not correct:** due to low exposure density, lenticular nature of the Hell Creek deposits and the small tectonic dip observed on the Murray Ranch, it is certainly possible that a misfit in the stratigraphic correlation of a couple of meters occurred (Fig. 3.17).

- **The biostratigraphic model of Nichols (2002) is of limited use:** this age model is made by only one author and at one location, namely the Mud Buttes region of North Dakota. To compare North Dakota with southern Garfield County is not straightforward as we have seen in paragraph 4.2.3. The proximity of the Western Interior Seaway is important, because vegetation might be severely influenced by sea level fluctuations (compare mangrove trees with pine trees for example) and this local biostratigraphic model can then not be applied for the entire HCF at a totally different location.

### 4.3.3. Comparison with other *T. rex* specimens

The Naturalis *Tyrannosaurus rex* can be seen as one of the geologically oldest specimens discovered so far. Together with for example Sue, B- rex and C-rex, it was found in the lower two-third of the HCF. In contrast to for example Stan and Wankel Rex, which are found stratigraphically high in the formation. As mentioned before, fine-tuning of the age of c. 67 Ma is difficult, but at least this gives a quick overview.

Ideally, the Table in Appendix 6 would be filled with stratigraphic age determinations, but unfortunately there are only a few attempts been made to place a T. rex skeleton in time. This would certainly be interesting to do, because a better age control can help to understand the evolution of Tyrannosaurus and its closest kin. Scannella and Keenan (2014) placed over 50 skulls of *Triceratops* within the stratigraphic framework of the HCF or Horner et al. (2011) and found a clear evolutionary transformation of the genus over the timespan of approximately 1 million years. Such an approach might also be possible for *T. rex* and could have interesting results.

# 5. Conclusions

Trix, the *Tyrannosaurus rex* of Naturalis Biociversity Center (RGM 792.000), is truly an exceptional and scientifically important specimen in many ways. Provisional bone count indicates approximately 53% of the skeleton has been recovered, which grants this discovery a position in the top three of most complete *Tyrannosaurus rex* specimens ever found. Only the *T. rex* specimens nicknamed Sue (FMNH PR2081) and Stan (BHI 3033) are more complete.

Furthermore, this fossil consists of specific bone elements that are rarely found, such as an articulated skull, a nearly complete pelvis, the furcula and an extraordinarily complete rib cage, which significantly helps in better understanding the anatomy of this dinosaur. The robust morphotype suggests the skeleton represents a female individual. The specimen displays multiple healed bone pathologies, which can shed light on its ancient (social) behavior and can give clues of its cause of death. Preliminary histological analysis suggests a very mature animal, of which not many have been found and using this c. 12 m long specimen it becomes possible to explore the far end of *T. rex* ontogeny.

Finally, the three-dimensional preservation of the skeleton is extraordinary; quoting renowned *T. rex*-expert Peter Larson: 'I must say that the preservation is superior to any other Rex." The nearly undistorted and uncompressed bone-elements have remained their original 3D shape over the course of millions of years and this 'pristinity' makes more accurate anatomical reconstructions (using correct, undeformed bone dimensions) and detailed geochemical studies possible.

In this Master Thesis, I studied the geological background of Trix in detail. The most important conclusions regarding its preservation, habitat and geological age, are listed below.

## 5.1. How did this *T. rex* get so well-preserved?

**The sequence of events leading to the extraordinary preservation of the skeleton of the Naturalis *Tyranosaurus rex* and its related evidence, can be summarized as follows:**

- A probably wounded, adult, female *T. rex* died at the bank of an active river.
- Soon after its death, minor scavenging of the carcass took place by probably a few *Nanotyrannus lancensis*, since shed theropod teeth were found at the dig site.
- Soon after this scavenging, the water level in the river began to rise due to prolonged rainfall.
- The river broke through one of its levees and flowed eastward into a dry, abandoned channel (meander scar) and caused some incision. This can be observed at the lacquer peel from the deposition of the rip-up clasts from the erosive base of Unit 2 of the MREX section.
- The decaying and partly disarticulated *T. rex* carcass was transported by a flood event into this abandoned channel. First, the skull came to rest in the deepest part of the channel and formed a flow obstacle which caused fast sedimentation of sand and of the other bone elements higher up in the channel sequence. The high flow velocities and paleocurrent direction were inferred from the presence of Type A climbing ripples and cross stratification.
- The entire skeleton was rapidly (within a couple of weeks) buried by a 3.2 m thick blanket of fine, well sorted sand. This could be derived from the well-constrained grain-size and en-member modelling dataset which show a unique grain-size fingerprint of Unit 2 compared to other sections in the study area.
- The encasing sandstone did not compact, so no bone deformation could occur in a later stage.
- After deposition of the bone bed, a normal pointbar sedimentation started with mudstones and organic accumulation that shielded of the sand unit.
- Acidic groundwater seepage, soil leeching and diagenetic alteration of the bones was strongly reduced due to the high carbonate content within the sandstone unit that protected the skeleton. This carbonate content was measured using thermogravimetry and together with petrography it revealed that angular dolomite and quartz grains dominated the matrix.

- After millions of years of deposition of rocks of the Hell Creek and Fort Union Formation on top, subsequent non-deposition during a phase of tectonic uplift in the Tertiary and intense Quaternary fluvial and fluvioglacial erosion, a beautifuly preserved skull of the Naturalis *T. rex* sticked out of the Montanan badlands and caught the eye of Blaine Lunstad in May 2013.

## 5.2. What did its paleoenvironment look like?

**The habitat of the Naturalis *Tyrannosaurus* rex was characterized by the following elements:**

- A lowland meandering river system, that can be subdivided in several sub-environments on basis of the determination of three paleonvironmental end-members: an active river channel (PEM1, characterized as a carbonate-rich fine sand), crevasse splay or proximal pointbar (PEM2, coarse silt to very fine sand and a mixture of both carbonate and organic material) and floodplain (PEM3, organic rich clay to fine silt).
- The floodplains consisted of shallow lakes inhabited by unionid bivalves, fish, turtles and crocodiles.
- A dense vegetation was present on the floodplains of mainly angiosperms. The canopy consisted of conifers, a middle vegetative cover comprised palm trees, cycads and broadleaf trees, and the undercover was dominated by mosses, horsetails and land and aquatic ferns. This ancient vegetation was derived from a detailed pollen study.
- The climate was subtropical with possible monsoonal activity, as was inferred from the cyclical appearing floodplain deposits related to enhanced and reduced rainfall.
- Occasional seasonal floods occurred, such as the one that transported and buried the Naturalis *T. rex* specimen.

## 5.3. How old are the *T. rex* bearing sediments?

**The Naturalis *T. rex* was found in rocks of the Lower to Middle Hell Creek Fm., older than 66.4 Ma, and possibly younger than 67.2 Ma, because:**

- Paleomagnetic measurements over a stratigraphic range of 47.5 m display all a normal polarity. This coincides with magnetochron c30n, which has its top at 66.4 Ma.
- The biostratigraphic marker species *Aquilapollenites collaris* was found in deposits c. 12 m above the *T. rex* excavation site and this angiosperm pollen taxon was used in the Hell Creek biozonation age model of Nichols (2002).
- Milankovitch forcing was suggested based on regular alternating floodplain deposits. However, high resolution cyclostratigraphy could not be performed because no accurate stratigraphic tie-point was found in the rock record of the study area (e.g. a geomagnetic reversal).
- An extented magneto- and biostratigraphic study on the Murray Ranch may constrain a more solid first order age model to place this fossil locality even better in time.
- The approximate geological age of 67 Ma shows that Trix is one of the oldest known *T. rex* specimens. It shows an age way older than Stan and similar to Sue. Applying similar (chrono) stratigraphic techniques to more *T. rex* specimens can shed light on possible anagenetic evolution within this theropod dinosaur.

# 6. Outlook

In this chapter, I briefly take a look into the future and provide questions and recommendations for further research related to this *T. rex* or the Hell Creek Formation in general.

## 6.1. Sedimentology and taphonomy

- It is recommended to perform detaile petrography and measure strontium isotopes in individual dolomite crystals to infer the provenance. Is the dolomite detrital or authigenic?
- Perform TGA measurements on more sandstone samples from other locations in the Williston Basin to determine whether the dolomite-richness at the Murray Ranch is a local phenomenon (and thereby contributing to this unique preservation) or just a common occurrence within the HCF.
- Take a closer look at the LIDAR-images made by Manchester University and create a rose diagram with bone elemental orientations (strike and dip) to infer paleocurrent directions. This way we better understand the 3D position of the skeleton and the conditions upon burial.
- Cooperation with vertebrate paleontologists and paleopathologists to study the cause of death and to make a realistic reconstruction of what happened when the *T. rex* died and the processes afterwards.
- Comparison with the Dueling Dinosaur discovery. At first glance, the locality looks similar to the Naturalis *T. rex* site with a thick package of sandstone encasing the predator and prey, but does it also have an unconsolidated structure similar to Unit 2 of the MREX section? And can its taphonomy also be explained by a massive flooding?

## 6.2. Paleoenvironment

- Microsampling the aragonitic shells of the collected unionid bivalves for studying seasonal cyclicity in oxygen and carbon isotopes. This may reveal some more evidence for a monsoonal climate prevailing during the time of the Naturalis *T. rex*.
- Coupling pollen and macroflora: how do these extinct Cretaceous plants look like? Cooperation with biologists to study the modern relatives of the discovered palynoflora.
- Closer cooperation with artists, to make a scientific accurate artist's impression of the Hell Creek ecosystems.

## 6.3. Integrated stratigraphy

- Performing integrated (litho-, bio-, magneto-, cyclo-, chemo-) stratigraphy on a long section from the base of the HCF crossing the KPg-boundary into the Paleocene to study in detail the possible cycles in the HCF and FUF. Absolute age control (Ar/Ar and U-Pb) on tuffs within Paleocene coals might be possible and this can be used as an accurate extrapolation into the HCF to create a solid chronostratigraphic framework for placing fossils (e.g. *T .rex*) better in time. The FUF yields a much better age control and the cycles are more pronounced compared to the HCF.
- When such outcrops are not available, then a continental drilling campaign is recommended to provide a series of long cores of both Paleocene and Cretaceous rocks. Focus area can be the Purgatory Hill region in McCone County in Montana, since this area is renowned for its good exposures that can be used to accurately correlate with the drill cores.
- Additional fieldwork on the Murray Ranch is recommended to focus specifically on the magnetostratigraphy. Furthermore, a (sub)surface model of the Murray Ranch with fence-diagrams might also be possible then, using software like 3D ArcScene and Rockworks.
- Search for dateable volcanic tuff layers and bentonites near the base of the HCF to have a better understanding of the basal contact with the Fox Hills Formation.

# Acknowledgements

First of all, I would like to sincerely thank Michele and Blaine Lunstad for finding the *Tyrannosaurus rex* specimen in the Hell Creek *badlands*. Without their discovery, this beautiful fossil and its wonderful story would still be entombed in its 67-million-year-old sandy grave or be destroyed by the harsh Montanan weather conditions within a couple of years. Now we can do amazing research on this specimen and with this inspiring museum object we can also make many people interested in natural sciences!

I am grateful to Mary Ann and Lige Murray for their hospitality and the permission to perform geological fieldwork on their private land. Clayton Phipps, the Dinosaur Cowboy, is thanked for its help with the identification of the skull, the subsequent excavation and for good company during my fieldwork. I thank Pete Larson, director of Black Hills Institute (BHI) in Hill City in South Dakota, for his help with the lacquer peel and enthusiasm and scientific advice regarding *Tyrannosaurus rex*. Servaas Neijens (National Geographic, The Netherlands), Tim Larson and Bob Farrar (both BHI) are thanked for sharing some of the video/photo material and ideas from the 2013 dig site.

Of course, I would like to sincerely thank my supervisors in the Netherlands - Jan Smit, Klaudia Kuiper, Anne Schulp and Hemmo Abels - for supporting me from the beginning of this project until the end. Jan, Klaudia and Hemmo, I learned a lot from you during the fieldwork in Montana and being part of the VU Montana Research Group (Fig. 7.1) was big fun! Lars Noorbergen and Edwin de Jong are thanked for help and good company during the field campaign in 2014. Anne, thanks for bringing me into the world of Trix and for giving me so many great opportunities within science, media and education! Sander van der Kaars is thanked for introducing me to the wonderful world of the extinct flora of the Hell Creek and for his excellent help with the pollen taxonomy. I thank Bert Boekschoten for his support and discussions.

Moreover, I would like to thank many people who helped me in a number of Dutch labs. First of all, I am grateful to Unze van Buuren, Martine Hagen, Maarten Prins and Kay Beets for help in the Sedimentology Lab at the VU with the preparation and interpretation of the data of the grain-size and thermogravimetric analysis. Bouke Lacet of the Geotechnical Laboratory at the VU is thanked for the thin sections he kindly provided. Roel van Elsas, Tineke Vogels and Koos de Jong are thanked for access and help with the microscope camera to make detailed pictures of pollen and thin sections. My short stay at the Paleomagnetic Laboratory in Utrecht was fun and I thank the people of Fort Hoofddijk for helping me out with the paleomagnetic measurements: Wout Krijgsman, Mark Dekkers, Maxim Krasnoperov, Karin Sant, Chris van Baak, and Marilyn Monster.

I thank Yorick Broekema (TU Delft) for help with the hydraulic equations for calculating the *T. rex* burial duration and I am grateful to Inge van Noortwijk for the beautiful sketch of the paleoenvironment of Trix. Lastly, I would like to thank my friends and room-mates at the VU for the enjoyable time and their support over the last 1.5 years or so. Max, Sietze, Edgar, Bart, Martijn, Esmee, Merrith, Nienke and Kirsten: thank you for the many nice discussions during lunchtime or the social drink of GeoVUsie, also about non-dinosaur related issues!

This research was made possible by the financial support from a personal grant from the Molengraaff Foundation, the Vidi-grant of Klaudia Kuiper, the VU University Amsterdam and Naturalis Biodiversity Center.

**Fig. 7.1.** The VU-Montana Research Team in action on the Murray Ranch, from left to right: Jan Smit, Klaudia Kuiper, Pim Kaskes and Lars Noorbergen.

# References


Abels, H.A., Kraus, M.J., and Gingerich, P.D., 2013, Precession-scale cyclicity in the fluvial lower Eocene Willwood Formation of the Bighorn Basin, Wyoming (USA): Sedimentology, v. 60, p. 1467–1483, doi: 10.1111/sed.12039.

Allen, J.R.L., 1970, A quantitative model of climbing ripples and their cross-laminated deposits: Sedimentology, v. 14, no. 1-2, p. 5–26.

Alvarez, L.W., Alvarez, W., Asaro, F., and Michel, H. V, 1980, Extraterrestrial Cause for the Cretaceous-Tertiary Extinction: Science, v. 208, no. 4448, p. 1095–1108.

Anna, L.O., Pollastro, R., and Gaswirth, S.B., 2010, Williston Basin Province—Stratigraphic and Structural Framework to a Geologic Assessment of Undiscovered Oil and Gas Resources: Assessment of Undiscovered Oil and Gas Resources of the Williston Basin Province of North Dakota, Montana, and South Dakota, 2010, p. Chapter 2/7, doi: 10.1306/M971332.

Archibald, J.D., Butler, R.F., Lindsay, E.H., Clemens, W.A., and Dingus, L., 1982, Upper Cretaceous-Paleocene biostratigraphy and magnetostratigraphy, Hell Creek and Tullock Formations, northeastern Montana: Geology, v. 10, no. 3, p. 153–159.

Arens, N.C., and Jahren, A.H., 2002, Chemostratigraphic correlation of four fossil-bearing sections in southwestern North Dakota: Geological Society of America Special Paper 361: The Hell Creek Formation and the Cretaceous-Tertiary boundary in the northern Great Plains: An integrated continental record of the end of the Cretaceous., p. 75–93, doi: 10.1130/0-8137-2361-2.75.

Arens, N.C., Jahren, A.H., and Amundson, R., 2000, Can C3 plants faithfully record the carbon isotopic composition of atmospheric carbon dioxide? Paleobiology, v. 26, no. 01, p. 137–164.

Arens, N.C., Jahren, A.H., and Kendrick, D.C., 2014, Carbon isotope stratigraphy and correlation of plant megafossil localities in the Hell Creek Formation of eastern Montana , USA: in Wilson, G.P., Clemens, W.A., Horner, J.R., and Hartman, J.H., eds., Through the End of the Cretaceous in the Type Locality of the Hell Creek Formation in Montana and Adjacent Areas: Geological Society of America Special Paper 503, p. 149–171, doi: 10.1130/2014.2503(05).

Asara, J.M., and Schweitzer, M.H., 2008, Response to comment on “protein sequences from mastodon and Tyrannosaurus rex revealed by mass spectrometry”: Science, v. 319, no. 5859, doi: DOI 10.1126/science.1147364.

Ashley, G.M., Southard, J.B., and Boothroyd, J.C., 1982, Deposition of climbing-ripple beds: a flume simulation: Sedimentology, v. 29, p. 67–79, doi: 10.1111/j.1365-3091.1982.tb01709.x.

Bakker, R.T., 1972, Anatomical and Ecological Evidence of Endothermy in Dinosaurs: Nature, v. 238, p. 81–85.

Bakker, R.T., Sullivan, R.M., Porter, V., Peter, L., and Saulsburgy, S.J., 2006, Dracorex Hogwartsia, n. gen., n., sp., A Spiked Flat-headed Pachycephalosaurid Dinosaur From the Upper Cretaceous Hell Creek Formation of South Dakota: New Mexico Museum of Natural History and Science Bulletin 35, p. 331–345.

Bakker, R.T., Williams, M., and Currie, P.J., 1988, Nanotyrannus, a new genus of pygmy tyrannosaur, from the latest Cretaceous of Montana: Hunteria, v. 1, no. 5, p. 1–30.

Baren, J.H.V. van, and Bomer, W., 1979, Procedures for the collection and preservation of soil profiles: International Soil Museum, Wageningen, The Netherlands, p. 22.

Barnosky, A.D., Matzke, N., Tomiya, S., Wogan, G.O.U., Swartz, B., Quental, T.B., Marshall, C., McGuire, J.L., Lindsey, E.L., Maguire, K.C., Mersey, B., and Ferrer, E. a, 2011, Has the Earth’s sixth mass extinction already arrived? Nature, v. 471, no. 7336, p. 51–57, doi: 10.1038/nature09678.

Bates, K.T., and Falkingham, P.L., 2012, Estimating maximum bite performance in Tyrannosaurus rex using multi-body dynamics.: Biology letters, v. 8, no. 4, p. 660–4, doi: 10.1098/rsbl.2012.0056.

Behrensmeyer, A.K., 1978, Taphonomic and ecologic information from bone weathering: Paleobiology, v. 4, no. 2, p. 150–162, doi: 10.2307/2400283.

Behrensmeyer, A.K., Kidwell, S.M., and Gastaldo, R. a, 2000, Taphonomy and paleobiology: Paleobiology, v. 26, no. 4, p. 103–147.

Belt, E.S., Hicks, J.F., and Murphy, D.A., 1997, A pre-Lancian regional unconformity and its relationship to Hell Creek paleogeography in south-eastern Montana: Rocky Mountain Geology, v. 31, no. 2, p. 1–26.

Benton, M.J., 1995, Diversification and extinction in the history of life: Science, v. 268, no. 5207, p. 52–58, doi: 10.1126/science.7701342.

Bercovici, A., Pearson, D., Nichols, D., and Wood, J., 2009, Biostratigraphy of selected K/T boundary sections in southwestern North Dakota, USA: toward a refinement of palynological identification criteria: Cretaceous Research, v. 30, no. 3, p. 632–658, doi: 10.1016/j.cretres.2008.12.007.

Bjørlykke, K., 2010, Petroleum Geoscience: From sedimentary Environments to Rock Physics: Springer.
Blakey, R.C., 2014, Paleogeography and paleotectonics of the Western Interior Seaway, Jurassic-Cretaceous of North America: Presentation at Tulsa Geological Society, p. 72.
Bohor, B.F., 1990, Shock-induced microdeformations in quartz and other mineralogical indications of an impact event at the Cretaceous-Tertiary boundary: Tectonophysics, v. 171, no. 1-4, p. 359–372, doi: 10.1016/0040-1951(90)90110-T.
Breithaupt, B.H., and Elizabeth, H., 2008, Wyoming's Dynamosaurus imperiosus and other early discoveries of Tyrannosaurus rex in the rocky mountain West: Tyrannosaurus Rex, the Tyrant King, p. 57–62.
Brett-Surman, M.K., Holtz, T.R., Farlow, J.O., and Walters, B., 2012, The complete dinosaur: Indiana University Press.
Brinkman, D.B., Newbrey, M.G., and Neuman, A.G., 2014, Diversity and paleoecology of actinopterygian fish from vertebrate microfossil localities of the Maastrichtian Hell Creek Formation of Montana: in Wilson, G.P., Clemens, W.A., Horner, J.R., and Hartman, J.H., eds., Through the End of the Cretaceous in the Type Locality of the Hell Creek Formation in Montana and Adjacent Areas: Geological Society of America Special Paper 503, p. 247–270, doi: 10.1130/2014.2503(09).For.
Brochu, C.A., 2002, Osteology of Tyrannosaurus Rex : Insights from a nearly complete Skeleton and High-Resolution Computed Tomographic Analysis of the Skull: Journal of Vertebrate Paleontology, v. 22, p. 1–138, doi: 10.1080/02724634.2003.10010947.
Brown, B., 1914, Cretaceous-Eocene correlation in New Mexico, Wyoming, Montana, Alberta: Bulletin of the Geological Society of America - Proceedings of the Paleontological Society, v. 25, p. 355–380.
Brown, J.L., 1993, Sedimentology and Depositional History of the Lower Paleocene Tullock Member of the Fort Union Formation, Powder River Basin, Wyoming and Montana: US Geological Survey Bulletin,.
Brown, B., 1907, The Hell Creek beds of the Upper Cretaceous of Montana: their relation to contiguous deposits, with faunal and floral lists and a discussion of their colleration: Bulletin of the American Museum of Natural History, v. 23, p. 823–845.
Brusatte, S.L., 2012, Dinosaur paleobiology: John Wiley & Sons.
Brusatte, S.L., Averianov, A., Sues, H.-D., Muir, A., and Butler, I.B., 2016, New tyrannosaur from the mid-Cretaceous of Uzbekistan clarifies evolution of giant body sizes and advanced senses in tyrant dinosaurs: Proceedings of the National Academy of Sciences, v. 113, no. 13, p. 1–6, doi: 10.1073/pnas.1600140113.
Brusatte, S.L., and Benson, R.B.J., 2013, The systematics of Late Jurassic tyrannosauroid theropods from Europe and North America: Acta Palaeontologica Polonica, v. 58, no. 1, p. 47–54, doi: 10.4202/app.2011.0141.
Brusatte, S.L., Butler, R.J., Barrett, P.M., Carrano, M.T., Evans, D.C., Lloyd, G.T., Mannion, P.D., Norell, M.A., Peppe, D.J., Upchurch, P., and Williamson, T.E., 2015, The extinction of the dinosaurs: Biological Reviews, v. 90, no. 2, p. 628–642, doi: 10.1111/brv.12128.
Brusatte, S.L., and Carr, T.D., 2016, The phylogeny and evolutionary history of tyrannosaurid dinosaurs: Scientific Reports, v. 6, no. 20252, p. 1–8, doi: 10.1038/srep20252.
Brusatte, S.L., Carr, T.D., Erickson, G.M., Bever, G.S., and Norell, M.A., 2009, A long-snouted, multihorned tyrannosaurid from the Late Cretaceous of Mongolia.: Proceedings of the National Academy of Sciences of the United States of America, v. 106, no. 41, p. 17261–17266, doi: 10.1073/pnas.0906911106.
Brusatte, S.L., Norell, M.A., Carr, T.D., Erickson, G.M., Hutchinson, J.R., Balanoff, A.M., Bever, G.S., Choiniere, J.N., Makovicky, P.J., and Xu, X., 2010, Tyrannosaur Paleobiology: New Research on Ancient Exemplar Organisms: Science, v. 329, no. 5998, p. 1481–1485, doi: 10.1126/science.1193304.
Butler, R.D., 1980, Stratigraphy, sedimentology and depositional environments of the Hell Creek Formation (Late Cretaceous) and adjacent strata, Glendive area, Montana: Unpublished Ph. D. Thesis - Grand Forks, University of North Dakota, p. 398.
Carr, T.D., 1999, Craniofacial ontogeny in Tyrannosauridae (Dinosauria, Coelurosauria): Journal of Vertebrate Paleontology, v. 19, no. 3, p. 497–520, doi: 10.1080/02724634.1999.10011161.
Chin, K., Tokaryk, T.T., Erickson, G.M., and Calk, L.C., 1998, A king-sized theropod coprolite: Nature, v. 393, no. 6686, p. 680–682, doi: 10.1038/31461.
Clausen, E.N., 1987, Late Cenozoic erosion of Williston Basin sediments: Fifth International Williston Basin Symposium, June 14 - 17, 1987, p. 190 – 195.
Clemens, W.A., 2002, Evolution of the mammalian fauna across the Cretaceous-Tertiary boundary in northeastern Montana and other areas of the Western Interior: The Hell Creek Formation and the Cretaceous-Tertiary boundary in the northern Great Plains: An integrated continental record of the end of the Cretaceous: Boulder, Colorado, Geological Society of America Special Paper 361, p. 217–245, doi: 10.1130/0-8137-2361-2.217.

Clemens, W.A., and Hartman, J.H., 2014, From Tyrannosaurus rex to asteroid impact: Early studies (1901 – 1980) of the Hell Creek Formation in its type area: in Wilson, G.P., Clemens, W.A., Horner, J.R., and Hartman, J.H., eds., Through the End of the Cretaceous in the Type Locality of the Hell Creek Formation in Montana and Adjacent Areas: Geological Society of America Special Paper 503, p. 1–87, doi: 10.1130/2014.2503(01).

Coleman, J.L., and Cahan, S.M., 2012, Preliminary Catalog of the Sedimentary Basins of the United States: U.S. Geological Survey Open-File Report 2012-111, p. 27.

Coleman Renick, B., and Riffenburg, H.B., 1929, Geology and ground-water resources of central and southern Rosebud County, Montana: US Geological Survey,.

Collier, A.J., and Knechtel, M.M., 1939, The coal resources of McCone county, Montana: US Government Printing Office,.

Condon, S.M., 2000, Stratigraphic Framework of Lower and Upper Cretaceous Rocks in Central and Eastern Montana: U.S. Geological Survey Digital Data Series DDS-57, p. 12.

Connor, C.W., 1992, The Lance Formation - petrography and stratigraphy, Powder River Basin and nearby basins, Wyoming and Montana: US Geological Survey Bulletin,.

Cook, T.D., Newbrey, M.G., Brinkman, D.B., and Kirkland, J.I., 2014, Euselachians from the freshwater deposits of the Hell Creek Formation of Montana: in Wilson, G.P., Clemens, W.A., Horner, J.R., and Hartman, J.H., eds., Through the End of the Cretaceous in the Type Locality of the Hell Creek Formation in Montana and Adjacent Areas: Geological Society of America Special Paper 503, p. 229–246, doi: 10.1130/2014.2503(08).

Cooley, J.B., and Schmitt, J.G., 2001, Taphonomy and sedimentology of a tyrannosaurid locality from the Late Cretaceous (Maastrichtian) Hell Creek Formation of eastern Montana, *in* Geological Society of America Annual Meeting 2001 - Poster Presentation,.

Currie, P.J., 2003, Allometric growth in tyrannosaurids (Dinosauria: Theropoda) from the Upper Cretaceous of North America and Asia: Canadian Journal of Earth Sciences, v. 40, no. May, p. 651–665, doi: 10.1139/e02-083.

Currie, P.J., and Eberth, D.A., 2010, On gregarious behavior in Albertosaurus: Canadian Journal of Earth Sciences, v. 47, no. 9, p. 1277–1289, doi: 10.1139/E10-072.

D'Hondt, S., 2005, Consequences of the Cretaceous/Paleogene mass extinction for marine ecosystems: Annual review of ecology, evolution, and Systematics, p. 295–317.

DeCelles, P.G., 2004, Late Jurassic to Eocene evolution of the Cordilleran thrust belt and foreland basin system, western U.S.A.: American Journal of Science, v. 304, no. February, p. 105–168, doi: 10.2475/ajs.304.2.105.

DePalma, R.A., Burnham, D.A., Martin, L.D., Larson, P.L., and Bakker, R.T., 2015, The first giant raptor (Theropoda: Dromaeosauridae) from the Hell Creek Formation: Paleontological Contributions of the University of Kansas, v. 0279, no. 14, p. 1–18.

DePalma, R.A., Burnham, D.A., Martin, L.D., Rothschild, B.M., and Larson, P.L., 2013, Physical evidence of predatory behavior in Tyrannosaurus rex: Proceedings of the National Academy of Sciences, v. 110, no. 31, p. 12560–12564, doi: 10.1073/pnas.1216534110.

DePalma, R., Cichocki, F., Dierick, M., and Feeney, R., 2010, Preliminary Notes on the First Recorded Amber Insects from the Hell Creek Formation: The Journal of Paleontological Sciences JPS., p. 1–7.

Derstler, K.L., and Myers, J.M., 2008, Taphonomy of the Tyrannosaurus rex Peck's rex from the Hell Creek Formation of Montana: Tyrannosaurus rex, the Tyrant King: Indiana University Press, Bloomington, p. 75–82.

Dietze, M., and Dietze, E., 2013, EMMAgeo: End-member modelling algorithm and supporting functions for grain-size analysis, R package version 0.9. 0:.

Dietze, E., Hartmann, K., Diekmann, B., IJmker, J., Lehmkuhl, F., Opitz, S., Stauch, G., Wünnemann, B., and Borchers, A., 2012, An end-member algorithm for deciphering modern detrital processes from lake sediments of Lake Donggi Cona, NE Tibetan Plateau, China: Sedimentary Geology, v. 243, p. 169–180.

Dietze, E., Maussion, F., Ahlborn, M., Diekmann, B., Hartmann, K., Henkel, K., Kasper, T., Lockot, G., Opitz, S., and Haberzettl, T., 2014, Sediment transport processes across the Tibetan Plateau inferred from robust grain-size end members in lake sediments: Climate of the Past, v. 10, no. 1, p. 91–106, doi: 10.5194/cp-10-91-2014.

Dingus, L., and Norell, M., 2010, Barnum Brown: the man who discovered Tyrannosaurus rex: University of California Press.

Dodson, P., Behrensmeyer, a K., Bakker, R.T., and Mcintosh, J.S., 1980, Taphonomy and Paleoecology of the Dinosaur Beds of the Jurassic Morrison Formation: Paleobiology, v. 6, no. 2, p. 208–232.

Dott, R.H., 1964, Wacke, Graywacke and Matrix--What Approach to Immature Sandstone Classification? Journal of Sedimentary Research, v. 34, no. 3, p. 625–632, doi: 10.1306/74D71109-2B21-11D7-

8648000102C1865D.
Eberth, D.A., 2015, Origins of dinosaur bonebeds in the Cretaceous of Alberta ,: v. 681, no. August, p. 655–681.
Erickson, J.M., 1992, Subsurface stratigraphy, lithofacies, and paleoenvironments of the Fox Hills Formation (Maastrichtian: Late Cretaceous) adjacent to the type area, North Dakota and South Dakota - toward a more holistic view: Proceedings of the F. D. Holland Jr. Symposium, North Dakota Geological Survey Miscellaneous Series 76, p. 199–243.
Erickson, G.M., Currie, P.J., Inouye, B.D., and Winn, A.A., 2006, Tyrannosaur life tables: an example of nonavian dinosaur population biology: Science, v. 313, no. 5784, p. 213–217, doi: 10.1126/science.1125721.
Erickson, G.M., Kirk, S.D. Van, Su, J., Levenston, M.E., Caler, W.E., and Carter, D.R., 1996, Bite-force estimation for Tyrannosaurus rex from tooth-marked bones: Nature, v. 382, no. 6593, p. 706–708, doi: 10.1038/382706a0.
Erickson, G.M., Makovicky, P.J., Currie, P.J., Norell, M.A., Yerby, S.A., and Brochu, C.A., 2004, Gigantism and comparative life-history parameters of tyrannosaurid dinosaurs: Nature, v. 430, no. 7001, p. 772–775, doi: 10.1038/nature02771.
Erickson, G.M., and Olson, K.H., 1996, Bite marks attributable to Tyrannosaurus rex: preliminary description and implications: Journal of Vertebrate Paleontology, v. 16, no. 1, p. 175–178.
Evans, D.C., Larson, D.W., and Currie, P.J., 2013, A new dromaeosaurid (Dinosauria: Theropoda) with Asian affinities from the latest Cretaceous of North America: Naturwissenschaften, v. 100, no. 11, p. 1041–1049, doi: 10.1007/s00114-013-1107-5.
Faegri, K., and Iversen, J., 1989, Textbook of Pollen Analysis, revised by Faegri K., Kaland P.E., Krzywinski K.: J Wiley, New York,.
Fassett, J.E., Heaman, L.M., and Simonetti, A., 2011, Direct U-Pb dating of Cretaceous and Paleocene dinosaur bones, San Juan Basin, New Mexico: Geology, v. 39, no. 2, p. 159–162.
Fastovsky, D.E., 1987, Paleoenvironments of vertebrate-bearing strata during the Cretaceous-Paleogene transition, eastern Montana and western North Dakota: Palaios, v. 2, no. 3, p. 282–295.
Fastovsky, D.E., and Bercovici, A., 2016, The Hell Creek Formation and its contribution to the Cretaceous–Paleogene extinction: A short primer: Cretaceous Research, v. 57, p. 368–390, doi: 10.1016/j.cretres.2015.07.007.
Fastovsky, D.E., and Dott, R.H., 1986, Sedimentology, stratigraphy, and extinctions during the Cretaceous-Paleogene transition at Bug Creek, Montana (USA): Geology, v. 14, no. 4, p. 279–282, doi: 10.1130/0091-7613(1986)14<279:SSAEDT>2.0.CO;2.
Fastovsky, D.E., and McSweeney, K., 1987, Paleosols spanning the Cretaceous-Paleogene transition, eastern Montana and western North Dakota: Geological Society Of America Bulletin, v. 99, p. 66–77.
Fiorillo, A.R., and Tykoski, R.S., 2014, A diminutive new tyrannosaur from the top of the world: PLoS ONE, v. 9, no. 3, p. e91287, doi: 10.1371/journal.pone.0091287.
Flight, J.N., 2004, Sequence stratigraphic analysis of the Fox Hills and Hell Creek Formations (Maastrichtian), eastern Montana and its relationship to dinosaur paleontology: Unpublished Master Thesis - Montana State University, Bozeman, p. 164, doi: 10.1007/s13398-014-0173-7.2.
Folk, R.L., 1966, A review of grain-size parameters: Sedimentology, v. 6, no. 2, p. 73–93, doi: 10.1111/j.1365-3091.1966.tb01572.x.
Foreman, B.Z., 2014, Climate-driven generation of a fluvial sheet sand body at the Paleocene-Eocene boundary in north-west Wyoming (USA): Basin Research, v. 26, no. 2, p. 225–241, doi: 10.1111/bre.12027.
Fowler, D.W., 2009, A sequence stratigraphic subdivision of the Hell Creek Formation: beginnings of a high-resolution regional chronostratigraphic framework for the terminal Cretaceous: 9th North American Paleontological Convention, abstracts volume: 136, p. 136.
Fowler, C.M.R., and Nisbet, E.G., 1985, The subsidence of the Williston Basin: Canadian Journal of Earth Sciences, v. 22, p. 408–415, doi: 10.1139/e85-039.
Fricke, H.C., Foreman, B.Z., and Sewall, J.O., 2010, Integrated climate model-oxygen isotope evidence for a North American monsoon during the Late Cretaceous: Earth and Planetary Science Letters, v. 289, no. 1-2, p. 11–21, doi: 10.1016/j.epsl.2009.10.018.
Frye, C.I., 1969, Stratigraphy of the Hell Creek Formation in North Dakota: North Dakota Geological Survey Bulletin 54, p. 65.
Fullerton, B.D.S., Colton, R.B., Bush, C.A., and Straub, A.W., 2004, Map Showing Spatial and Temporal Relations of Mountain and Continental Glaciations on the Northern Plains, Primarily in Northern Montana and Northwestern North Dakota: USGS report,.
Funkhouser, J.W., 1961, Pollen of the genus Aquilapollenites: Micropaleontology, p. 193–198.

Garrity, C.P., and Soller, D.R., 2009, Database of the Geologic Map of North America—Adapted from the Map by J.C. Reed, Jr. and others (2005): USGS Data Series, , no. 424, p. 10.

Gerhard, L.C., Anderson, S.B., and Fischer, D.W., 1990, Petroleum geology of the Williston Basin: Interior cratonic basins: AAPG Memoir, v. 51, p. 507–559.

Glut, D., 2008, Tyrannosaurus rex: A century of celebrity: Tyrannosaurus rex, the Tyrant King, p. 398–425.

Goedert, J., Amiot, R., Boudad, L., Buffetaut, E., Fourel, F., Godefroit, P., Kusuhashi, N., Suteethorn, V., Tong, H., Watabe, M., and Lécuyer, C., 2016, Preliminary Investigation of Seasonal Patterns Recorded in the Oxygen Isotope Compositions of Theropod Dinosaur Tooth Enamel: Palaios, v. 31, no. 1, p. 10–19, doi: 10.2110/palo.2015.018.

Gradstein, F.M., Ogg, J.G., Schmitz, M., and Ogg, G., 2012, The geologic time scale 2012 2-volume set: elsevier.

Hall, L.A., and Keenan, 2010, Taphonomy of a new specimen of Tyrannosaurus rex from the Hell Creek Formation, Montana: Society for Vertebrate Paleontology Annual Meeting 2010 - Poster Presentation,.

Haq, B.U., 2014, Cretaceous eustasy revisited: Global and Planetary Change, v. 113, p. 44–58, doi: 10.1016/j.gloplacha.2013.12.007.

Haq, B.U., Hardenbol, J., and Vail, P.R., 1987, Chronology of fluctuating sea levels since the Triassic: Science, v. 235, no. 4793, p. 1156–1167, doi: 10.1126/science.235.4793.1156.

Harrison, W.F., Nichols, D.J., Henderson, M.D., and Scherer, R.P., 2013, Using pollen, leaves and paleomagnetism to date a juvenile tyrannosaurid in Upper Cretaceous rock: Tyrannosaurid Paleobiology, p. 239–249.

Hartman, J.H., 1998, The biostratigraphy and paleontology of Latest Cretaceous and Paleocene freshwater bivalves from the Western Williston Basin, *in* Montana, USA: in Johnston, PA, and Haggart, JW, eds., International Symposium on the Paleobiology and Evolution of the Bivalvia, Drumheller (Bivalves: An Eon of Evolution—Paleobiological Studies Honoring Norman D. Newell): University of Calgary Press, Cal, p. 317–345.

Hartman, J.H., Johnson, K.R., and Nichols, D.J., 2002, The Hell Creek Formation and the Cretaceous-Tertiary boundary in the northern Great Plains: an integrated continental record of the end of the Cretaceous: Geological Society of America.

Hartman, J.H., and Kirkland, J.I., 2002, Brackish and marine mollusks of the Hell Creek Formation of North Dakota: Evidence for a persisting Cretaceous seaway: The Hell Creek Formation and the Cretaceous-Tertiary boundary in the northern Great Plains: An integrated continental record of the end of the Cretaceous: Boulder, Colorado, Geological Society of America Special Paper 361, p. 271–296, doi: 10.1130/0-8137-2361-2.271.

Heiri, O., Lotter, A.F., and Lemcke, G., 2001, Loss on Ignition as a Method for Estimating Organic and Carbonate Content in Sediments: Reproducibility and Comparability of Results: Journal of Paleolimnology, v. 25, p. 101–110, doi: 10.1023/A.

Henderson, M.D., and Harrison, W.H., 2008, Taphonomy and environment of deposition of juvenile tyrannosaurid skeleton from the Hell Creek Formation (latest Maastrichtian) of southeastern Montana: Tyrannosaurus rex, the Tyrant King: Indiana University Press, Bloomington, p. 82–90.

Henderson, M.D., and Peterson, J.E., 2006, An azhdarchid pterosaur cervical vertebra from the Hell Creek Formation (Maastrichtian) of southeastern Montana: Journal of Vertebrate Paleontology, v. 26, no. 1, p. 192–195.

Heslop, D., 2008, A quick guide to DRS-UNMIXER:.

Hicks, J.F., Johnson, K.R., Obradovich, J.D., Tauxe, L., and Clark, D., 2002, Magnetostratigraphy and geochronology of the Hell Creek and basal Fort Union Formations of southwestern North Dakota and a recalibration of the age of the Cretaceous-Tertiary boundary: The Hell Creek Formation and the Cretaceous-Tertiary boundary in the northern Great Plains: An integrated continental record of the end of the Cretaceous: Boulder, Colorado, Geological Society of America Special Paper 361, p. 35–55, doi: 10.1130/0-8137-2361-2.35.

Hildebrand, A.R., Penfield, G.T., Kring, D.A., Pilkington, M., Camargo Z., A., Jacobsen, S.B., and Boynton, W. V., 1991, Chicxulub crater - a possible Cretaceous/Tertiary boundary impact crater on the Yucatan Peninsula, Mexico: Geology, v. 19(9), p. 867–871, doi: 10.1130/0091-7613(1991)019<0867.

Hilgen, F.J., Hinnov, L.A., Abdul Aziz, H., Abels, H.A., Batenburg, S., Bosmans, J.H.C., de Boer, B., Hüsing, S.K., Kuiper, K.F., Lourens, L.J., Rivera, T., Tuenter, E., van de Wal, R.S.W., Wotzlaw, J.-F., et al., 2015, Stratigraphic continuity and fragmentary sedimentation: the success of cyclostratigraphy as part of integrated stratigraphy: Geological Society, London, Special Publications, v. 404, no. 1, p. 157–197, doi: 10.1144/SP404.12.

van Hinsbergen, D.J.J., de Groot, L. V, van Schaik, S.J., Spakman, W., Bijl, P.K., Sluijs, A., Langereis, C.G., and Brinkhuis, H., 2015, A Paleolatitude Calculator for Paleoclimate Studies: PloS one, v. 10, no. 6, p.

e0126946, doi: 10.1371/journal.pone.0126946.
Hoganson, J.W., and Murphy, E.C., 2002, Marine Breien Member (Maastrictian) of the Hell Creek Formation in North Dakota: stratigraphy, vertebrate fossil record, and age.: The Hell Creek Formation and the Cretaceous-Tertiary boundary in the northern Great Plains: An integrated continental record of the end of the Cretaceous: Boulder, Colorado, Geological Society of America Special Paper 361, p. 247–269, doi: 10.1130/0-8137-2361-2.247.
Holroyd, P.A., Wilson, G.P., and Hutchison, J.H., 2014, Temporal changes within the latest Cretaceous and early Paleogene turtle faunas of northeastern Montana: in Wilson, G.P., Clemens, W.A., Horner, J.R., and Hartman, J.H., eds., Through the End of the Cretaceous in the Type Locality of the Hell Creek Formation in Montana and Adjacent Areas: Geological Society of America Special Paper 503, p. 299–312, doi: 10.1130/2014.2503(11).
Hone, D.W.E., Farke, A.A., and Wedel, M.J., 2016, Ontogeny and the fossil record: what, if anything, is an adult dinosaur? Biology Letters, v. 12, no. 2, p. 20150947, doi: 10.1098/rsbl.2015.0947.
Horner, J.R., 2014, Introduction: in Wilson, G.P., Clemens, W.A., Horner, J.R., and Hartman, J.H., eds., Through the End of the Cretaceous in the Type Locality of the Hell Creek Formation in Montana and Adjacent Areas: Geological Society of America Special Paper 503, p. ix–x, doi: 10.1130/2014.2503(001).
Horner, J.R., and Goodwin, M.B., 2009, Extreme cranial ontogeny in the upper cretaceous dinosaur Pachycephalosaurus: PLoS ONE, v. 4, no. 10, doi: 10.1371/journal.pone.0007626.
Horner, J.R., Goodwin, M.B., and Myhrvold, N., 2011, Dinosaur census reveals abundant Tyrannosaurus and rare ontogenetic stages in the upper Cretaceous Hell Creek Formation (Maastrichtian), Montana, USA: PLoS ONE, v. 6, no. 2, doi: 10.1371/journal.pone.0016574.
Horner, J.R., Varricchio, D.J., and Goodwin, M.B., 1992, Marine transgressions and the evolution of Cretaceous dinosaurs: Nature, v. 358, p. 59–61.
Husson, D., Galbrun, B., Laskar, J., Hinnov, L. a., Thibault, N., Gardin, S., and Locklair, R.E., 2011, Astronomical calibration of the Maastrichtian (Late Cretaceous): Earth and Planetary Science Letters, v. 305, no. 3-4, p. 328–340, doi: 10.1016/j.epsl.2011.03.008.
Hutchinson, J.R., Bates, K.T., Molnar, J., Allen, V., and Makovicky, P.J., 2011, A computational analysis of limb and body dimensions in tyrannosaurus rex with implications for locomotion, ontogeny, and growth: PLoS ONE, v. 6, no. 10, doi: 10.1371/journal.pone.0026037.
Hutchinson, J.R., and Garcia, M., 2002, Tyrannosaurus was not a fast runner: Nature, v. 415, no. 6875, p. 1018–1021.
Jensen, F., and Varnes, H.D., 1964, Geology of the Fort Peck area, Garfield, McCone, and Valley counties, Montana: U. S. Geological Survey Professional Paper, p. 49.
Jerrett, R.M., Price, G.D., Grimes, S.T., and Dawson, A.T., 2015, A paleoclimatic and paleoatmospheric record from peatlands accumulating during the Cretaceous-Paleogene boundary event, Western Interior Basin, Canada: Bulletin of the Geological Society of America, v. 127, no. 11-12, p. 1564–1582, doi: 10.1130/B31166.1.
Johnson, K.R., 1992, Leaf-fossil evidence for extensive floral extinction at the Cretaceous-Tertiary boundary, North Dakota, USA: Cretaceous Research, v. 13, no. 1, p. 91–117.
Johnson, K.R., 2002, Megaflora of the Hell Creek and lower Fort Union Formations in the western Dakotas: Vegetational response to climate change, the Cretaceous-Tertiary boundary event, and rapid marine transgression: Geological Society of America, Special Paper, v. 361, p. 329–391, doi: 10.1130/0-8137-2361-2.329.
Johnson, K.R., Nichols, D.J., and Hartman, J.H., 2002, Hell Creek Formation: A 2001 synthesis: The Hell Creek Formation and the Cretaceous-Tertiary boundary in the northern Great Plains: An integrated continental record of the end of the Cretaceous: Boulder, Colorado, Geological Society of America Special Paper 361, p. 503–510, doi: 10.1130/0-8137-2361-2.503.
Kauffman, E.G., 1984, Paleobiogeography and evolutionary response dynamic in the Cretaceous Western Interior Seaway of North America, *in* Jurassic-Cretaceous biochronology and paleogeography of North America, Geol. Assoc. Can. Sp. Pap, p. 273–306.
Kent, D.M., and Christopher, J.E., 1994, Geological history of the Williston Basin and Sweetgrass arch: Geological atlas of the Western Canada Sedimentary Basin: Canadian Society of Petroleum Geologists and Alberta Research Council, p. 421–429.
Kirschvink, J.L., 1980, The least-squares line and plane and the analysis of palaeomagnetic data: Geophysical Journal of the Royal Astronomical Society, v. 62, no. 3, p. 699–718, doi: 10.1111/j.1365-246X.1980.tb02601.x.
Koenig, A.E., Lucas, S.G., Neymark, L.A., Heckert, A.B., Sullivan, R.M., Jasinski, S.E., and Fowler, D.W., 2012, Direct U-Pb dating of Cretaceous and Paleocene dinosaur bones, San Juan Basin, New Mexico: Comment: Geology, v. 40, no. 4, p. 262, doi: 10.1016/j.

Konert, M., and Beets, C.J. Simultaneous analysis of organic matter and carbonates in sediments with a thermo-gravimetric analyzer (TGA): comparison to classical analytical techniques: Submitted,.

Konert, M., and Vandenberghe, J., 1997, Comparison of laser grain size analysis with pipette and sieve analysis: a solution for the underestimation of the clay fraction: Sedimentology, v. 44, p. 523–535.

Kowallis, B.J., Christiansen, E.H., Deino, A.L., Petersonc, F., Turner, C.E., Kunk, M.J., and Obradovich, J.D., 1998, The age of the Morrison Formation: Modern Geology, v. 22, p. 235–260.

Koymans, M.R., Langereis, C.G., Pastor-Galán, D., and van Hinsbergen, D.J.J., 2016, Paleomagnetism.org: an online multi-platform open source environment for paleomagnetic data analysis: Computers & Geosciences, v. 93, p. 127–137, doi: 10.1016/j.cageo.2016.05.007.

Kring, D.A., 2007, The Chicxulub impact event and its environmental consequences at the Cretaceous-Tertiary boundary: Palaeogeography, Palaeoclimatology, Palaeoecology, v. 255, no. 1-2, p. 4–21, doi: 10.1016/j.palaeo.2007.02.037.

Kroeger, T.J., 2002, Palynology of the Hell Creek Formation (Upper Cretaceous, Maastrichtian) in northwestern South Dakota: Effects of paleoenvironment on the composition of palynomorph assemblages: The Hell Creek Formation and the Cretaceous-Tertiary boundary in the northern Great Plains: An integrated continental record of the end of the Cretaceous: Boulder, Colorado, Geological Society of America Special Paper 361, p. 457–472, doi: 10.1130/0-8137-2361-2.457.

Kuiper, K.F., 2003, Direct intercalibration of radio-isotopic and astronomical time in the Mediterranean Neogene:.

Kuiper, K.F., Deino, A., Hilgen, F.J., Krijgsman, W., Renne, P.R., and Wijbrans, J.R., 2008, Synchronizing Rock Clocks of Earth History: Science, v. 320, no. 5875, p. 500–504, doi: 10.1126/science.1154339.

Labandeira, C.C., Johnson, K.R., and Lang, P., 2002, Preliminary assessment of insect herbivory across the Cretaceous-Tertiary boundary: Major extinction and minimum rebound: The Hell Creek Formation and the Cretaceous-Tertiary boundary in the northern Great Plains: An integrated continental record of the end of the Cretaceous: Boulder, Colorado, Geological Society of America Special Paper 361, p. 297–327, doi: 10.1130/0-8137-2361-2.297.

Lamanna, M.C., Sues, H.D., Schachner, E.R., and Lyson, T.R., 2014, A new large-bodied oviraptorosaurian theropod dinosaur from the latest Cretaceous of western North America: Plos One, v. 9, no. 3, doi: 10.1371/journal.pone.0092022.

Larson, N.L., 2008a, One hundred years of Tyrannosaurus rex: the skeletons: Tyrannosaurus rex, the Tyrant King, p. 1–55.

Larson, P., 2013a, The case for Nanotyrannus: Tyrannosaurid Paleobiology, p. 15–53.

Larson, P., 2013b, The validity of Nanotyrannus Lancensis (Theropoda, Lancian—Upper Maastrichtian of North America), *in* Society of paleontology: 73rd annual meeting, abstracts with programs,.

Larson, P., 2008b, Variation and sexual dimorphism in Tyrannosaurus rex: Tyrannosaurus rex, the Tyrant King, p. 103–130.

Larson, P.L., and Carpenter, K., 2008, Tyrannosaurus rex, the Tyrant King: Indiana University Press.

Larson, P.L., and Donnan, K., 2002, Rex appeal: the amazing story of Sue, the dinosaur that changed science, the law, and my life: Invisible Cities Press.

LeCain, R., Clyde, W.C., Wilson, G.P., and Riedel, J., 2014, Magnetostratigraphy of the Hell Creek and lower Fort Union Formations in northeastern Montana: in Wilson, G.P., Clemens, W.A., Horner, J.R., and Hartman, J.H., eds., Through the End of the Cretaceous in the Type Locality of the Hell Creek Formation in Montana and Adjacent Areas: Geological Society of America Special Paper 503, p. 137–147, doi: 10.1130/2014.2503(04).

Lehman, T.M., 1987, Late Maastrichtian Paleoenvironments and Dinosaur Biogeography in the Western Interior of North America: Palaeogeography Palaeoclimatology Palaeoecology, v. 60, p. 189–217.

Lerbekmo, J.F., 2009, Glacioeustatic sea level fall marking the base of supercycle TA-1 at 66.5 Ma recorded by the kaolinization of the Whitemud Formation and the Colgate Member of the Fox Hills Formation: Marine and Petroleum Geology, v. 26, no. 7, p. 1299–1303, doi: 10.1016/j.marpetgeo.2008.08.001.

Li, D., Norell, M.A., Gao, K., Smith, N.D., and Makovicky, P.J., 2010, A longirostrine tyrannosauroid from the Early Cretaceous of China.: Proceedings. Biological sciences / The Royal Society, v. 277, no. 1679, p. 183–190, doi: 10.1098/rspb.2009.0249.

Linkevich, G.D., 2013, Manual and landmark-based morphometric comparison of two populations of Campeloma , sp. across the K-Pg boundary: Senior Capstone Projects - Paper 236 (Bachelor Thesis),.

Lipkin, C., and Carpenter, K., 2008, Looking again at the forelimb of Tyrannosaurus rex: Tyrannosaurus rex, the Tyrant King, p. 166–189.

Lockley, M., Kuhihara, R., and Mitchell, L., 2008, Why Tyrannosaurus rex had puny arms: an integral morphodynamic solution to a simple puzzle in theropod paleobiology: Tyrannosaurus rex, the Tyrant King, p. 130–164.

Loewen, M.A., Irmis, R.B., Sertich, J.J.W., Currie, P.J., and Sampson, S.D., 2013, Tyrant dinosaur evolution tracks the rise and fall of late Cretaceous oceans: PLoS ONE, v. 8, no. 11, doi: 10.1371/journal.pone.0079420.

Longrich, N.R., Bhullar, B.-A.S., and Gauthier, J.A., 2012, Mass extinction of lizards and snakes at the Cretaceous–Paleogene boundary: Proceedings of the National Academy of Sciences, v. 109, no. 52, p. 21396–21401.

Longrich, N.R., Horner, J.R., Erickson, G.M., and Currie, P.J., 2010, Cannibalism in Tyrannosaurus rex: PLoS ONE, v. 5, no. 10, doi: 10.1371/journal.pone.0013419.

Longrich, N.R., Tokaryk, T., and Field, D.J., 2011, Mass extinction of birds at the Cretaceous-Paleogene (K-Pg) boundary.: Proceedings of the National Academy of Sciences of the United States of America, v. 108, no. 37, p. 15253–7, doi: 10.1073/pnas.1110395108.

Lü, J., Yi, L., Brusatte, S.L., Yang, L., Li, H., and Chen, L., 2014, A new clade of Asian Late Cretaceous long-snouted tyrannosaurids: Nat Commun, v. 5.

Van der Lubbe, J.H.J.L., Tjallingii, R., Prins, M.A., Brummer, G.J.A., Jung, S.J.A., Kroon, D., and Schneider, R.R., 2014, Sedimentation patterns off the Zambezi River over the last 20,000 years: Marine Geology, v. 355, p. 189–201, doi: 10.1016/j.margeo.2014.05.012.

Lund, S.P., Hartman, J.H., and Banerjee, S.K., 2002, Magnetostratigraphy of interfingering upper Cretaceous–Paleocene marine and continental strata of the Williston Basin, North Dakota and Montana: The Hell Creek Formation and the Cretaceous-Tertiary boundary in the northern Great Plains: An integrated continental record of the end of the Cretaceous: Boulder, Colorado, Geological Society of America Special Paper 361, p. 57–74, doi: 10.1130/0-8137-2361-2.57.

Lyman, R.L., 1994, Vertebrate taphonomy: Cambridge University Press.

Lyson, T.R., and Longrich, N.R., 2011, Spatial niche partitioning in dinosaurs from the latest cretaceous (Maastrichtian) of North America.: Proceedings of The Royal Society B Biological Sciences, v. 278, no. 1709, p. 1158–1164, doi: 10.1098/rspb.2010.1444.

Maarse, H., and Terwindt, J.H.J., 1964, A new method of making lacquer peel sections: Marine Geology, v. 1, p. 98–105, doi: 10.1163/187529271X00756.

Manning, P.L., 2008, T. rex speed trap: Tyrannosaurus rex: The Tyrant King, p. 205–231.

Manning, P.L., Ott, C., and Falkingham, P.L., 2008, A Probable Tyrannosaurid Track from the Hell Creek Formation (Upper Cretaceous), Montana, United States: Palaios, v. 23, no. 10, p. 645–647, doi: 10.2110/palo.2008.p08-030r.

McCrea, R.T., Buckley, L.G., Farlow, J.O., Lockley, M.G., Currie, P.J., Matthews, N.A., and Pemberton, S.G., 2014, A "terror of tyrannosaurs": The first trackways of tyrannosaurids and evidence of gregariousness and pathology in tyrannosauridae: PLoS ONE, v. 9, no. 7, doi: 10.1371/journal.pone.0103613.

McGookey, D.P., Haun, J.D., Hale, L.A., Goodell, H.G., McCubbin, D.G., Weimer, R., and Wulf, G.R., 1972, Cretaceous system: Geologic Atlas of the Rocky Mountain Region: Rocky Mountain Association of Geologists, p. 190–228.

McIver, E.E., 2002, The paleoenvironment of Tyrannosaurus rex from southwestern Saskatchewan, Canada: Canadian Journal of Earth Sciences, v. 39, p. 207–221, doi: 10.1139/E01-073.

Moore, W.L., 1976, The stratigraphy and environments of deposition of the Cretaceous Hell Creek Formation (reconnaissance) and the Paleocene Ludlow Formation (detailed), southwestern North Dakota: North Dakota Geological Survey Report of Investigations, v. 56, p. 40.

Moore, J.R., Wilson, G.P., Sharma, M., Hallock, H.R., Braman, D.R., and Renne, P.R., 2014, Assessing the relationships of the Hell Creek-Fort Union contact, Cretaceous-Paleogene boundary, and Chicxulub impact ejecta horizon at the Hell Creek Formation lectostratotype, Montana, USA: in Wilson, G.P., Clemens, W.A., Horner, J.R., and Hartman, J.H., eds., Through the End of the Cretaceous in the Type Locality of the Hell Creek Formation in Montana and Adjacent Areas: Geological Society of America Special Paper 503, p. 123–135, doi: 10.1130/2014.2503(03).

Murphy, E.C., Hoganson, J.W., and Johnson, K.R., 2002, Lithostratigraphy of the Hell Creek Formation in North Dakota: The Hell Creek Formation and the Cretaceous-Tertiary boundary in the northern Great Plains: An integrated continental record of the end of the Cretaceous: Boulder, Colorado, Geological Society of America Special Paper 361, p. 9–34.

Nichols, D.J., 2002, Palynology and palynostratigraphy of the Hell Creek Formation in North Dakota: A microfossil record of plants at the end of Cretaceous time: The Hell Creek Formation and the Cretaceous-Tertiary boundary in the northern Great Plains: An integrated continental record of the end of the Cretaceous: Boulder, Colorado, Geological Society of America Special Paper 361, p. 393–456, doi: 10.1130/0-8137-2361-2.393.

Nichols, D.J., and Johnson, K.R., 2008, Plants and the KT Boundary: Cambridge University Press.

Ogg, J.G., 2012, Geomagnetic Polarity Time Scale: Felix M. Gradstein, James G. Ogg, Mark Schmitz and Gabi

Ogg.
Osborn, H.F., 1905, Tyrannosaurus and other Cretaceous carnivorous dinosaurs: Bulletin of the American Museum of Natural History, v. 21, p. 259–265.
Osborn, H.F., 1906, Tyrannosaurus, Upper Cretaceous carnivorous dinosaur (second communication): Bulletin of the American Museum of Natural History, v. 22, p. 281–296.
Paillard, D., 1996, AnalySeries 1.0: a Macintosh software for the analysis of geophysical time-series.:.
Paillard, D., 1998, The timing of Pleistocene glaciations from a simple multiple-state climatemodel: Nature, v. 391, p. 916–918, doi: 10.1038/34891.
Paterson, G.A., and Heslop, D., 2015, New methods for unmixing sediment grain size data: Geochemistry, Geophysics, Geosystems, v. 16, no. 12, p. 4494–4506, doi: 10.1002/2015GC006070.
Pearson, D.A., Schaefer, T., Johnson, K.R., Nichols, D.J., and Hunter, J.P., 2002, Vertebrate biostratigraphy of the Hell Creek Formation in southwestern North Dakota and northwestern South Dakota: The Hell Creek Formation and the Cretaceous-Tertiary boundary in the northern Great Plains: An integrated continental record of the end of the Cretaceous: Boulder, Colorado, Geological Society of America Special Paper 361, p. 145–167, doi: 10.1130/0-8137-2361-2.145.
Persons IV, W.S., and Currie, P.J., 2016, An approach to scoring cursorial limb proportions in carnivorous dinosaurs and an attempt to account for allometry: Scientific reports, v. 6, p. 19828, doi: 10.1038/srep19828.
Peterson, J.A., and MacCary, L.M., 1987, Regional Stratigraphy and General Petroleum Geology of the U . S . Portion of the Williston Basin and Adjacent Areas: Rocky Mountain Association of Geologists Symposium: Williston Basin: Anatomy of a Cratonic Oil Province, p. 9–43.
Pevzner, P.A., Kim, S., and Ng, J., 2008, Response to comment on “protein sequences from mastodon and Tyrannosaurus rex revealed by mass spectrometry”: Science, v. 319, no. 5859, doi: DOI 10.1126/science.1147364.
van der Plicht, J., van der Wijk, A., and Bartstra, G.J., 1989, Uranium and thorium in fossil bones: activity ratios and dating: Applied Geochemistry, v. 4, no. 3, p. 339–342, doi: 10.1016/0883-2927(89)90039-5.
Pollastro, R.M., Roberts, L.N.R., and Cook, T.A., 2010, Geologic assessment of technically recoverable oil in the Devonian and Mississippian Bakken Formation: Assessment of Undiscovered Oil and Gas Resources of the Williston Basin Province of North Dakota, Montana, and South Dakota, 2010, p. Chapter 5/7, doi: 10.1306/M971332.
Pope, K.O., Baines, K.H., Ocampo, A.C., and Ivanov, B.A., 1997, Energy, volatile production, and climatic effects of the Chicxulub Cretaceous/Tertiary impact: Journal of Geophysical Research-Planets, v. 102, no. E9, p. 21645–21664, doi: 10.1029/97je01743.
Pringle, H., 2014, Selling America ’ s Fossil Record: Science, v. 343, no. January, p. 364–367.
Prins, M.A., Bouwer, L.M., Beets, C.J., Troelstra, S.R., Weltje, G.J., Kruk, R.W., Kuijpers, A., and Vroon, P.Z., 2002, Ocean circulation and iceberg discharge in the glacial North Atlantic: Inferences from unmixing of sediment size distributions: Geology, v. 30, no. 6, p. 555–558, doi: 10.1130/0091-7613(2002)030<0555:OCAIDI>2.0.CO;2.
Prins, M.A., and Vriend, M., 2007, Glacial and interglacial eolian dust dispersal patterns across the Chinese Loess Plateau inferred from decomposed loess grain-size records: Geochemistry, Geophysics, Geosystems, v. 8, no. 7, p. 1–17, doi: 10.1029/2006GC001563.
Prins, M.A., and Weltje, G.J., 1999, End-member modeling of siliciclastic grain-size distributions: the late Quaternary record of eolian and fluvial sediment supply to the Arabian Sea and its paleoclimatic significance: SEPM Special Publication, v. 63, p. 91–111, doi: -.
Rayfield, E.J., 2004, Cranial mechanics and feeding in Tyrannosaurus rex.: Proceedings. Biological sciences / The Royal Society, v. 271, no. 1547, p. 1451–1459, doi: 10.1098/rspb.2004.2755.
Renne, P.R., Deino, A.L., Hilgen, F.J., Kuiper, K.F., Mark, D.F., Mitchell, W.S., Morgan, L.E., Mundil, R., and Smit, J., 2013, Time Scales of Critical Events Around the Cretaceous-Paleogene Boundary: Science, v. 339, no. 6120, p. 684–687, doi: 10.1126/science.1230492.
Retallack, G.J., 1994, A pedotype approach to latest Cretaceous and earliest Tertiary paleosols in eastern Montana: Geological Society of America Bulletin, v. 106, no. 11, p. 1377–1397.
Retallack, G.J., 1984, Completeness of the rock and fosil record: some estimates using fossil soils: Paleobiology, v. 10, no. 1, p. 59–78.
Retallack, G.J., 1997, Dinosaurs and dirt: Dinofest international, p. 345–359.
Rigby Jr, J.K., 1987, The last of the North American dinosaurs: In Czerkas, S. J., and Olson, E. C. (eds), Dinosaurs Past and Present, v. 2: Natural History Museum of Los Angeles County and University of Washington Press, p. 119–135.
Rigby, J.K., and Rigby Jr, J.K., 1990, Geology of the Sand Arroyo and Bug Creek Quadrangles, McCone County,

Montana: Brigham Young University Geology Studies, v. 36, p. 69–134.
van Rijn, L.C., 2007a, Unified View of Sediment Transport by Currents and Waves. I: Initiation of Motion, Bed Roughness, and Bed-Load Transport: Journal of Hydraulic Engineering, v. 133, no. 6, p. 649–667, doi: 10.1061/(ASCE)0733-9429(2007)133:7(776).
van Rijn, L.C., 2007b, Unified View of Sediment Transport by Currents and Waves. II: Suspended Transport: Journal of Hydraulic Engineering, v. 133, no. 6, p. 668–689, doi: 10.1061/(ASCE)0733-9429(2007)133:7(776).
Roberts, L.N., Finn, T.M., Lewan, M.D., and Kirschbaum, M.A., 2008, Burial History, Thermal Maturity, and Oil and Gas Generation History of Source Rocks in the Bighorn Basin, Wyoming and Montana: U.S. Geological Survey - Scientific Investigations Report, v. 5037, p. 28.
Robertson, D.S., McKenna, M.C., Toon, O.B., Hope, S., and Lillegraven, J.A., 2004, Survival in the first hours of the Cenozoic: Geological Society of America Bulletin, v. 116, no. 5-6, p. 760–768.
Rogers, R.R., 1990, Taphonomy of Three Dinosaur Bone Beds in the Upper Cretaceous Two Medicine Formation of Northwestern Montana: Evidence for Drought-Related Mortality: Palaios, v. 5, no. 5, p. 394–413, doi: 10.2307/3514834.
Rogers, R.R., and Kidwell, S.M., 2000, Associations of Vertebrate Skeletal Concentrations and Discontinuity Surfaces in Terrestrial and Shallow Marine Records: A Test in the Cretaceous of Montana: The Journal of Geology, v. 108, no. 2, p. 131–154, doi: 10.1086/314399.
Russell, D.A., and Manabe, M., 2002, Synopsis of the Hell Creek (uppermost Cretaceous) dinosaur assemblage: The Hell Creek Formation and the Cretaceous-Tertiary boundary in the northern Great Plains: An integrated continental record of the end of the Cretaceous: Boulder, Colorado, Geological Society of America Special Paper 361, p. 169–176, doi: 10.1130/0-8137-2361-2.169.
Sampson, S.D., and Loewen, M.A., 2005, Tyrannosaurus rex from the Upper Cretaceous (Maastrichtian) North Horn Formation of Utah: biogeographic and paleoecologic implications: Journal of Vertebrate Paleontology, v. 25, no. 2, p. 469–472, doi: 10.1671/0272-4634(2005)025.
Sampson, S.D., Loewen, M.A., Farke, A.A., Roberts, E.M., Forster, C.A., Smith, J.A., and Titus, A.L., 2010, New horned dinosaurs from Utah provide evidence for intracontinental dinosaur endemism: PLoS ONE, v. 5, no. 9, p. 1–12, doi: 10.1371/journal.pone.0012292.
Santisteban, J.I., Mediavilla, R., Lopez-Pamo, E., Dabrio, C.J., Zapata, M.B.R., Garcia, M.J.G., Castano, S., and Martinez-Alfaro, P.E., 2004, Loss on ignition: a qualitative or quantitative method for organic matter and carbonate mineral content in sediments? Journal of Paleolimnology, v. 32, no. 3, p. 287–299, doi: 10.1023/B:JOPL.0000042999.30131.5b.
Scannella, J.B., and Fowler, D.W., 2014, A stratigraphic survey of Triceratops localities in the Hell Creek Formation , northeastern Montana ( 2006 – 2010 ): in Wilson, G.P., Clemens, W.A., Horner, J.R., and Hartman, J.H., eds., Through the End of the Cretaceous in the Type Locality of the Hell Creek Formation in Montana and Adjacent Areas: Geological Society of America Special Paper 503, p. 313–332, doi: 10.1130/2014.2503(12).
Scannella, J.B., and Fowler, D.W., 2009, Anagenesis in Triceratops: evidence from a newly resolved stratigraphic framework for the Hell Creek Formation: North American Paleontological Convention, abstracts volume: 148,.
Scannella, J.B., and Horner, J.R., 2010, *Torosaurus* Marsh, 1891, is *Triceratops* Marsh, 1889 (Ceratopsidae: Chasmosaurinae): synonymy through ontogeny: Journal of Vertebrate Paleontology, v. 30, no. 4, p. 1157–1168, doi: 10.1080/02724634.2010.483632.
Schaeffer, J., 2016, Feeding habits and migratory behaviour of Tyrannosaurus rex Using Stable Calcium and Strontium isotopes: Vrije Universiteit Amsterdam [Unpublished BSc Thesis], p. 32.
Schmerge, J.D., and Rothschild, B.M., 2016, Distribution of the dentary groove of theropod dinosaurs: Implications for theropod phylogeny and the validity of the genus Nanotyrannus Bakker et al., 1988: Cretaceous Research, v. 61, p. 26–33, doi: 10.1016/j.cretres.2015.12.016.
Scholz, H., and Hartman, J.H., 2007, Paleoenvironmental Reconstruction of the Upper Cretaceous Hell Creek Formation of the Williston Basin, Montana, Usa: Implications From the Quantitative Analysis of Unionoid Bivalve Taxonomic Diversity and Morphologic Disparity: Palaios, v. 22, p. 24–34, doi: 10.2110/palo.2005.p05-059r.
Schulp, A.S., Bastiaans, D., Kaskes, P., Manning, P.L., and Larson, P.L., 2015, A new, mature and pathologic specimen of Tyrannosaurus rex: Society for Vertebrate Paleontology Annual Meeting 2015 - Poster Presentation,.
Schulte, P., Alegret, L., Arenillas, I., Arz, J.A., Barton, P.J., Bown, P.R., Bralower, T.J., Christeson, G.L., Claeys, P., Cockell, C.S., Collins, G.S., Deutsch, A., Goldin, T.J., Goto, K., et al., 2010, The Chicxulub Asteroid Impact and Mass Extinction at the Cretaceous-Paleogene Boundary: Science, v. 327, no. 5970, p. 1214–1218.

Schweitzer, M.H., Wittmeyer, J.L., Horner, J.R., and Toporski, J.K., 2005, Soft-Tissue Vessels and Cellular Preservation in Tyrannosaurus rex: Science, v. 307, no. 5717, p. 1952–1955, doi: 10.1126/science.1108397.

Schweitzer, M.H., Zheng, W., Zanno, L., Werning, S., Sugiyama, T., Schweitzer, M.H., Elsey, R.M., Dacke, C.G., Horner, J.R., Lamm, E.-T., Kyes, P., Potter, T.S., Bloom, M.A., Domm, L. V., et al., 2016, Chemistry supports the identification of gender-specific reproductive tissue in Tyrannosaurus rex: Scientific Reports, v. 6, no. November 2015, p. 23099, doi: 10.1038/srep23099.

Sereno, P.C., Tan, L., Brusatte, S.L., Kriegstein, H.J., Zhao, X., and Cloward, K., 2009, Tyrannosaurid skeletal design first evolved at small body size.: Science, v. 326, no. 5951, p. 418–422, doi: 10.1126/science.1177428.

Serrano-Brañas, C.I., Torres-Rodríguez, E., Reyes Luna, P.C., González, I., and González-León, C., 2014, Tyrannosaurid teeth from the Lomas Coloradas Formation, Cabullona Group (Upper Cretaceous) Sonora, México: Cretaceous Research, v. 49, p. 163–171, doi: 10.1016/j.cretres.2014.02.018.

Sheehan, P.M., and Fastovsky, D.E., 1992, Major extinctions of land-dweling vertebrates at the Cretaceous-Tertiary boundary, eastern Montana: Geology, v. 20, no. June, p. 556–560, doi: 10.1130/0091-7613(1992)020<0556.

Sheehan, P.M., Fastovsky, D.E., Hoffmann, R.G., Berghaus, C.B., and Gabriel, D.L., 1991, Sudden extinction of the Dinosaurs: Latest Cretaceous, Upper Great Plains, U.S.A.: Science, v. 254, no. 5033, p. 835–839.

Shurr, G.W., and Monson, L.M., 1995, Tectonic setting and paleotectonic history of Fort Peck Reservation in northeastern Montana: Williston Basin Symposium,.

Sloan, R.E., and Van Valen, L., 1965, Cretaceous mammals from Montana: Science, v. 148, no. 3667, p. 220–227.

Sloss, L.L., 1963, Sequences in the Cratonic Interior of North America: Geological Society Of America Bulletin, v. 74, p. 93–114, doi: 10.1130/0016-7606(1963)74[93:SITCIO]2.0.CO;2.

Smit, J., 1999, The Global Stratigraphy of the Cretaceous-Tertiary Boundary Impact Ejecta: Annual Review of Earth and Planetary Sciences, v. 27, no. 1, p. 75–113, doi: 10.1146/annurev.earth.27.1.75.

Smit, J., and Van der Kaars, W.A., 1984, Terminal Cretaceous Extinctions in the Hell Creek Area, Montana: Compatible with Catastrophic Extinction: Science, v. 223, no. 4641, p. 1177–1179.

Smit, J., Van der Kaars, W.A., and Rigby J. K., J., 1987, Stratigraphic aspects of the Cretaceous-Tertiary boundary in the Bug Creek area of eastern Montana, U.S.A: Mémoires de la Société Géologique de France, New Series, v. 150, p. 53–73.

Smit, J., Hertogen, J., 1980, An extraterrestrial event at the Cretaceous-Tertiary boundary: Nature, v. 285, no. 5762, p. 198–200, doi: 10.1038/285198a0.

Smith, S.D., Persons, W.S., and Xing, L., 2016, A tyrannosaur trackway at Glenrock, Lance Formation (Maastrichtian), Wyoming: Cretaceous Research, v. 61, p. 1–4, doi: 10.1016/j.cretres.2015.12.020.

Soil Survey Division Staff (1993), 1993, Soil Survey Manual, vol. 18. Soil Conservation Service: U.S. Department of Agriculture, USA.,.

Soller, D.R., 2001, Map showing the thickness and character of Quaternary sediments in the glaciated United States east of the Rocky Mountains: US Geological Survey,.

Soulsby, R., 1997, Dynamics of marine sands: Thomas Telford, UK.

Sprain, C.J., Feinberg, J.M., Renne, P.R., and Jackson, M., 2016, Importance of titanohematite in detrital remanent magnetizations of strata spanning the Cretaceous-Paleogene boundary, Hell Creek region, Montana: Geochemistry, Geophysics, Geosystems, v. 17, no. 3, p. 660–678, doi: 10.1002/2015GC006191.

Sprain, C.J., Renne, P.R., Wilson, G.P., and Clemens, W.A., 2015, High-resolution chronostratigraphy of the terrestrial Cretaceous-Paleogene transition and recovery interval in the Hell Creek region, Montana: Geological Society of America Bulletin, v. 127, no. 3-4, p. 393–409, doi: 10.1130/B31076.1.

Stanley, E.A., 1965, Upper Cretaceous and Paleocene plant microfossils and Paleocene dinoflagellates and hystrichosphaerids from northwestern South Dakota: Bulletins of American Paleontology, v. 49, no. 222, p. 177–384.

Stevens, K.A., 2006, Binocular vision in theropod dinosaurs: Journal of Vertebrate Paleontology, v. 26, no. 2, p. 321–330, doi: 10.1671/0272-4634(2006)26.

Sweet, A.R., and Braman, D.R., 1992, The K-T boundary and contiguous strata in western Canada: interactions between paleoenvironments and palynological assemblages: Cretaceous Research, v. 13, no. 1, p. 31–79, doi: 10.1016/0195-6671(92)90027-N.

Swisher, C.C., Dingus, L., and Butler, R.F., 1993, 40Ar/39Ar dating and magnetostratigraphic correlation of the terrestrial Cretaceous-Paleogene boundary and Puercan Mammal Age, Hell Creek-Tullock formations, eastern Montana: Canadian Journal of Earth Sciences, v. 30, no. 9, p. 1981–1996.

Switek, B., 2013, The truth about T. rex: Nature, v. 502, no. 7472, p. 424–426, doi: 10.1038/502424a.

Tauxe, L., Butler, R.F., Van der Voo, R., and Banerjee, S.K., 2010, Essentials of Paleomagnetism: University of California Press.

Therrien, F., Eberth, D.A., Braman, D.R., and Zelenitsky, D.K., 2007, High-resolution organic carbon isotope record across the Cretaceous-Tertiary boundary in south-central Alberta: Implications for the post-impact recovery rate of terrestrial ecosystems and use of δ13C as a boundary marker: Canadian Journal of Earth Sciences, v. 44, no. 4, p. 529–542.

Thibault, N., Husson, D., Harlou, R., Gardin, S., Galbrun, B., Huret, E., and Minoletti, F., 2012, Astronomical calibration of upper Campanian-Maastrichtian carbon isotope events and calcareous plankton biostratigraphy in the Indian Ocean (ODP Hole 762C): Implication for the age of the Campanian-Maastrichtian boundary: Palaeogeography, Palaeoclimatology, Palaeoecology, v. 337-338, p. 52–71, doi: 10.1016/j.palaeo.2012.03.027.

Toonen, W.H.J., 2013, A Holocene flood record of the Lower Rhine: Utrecht University - [Unpublished Ph.D Thesis],.

Toonen, W.H.J., Kleinhans, M.G., and Cohen, K.M., 2012, Sedimentary architecture of abandoned channel fills: Earth Surface Processes and Landforms, v. 37, no. 4, p. 459–472, doi: 10.1002/esp.3189.

Toonen, W.H.J., Winkels, T.G., Cohen, K.M., Prins, M.A., and Middelkoop, H., 2015, Lower Rhine historical flood magnitudes of the last 450 years reproduced from grain-size measurements of flood deposits using End Member Modelling: Catena, v. 130, no. June, p. 69–81, doi: 10.1016/j.catena.2014.12.004.

Tryon, R.M., and Tryon, A.F., 1982, Ferns and Allied Plants: New York, Springer-Verlag.

Tschudy, B.D., and Leopold, E.B., 1970, Aquilapollenites ( Rouse ) Funkhouser — Selected Rocky Mountain Taxa and Their Stratigraphic Ranges: Geological Society of America Special Papers 127, p. 113–168.

Tschudy, R.H., Pillmore, C.L., Orth, C.J., Gilmore, J.S., and Knight, J.D., 1984, Disruption of the terrestrial plant ecosystem at the Cretaceous-Tertiary boundary, Western Interior: Science, v. 225, no. 4666, p. 1030–1032.

Vail, P.R., Mitchum Jr, R.M., and Thompson III, S., 1977, Seismic Stratigraphy and Global Changes of Sea Level: Part 4. Global Cycles of Relative Changes of Sea Level: Section 2. Application of Seismic Reflection Configuration to Stratigraphic Interpretation: AAPG Special Volumes,.

Vajda, V., and Bercovici, A., 2014, The global vegetation pattern across the Cretaceous-Paleogene mass extinction interval: A template for other extinction events: Global and Planetary Change, v. 122, p. 29–49, doi: 10.1016/j.gloplacha.2014.07.014.

Vajda, V., Lyson, T.R., Bercovici, A., Doman, J.H., and Pearson, D.A., 2013, A snapshot into the terrestrial ecosystem of an exceptionally well-preserved dinosaur (Hadrosauridae) from the Upper Cretaceous of North Dakota, USA: Cretaceous Research, v. 46, p. 114–122, doi: 10.1016/j.cretres.2013.08.010.

Vajda, V., Raine, J.I., and Hollis, C.J., 2001, Indication of global deforestation at the Cretaceous-Tertiary boundary by New Zealand fern spike.: Science (New York, N.Y.), v. 294, no. 5547, p. 1700–2, doi: 10.1126/science.1064706.

Valverde, J.M., Perejon, A., Medina, S., and Perez-Maqueda, L.A., 2015, Thermal decomposition of dolomite under CO2: insights from TGA and in situ XRD analysis: Physical chemistry chemical physics: PCCP, v. 17, no. 44, p. 30162–76, doi: 10.1039/c5cp05596b.

Vellekoop, J., Sluijs, A., Smit, J., Schouten, S., Weijers, J.W.H., Sinninghe Damsté, J.S., and Brinkhuis, H., 2014, Rapid short-term cooling following the Chicxulub impact at the Cretaceous-Paleogene boundary.: Proceedings of the National Academy of Sciences of the United States of America, v. 111, no. 21, p. 1–5, doi: 10.1073/pnas.1319253111.

Versteegh, E.A.A., Vonhof, H.B., Troelstra, S.R., Kaandorp, R.J.G., and Kroon, D., 2010, Seasonally resolved growth of freshwater bivalves determined by oxygen and carbon isotope shell chemistry: Geochemistry, Geophysics, Geosystems, v. 11, no. 8, doi: 10.1029/2009GC002961.

Visher, G.S., 1969, Grain size distributons and depositional processes: Journal of Sedimentary Petrology, v. 39, no. 3, p. 1074–1106.

Voigt, E., 1949, Die Anwendung der Lackfilm-Methode bei der Bergung geologischer und bodenkundlicher Profile: Mitt. Geol. Staatsinst. Hamburg, v. 19, p. 111–129.

Vuke, S.M., and Wilde, E.M., 2004, Geologic map of the Melstone 30’ x 60’ quadrangle, eastern montana: Montana Bureau of Mines and Geology - Open File Report,.

Weishampel, D.B., Dodson, P., and Osmólska, H., 2004, The dinosauria: University of California Press.

Weltje, G.J., 1997, End-member modeling of compositional data: Numerical-statistical algorithms for solving the explicit mixing problem: Mathematical Geology, v. 29, no. 4, p. 503–549, doi: 10.1007/BF02775085.

Weltje, G.J., and Prins, M.A., 2007, Genetically meaningful decomposition of grain-size distributions: Sedimentary Geology, v. 202, no. 3, p. 409–424, doi: 10.1016/j.sedgeo.2007.03.007.

Weltje, G.J., and Prins, M.A., 2003, Muddled or mixed? Inferring palaeoclimate from size distributions of

deep-sea clastics: Sedimentary Geology, v. 162, no. 1-2, p. 39–62, doi: 10.1016/S0037-0738(03)00235-5.
Westerhoff, W.E., 2008, The Rhine - A major fluvial record: Netherlands Journal of Geosciences - Geologie en Mijnbouw,.
White, P.D., Fastovsky, D.E., and Sheehan, P.M., 1998, Taphonomy and suggested structure of the dinosaurian assemblage of the Hell Creek Formation (Maastrichtian), eastern Montana and western North Dakota: Palaios, v. 13, no. 1, p. 41–51.
Wick, S.L., 2014, New evidence for the possible occurrence of Tyrannosaurus in West Texas, and discussion of Maastrichtian tyrannosaurid dinosaurs from Big Bend National Park: Cretaceous Research, v. 50, p. 52–58, doi: 10.1016/j.cretres.2014.03.010.
Wiersma, J.P., 2013, Taphonomy of a subadult Teratophoneus curriei (Tyrannosauridae) from the Upper Campanian Kaiparowits Formation of Utah: Vrije Universiteit Amsterdam [Unpublished BSc Thesis], p. 80.
Wilf, P., Johnson, K.R., and Huber, B.T., 2003, Correlated terrestrial and marine evidence for global climate changes before mass extinction at the Cretaceous-Paleogene boundary: Proceedings of the National Academy of Sciences of the United States of America, v. 100, no. 2, p. 599–604, doi: 10.1073/pnas.0234701100.
Wilson, G.P., 2014, Extinction and survival of salamander and salamander-like amphibians across the Cretaceous-Paleogene boundary in northeastern Montana, USA: in Wilson, G.P., Clemens, W.A., Horner, J.R., and Hartman, J.H., eds., Through the End of the Cretaceous in the Type Locality of the Hell Creek Formation in Montana and Adjacent Areas: Geological Society of America Special Paper 503, p. 271–297, doi: 10.1130/2014.2503(15).
Wilson, G.P., Clemens, W.A., Horner, J.R., and Hartman, J.H., 2014, Through the end of the Cretaceous in the type locality of the Hell Creek Formation in Montana and adjacent areas: Geological Society of America.
Wilson, M.R., and Kyser, T.K., 1988, Geochemistry of porphyry-hosted Au-Ag deposits in the Little Rocky Mountains, Montana: Economic Geology, v. 83, no. 7, p. 1329–1346.
Witmer, L.M., and Ridgely, R.C., 2009, New insights into the brain, braincase, and ear region of tyrannosaurs (Dinosauria, Theropoda), with implications for sensory organization and behavior: Anatomical Record, v. 292, no. 9, p. 1266–1296, doi: 10.1002/ar.20983.
Witmer, L.M., and Ridgely, R.C., 2010, The Cleveland tyrannosaur skull (Nanotyrannus or Tyrannosaurus) - New findings based on CT scanning, with special reference to the braincase: Kirtlandia, v. 57, no. 57, p. 61–81.
Xu, X., Norell, M.A., Kuang, X., Wang, X., Zhao, Q., Jia, C., Zhoa, Q., and Jia, C., 2004, Basal tyrannosauroids from China and evidence for protofeathers in tyrannosauroids: Letters to Nature, v. 431, p. 680–884, doi: 10.1029/2001JD001278.
Xu, X., Wang, K., Zhang, K., Ma, Q., Xing, L., Sullivan, C., Hu, D., Cheng, S., and Wang, S., 2012, A gigantic feathered dinosaur from the Lower Cretaceous of China: Nature, v. 484, no. 7392, p. 92–95, doi: 10.1038/nature10906.
Yu, S.-Y., Colman, S.M., and Li, L., 2015, BEMMA: A Hierarchical Bayesian End-Member Modeling Analysis of Sediment Grain-Size Distributions: Mathematical Geosciences, doi: 10.1007/s11004-015-9611-0.
Zijderveld, J.D.A., 1967, AC demagnetization of rocks: analysis of results: Methods in paleomagnetism, v. 3, p. 254.

# Appendices

**Appendix 1: Maps of the study area of the Naturalis *T. rex*, including:**
- Digital Elevation Model of the entire study area
- Digital Elevation Model of the zoom-in study area
- ArcScene 3D model of the entire study area
- Geological map of the entire study area

**Appendix 2: Photo-overview of all sections and (when sampled) accompanied with sedimentological and geochemical data plotted versus stratigraphic height (see main text for explanations associated with the graphs):**
- Black Hills Institute Pelvis Block #1 (BHI)
- Naturalis (Murray) *T. rex* section (MREX)
- Cyclic Butte (CB)
- Shelly Butte A & B section (SBA & SBB)
- Rex Hills A & B section (RHA & RHB)
- Piney Ridge A & B section (PRA(B))

**Appendix 3: Raw sedimentological, geochemical and Munsell data of all sections**
- Attached Excel file
- Attached Matlab script

**Appendix 4: Raw palynology data**
- Attached Excel file

**Appendix 5: Raw paleomagnetism data**
- Attached Excel file

**Appendix 6: List of all known *Tyrannosaurus rex* specimens**
- Attached Excel file

## Appendix 1: Maps of the study area

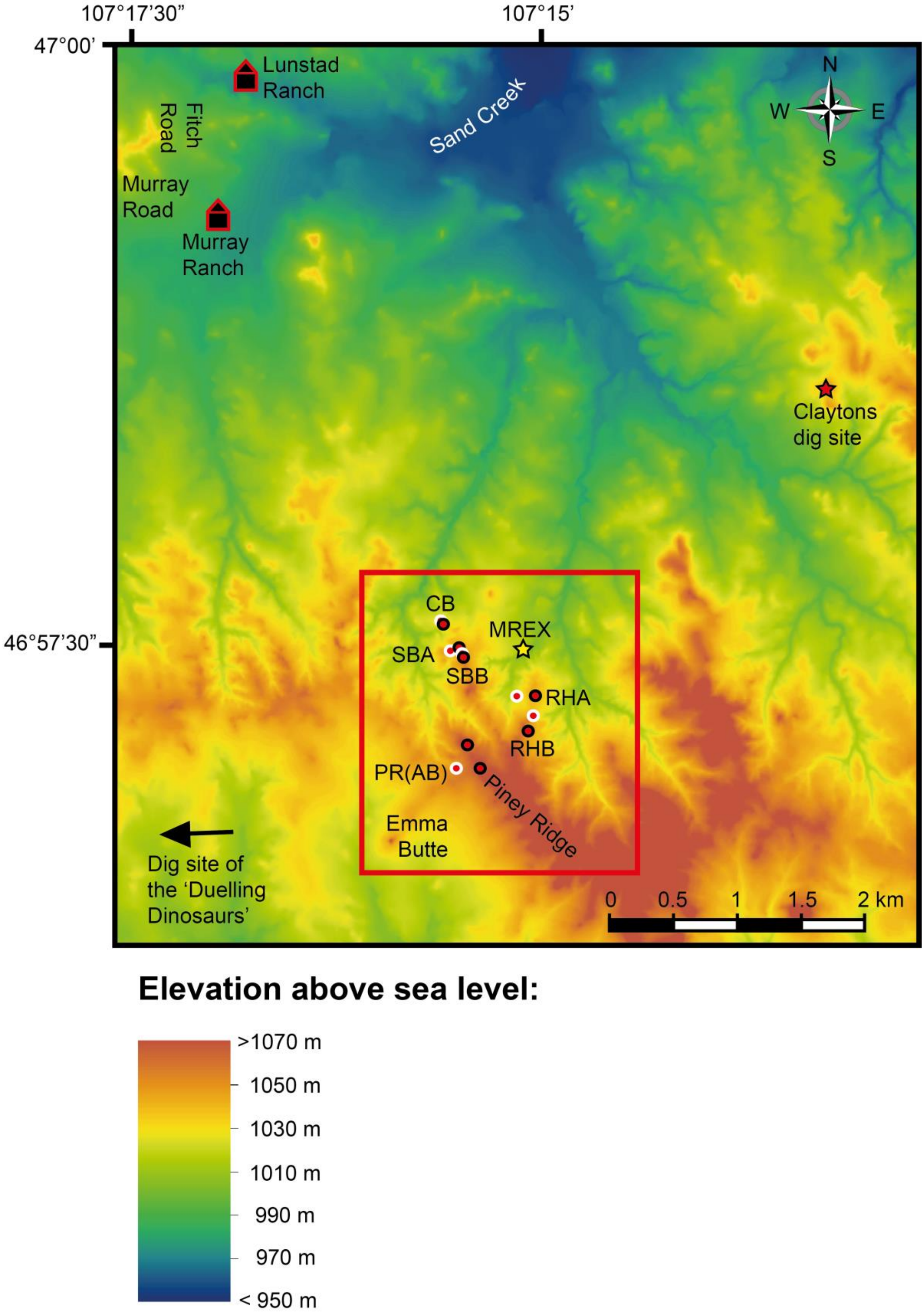


**Fig. A1.1.** Digital elevation model of the entire study area showing high elevations in the southern part and deep incision in the north. The elevation data used for this ArcGIS image is derived from the USGS National Elevation Data (NED, file: n47w108 1/3 arc-second 2013 1 x 1 degree ArcGrid).

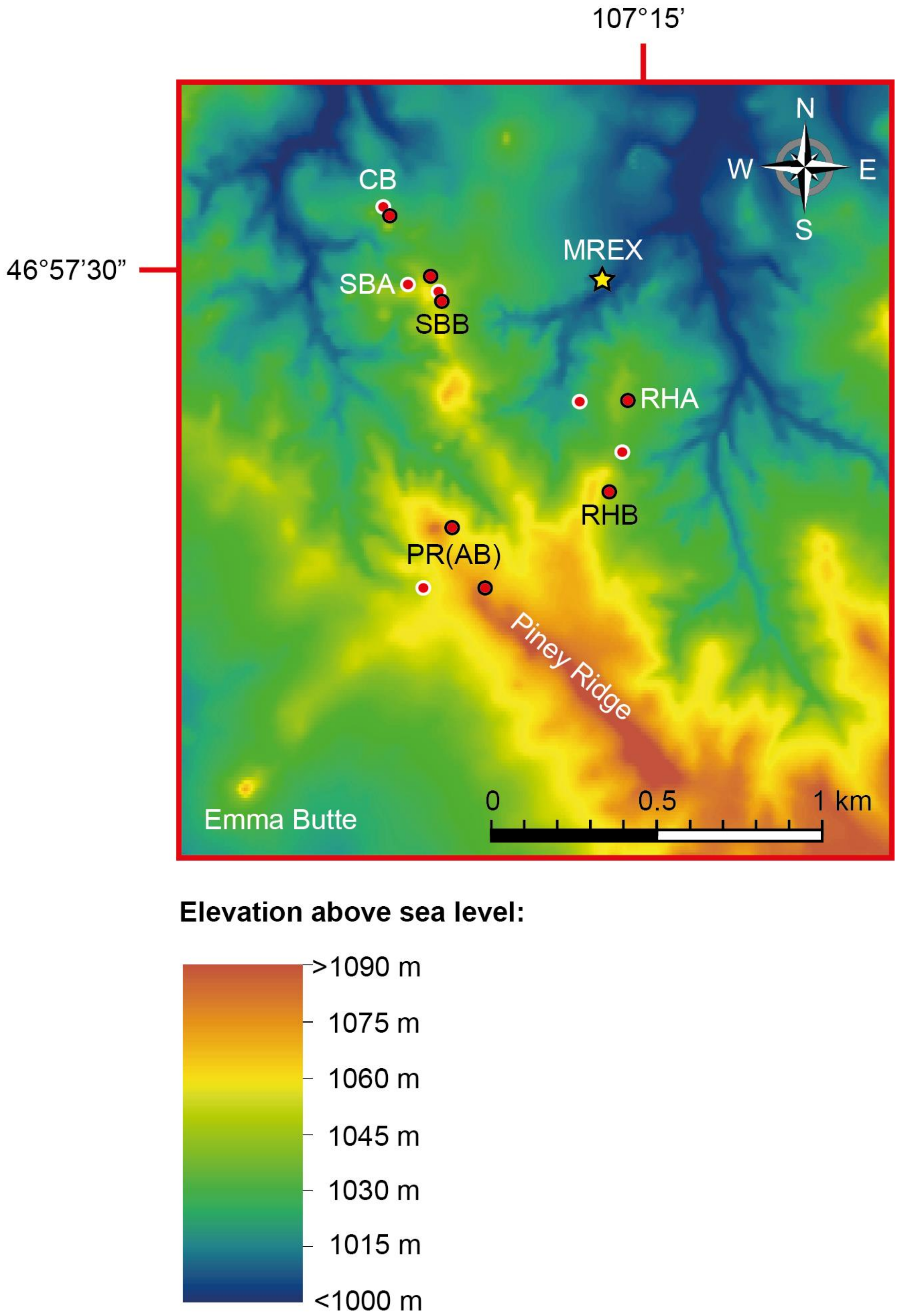


**Fig. A1.2.** Digital elevation model of a zoom-in of the study area showing high elevations in the southern part and two deep incisions in the north. The MREX section is located on the edge of a branch of one of these canyons. The elevation data used for this image is derived from the USGS National Elevation Data (NED, file: n47w108 1/3 arc-second 2013 1 x 1 degree ArcGrid).

**Fig. A1.3.** 3D Digital Elevation Model of the entire study area with an aerial photograph as overlay, produced in ArcScene. This model is possible to print in a 3D printer to use e.g. as a maquette in a museum exhibition.

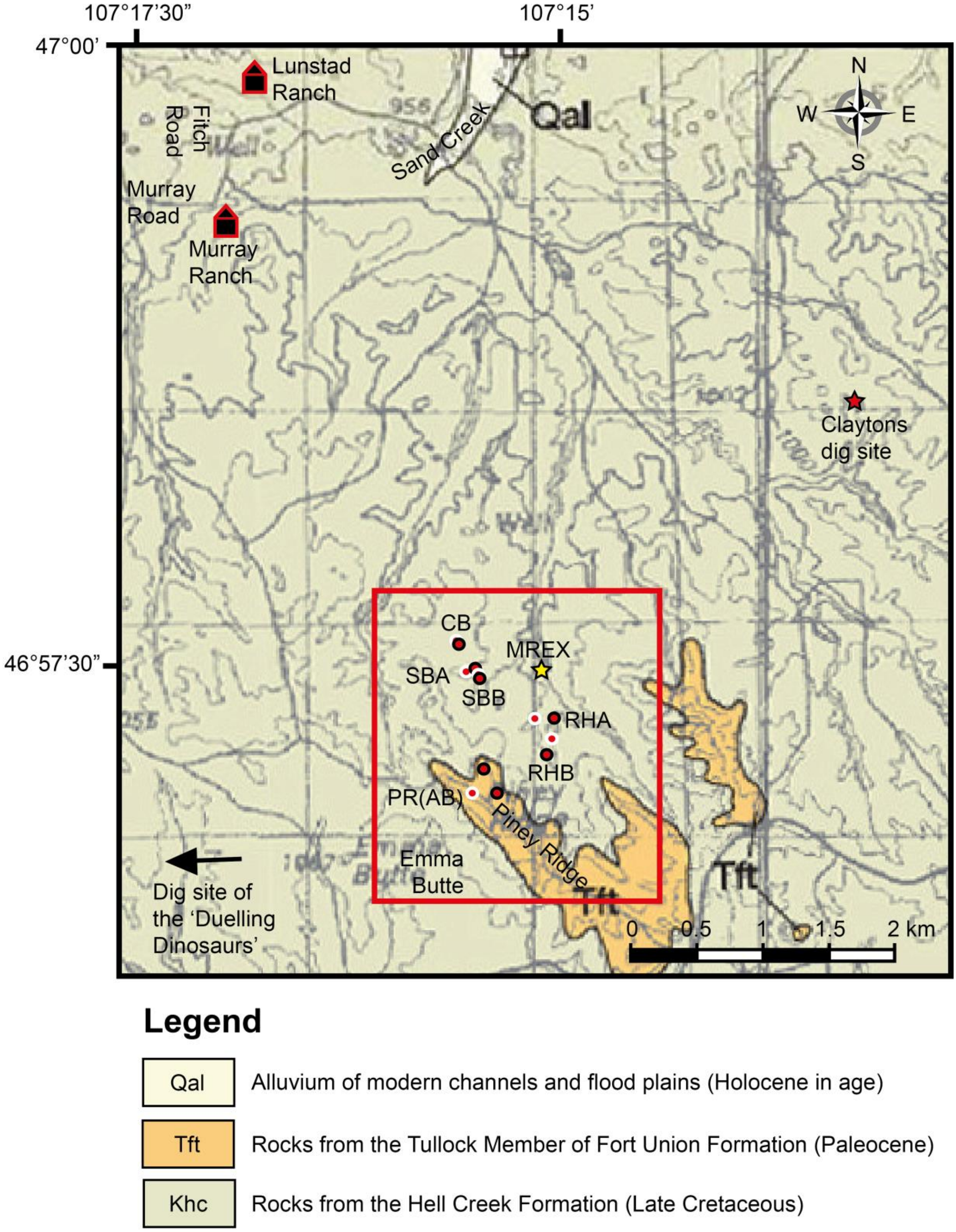


**Fig. A.1.4.** Simplified geological map of the study area using a cropped version of the map from Vuke & Wilde (2004) of the Melstone 30' x 60' Quadrangle Eastern Montana (Montana Bureau of Mines and Geology Open File 513). In most of the area sedimentary rock from the Upper Cretaceous Hell Creek Formation is exposed, but it is interpreted by Vuke & Wilde (2004) that outcrops from the Paleocene Fort Union Formation are present in the high elevation area in the south, such as Piney Ridge. The Sand Creek area in the north is interpreted as alluvium from a Holocene river channel.

# Appendix 2: Photo-overviews and graphs

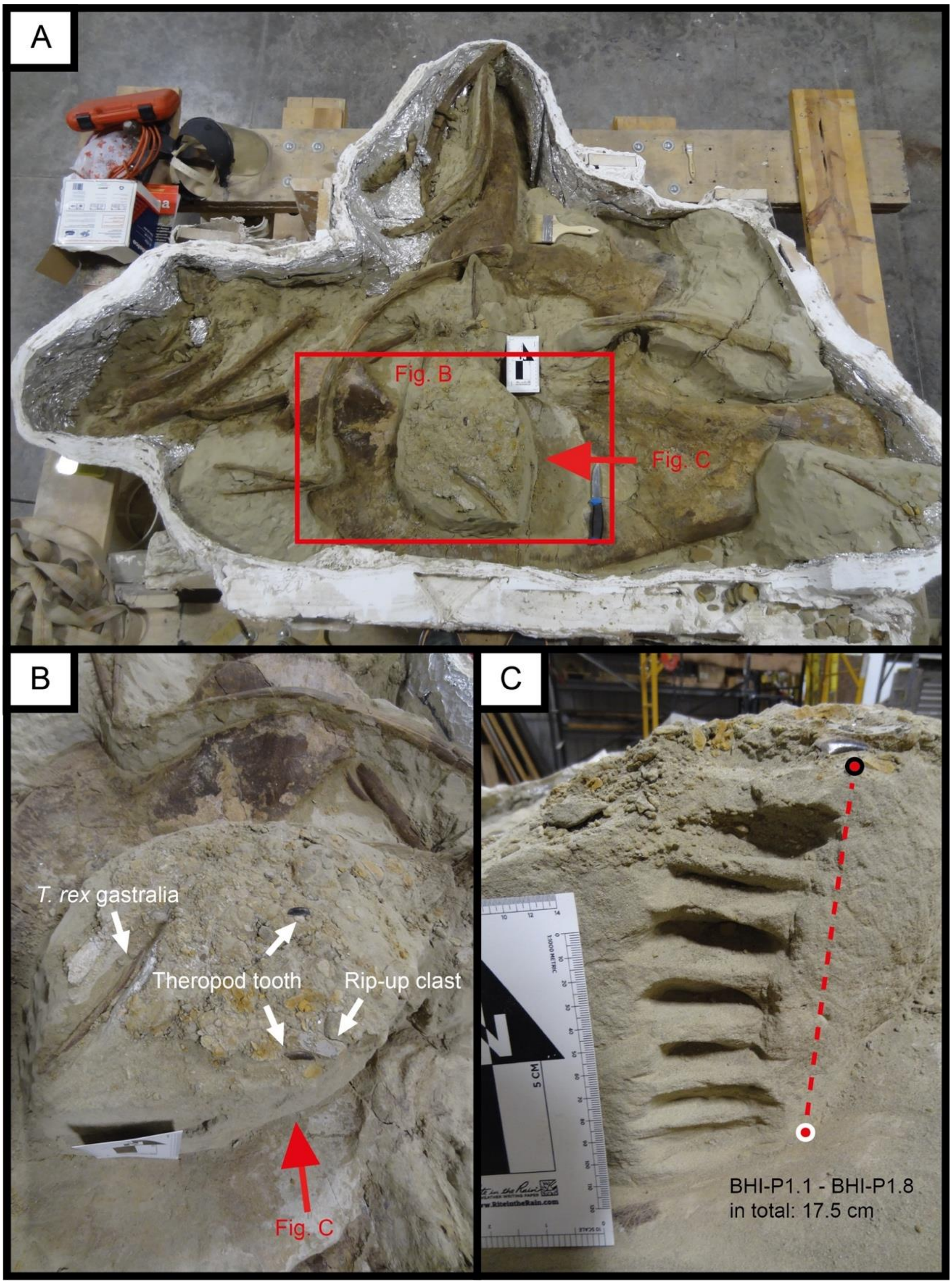


**Fig. A2.1.** Overview of the pelvis block of the Naturalis *T. rex*, as stored in the Black Hills Institute in September 2014. The sample location of BHI-P1.1.-P1.8 is indicated in C.

**Fig. A2.2**

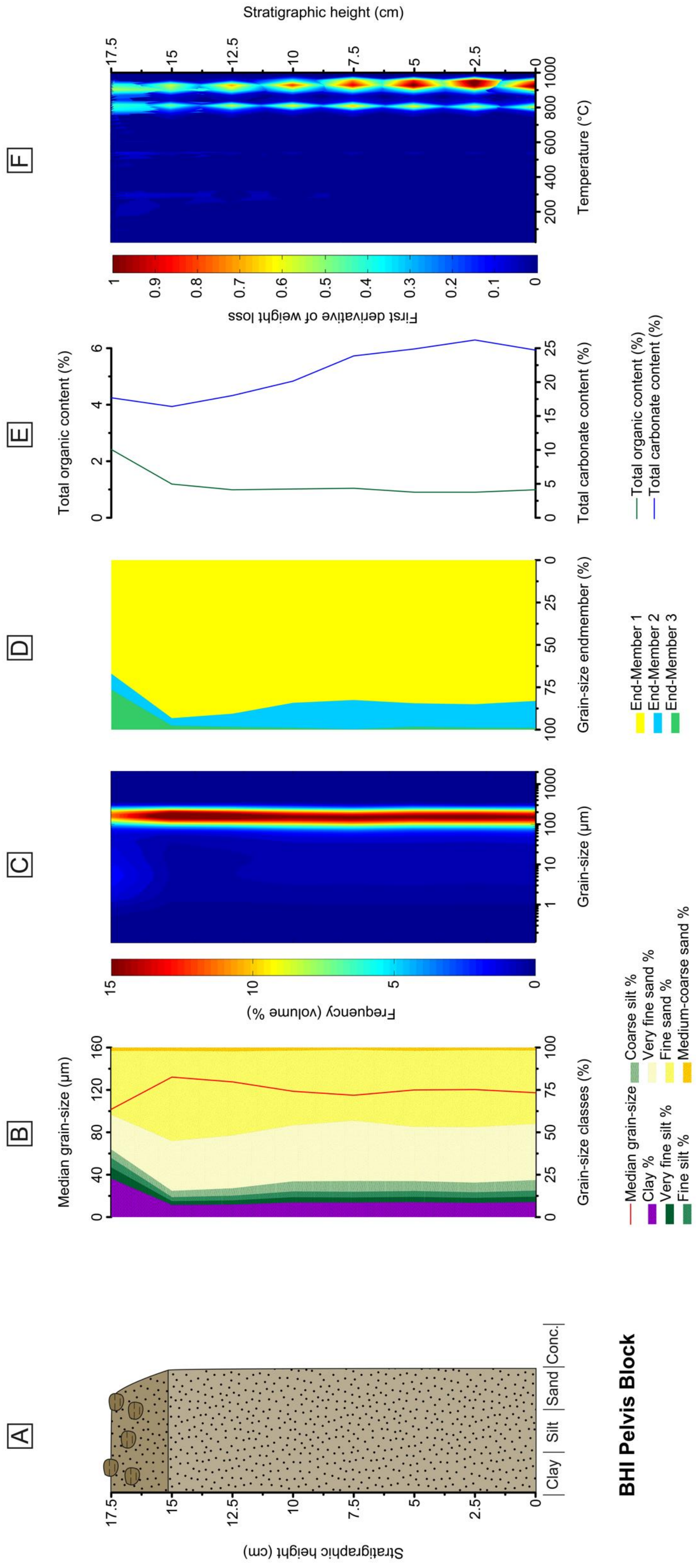

A
B
C
D
E
F
BHI Pelvis Block
Stratigraphic height (cm)
Clay
Silt
Sand
Conc.
Median grain-size (µm)
Grain-size classes (%)
Median grain-size
Clay %
Very fine silt %
Fine silt %
Coarse silt %
Very fine sand %
Fine sand %
Medium-coarse sand %
Frequency (volume %)
Grain-size (µm)
Grain-size endmember (%)
End-Member 1
End-Member 2
End-Member 3
Total organic content (%)
Total carbonate content (%)
First derivative of weight loss
Temperature (°C)

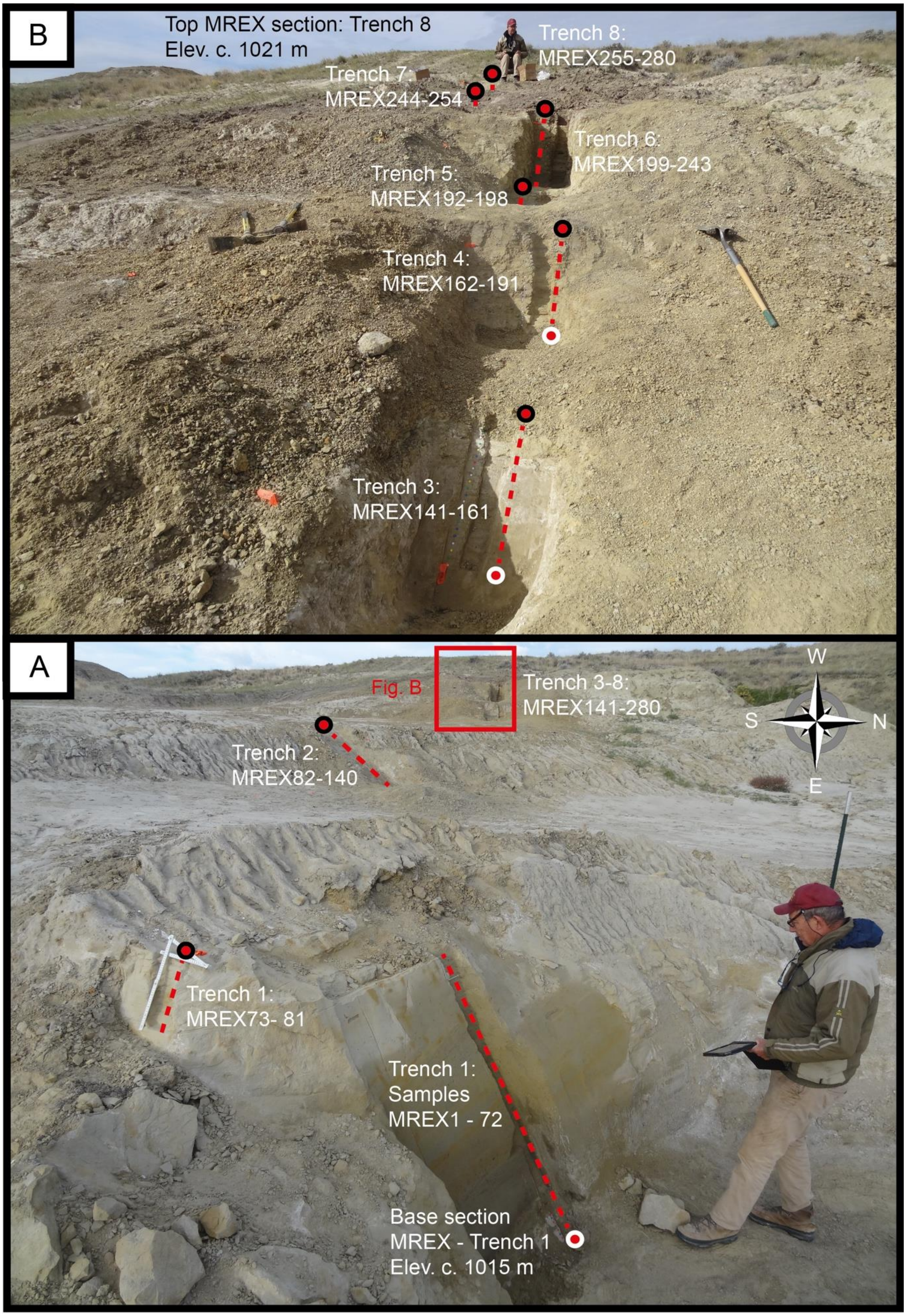


**Fig. A2.3.** Overview of the Naturalis *T. rex* section (MREX) indicating the stratigraphic position of the trenches and sample numbers. The basal part with the lacquer peel surface is shown in A and the upper part of the section is displayed in B. Jan Smit (c. 2 m) for scale.

**Fig. A2.4**

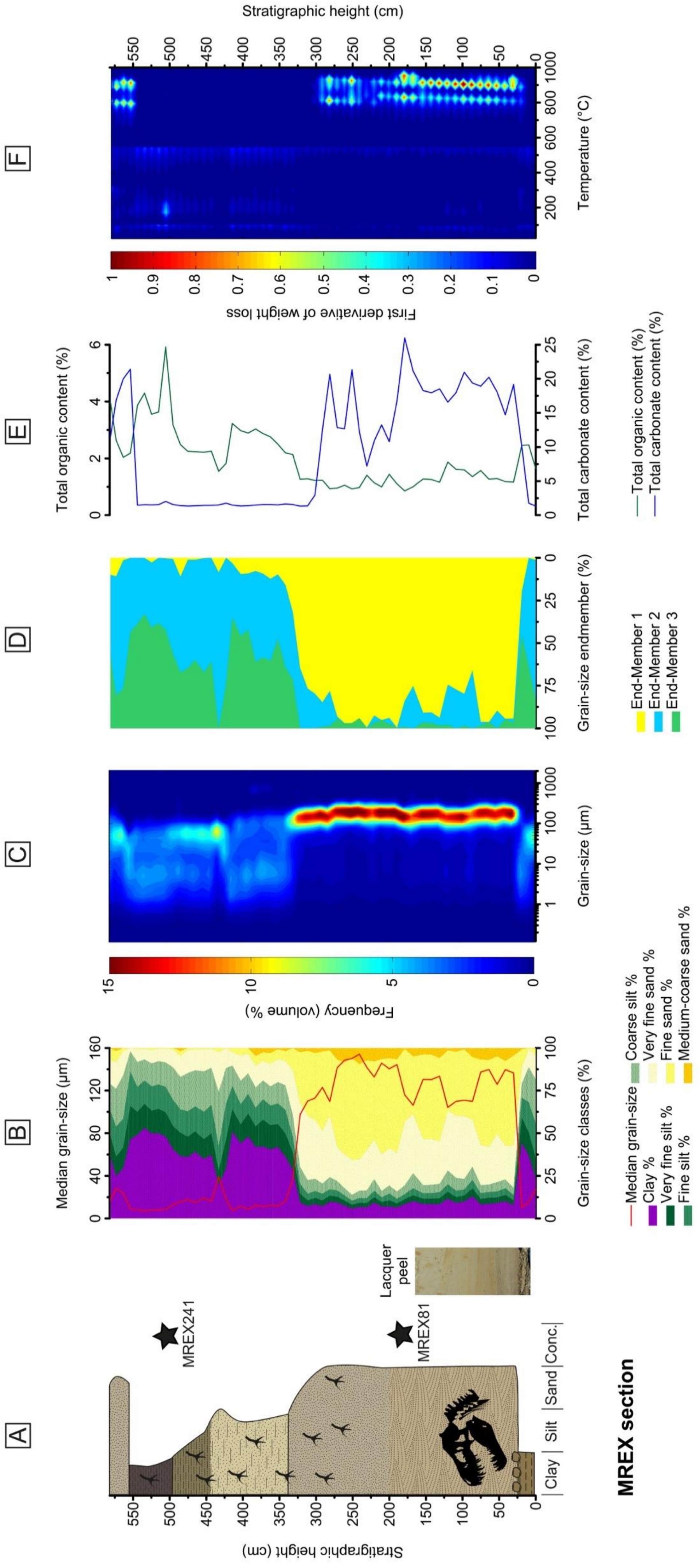

A
B
C
D
E
F
MREX section
Stratigraphic height (cm)
MREX241
MREX81
Lacquer peel
Clay
Silt
Sand
Conc.
Median grain-size (µm)
Grain-size classes (%)
Median grain-size
Clay %
Very fine silt %
Fine silt %
Coarse silt %
Very fine sand %
Fine sand %
Medium-coarse sand %
Frequency (volume %)
Grain-size (µm)
Grain-size endmember (%)
End-Member 1
End-Member 2
End-Member 3
Total organic content (%)
Total carbonate content (%)
First derivative of weight loss
Temperature (°C)

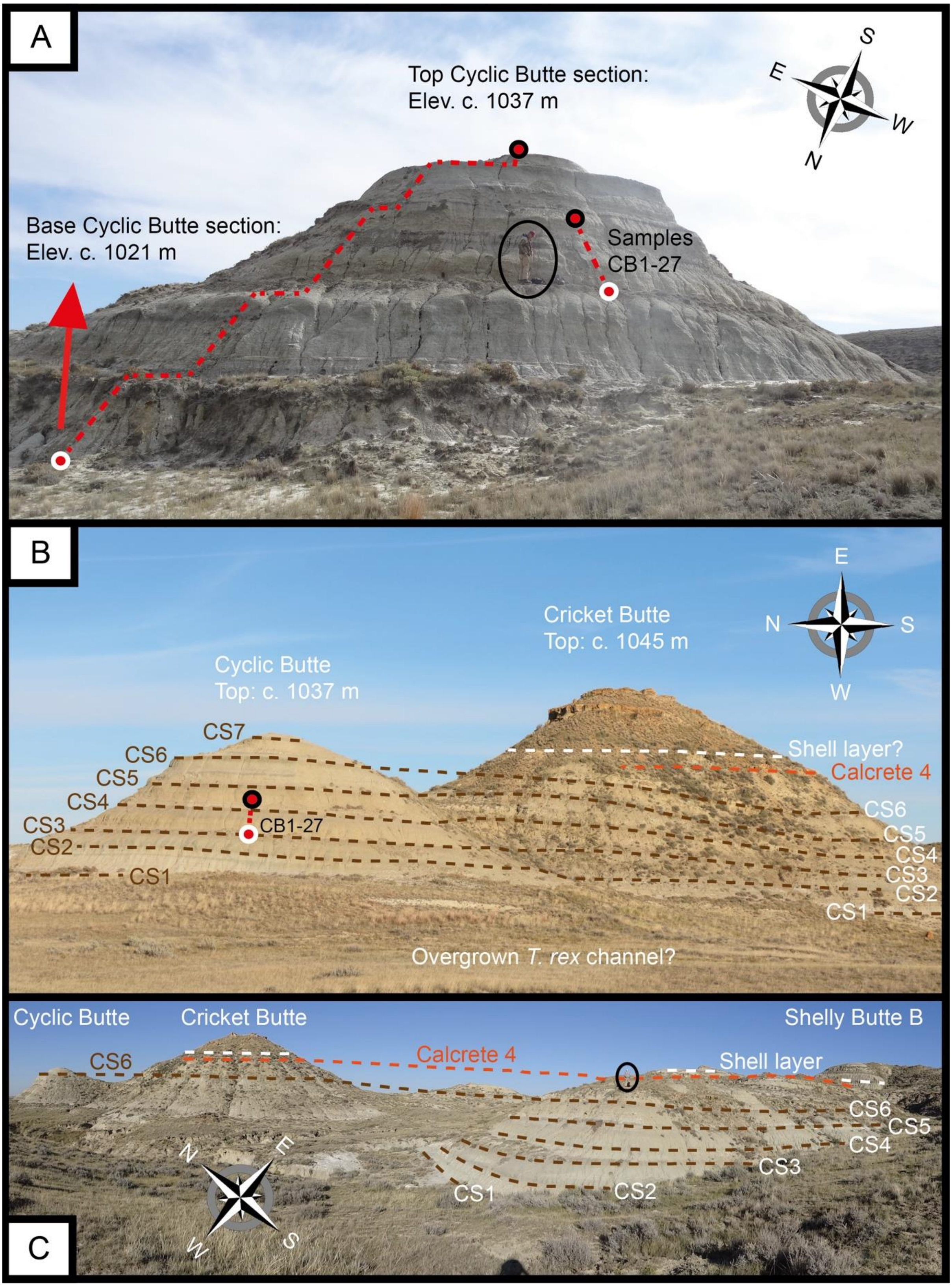


**Fig A2.5.** Photo overviews of Cyclic Butte indicating the entire stratigraphic log and position of samples CB1-27 (at a stratigraphic height of 13.9 – 16.5 m) **(A)** and the field correlations with the neighboring Cricket Butte **(B)** and Shelly Butte **(C)**. As correlation horizons, several carbonaceous shales (CS), a prominent calcrete level (Calcrete 4) and a shell layer (beautifully exposed in Shelly Butte B) were used. Jan Smit (c. 2 m) for scale.

**Fig. A2.6**

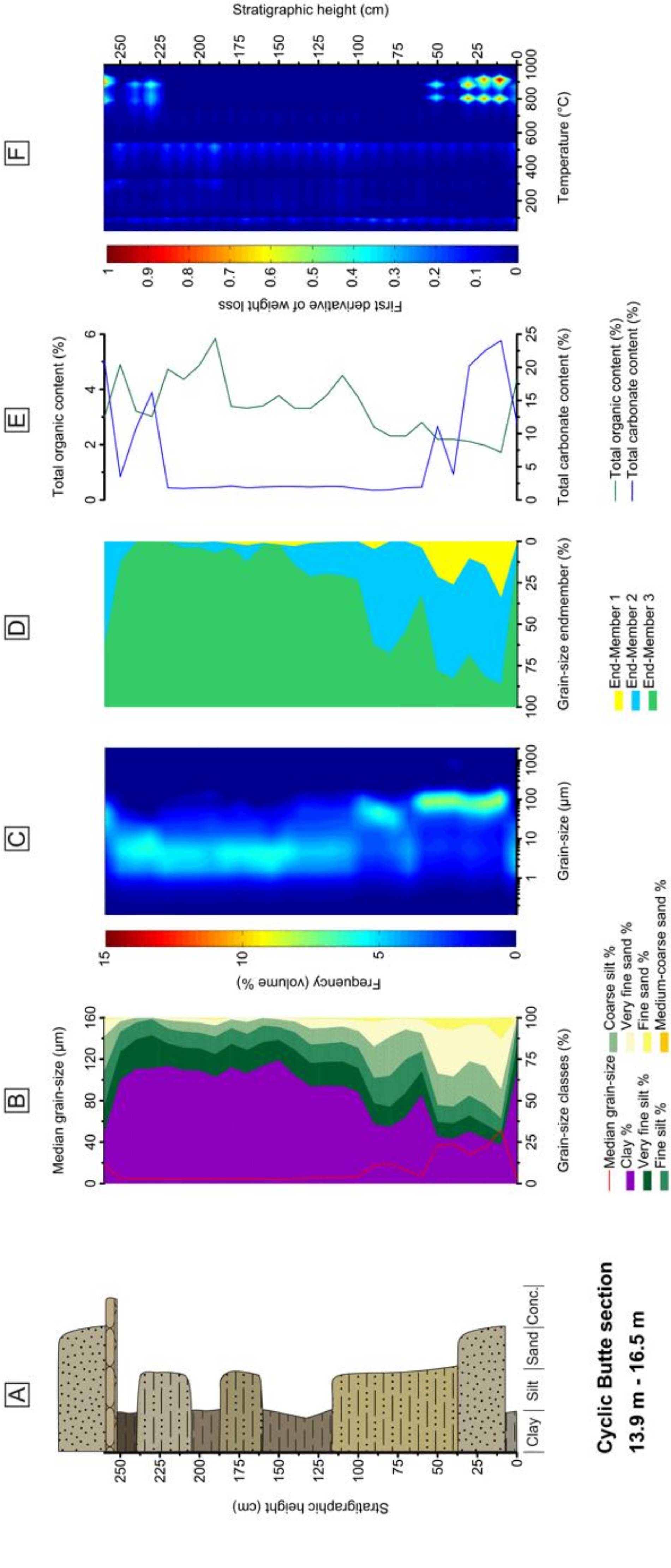

A
B
C
D
E
F
Stratigraphic height (cm)
Clay
Silt
Sand
Conc.
Cyclic Butte section
13.9 m - 16.5 m
Median grain-size (μm)
Grain-size classes (%)
Median grain-size
Clay %
Very fine silt %
Fine silt %
Coarse silt %
Very fine sand %
Fine sand %
Medium-coarse sand %
Frequency (volume %)
Grain-size (μm)
Grain-size endmember (%)
End-Member 1
End-Member 2
End-Member 3
Total organic content (%)
Total carbonate content (%)
First derivative of weight loss
Temperature (°C)

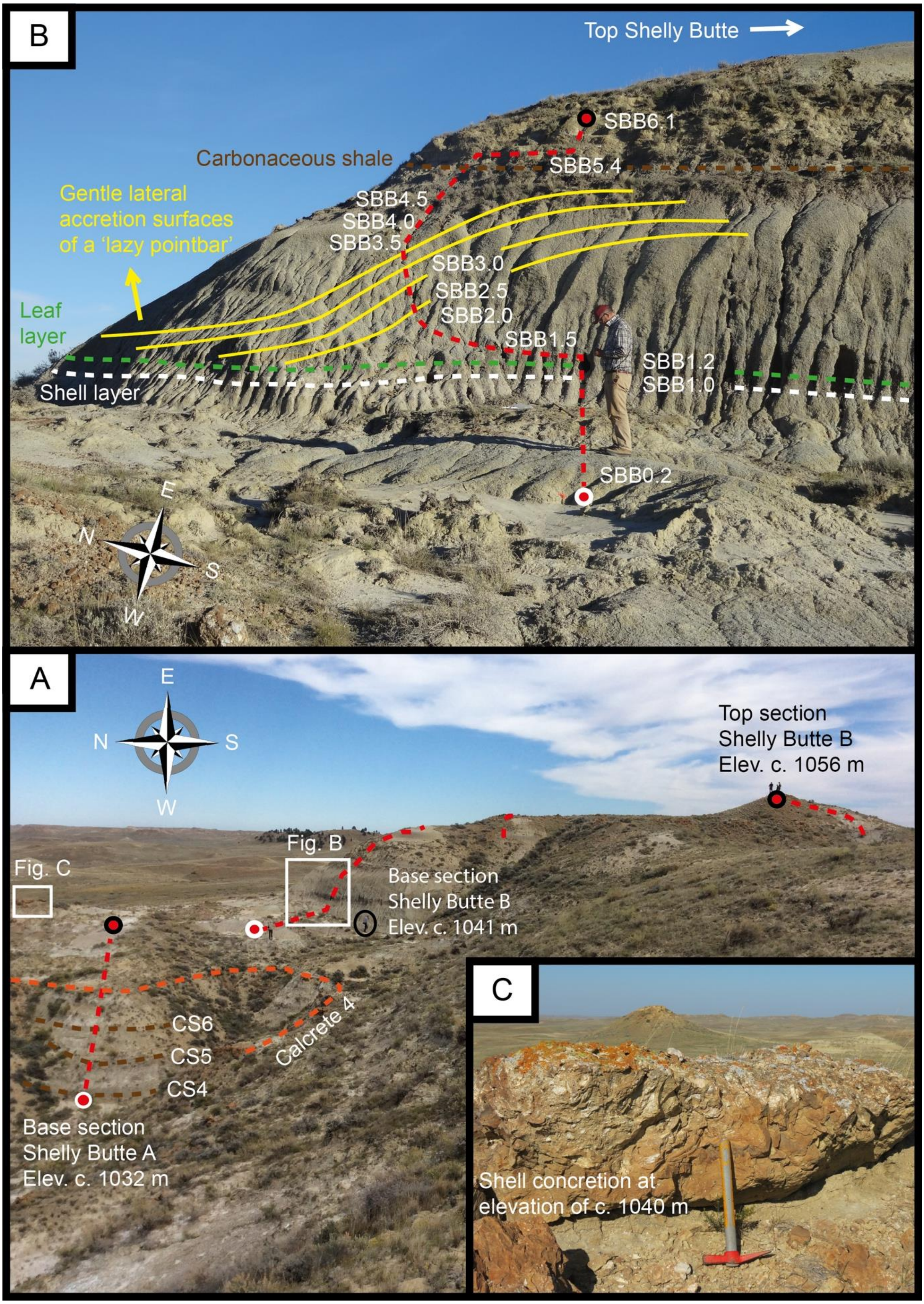


**Fig. A2.7.** Photo overviews of Shelly Butte indicating the entire stratigraphic log and position of the samples taken.

**Fig. A2.8**

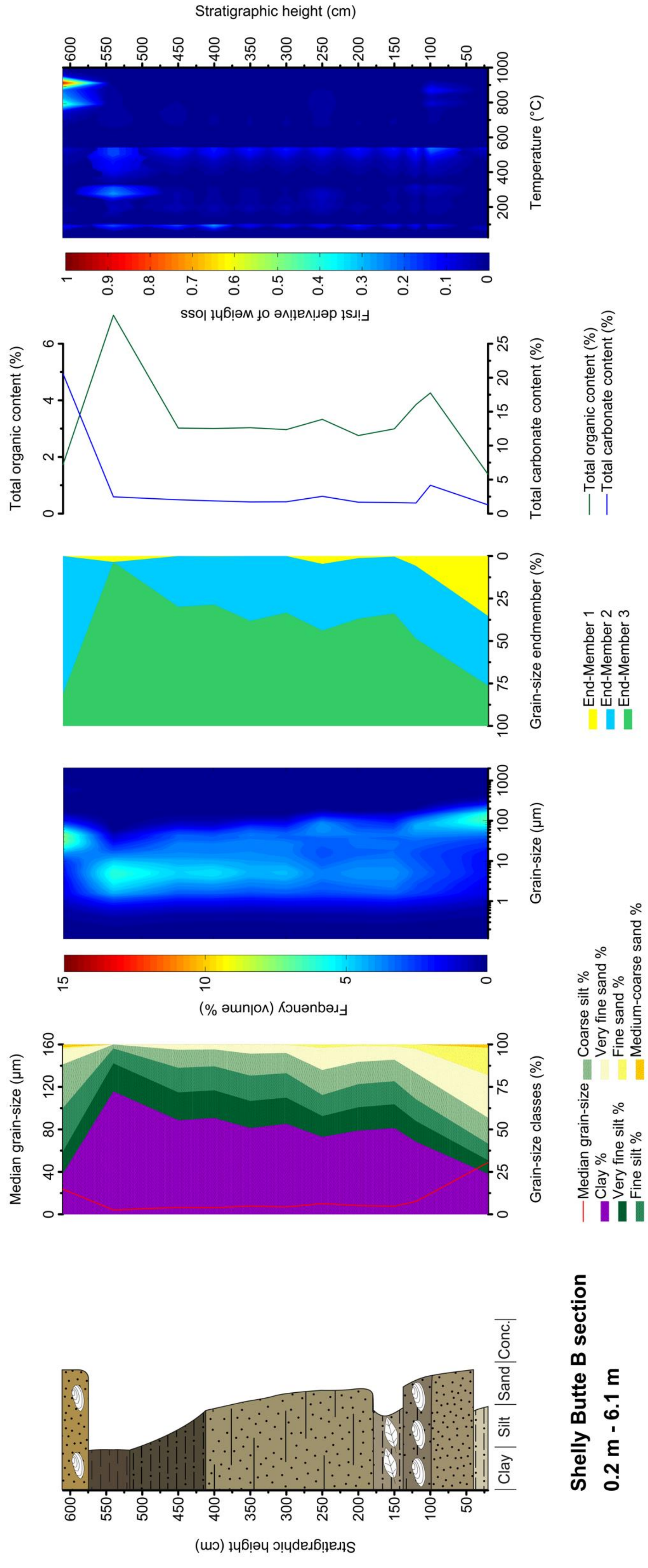

Shelly Butte B section
0.2 m - 6.1 m
A
B
C
D
E
F
Stratigraphic height (cm)
Clay
Silt
Sand
Conc.
Median grain-size (µm)
Grain-size classes (%)
Median grain-size
Clay %
Very fine silt %
Fine silt %
Coarse silt %
Very fine sand %
Fine sand %
Medium-coarse sand %
Frequency (volume %)
Grain-size (µm)
Grain-size endmember (%)
End-Member 1
End-Member 2
End-Member 3
Total organic content (%)
Total carbonate content (%)
First derivative of weight loss
Temperature (°C)

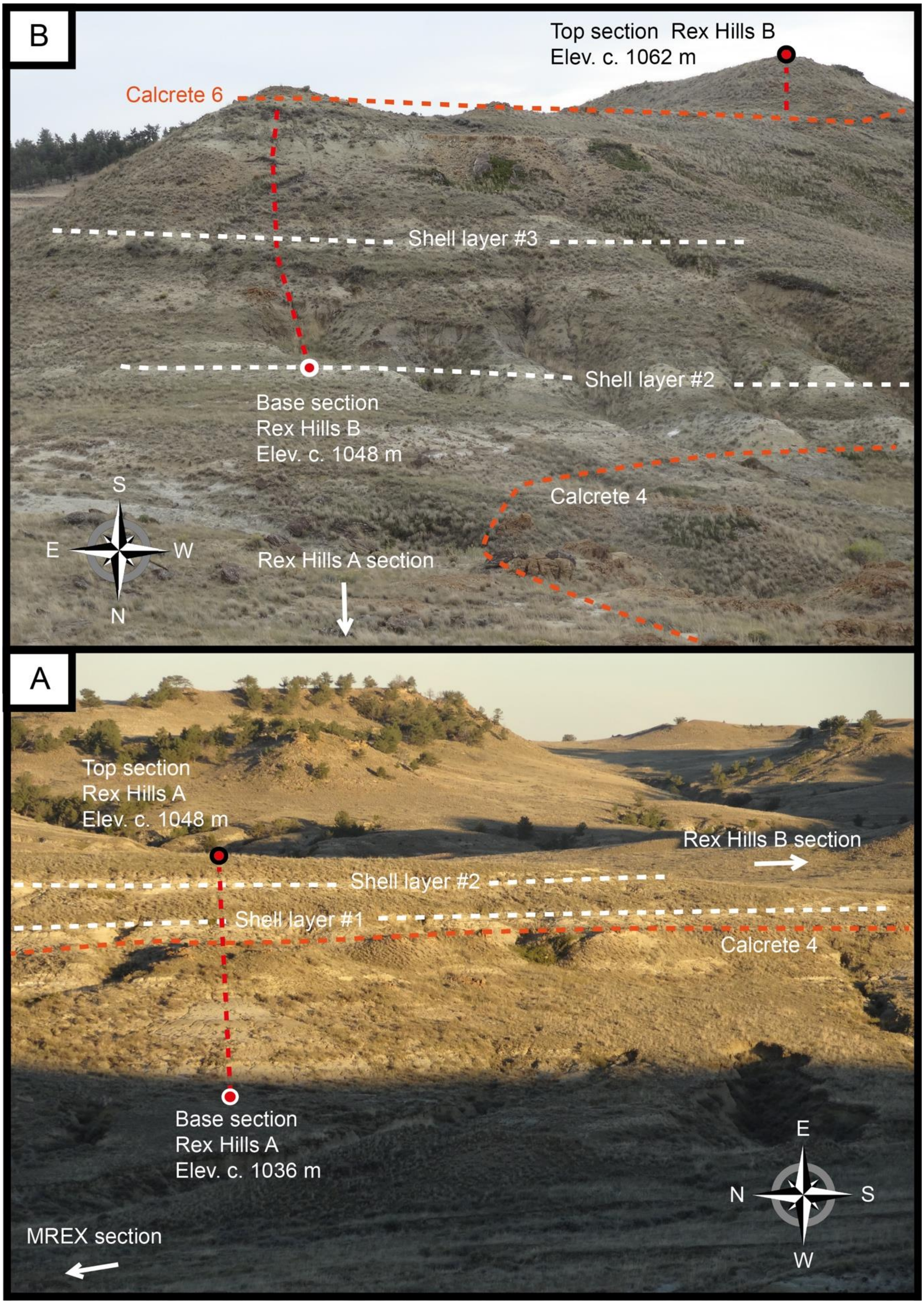


**Fig. A2.9.** Photo overview of Rex Hills A & B sections.

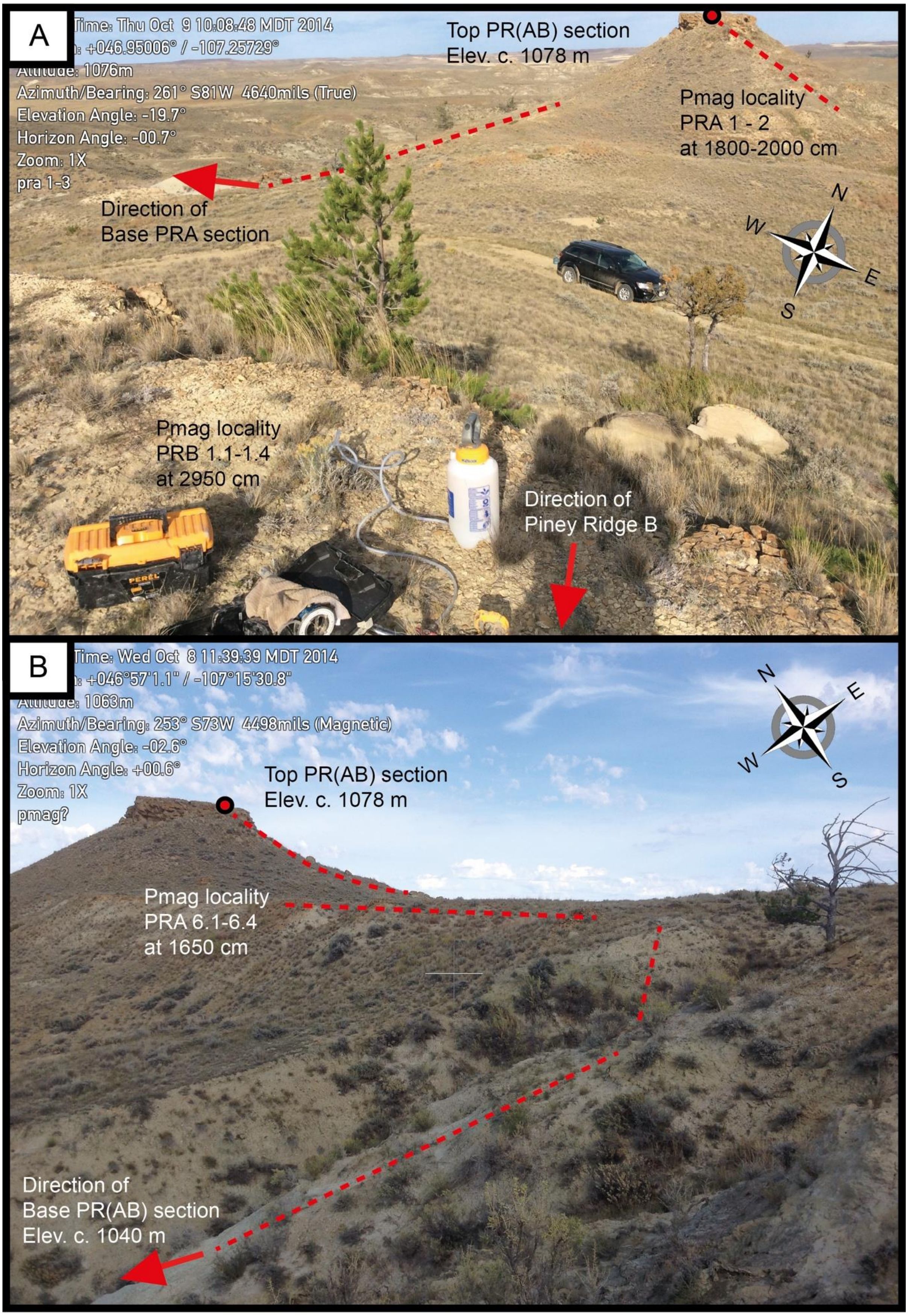


**Fig. A2.10.** Photo overview of the Piney Ridge A & B section.

## Appendix 3: Raw sedimentological and geochemical data

This Appendix, the attached Excel file and Matlab script are available upon request (by e-mail: pim.kaskes@gmail.com)

## Appendix 4: Raw palynology data

This Appendix and attached Excel file are available upon request.

## Appendix 5: Raw paleomagnetic data

This Appendix and attached Excel file are available upon request.

## Appendix 6: *T. rex* list

This Appendix and attached Excel file (with an overview of all *Tyrannosaurus rex* skeletons known so far (as of May 2016)) are available on request.